

https://dspace.org/

Shock wave interaction with porous compressible foams

Atkins, Mark D

2016
http://hdl.handle.net/10539/21333

Downloaded from a DSpace repository. https://dspace.org/

SHOCK WAVE INTERACTION WITH POROUS COMPRESSIBLE FOAMS

Mark D Atkins

DEGREES AWARDED WITH DISTINCTION 24 June 1993

A dissertation submitted to the Faculty of Engineering, University of the Witwatersrand, Johannesburg, in fulfillment of the requirements for the degree of Masters of Science in Engineering

Johannesburg, 1992

Abstract

Two foams, a polyether (density 32.5 kg/m^3) and a polyester (density 38 kg/m^3) foam were tested in a shock tube to analyze the interaction of a normal shock wave and a compressible porous material. The foam specimens were placed in the shock tube test section, the foam being bounded by two steel walls, two glass windows and a solid back plate. The compression chamber of the shock tube was pressurized and the diaphragm separating the compression chamber and the expansion chamber was ruptured, thus producing a normal shock wave which travels down the shock tube and strikes the foam.

Piezoelectric pressure transducers were used to record the pressure before, alongside and behind the foam. A complete set of schlieren photographs, recording the interaction of the incident shock wave and the porous material were taken for each foam. A method for tracking the path of particles of foam (path photographs) was developed. Combining the information obtained from the pressure records, schlieren photographs and path photographs a complete picture of the shock wave foam interaction was developed.

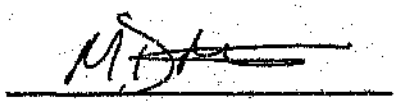
All the gas waves were identified and analyzed. A foam wave (velocity 90 m/s) travelling through the skeleton of the material was discovered. A physical model was developed to explain the high pressure recorded behind the foam. This model is based upon the foam being compressed and forming an almost solid piston, thus forcing the trapped gas into a diminishing volume and creating a high pressure behind the foam.

The theoretical analyses of Monti [30], Gel'fand [20] and Gvozdeva [22] were analyzed and compared. The general finding was that for the range of incident mach numbers 1.37 to 1.46 Monti's analysis under predicts the reflected Mach number by 3 % and Gel'fand's analysis over predicts the reflected Mach number by 6 %.

The coefficient of pressure increase (the ratio of the maximum pressure recorded behind the foam to the equivalent pressure recorded during the reflection of a shock wave from a solid wall) as predicted by Gvozdeva's analysis for the polyether foam lies within the scatter of the experimental results. However for the polyester foam Gvozdeva's analysis under predicts the coefficient of pressure increase by 15%.

Declaration

I declare that this dissertation is my own, unaided work. It is being submitted for the degree of Master of Science in Engineering in the University of the Witwatersrand, Johannesburg. It has not been submitted before for any degree or examination in any other University.



29 day of JULY 1992

Table of Contents

	Abstract	**I**
	Declaration	**ii**
	Contents	**iii**
	Nomenclature	**vi**
	List of Figures	**x**
	List of Photographs	**xviii**
	List of Tables	**xxi**
1	**Introduction**	**1**
1.1	Background	1
1.2	Literature Review	4
1.3	Objectives	35
2	**Theoretical Analysis**	**36**
2.1	Monti Analysis	37
2.2	Gel'fand et al Analysis	44
2.3	Gvozdeva et al Analysis	47
3	**Experimental Facilities**	**50**
3.1	Shock Tube	50
3.1.1	Expansion Chamber	50
3.1.2	Test Section	54
3.1.3	Diaphragm Bursting System	58
3.2	Schlieren System	61
3.2.1	Schlieren Layout	62
3.2.2	Argon Jet Light Source	63
3.2.3	Argon Jet Timing Unit	65
3.2.4	Optical Light Sensor	67
3.3	Foam	68
3.4	Instrumentation	69
3.4.1	PCB 113A21 Pressure Transducers	69
3.4.2	PCB 482A10 Line Power Supply	69
3.5	Computer Hardware	70

3.5.1	XT Portable Personal Computer	70
3.5.2	AT Personal Computer	70
3.5.3	ISC-16 Hardware System	70
3.6	Computer Software	72
3.6.1	ISC-16 Scope Driver	72
3.6.2	ISC - 16 Mass Storage Scope Driver	73
4	**Experimentation**	**74**
4.1	Procedure	74
4.2	Path Photographs	78
4.3	Observations	81
4.4	Data Processing	85
5	**Results and Discussion**	**95**
5.1	Pressure Variation	95
5.1.1	Reflected Shock Wave	105
5.1.2	Rear Wall Pressure	110
5.2	Schlieren Photographs	113
5.3	Path Photographs	126
5.3.1	Foam Skeleton Wave	133
5.3.2	Transmitted Compression Wave	143
5.4	Theoretical Analysis	146
5.4.1	Solid Wall Reflection	146
5.4.2	Monti's Theoretical Analysis	148
5.4.3	Gel'fand's Theoretical Analysis	151
5.4.4	Gvozdeva's Theoretical Analysis	157
5.5	Foam Model	161
5.6	Two Dimensional Effects	171
6	**Conclusions**	**177**
References		**180**
Appendix A		**184**
A.1	Transducer Specifications	184
A.2	Power Supply Specifations	185
Appendix B		**186**
B.1	Pressure Transducer Calibration	186
Appendix C		**189**
C.1	Pressure Traces	189

Appendix D **194**

D.1 Program Photograph Conversion 194

Appendix E **198**

E.1 Program Reflected Sound Wave Propagation 199

Appendix F **205**

F.1 Schlieren Photographs 205

Appendix G **211**

G.1 Path Photographs 211

Appendix H **219**

H.1 Program Compressed Foam Boundary 219

Nomenclature

Symbol	Quantity	units
a	speed of sound	m/s
b	force as a result of the material skeleton elasticity	
c	specific heat capacity	J/kg
C	compression wave	
d	length of the porous material	m
dp	particle diameter	m
D	velocity of thee wave	m/s
e	internal energy of the porous medium	
E	Young's modulus .	Pa
fx	force per unit area	N/m^2
I	shock wave intensity	
L	length of specimen	m
m	material deformation parameter	
M	Mach number	
n	number of internal degrees of freedom (n=5 for a bia-tomic gas)	
np	mass concentration of particles	
p	pressure average over a unit volume	Pa
P	pressure	Pa

Symbol	Quantity	units
Pn	stress in the medium normal to the shock wave front	Pa
R	coefficient of pressure increase (P_{III}/P_{3O})	
R	rarefaction wave	
S	shock wave	
S	sensitivity	Pa/mv
t	time	s
u	velocity of gas	m/s
v	volume per unit mass	m^3/kg
v_l	average voltage	mv
V	velocity	m/s
Q	heat flux from the gaseous phase to the material skeleton	

Greek Notation

α,η	porosity	
α	volume fraction of air in the foam (porosity coefficient)	
δ	shock wave strength	kg/m^3
η	one dimensional strain	
ηO	volume fraction of foam in the porous sample	
γ	hydraulic drag coefficient	
γ	the ratio of specific heat of gas to the specific heat of the porous medium	

Symbol	Quantity	units
Γ	equivalent adiabatic exponent of the foam	
π	average stiffness modulus	Pa
ρ	density	kg/m^3
ρc	acoustic resistance	$kg/m^3\ s$
τ	nondimensional time	
Θ	average stiffness modulus for the porous material	Pa

Subscripts

I	incident shock wave
R	reflected shock wave
S	incident shock wave
SR	reflected shock wave
T	transmitted shock wave
TRT	shock wave transmitted into the air as a result of the shock wave foam / air interaction
TRTT	shock wave formed when the reflected shock wave SR interacts with the shock wave STRT
1	region of gas ahead the incident shock wave
2	region of gas after the incident shock wave
3O	region of gas behind the reflected shock wave from a solid wall
I	region of gas in the foam ahead of the incident shock wave
II	region of gas in the foam behind the transmitted compression wave

Symbol	Quantity
III	region of gas in the foam behind the compression wave reflected from the solid wall
s	skeleton of the porous material

List of Figures

Figure		Page
1.1	Pressure variation, 190 mm of polyether foam (ρ = 14.8 kg/m^3), incident shock wave Mach number 1.343	2
1.2	Shock wave positions as a function of time for shock wave impingementon a deformable material	4
1.3	Typical pressure history recorded upstream of the foam model	5
1.4	Experimental layout for shock wave interactions generated by a rifle bullet	6
1.5	Schlieren photographs of the reflection of a weak shock wave from the surfaces (a) 7.0 lb/ft^3 fibreglass board (b) 3.0 lb/ft^3 fibreglass board	7
1.6	Experimental configuration (Beavers and Matta [3])	9
1.7	Dependence of reflected shock wave Mach number on incident shock wave Mach number and material parameters	10
1.8	Shock tube test sections (a) two dimension expansion duct (b) cylindrical expansion duct	11
1.9	Shock reflection in a two dimensional duct (a) no foam lining (b) 2.5 cm foam lining	12
1.10	Axial pressure variation in cylindrical ducts (a) no foam lining (b) 2.5 cm foam lining	13
1.11	Pressure variation, incident Mach number 2, polyurethane foam length 150 mm	14
1.12	Dependence of the reflected shock wave strength on the incident shock wave strength	15

Figure		Page
1.13	Configuration of the incident and reflected shock waves interacting with a porous material	16
1.14	Shock tube with a perforated plug	17
1.15	Shock tube with porous walls	18
1.16	Pressure variation, polyurethane foam length 300 mm, incident shock wave strength $\delta_i 1 = 3.3$	20
1.17	Variation of the coefficient of pressure increased at the wall, behind a block of polyurethane foam	21
1.18	Oscillogram records, upper trace : pressure behind the porous material, lower trace : pressure on the lateral wall left side : polystyrene, length (1a) 0 mm (2a) 18 mm (3a) 36 mm (4a) 54 mm, right side : polyurethane , length (1b) 0 mm (2b) 65 mm (3b) 130 mm (4b) 185 mm	23
1.19	Variation of the coefficient of pressure increased at the wall, behind a 130 mm block of polyurethane foam	24
1.20	Variation of the coefficient of pressure increased at the wall, behind various thickness of polystyrene foam	25
1.21	Oscillogram records, upper trace : pressure behind the porous material, lower trace : pressure on the lateral wall left side : polyurethane foam , $M_I = 1.9$, positive density gradient, right side : polyurethane foam $M_I = 1.5$, negative density gradient	26
1.22	Theoretical and experimental pressure profiles , (1) and (3) experimental, (2) and (4) theoretical	27
1.23	Experimental and numerical pressure time history of the end of the shock tube (1,2) and on the side wall (3,4)	32
1.24	Variation of the coefficient of pressure increase at the rear shock tube wall covered by polyurethane foam : (1,3,5) - numerical simulation, (2,5) - experimental	32

Figure		Page
1.25	Experimental and numerical pressure time history of the solid plate covered with polyurethane foam after a weak blast wave reflection : experimental - solid curve, computed - dotted curve	33
1.26	Variation of the coefficient of pressure increase at the rear shock tube wall covered by polyurethane foam, for blast wave reflection : solid curve - experimental data, dotted curve - computed data	34
2.1	Shock wave interaction notation	36
2.2	Shock wave motion as a function of time for a shock wave striking a discontinuity surface	39
3.1	Shock tube	51
3.2	Square tube	52
3.3	Square block template	53
3.4	Sealing flange	54
3.5	Test section	55
3.6	Back plate assembly	56
3.7	Diaphragm breaker circuit diagram 1	58
3.8	Diaphragm breaker circuit diagram 2	59
3.9	Simple schlieren system	61
3.10	Schlieren layout	62
3.11	Argon jet light source	64
3.12	Argon jet light system layout	66
4.1	Part of the standard optical setup for schlieren photographs	78

Figure		Page
4.2	Optical equipment layout for Path photographs	79
4.3	Foam sides	82
4.4	Transducer positions in the test section of the shock tube	83
5.1	Transducer positions in the test section	95
5.2	Pressure variation at P1, 70 mm of polyether foam, incident shock Mach number 1.4	96
5.3	Pressure variation at P3, 70 mm of polyether foam, incident shock Mach number 1.4	97
5.4	Pressure variation at P4, 70 mm of polyether foam, incident shock Mach number 1.4	97
5.5	Pressure variation at P5, 70 mm of polyether foam, incident shock Mach number 1.4	98
5.6	Pressure variation at P6, 70 mm of polyether foam, incident shock Mach number 1.4	99
5.7	Pressure variation at P7, 70 mm of polyether foam, incident shock Mach number 1.4	99
5.8	Pressure variation at P8, 70 mm of polyether foam, incident shock Mach number 1.4	100
5.9	Pressure variation at P9, 70 mm of polyether foam, incident shock Mach number 1.4	101
5.10	Pressure variation at P10, 70 mm of polyether foam, incident shock Mach number 1.4	101
5.11	Pressure contour plot, 70 mm of polyether foam, incident shock wave Mach number 1.4	102
5.12	Pressure contour plot, 70 mm of polyester foam, incident shock wave Mach number 1.4	104
5.13	Pressure variation in the expansion chamber 70 mm of polyether foam, incident shock wave Mach number 1.426	105

Figure		Page
5.14	Pressure variation in the expansion chamber 70 mm of polyester foam, incident shock wave Mach number 1.426	106
5.15	Pressure variation in the expansion chamber 70 mm of polyether foam, incident shock wave Mach number 1.449	107
5.16	Intersection of shock waves	108
5.17	Reflected shock wave Mach number variation with incident shock wave Mach number	110
5.18	Coefficient of pressure increase variation variation with incident shock wave Mach number	112
5.19	Sound wave pattern	116
5.20	Photograph measurement	121
5.21	Foam face movement	123
5.22	Motion of polyether foam (square - foam, triangle - gas, diamond - contact surface)	124
5.23	Motion of polyester foam (square - foam, triangle - gas, diamond - contact surface)	125
5.24	Diagonal lines for Path photographs.	133
5.25	Particle paths, polyester foam 38 kg/m^3 $M_I = 1.4$	134
5.26	Polyester foam face motion, schlieren photographs (crosses) Path photographs (squares)	136
5.27	Particle paths, polyether foam 32.5 kg/m^3 $M_I = 1.4$	138
5.28	Polyether foam face motion	139
5.29	Polyester foam face motion	141
5.30	Polyether foam face motion, schlieren photographs (crosses) path photographs (squares)	142

Figure		Page
5.31	Transmitted compression wave and foam skeleton wave comparison, polyester foam 38 kg/m^3	144
5.32	Transmitted compression wave and foam skeleton wave comparison, polyether foam 32.5 kg/m^3	145
5.33	Shock wave interaction with a solid wall	146
5.34	Experimental force-deformation curve for the polyester foam	149
5.35	Reflected shock wave Mach number variation with incident shock wave Mach number, experimental and Monti's [30] theoretical results	150
5.36	Reflected shock pressure variation with incident shock wave Mach number, experimental and Monti's [30] theoretical results	150
5.37	Reflected shock wave Mach number variation with incident shock wave Mach number, experimental and Gel'fand's [19] theoretical results	152
5.38	Reflected shock wave pressure variation with incident shock wave Mach number, experimental and Gel'fand's [19] theoretical results	153
5.39	Reflected shock wave Mach number variation with incident shock wave Mach number, polyester foam	154
5.40	Reflected shock wave Mach number variation with incident shock wave Mach number, polyether foam	155
5.41	Reflected shock wave pressure variation with incident shock wave Mach number, polyester foam	156
5.42	Reflected shock wave pressure variation with incident shock wave Mach number, polyether foam	156
5.43	Coefficient of pressure increase variation with incident shock wave Mach number, polyester foam	159

Figure		Page
5.44	Coefficient of pressure increase variation with incident shock wave Mach number, polyether foam	160
5.45	Transmitted shock Mach number variation with incident shock wave Mach number (Gvozdeva's analysis)	160
5.46	Pressure contour plot and motion of 70 mm of polyester foam, incident shock wave Mach number 1.4	162
5.47	Pressure contour plot and motion of 70 mm of polyether foam, incident shock wave Mach number 1.4	163
5.48	Composite wave diagram, polyether foam [38]	164
5.49	Motion of polyester foam (square - foam, triangle - gas, diamond - contact surface, x - calculated compressed foam boundary)	169
5.50	Motion of polyether foam (square - foam, triangle - gas, diamond - contact surface, x - calculated compressed foam boundary)	170
C.1	Pressure variation at P1, 70 mm of polyester foam, incident shock wave Mach number 1.4	189
C.2	Pressure variation at P3, 70 mm of polyester foam, incident shock wave Mach number 1.4	190
C.3	Pressure variation at P4, 70 mm of polyester foam, incident shock wave Mach number 1.4	190
C.4	Pressure variation at P5, 70 mm of polyester foam, incident shock wave Mach number 1.4	191
C.5	Pressure variation at P6, 70 mm of polyester foam, incident shock wave Mach number 1.4	191
C.6	Pressure variation at P7, 70 mm of polyester foam, incident shock wave Mach number 1.4	192
C.7	Pressure variation at P8, 70 mm of polyester foam, incident shock wave Mach number 1.4	192

Figure		Page
C.8	Pressure variation at P9, 70 mm of polyester foam, incident shock wave Mach number 1.4	193
C.9	Pressure variation at P10, 70 mm of polyester foam, incident shock wave Mach number 1.4	193
D.1	Shock tube test section	194
E.1	Reflected sound wave propagation	199

List of Photographs

Plate		Page
3.1	Polyether and polyester foam	68
5.1	Schlieren photograph, polyether foam, density 32.5 kg/m^3, time 195 μs	114
5.2	Schlieren photograph, polyether foam, density 32.5 kg/m^3, time 261 μs	114
5.3	Schlieren photograph, polyether foam, density 32.5 kg/m^3, time 380 μs	115
5.4	Schlieren photograph, polyether foam, density 32.5 kg/m^3, time 1100 μs	117
5.5	Schlieren photograph, polyether foam, density 32.5 kg/m^3, time 1160 μs	118
5.6	Schlieren photograph, polyether foam, density 32.5 kg/m^3, time 1340 μs	118
5.7	Schlieren photograph, polyether foam, density 32.5 kg/m^3, time 1580 μs	119
5.8	Schlieren photograph, polyether foam, density 32.5 kg/m^3, time 1880 μs	120
5.9	Path photograph, polyester foam, density 38 kg/m^3, time 0 μs	127
5.10	Path photograph, polyester foam, density 38 kg/m^3, time 440 μs	128
5.11	Path photograph, polyester foam, density 38 kg/m^3, time 800 μs	129

Plate		Page
5.12	Path photograph, polyester foam, density 38 kg/m^3, time104 0 μs	130
5.13	Path photograph, polyester foam, density 38 kg/m^3, time1400 μs	131
5.14	Path photograph, polyether foam, density 32.5 kg/m^3, time 440 μs	132
5.15	Path photograph, polyester foam, density 38 kg/m^3, (72 mm × 72 mm), time 0 μs	172
5.16	Path photograph, polyester foam, density 38 kg/m^3, (72 mm × 72 mm), time 500 μs	173
5.17	Path photograph, polyester foam, density 38 kg/m^3, (72 mm × 72 mm), time 800 μs	174
5.18	Schlieren photograph, polyester foam density 38 kg/m^3, cling rap side, time 1340 μs	175
F.1	Schlieren photographs, polyether foam, density 32.5 kg/m^3, (S3.1 to S3.4)	206
F.2	Schlieren photographs, polyether foam, density 32.5 kg/m^3, (S79 to S82)	206
F.3	Schlieren photographs, polyether foam, density 32.5 kg/m^3, (S83 to S86)	207
F.4	Schlieren photographs, polyether foam, density 32.5 kg/m^3, (S87 to S89)	207
F.5	Schlieren photographs, polyester foam, density 38 kg/m^3, (S90 to S93)	208
F.6	Schlieren photographs, polyester foam, density 38 kg/m^3, (S94 to S97)	208

Plate		Page
F.7	Schlieren photographs, polyester foam, density 38 kg/m^3, (S98 to S2)	209
F.8	Schlieren photographs, polyester foam, density 38 kg/m^3, (S3 to S6)	209
F.9	Schlieren photographs, polyester foam, density 38 kg/m^3, (S7 to S10)	210
G.1	Path photographs, polyester foam, density 38 kg/m^3, (P2 to P19)	212
G.2	Path photographs, polyester foam, density 38 kg/m^3, (P20 to P35)	213
G.3	Path photographs, polyether foam, density 32.5 kg/m^3, (P1 to P14)	214
G.4	Path photographs, polyether foam, density 32.5 kg/m^3, (P15 to P32)	215
G.5	Path photographs, polyether foam, density 32.5 kg/m^3, (P33 to P36)	216
G.6	Path photographs, polyester foam, density 38 kg/m^3, (72 mm x 72 mm), (P1 to P14)	217
G.7	Path photographs, polyester foam, density 38 kg/m^3, (72 mm x 72 mm), (P15 to P26)	218

List of Tables

Table		Page
1.1	Relative amplitude of weak shock waves reflected from surfaces of various materials at atmospheric pressure	8
3.1	Suppression circuit components	60
4.1	Foam specifications	82
4.2	Transducer positions	83
4.3	Porous compressible foam tests	87
5.1	Reflected shock waves from polyether foam	108
5.2	Reflected shock waves from polyester foam	109
5.3	Rear wall pressure polyether foam	111
5.4	Rear wall pressure polyester foam	111
5.5	Foam and gas motion	121
5.6	Polyester foam particle path equations	135
5.7	Polyether foam particle path equations	137
5.8	Solid wall reflection	147
5.9	Results of Monti's [30] theoretical analysis	149
5.10	Results of Gel'fand's [19] theoretical analysis	151
5.11	Results of Gvozdeva's [22] theoretical analysis for polyester foam	158
5.12	Results of Gvozdeva's [22] theoretical analysis for polyether foam	158

Table		Page
5.13	Path of the polyester compressed foam boundary	165
5.14	Path of the polyether compressed foam boundary	167
B.1	Calibration of transducer SN 4815	187
B.2	Transducer sensitivity	187
H.1	Pressure recorded along side the polyester foam (input for the compressed foam boundary program)	219
H.2	Pressure recorded along side the polyether foam (input for the compressed foam boundary program)	221

1 Introduction

1.1 Background

When an explosion occurs a spherical blast wave is generated which propagates outwards, reflecting off any solid surface. The reflected blast waves can cause a larger proportion of the damage during an explosion due to the higher pressure. Thus if the destructive power of the reflected blast wave could be reduced, the overall effect of the explosion would be reduced.

The idea of placing a porous material in front of a solid surface to reduce the reflected shock wave and attenuate the transmitted wave, was the initial reason for starting a research program into the interaction of shock waves and porous materials. A number of porous materials were considered, a collection of straws bound together, metal ball bearings bound in a lattice structure and porous compressible foams. The initial experimentation indicated that the porous compressible foams showed the most promise as a reflected shock wave reducer. Further experimentation was confined to porous compressible foams.

Atkins [1] documented an investigation into the interaction of shock waves and porous compressible foams. The research was carried out with the following objectives in mind:

- to determine the effect of foam density on the reflected shock wave strength
- to determine the effect of the foam length on the reflected shock wave strength
- to determine the variation of the shock wave Mach number of the reflected shock wave with the incident shock wave Mach number.

Five different foams having densities ranging from 14.8 kg/m^3 to 38.0 kg/m^3 were tested. Three different lengths of each foam were tested, namely 50 mm, 120 mm and 190 mm.

The results were limited to pressure traces obtained from four piezoelectric pressure transducers. Two transducers were located in front of the foam, one alongside and one behind the foam.

A typical pressure trace is shown in figure 1.1. The pressure trace is from the interaction of a shock wave having a Mach number of 1.343 and 190 mm of polyether foam (ρ = 14.8 kg/m^3).

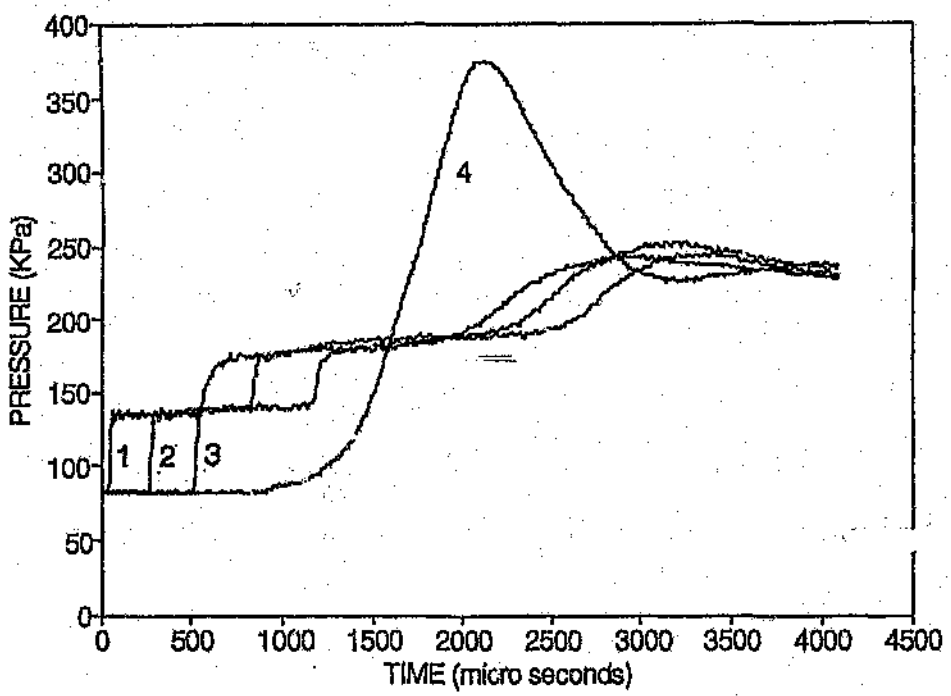


Figure 1.1 Pressure variation, 120 mm of polyether foam (ρ = 14.8 kg/m^3), incident shock wave Mach number 1.343 (1)

Analysing curves (1) and (2), the pressure from the two transducers located in front of the foam, three waves can clearly be identified. The first rise in pressure is as a result of the incident shock wave passing the transducer. The second rise in pressure is the shock wave that has been reflected from the front face of the foam. The third distinct rise in pressure is a compression wave travelling in the same direction as the reflected shock wave.

Analysing curve (3), the pressure recorded alongside the foam, all that can confidently be stated is that two waves can be seen travelling through the foam, one towards the back plate, the other away from it.

The analysis of curve (4) provided the most difficult challenge that had to be solved in order to understand the shock wave porous foam interaction. Considering that the rise in pressure across the incident shock wave is approximately 100 kPa and the pressure measured behind the 190 mm of polyether foam was 600 kPa, the foam was acting as a pressure amplifier. Extensive precautions were taken to ensure that the pressure that was being

measured was gas pressure and that the foam was not striking the face of the transducer.

Atkins [1] came to the following conclusions:

- foam reduced the reflected shock wave strength for a limited time
- the denser the foam the larger the pressure behind the reflected shock wave
- the time taken for the reflected pressure to rise to that which was obtained without the foam increases as the density increases and increases as the foam length increases
- the pressure behind the reflected shock wave does not change as the length increases.

No explanation of the pressure amplification behind the foam was attempted. The following recommendations were made:

- the shock tube be fitted with a window to allow the foam specimen to be viewed
- further studies are required on the wave transmitted through the foam.

The literature survey and the experimental results Atkins [1] obtained highlighted that a large proportion of the waves present in the shock wave porous foam interaction were not clearly understood. This led to the formulation of a test matrix for further research. Since the basic dependence of the shock wave parameters on the length and density of the foam had been determined (Atkins [1]), it was logical to limit further research to two foams of differing density, each having the same length. Thus enabling a larger number of tests to be carried out to identify the waves present and to determine what was physically happening in the shock wave porous foam interaction.

1.2 Literature Review

Monti [30] in 1970 published the results of a theoretical and experimental investigation on normal shock wave reflection from cellular and open structure foams. A block of material was placed in front of a solid rigid wall and struck by a normal shock wave.

Starting with the equations governing the propagation of normal, plane shock waves in continuous and isotropic media, Monti develops a simple solution for the strength of the reflected and transmitted shock waves away from and into linear (Hooke type) materials. The solution is a function of a single parameter which measures the deformability of the material.

Based on his theoretical analysis Monti stated that if tests were conducted on the reflection of shock waves from a foam material in front of a solid wall and a solid wall, with the incident shock wave having the same Mach number, the pressure on the solid wall could be larger in the case with foam in front of it.

Figure 1.2 is a distance - time graph showing the waves that Monti assumed were present during the shock wave interaction with the foam material.

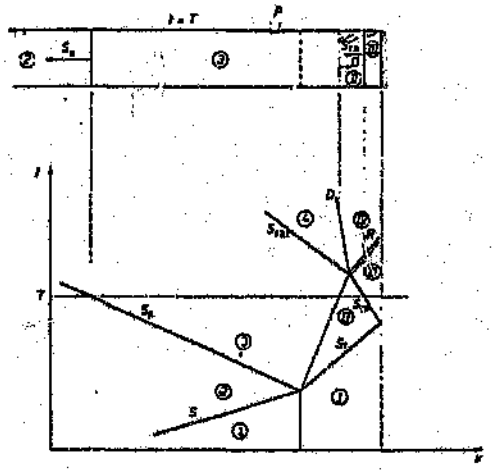


Figure 1.2 Shock wave positions as a function of time for shock wave impingement on a deformable material [30]

The incident shock wave (S_I) strikes the material face (D), a shock wave is reflected (S_R) and the material interface begins to move. A shock wave (S_T) is transmitted into the material, this shock wave then strikes the solid wall behind the material and a shock wave (S_{TR}) is reflected back into the foam. This shock wave then strikes the material interface, a rarefaction wave (R) is reflected back into the material, a shock wave (S_{TRT}) is transmitted into the air and the material interface changes direction.

Monti's experimental setup consisted of a shock tube having a cross-section of 49 mm by 49 mm, with one piezometer located in front of the foam. Tests were conducted on cellular and open structure foams, with incident shock wave Mach numbers ranging from 1.3 to 2.2.

The test specimens were parrallelepiped in shape. A 1 mm gap was left between the walls of the shock tube and the material. The gap was left to avoid friction between the foam and the tube walls.

The experimental data was limited to one pressure history at a particular distance away from the front face of the foam. An example of this is shown in figure 1.3. The pressure jumps S_I and S_R can clearly be seen. The shock wave S_{TRT} or strictly speaking a compression wave, is the third rise in pressure.

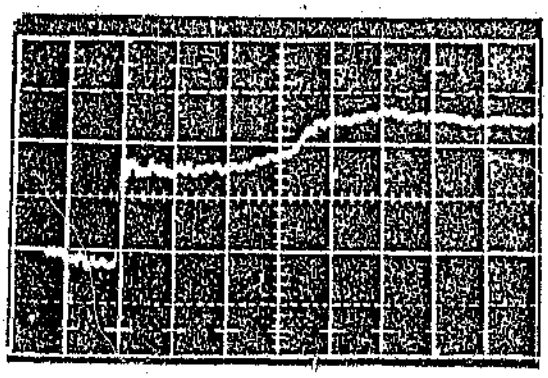


Figure 1.3 Typical pressure history recorded upstream of the foam model [30]

The results presented by Monti are a comparison between the experimental reflected shock wave pressure and the predicted theoretical values. The agreement between the experimental and theoretical shock wave S_R pressure is satisfactory.

In 1971 Cloutier et al. [11] published experimental results that were carried out for the Defence Research Establishment Valcartier, Canada. The DREV had been faced with the problem of finding a means to attenuate the out going shock wave system from a hypersonic model flown in a freeflight ballistic range, so that the reflected shock waves did not interfere with the turbulent wake of the model that was being studied.

Rifle bullets were used to generate the weak shock waves so the relative effectiveness of different materials to attenuate shock waves could be determined. The shock waves were monitored by pressure transducers, shadowgraph and schlieren photographic techniques.

Figure 1.4 shows the experimental layout. The fibreglass board was placed upon a solid backup plate and a 303 rifle bullet fired 4 in. above the surface. The angle between the incident shock wave and the plane of the material was approximately 28 degrees.

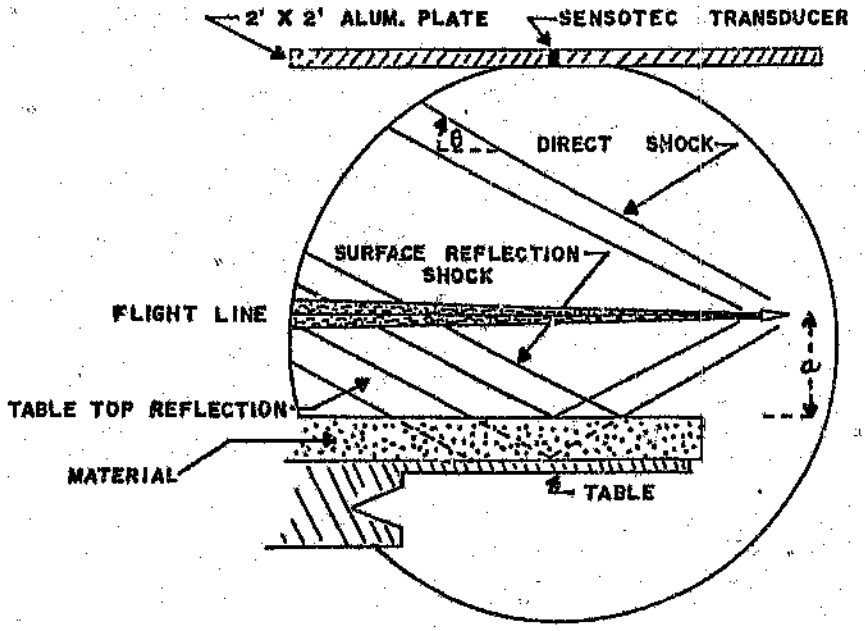
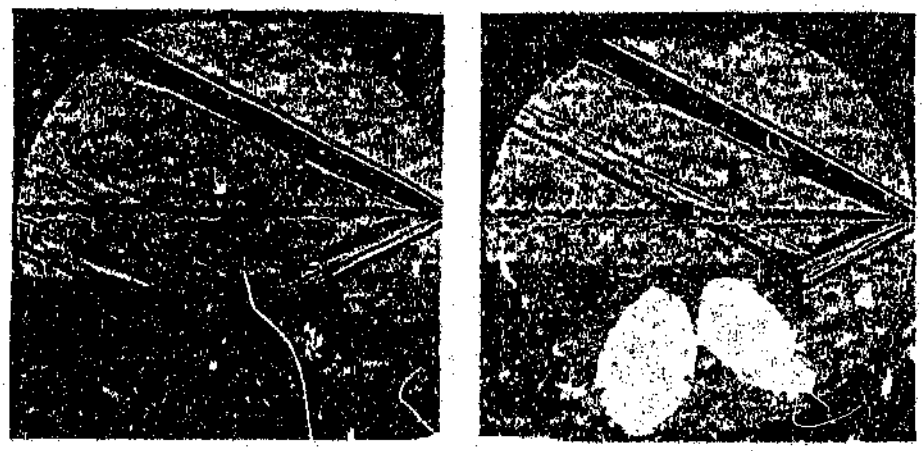


Figure 1.4 Experimental layout for shock wave reflection generated by a rifle bullet [11]

Figure 1.5 shows two schlieren photographs of the reflection of weak shock waves from 2 in. thick fibreglass boards having densities of (a) 7.0 lb/ft^3 and (b) 3.0 lb/ft^3.



(a) (b)

Figure 1.5 Schlieren photographs of the reflection of a weak shock wave from the surfaces (a) 7.0 lb/ft^3 fibreglass board (b) 3.0 lb/ft^3 fibreglass board [11]

The reflection from the backup plate can be seen in photograph (b). This phenomenon occurred with thin layers of low density fibreglass material, which was the material with a low surface reflection property. Cloutier et al. found that by increasing the thickness of the material or adding layers of different density fibreglass, the reflections from the backup plate could be eliminated, while still having a low surface reflection property.

Table 1.1 shows the relative amplitude of the weak shock wave reflected from various materials. The results indicate that the fibreglass materials tested gave weaker surface reflections that the urethane foams and the lower density fibreglass materials gave less surface reflections that the higher density fibreglass.

Table 1.1 Relative amplitude of weak shock waves reflected from surfaces of various materials at atmospheric pressure. [11]

Material	Density (lb/ft^3)	Relative reflected amplitude (%)
Metal plate		100
Vinyl-faced fibreglass	0.75	90
Urethane foam	3.2	55
Urethane foam	1.1	25
Fibreglass board	7	11
Fibreglass board	3	8
Fibreglass board	1.3	6
Fibreglass blanket	0.75	4
Fibreglass blanket	0.5	4

Beavers and Matta [3] in 1972 published the results of an analytical and experimental program on the reflection of weak shock waves from permeable materials for the Department of Defense (U.S.) An analytical model was developed which allowed the calculation of the reflected shock wave velocity for a given incident velocity and known properties of the permeable material. The model is based on a non linear extension to Darcy's law. Beavers and Matta assumed that there were no shock waves transmitted into the material and the velocity behind the reflected shock wave was zero.

Figure 1.6 shows the experimental setup, the permeable material was fixed in the shock tube and had no back plate. The only recording devices were timing units in front of the permeable material which were used to calculate the velocity of the incident and reflected shock waves.

The experiments were carried out in a 3 in. by 3 in. shock tube. Three materials were tested, namely;

- foametal - a latticework of metallic fibres with no free fibre ends within the material

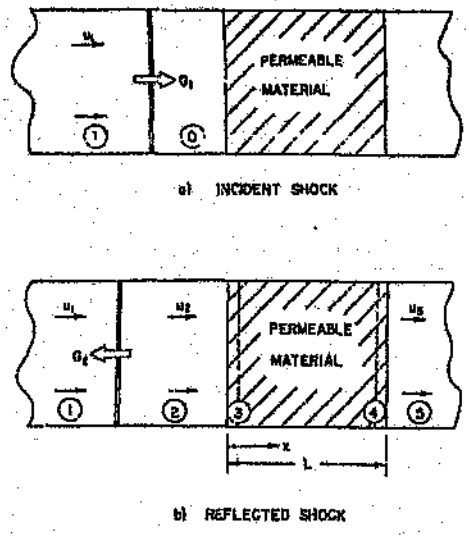


Figure 1.6 Experimental configuration [3]

- Feltmetal - collection of short sintered fibres with free ends within the metal

- granular - aluminium oxide grains of uniform size held together in a ceramic bond

Figure 1.7 shows the results published by Beavers and Matta [3] The dependence of the reflected shock wave Mach number (MR) on the incident shock wave Mach number (MI) and material parameters can be seen. Fair agreement between experimental and theoretical results were obtained for all the materials, but one. Beavers and Matta [3] assumed that there was a shock wave transmitted in to the permeable material when the incident shock wave struck it, which was in contradiction to the assumptions made in formulating the analytical model. This they stated was the reason for the discrepancy between the experimental and theoretical results for the foame-tal.

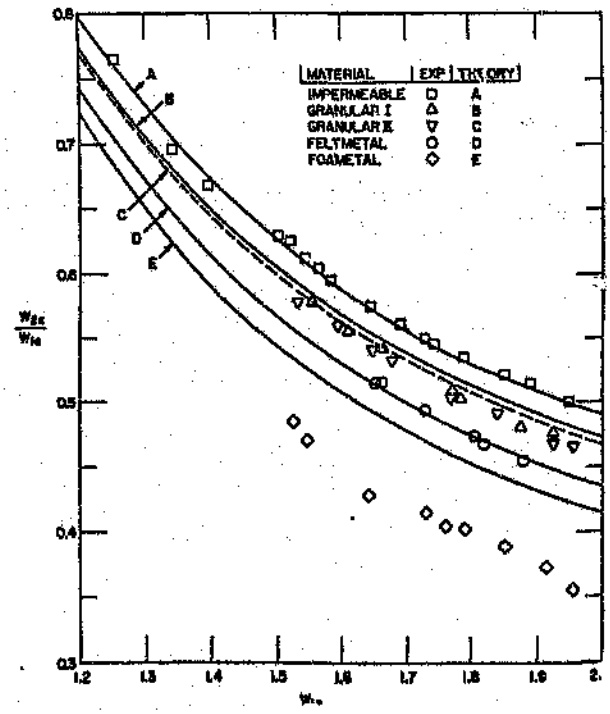


Figure 1.7 Dependence of reflected shock wave Mach number on incident shock wave Mach number and material parameters [3]

In 1973 Guy [21] published his experimental results for the attenuation of shock waves in a duct with absorbent lining, carried out for the Australian Atomic Energy Commission. As a shock wave travels into an abrupt expansion duct, complex patterns of diffracting and reflecting shock waves are produced, which interfere with the unsteady flow moving along the duct. It is this interference, which is undesirable in ballistic range enclosures.

Guy [21] stated that the complexity of the shock wave propagation precluded any theoretical investigation.

The experimental investigation was carried out in a 4 cm diameter cylindrical shock tube. Two test sections were used. The first shown in figure 1.8 (a) was a two dimensional abrupt expansion duct with an expansion ratio of 2:1.

This test section had glass windows which allowed schlieren photographs to be taken. The second test section figure 1.8 (b) was a cylindrical expansion duct with an expansion ratio of 4:1. Mounted on the axis of the duct was a pressure transducer. Both test sections were lined with 2.5 cm thick polyurethane strips.

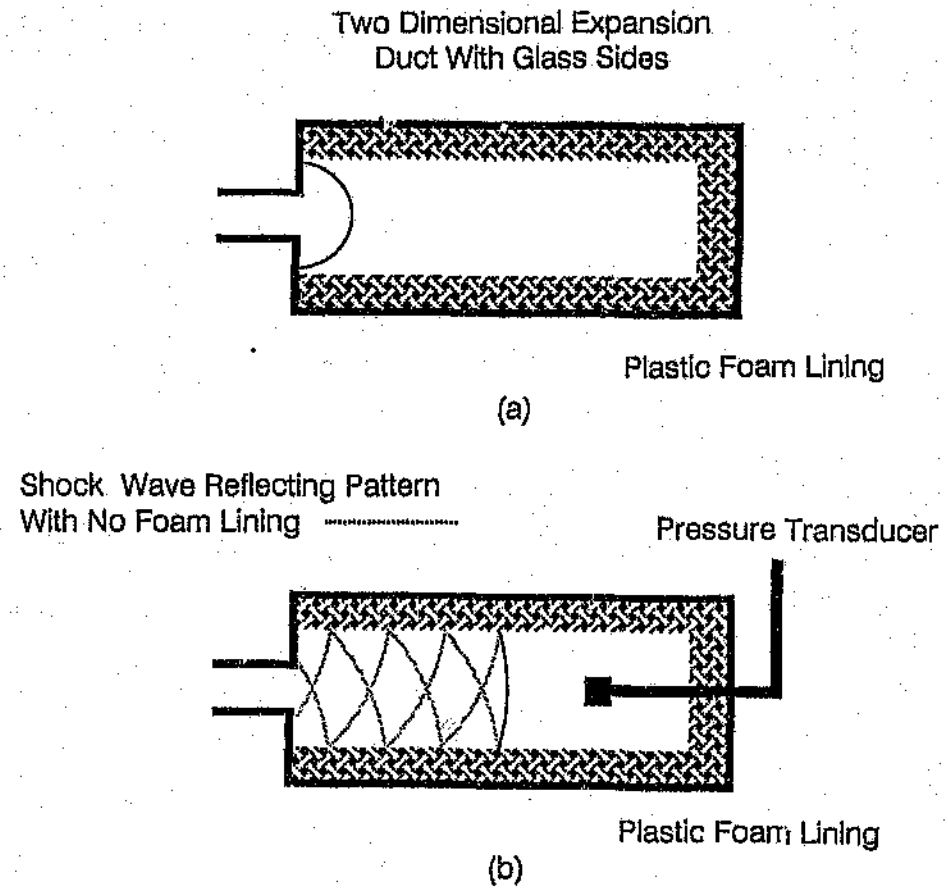
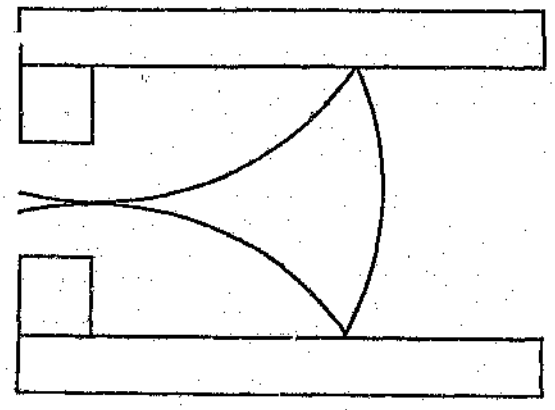
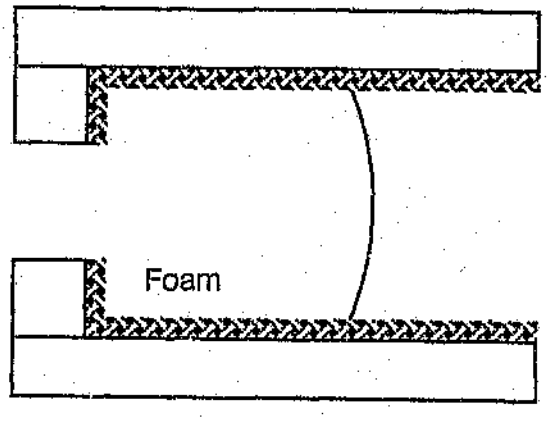


Figure 1.8 Shock tube test section (a) two dimensional expansion duct (b) cylindrical expansion duct [21]

Test were run with an incident Mach number ranging from 1.1 to 1.4. Figure 1.9 shows a drawing replica of the schlieren photographs taken of the two dimensional test section (a) with no foam (b) with 2.5 cm foam lining. The lining almost totally eliminated the shock wave reflection.



(a)



(b)

Figure 1.9 Shock reflection in a two dimensional duct (a) no foam lining (b) 2.5 cm foam lining [21]

Figure 1.10 is the pressure variation in the centre of the cylindrical expansion duct (a) with no foam (b) with 2.5 cm foam lining, for an incident shock wave strength of $P_2/P_1 = 1.4$. No scale for the traces was published.

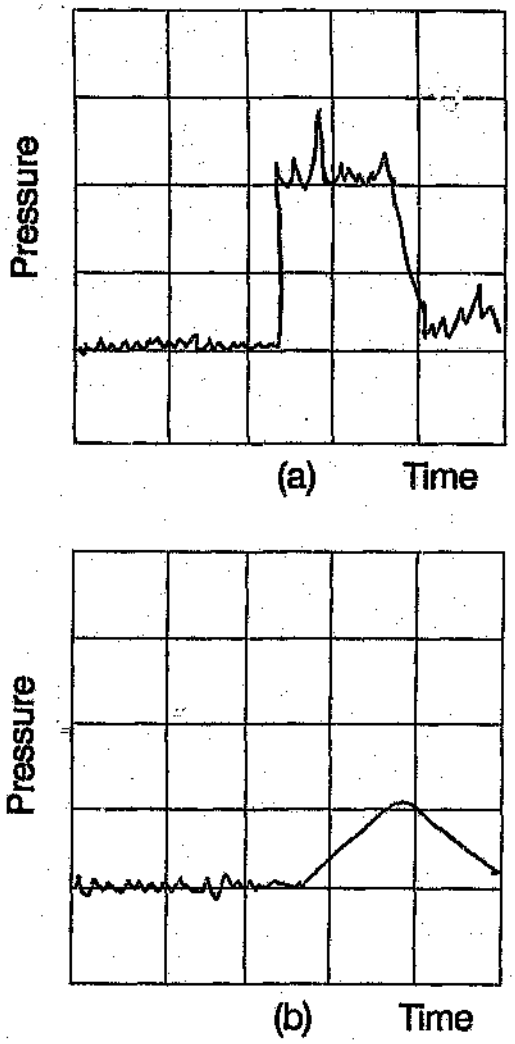


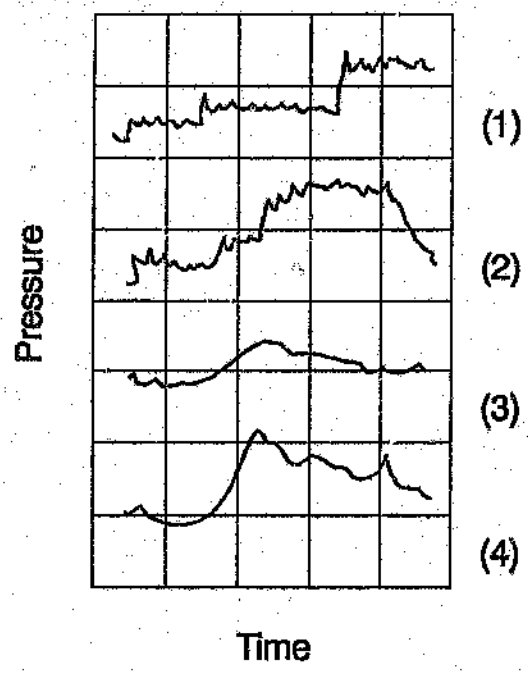
Figure 1.10 Axial pressure variation in cylindrical ducts (a) no foam lining (b) 2.5 cm foam lining [21]

The high frequency noise associated with the pressure peak in the unlined duct is eliminated by the presence of the lining and the peak pressure is significantly reduced. Guy [21] concluded that a polyurethane duct lining could be extremely effective in reducing the strength of shock wave reflections.

Gel'fand et al. [18] in 1975 published experimental results on the propagation and reflection of pressure waves in a porous medium. Test were carried out in a 45 mm by 30 mm shock tube. Piezoelectric pressure pickups were located before, alongside and behind the porous material. The pressure variation from the pickups was monitored on a two beam oscillograph.

Blocks of polyurethane foam ranging in length from 150 mm to 600 mm were mounted in the test section, with the rear of the foam fitting flush against the back plate.

Figure 1.11 shows an oscillograph of the readings from the pressure pickups for a test with an incident shock wave Mach number of 2.0, striking a 150 mm polyurethane block. Below is a schematic of the shock tube showing the location of the pressure pickups.



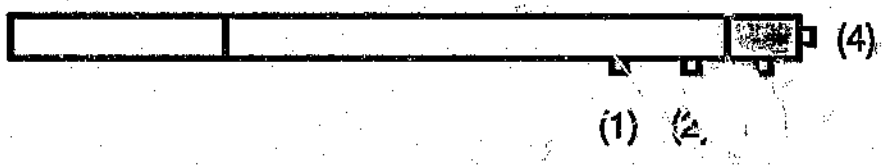


Figure 1.11 Pressure variation, incident Mach number 2, polyurethane foam length 150 mm [18]

The scale for each trace is as follows;

- pressure pickup (1) - y axis 60 bar/division, x axis 100 μs/division
- pressure pickup (2) - y axis 80 bar/division, x axis 100 μs/division

- pressure pickup (3) - y axis 11 bar/division, x axis 300 μs/division

- pressure pickup (4) - y axis 34.6 bar/division, x axis 300 μs/division

Analyzing curves (1) and (2), located in front of the foam, the first pressure rise is the incident shock wave passing the pressure pickup. The second rise is the shock wave that has been reflected from the front face of the foam. Gel'fand et al. [18] states that there is a wave which is refracted in the polyurethane foam which strikes the closed end of the tube which after reflection gives rise to the third pressure rise.

Looking at curve (3), located alongside the foam, Gel'fand et al. [18] assumes that the reason for the long rise time of this wave as compared to the incident shock wave is as a result of the large difference in acoustic resistances of air and foam. (air - $\rho c = 4.2 \times 10^2$ kg/m^2s, porous medium - $\rho c = 4 \times 10^3$ kg/m^2s)

Gel'fand et al. [18] were the first to show experimentally that the peak pressure recorded behind the foam was considerably larger than the pressure recorded for normal solid wall reflection, with the same incident Mach number. This phenomenon can be inferred from curve (4). Gel'fand et al. [18] states that the high pressure recorded behind the foam on the rigid wall was obviously explained by the fact that the solid phase of the porous medium is set into motion behind the wave and this momentum is transmitted to the wall.

The dependence of the reflected shock wave strength on the strength of the incident shock wave is shown in figure 1.12. ΔP_I and ΔP_R represent the pressure rise across the incident and reflected shock waves. P_O represents the atmospheric pressure.

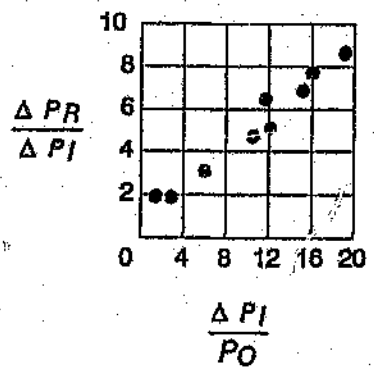


Figure 1.12 Dependence of the reflected shock wave strength on the incident shock wave strength [18]

During the period 1983 to 1985 J.F. Clarke published five papers on shock wave reflection from a porous medium.

Clarke [6] in his paper titled Regular Reflection of a Weak Shock Wave from a Rigid Porous Wall theoretically investigated the reflection of a shock wave from a porous material, placed parallel to the direction of flow. Figure 1.13 shows the waves Clarke assumed were present during the shock wave and foam interaction. The incident shock wave (I) strikes the porous material at an angle Θ, an expansion wave (E) is reflected from the surface of the material. The reflected shock wave (R) then forms at the tail of the expansion wave.

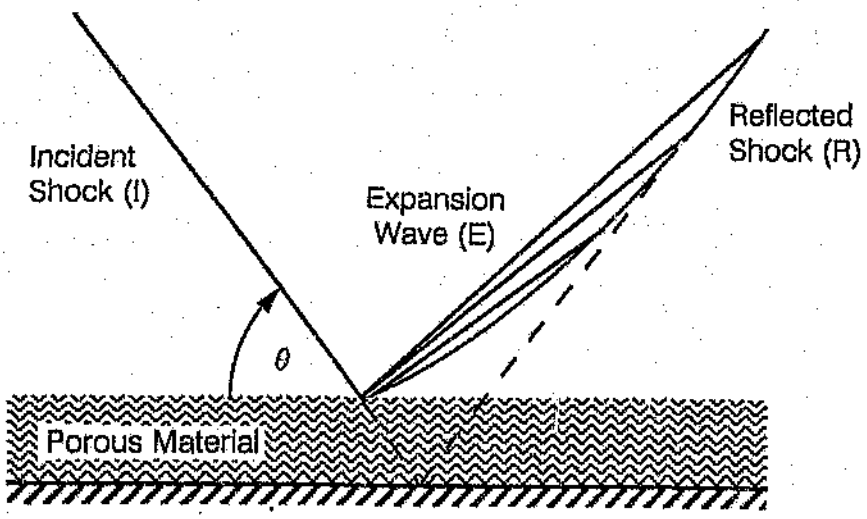


Figure 1.13 Configuration of the incident and reflected shock waves interacting with a porous material [6]

Clarke [6] concluded that a reduction in the reflected shock wave strength could take place over distances of centimetres from the interface. He suggested the need for experimental results to validate his assumptions.

In October 1982 Clarke [7] published some additional results concerning his first paper. He simplified his previous theoretical approach to a case of one dimensional unsteady field, by assuming that the angle of the incident shock wave Θ, tended to zero. Thus he was able to compare his theoretical predictions to the experimental results of a reflected weak shock wave from a porous plug. In his own words "Agreement between calculation and observation is more in the nature of tolerable than excellent." Clarke [7] expressed the need for further and more careful experimental study.

Clarke [8] continued his investigation of the reflected shock waves from porous mediums, the results of which were published in a paper entitled Reflection of a Weak Shock Wave from a Perforated Plug. He considered a weak normal shock wave striking a plug, consisting of a number of slender hollow tubes. The perforated plug is shown in figure 1.14.

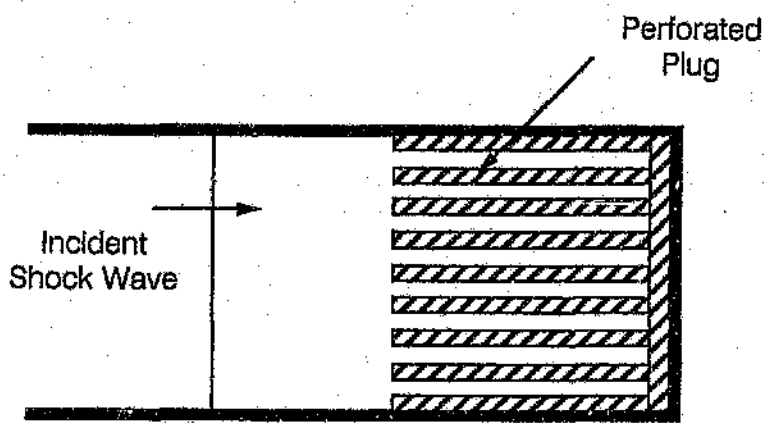


Figure 1.14 Shock tube with a perforated plug [8]

The primary objective was to determine the reflected shock wave strength and it's variation with time. He based his theoretical analysis upon the assumption that the motion of the air in the tubes could be modeled as a one-dimensional unsteady polytropic compressible flow. He concluded that the reflected wave field is dependent upon the tube length, the tube diameter and the acoustic impedance ratio of the ambient air and air within the tubes. Clarke [8] found the comparison between theory and experiment to be satisfactory.

To predict the reflected shock wave from a polyurethane porous plug Clarke,[9] in his paper titled The Reflection of Weak Shock Waves from Absorbent Surfaces, proposed an additional model. The model assumes that the porous material consisted of an aggregate of long thin tubes of different irregular lengths. Shock tube experiments with a solid backed porous plug of polyurethane foam were carried out to test this theory. Clarke [9] states that scatter in the experimental data makes it difficult to be positive about agreement between predicted and experimental results, but that the orders of magnitude of the observed reflected shock wave strengths are right. He did not publish any experimental results of the reflected shock wave

strengths and then goes on to state that agreement between the measurements and predictions is tolerable.

Clarke's [10] latest publication titled The Effect of a Porous Surface on a Shock Wave Initially Normal to it, considers a porous material placed parallel to the direction of flow. The experimental apparatus is shown in figure 1.15.

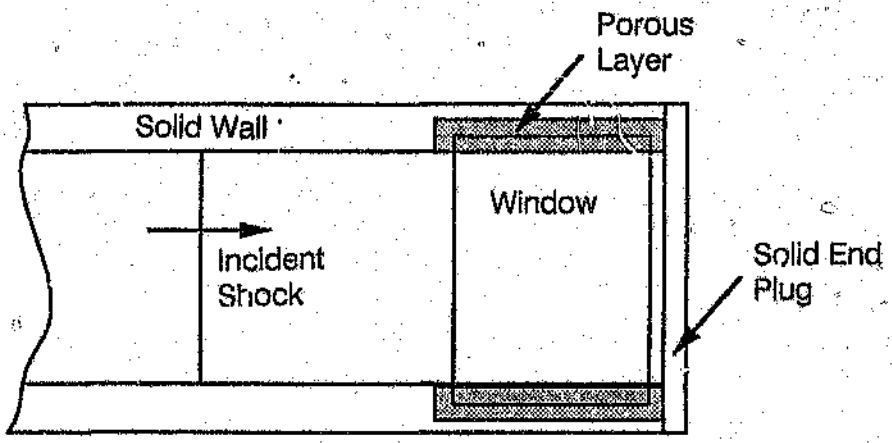


Figure 1.15 Shock tube with porous walls [10]

The theoretical analysis is based upon his previous work, expanding upon the air inflow to the porous layer. This theory may be used in the case of the shock wave striking a porous plug perpendicular to the direction of flow, by considering the angle between the incident shock wave and the foam to be zero. Clarke [10] states that this theory is largely explanatory, rather that predictive. He concludes by stating that to understand the interaction between the shock wave and a porous surface it is imperative that more extensive tests be undertaken with stronger shock waves and a range of porous materials.

In 1983 Gel'fand et al. [20] published their results of a theoretical and experimental analysis of the reflected and transmitted shock waves in polyurethane foam. The interaction of shock waves with a porous screen was investigated in a shock tube. The shock tube was rectangular in section and had internal dimensions of 30 mm by 45 mm. Pressure piezosensors were located along the walls of the shock tube. Two oscillographs were used to record the pressure from the piezosensors.

Two different polyurethane foams, having densities of 20 kg/m^3 and 35 kg/m^3 were tested. The length of the polyurethane samples was varied between 300 mm and 800mm. The incident shock wave intensities were in the range $\delta_1 = P_2/P_1 = 1.3$ to 9.0, where P_2 is the pressure behind the incident shock wave and P_1 is the atmospheric pressure.

The results published by Gel'fand et al. [20] are shown in figure 1.16. Below the oscillograph is a schematic of the shock tube showing the location of the piezosensors and polyurethane foam. There is no rigid wall behind the foam. The incident shock wave had a strength of $\delta_1 = 3.3$, the polyurethane foam having a density of 20 kg/m^3 and being 300 mm in length. The x- axis for all the traces has a scale of 1000 μs/division, no y-axis scale was given.

Analysing curves (1) and (2), the only waves present are the incident and reflected shock waves. Curves (3a) and (3b) were obtained from the transducer alongside the foam. In the case of curve (3b) there was a 1 mm gap between the foam and the shock tube walls. Gel'fand et al. [20] stated that the first rise in pressure in curve (3b) was due to a pressure perturbation slipping along the air gap between the wall of the tube and the polyurethane, the second rise being a wave traveling thorough the foam. It must be noted that Gel'fand et al.[20] stated that the foam was set into motion and travelled down the tube, but no quantitive information about the foam's motion was published.

Gel'fand et al.[20] explained the waves present in curve (4) as follows: the first rise in pressure is as a result of the leading edge of the wave that has traveled through the foam and then reached the foam-air interface. The subsequent pressure rise is due to waves successively emitted from the sample as it is set in motion by the air wave.

The experiments showed that at the gas-foam interface the shock waves are reflected with an increase in pressure, while at the foam-gas interface they attenuate to a value lower than the incident shock wave.

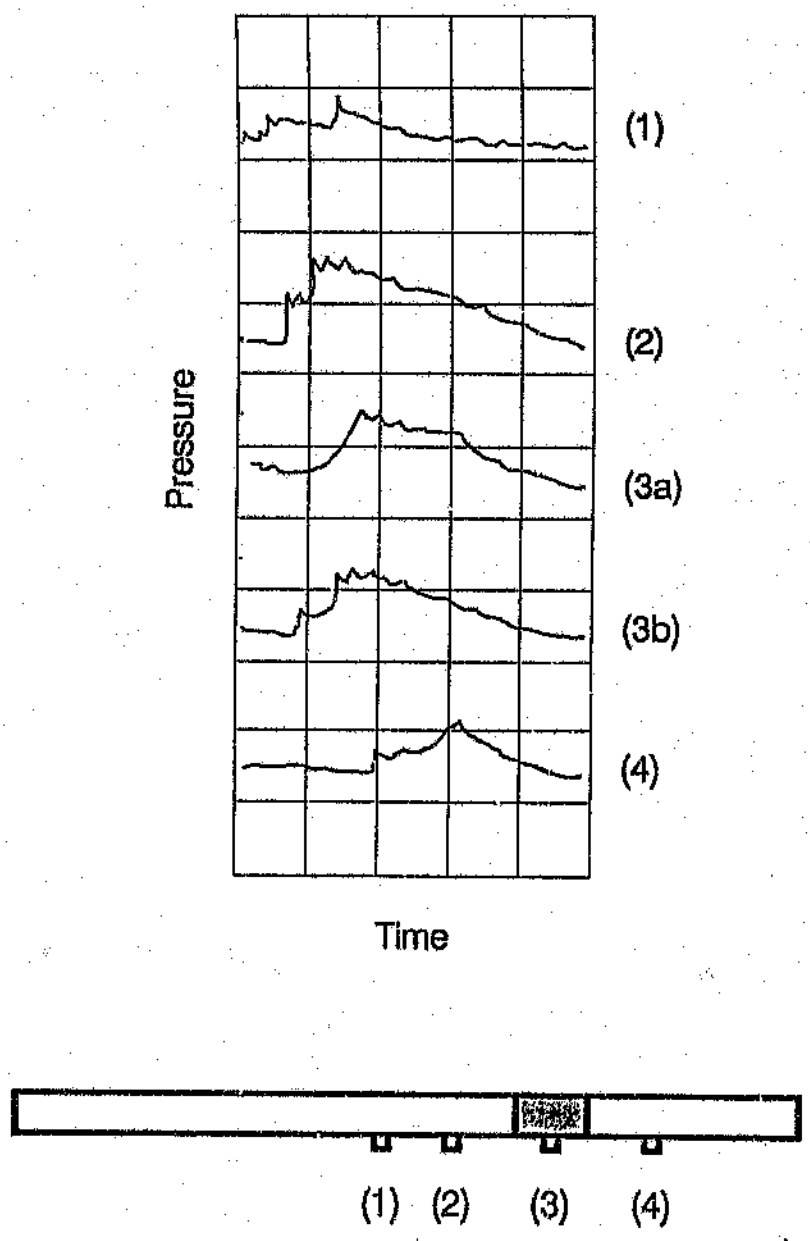


Figure 1.16 Pressure variation, polyurethane foam length 300 mm, incident shock wave strength $\delta_1 = 3.3$ [20]

The theoretical analysis was based upon the Rudinger [33] model in which the foam is treated as a pseudo-gas with an equivalent adiabatic exponent and acoustic velocity. A detailed analysis of this theoretical model is carried out in section 2.2. Gel'fand et al.[20] established that the Rundinger model adequately predicted the shock wave parameters in the polyurethane foam. But the model did not completely account for the damping of the reflected shock wave.

Gvozdeva and Faresov [22] in 1985 published an approximate analytic method for calculating the parameters for the propagation of steady shock waves in porous compressible media.

The analytical model is based on the elasticity of the porous material being determined by the pressure of the gas in the pores. Gvozdeva and Faresov[22] assumes that this is justified since for the polyurethane foams the compressive stress on the skeleton of the material at 40 percent deformation is $P_1 = (0.4 - 1.0) \times 10^4$ *Pa*, thus for gas pressures $P_1 \geq 10^5$ *Pa* in the pores, the elasticity of the skeleton can be neglected. The foams are modelled as a single phase collection of non-interacting solid particles suspended in a gas or as a liquid containing gas bubbles.

Gvozdeva and Faresov [22] develop a set of formulas to analyse how a steady shock wave in air is reflected by a rigid wall padded with polyurethane foam. The results are compared with previous experimental work carried out by other researchers. This comparison is shown in figure 1.17.

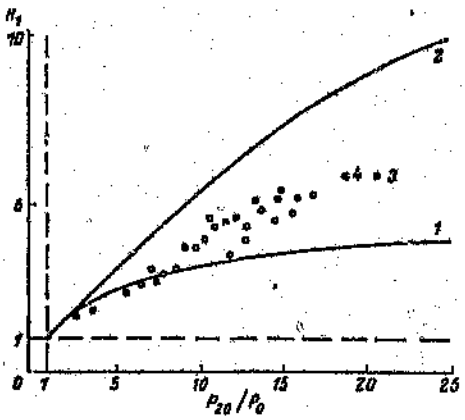


Figure 1.17 Variation of the coefficient of pressure increased at the wall, behind a block of polyurethane foam [22]

The coefficient of pressure increase at the wall R_1 is defined as $R_1 = P_{III}/P_{3O}$, where P_{III} is the peak pressure recorded on the rigid wall behind the foam, and P_{3O} is the pressure corresponding to normal reflection of an incident shock wave from a rigid wall. The analytic results are represented by curve (1) and (2). In curve (2) thermal equilibrium between the gas and foam phase has been assumed. The experimental results are represented by the circles. Curves (1) and (2) were calculated with the input conditions $P_1 = 10^5\ Pa$ foam porosity $\alpha = 0.975$ and density $\rho_I = 33\ kg/m^3$.

No comment can be made on the reliability of the model since the experimental data that the analytical curves are compared to are for foams of different densities and porosities.

Gvozdeva and Faresov from the Institute for High Temperatures, Moscow in collaboration with Brossard and Charpentier [23] from the University of Orleans, France, in 1986, published the results of an experimental study of the interaction of a plane shock wave in air and a rigid wall coated with flat layers of polyurethane and polystyrene.

The experiments were carried out on the two porous materials in a shock tube with a cross-section of 100 mm by 100 mm. The incident shock wave Mach number ranged from 1.1 to 2.7. Two piezoelectric pressure gauges were used to record the pressure variation. One gauge was mounted in the rigid wall at the end of the shock tube and the other 133 mm from the end of the shock tube on the side wall. Thus depending on the length of the material tested the gauge may record the pressure in front of or alongside the foam. The length of the polystyrene (density $\rho = 26\ kg/m^3$) was varied between 18 mm and 54 mm. The length of the polyurethane foam (density $\rho = 23.5\ kg/m^3$)) was varied between 65 mm and 185 mm. It must be noted that a 1 mm gap was left between the material and the walls of the shock tube, this was done to avoid friction.

Figure 1.18 show the oscilloscope records that Gvozdeva et al. [23] published. The upper trace in each set of oscillograms is the pressure variation behind the porous material and the lower trace is the side wall pressure variation. The left set of traces is the pressure variation for the polystyrene, the incident Mach number ranging from 1.7 to 1.8. The x-axis scale is 200 μs/division, no y-axis scale was given. The length of the polystyrene was (1a) 0 mm, (2a) 18 mm, (3a) 36 mm and (4a) 54 mm. The set of pressure traces on the right are for the polyurethane foam, the incident Mach number ranging from 1.8 to 1.9. The x-axis scale is 500 μs/division, no y-axis scale was given. The length of the polyurethane was (1b) 0 mm, (2b) 65 mm, (3b) 130 mm and (4b) 185 mm.

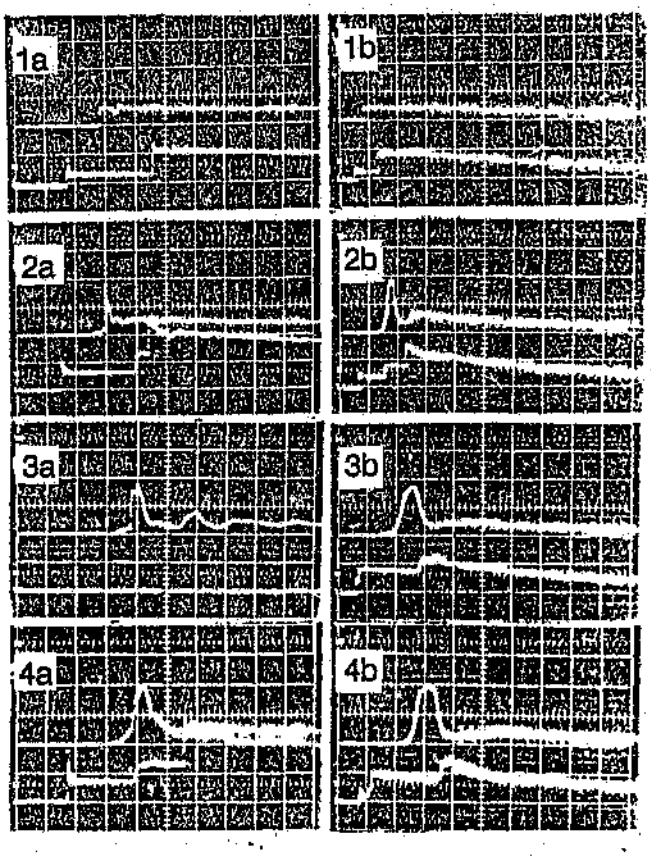


Figure 1.18 Oscillogram records, upper trace : pressure behind the porous material, lower trace : pressure on the lateral wall left side : polystyrene, length (1a) 0 mm (2a) 18 mm (3a) 36 mm (4a) 54 mm, right side : polyurethane , length (1b) 0 mm (2b) 65 mm (3b) 130 mm (4b) 185 mm [23]

Analysing the pressure variation behind the polystyrene, Gvozdeva et al.[23] divides the pressure rise into two parts, the first increase they attribute to a small precursor elastic wave that propagates through the skeleton of the material. The second she does not comment on. The pressure then peaks and reduces to approximately the value of the pressure for normal solid wall reflection (trace (1a)) after a number of oscillations. Gvozdeva et al. [23] state that the number of oscillations required to stabilize the pressure behind the polystyrene is proportional to the length of the material.

The dependence of the coefficient of pressure increase at the wall $R_1 = P_{III}/P_{3O}$ on the incident Mach number is shown in figure 1.19. P_{III} is the peak pressure recorded on the rigid wall behind the foam, P_{3O} is the pressure corresponding to normal reflection of an incident shock wave from a rigid wall. The test material was 130 mm of polyurethane foam.

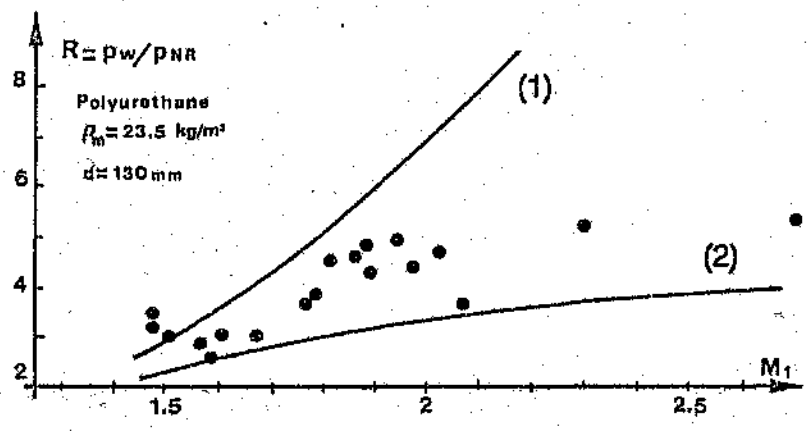


Figure 1.19 Variation of the coefficient of pressure increased at the wall, behind a 130 mm block of polyurethane foam [23]

Curves (1) and (2) are the predicted curves based on the model described in Gvozdeva et al's. [23] previous paper where the mixture of the two phases (gas and foam) is considered to be (1) isothermal and (2) adiabatic.

The dependence of the coefficient of pressure increase R_1 on the incident Mach number and length for polystyrene is shown in figure 1.20. The scatter in the data is too large to determine any relationship between the length of the polystyrene and the coefficient of pressure increase R_1.

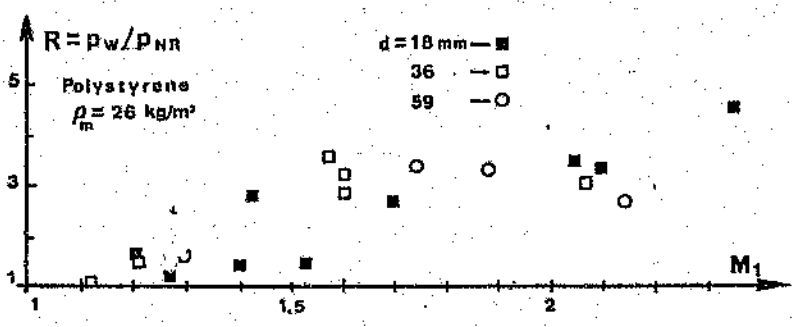


Figure 1.20 Variation of the coefficient of pressure increased at the wall, behind various thickness of polystyrene foam [23]

Gvozdeva et al. [23] carried out some experiments to determine the effect of a density gradient in the polyurethane foam on the various shock wave reflection parameters. Figure 1.21 shows the oscillograms obtained with a positive density gradient (a) and a negative gradient (b). The positive gradient was obtained by placing two layers of polyurethane foam next to each other, the first 65 mm in length having a density of $\rho = 23.5\ kg/m^3$ and the second 40 mm in length having a density of $\rho = 198\ kg/m^3$. The negative gradient was obtained by reversing the order of the foams.

The negative gradient has the effect of reducing the peak pressure behind the foam and increasing the duration of the pressure signal.

Gvozdeva et al. [23] concludes by saying the amplification of the reflected pressure behind the porous material is strongly dependent on the mechanical properties of the material, the thickness of the compressible material, the gradient of the densities of the material and the Mach number of the incident shock wave.

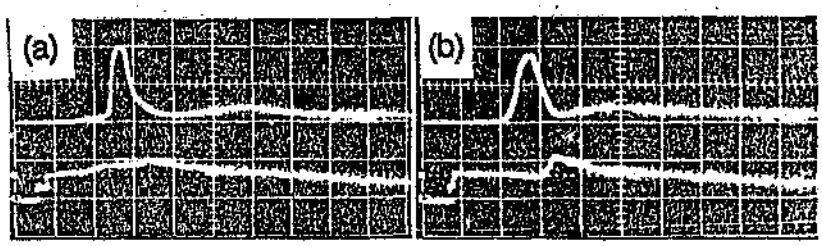


Figure 1.21 Oscillogram records, upper trace : pressure behind the porous material, lower trace : pressure on the lateral wall, left side : polyurethane foam , M_i = 1.9, positive density gradient, right side : polyurethane foam M_i = 1.5, negative density gradient [23]

In 1987 Gvozdeva et al.[24] published another paper that examined the shock wave propagation in a gas and a porous medium. The results of a numerical and experimental investigation were presented.

The numerical model is based on the assumption that the porous medium is a single velocity continuum or "quasigas". That is, the elasticity of the skeleton of the foam is ignored. The system of non steady equations for the motion of the foam is solved using the shock - smearing approach, with the McCormick finite difference scheme. The calculation array used had 100 points 50 of which initially belonged to the foam.

The experiments were carried out in a shock tube having a cross- section of 100 mm by 100 mm. The elastic polyurethane foam test specimens were varied in length from 50 mm to 100 mm. No gap was left between the wall of the shock tube and the foam material. Two piezoelectric sensors were used to record the pressure variation in front of and behind the foam. The latter was mounted 0.2 mm from the back plate of the shock tube , on the side wall.

The experimental and numerical results are shown in figure 1.22. The foam test specimen had a length of 80 mm, a density of $\rho = 38.6\ kg/m^3$, and a porosity of $\alpha = 0.975$. The incident shock wave Mach number was 1.7. Curve (1) is the pressure variation from a piezoelectric sensor located 200 mm from the back of the shock tube. Curve (3) is the pressure measured behind the foam. Curves (2) and (4) are the corresponding theoretical

curves. $P_{2O} = P_2/P_O$ is the normal reflection pressure of an air shock wave from a solid wall without a porous material coating.

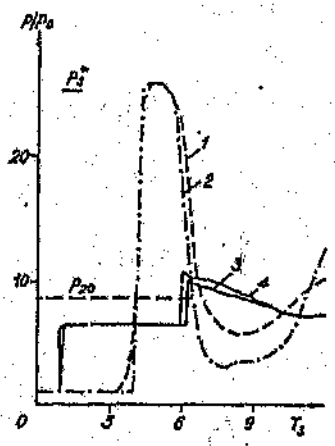


Figure 1.22 Theoretical and experimental pressure profiles , (1) and (3) experimental, (2) and (4) theoretical [24]

Gvozdeva et al. [24] states that the comparison indicates satisfactory qualitative and quantitative description of the dynamic deformation of a layer of real porous material using the given model. However the numerical and experimental pressure profiles at the wall under the layer of porous material is in good agreement only up until time Ts = 6, which Gvozdeva et al. concludes indicates the need for further refinement of the calculation model.

At the 17 th International Symposium on Shock Tubes and Waves, 1989 Frolov et al. [16] presented a simple approximate analytical theory to predict the rate of decay of a planar shock wave travelling through a gaseous medium blocked by barriers and screens. By considering the evolution of a planar stepwise shock wave after its entry into a permeable screen located in section $(x_2 - x_1)$ and making the following assumptions;

- the flow is uni-dimensional
- the gas obeys the perfect gas law

- heat transfer is neglected
- the shock wave velocity is independent of the conditions behind it , and depends only on the confinement geometry, distance travelled by the shock wave through the blocked space and its initial Mach number.

Frolov et al. [16] developed the equation

$$G(M_O, \gamma) - G(M_1, \gamma) = f(x_2 - x_1)/2 \qquad (1.1)$$

where $G(M_O, \gamma) - G(M_1, \gamma) = \int_{M_1}^{M_O} \Phi(M, \gamma)\, dx$

The integral is evaluated numerically using the Simpson technique. The parameter f was determined for various permeable screens

Granular Solid material

$$f = \frac{3.5\,(1-\varepsilon)}{\varepsilon\, d_p} \qquad (1.2)$$

where ε is the porosity
d_p is the particle diameter

Air dust suspension

$$f = \frac{0.63\, n_p}{\rho p\, d_p} \qquad (1.3)$$

where n_p is the mass concentration of particles
ρp is the density

Lattices and porous packings

$$f = \frac{(1-\alpha)}{S} \qquad (1.4)$$

where S is the layer spacing
α is the porosity

Rough tubes

$$f = \lambda \qquad (1.5)$$

where λ is the hydraulic drag coefficient.

Experimental data on shock wave attenuation in beds of granular solid material, gas-solid suspension, gauzes, porous packings, rough tubes etc were used to verify the theory.

Frolov et al. [16] concluded that the theory may be used for applications in engineering practice, but it must be used with some reserve for working out optimal safety measures.

At the 17 th International Symposium on Shock Tubes and Waves, 1989 Henderson et al. [27] presented the results of their experiments with shock waves passing from nitrogen gas into polyurethane foam plastics.

The speed of sound in the foam was determined experimentally using two techniques. Firstly the speed of a pressure disturbance was measured. The results were plotted, and extrapolated to zero pressure to infer the speed of sound. The second method was to measure the mechanical properties, Young's modulus and Poisson's ratio of the foam and then to calculate the speed of sound. Both methods gave the speed of sound in the foam as 139 *m/s* .

In the initial abstract for the conference Henderson et al. [27] stated that they were measuring the movement of the foam/nitrogen interface using an array of thirty optical fibres feeding light sensitive diodes. From this they intended to calculate the velocity of the interface and compare it to the gas velocity at the interface and thereby determine whether the gas was penetrating the foam or not. However in the conference paper no mention was made of this portion of the experiment.

Korobeinikov [28] in 1989 published a book titled Unsteady Interaction of Shock and Detonation Waves in Gases, in which he devoted a chapter to the interaction of shock waves with porous compressible medium. The chapter was written by Faresov and is a systematic presentation of the experimental and theoretical work in this field undertaken by Russian researchers. The papers on porous polyurethane foam used to write the chapter have previously been reviewed in this section.

At the 12 th International Colloquium on Dynamics of Explosions and Reactive Systems, 1389 Rayevsky et al. [32] from the Institute of High Temperatures of the Academy of Sciences of the USSR and Brossard et al. from the University of Orleans, France presented a paper on the numerical

and experimental study of shock and blast wave reflection from solid surfaces covered with layers of polyurethane foam.

The experiments were conducted in a square channel shock tube having a cross-section of 100 mm by 100 mm. Nitrogen or Helium was used as a driver gas and air as the working gas. The elastic polyurethane foam tested ranged in density from $\rho_f = 25\ kg/m^3$ to $\rho_f = 33\ kg/m^3$ and a porosity of $\alpha_f = 0.95 - 0.98$. Piezoelectric pressure gauges developed at the Institute of High Temperatures and PCB 113A24 transducers were used to record the pressure variation.

To produce a blast wave Rayevsky et al. [3.2] used the shock tube described above as a blast simulator. The foam attached to a solid back plate was placed 300 mm or 500 mm behind the open end of the shock tube. The shock tube back plate had a 20 mm diameter hole in the centre. This allowed blast pressure jumps of up to 3.0 to be produced.

The numerical model assumes the porous medium to be a one-fluid, two temperature continuum and by regarding the skeleton of the material as an aggregate of absolutely hard particles the following system of equations for conservation of mass, impulse and energy is developed.

$$\frac{\partial \rho}{\partial t} + \frac{\partial}{\partial x}(\rho u) = 0 \tag{1.6}$$

$$\frac{\partial \rho u}{\partial t} + \frac{\partial}{\partial x}((1-\alpha_f)\, b + \alpha\, p + \rho\, u^2) = 0 \tag{1.7}$$

$$\frac{\partial}{\partial t}\left[\rho\left(e + \frac{u^2}{2}\right)\right] + \frac{\partial}{\partial x}\left[\rho\, u\left(e + \frac{u^2}{2}\right) + ((1-\alpha)\, b + \alpha\, p)\, u\right] = Q \tag{1.8}$$

$$e = \frac{p\alpha}{p(\gamma - 1)} + e_s\,(\rho/\rho_f)\,(1-\alpha) \tag{1.9}$$

$$b = E\,(\rho/\rho_f) \tag{1.10}$$

where b is the force as a result of the material skeleton elasticity
e is the internal energy of the porous medium
e_s is the internal energy of the skeleton of the porous medium due to elasticity
E is Young's modulus
p is the pressure averaged over a unit volume
Q is the heat flux from the gaseous phase to the material skeleton
t is the current time

u is the averaged velocity over a unit volume
α is the porosity
γ is the ratio of specific heat of gas to the specific heat of the porous medium
ρ is the density averaged over a unit volume

The system of equations was solved using the second order McCormick "shock capturing " algorithm.

The results of the numerical and experimental investigation for the shock wave interaction with a polyurethane foam are shown in figure 1.23. The polyurethane foam had a density of $\rho_0 = 33.0\ kg/m^3$, a porosity of $\alpha_0 = 0.975$ and a length of $d = 100$ mm. The incident shock wave Mach number was 1,7 and the initial pressure in the shock tube $P_0 = 1$ bar. The numerical results are represented by solid lines and the experimental results by dotted lines. Curves (1) and (2) are the pressure variation on the back wall of the shock tube behind the porous material. P_n is the maximum pressure for solid wall reflection (no foam). Curves (3) and (4) are the pressure variation at the initial location of the front face of the foam. The nondimensional time scale is given by equation (1.11).

$$\tau = \frac{D_1 t}{d} \qquad (1.11)$$

where d is the length of the porous material
D_1 is the speed of the incident shock wave front
τ is the nondimensional time

Comparing the curves, there is good agreement between the numerical and experimental data up until the rarefaction wave is formed at the foam boundary ($\tau = 6$). Rayevsky et al. [32] stated that this discrepancy may be caused by the effect of non zero interface velocity.

Figure 1.24 shows the numerical and experimental variation of the coefficient of pressure increase at the wall (P_1/P_0) with incident Mach number (M_1) of a shock wave. The foam test specimen had a density of $\rho_f = 25\ kg/m^3$, a porosity of $\alpha_f = 0.98$ and a length of $d = 80$ mm. The solid curve represents the numerical simulation and the experimental points are shown as circles. The heat exchange between the gas phase and the skeleton of the porous medium is taken into account in the model represented by curve (1).

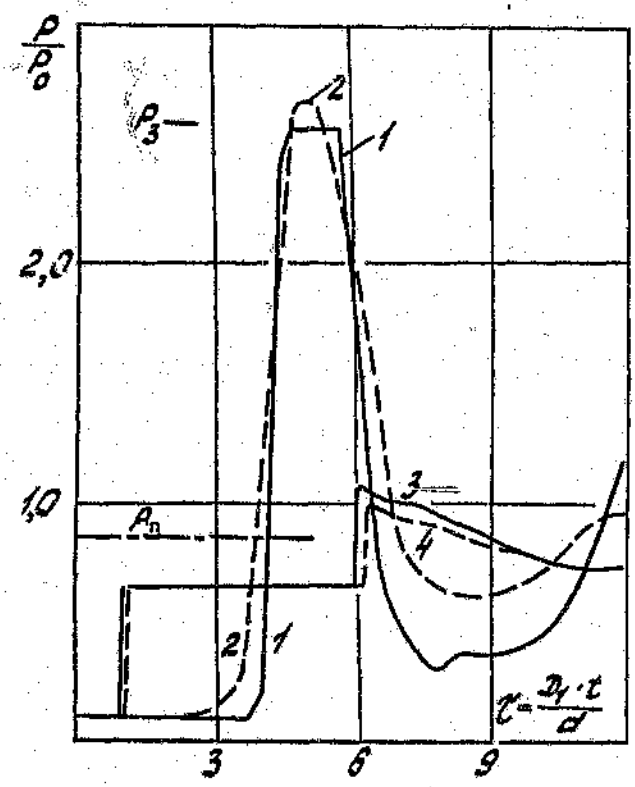


Figure 1.23 Experimental and numerical pressure time history of the end of the shock tube (1,2) and on the side wall (3,4)[32]

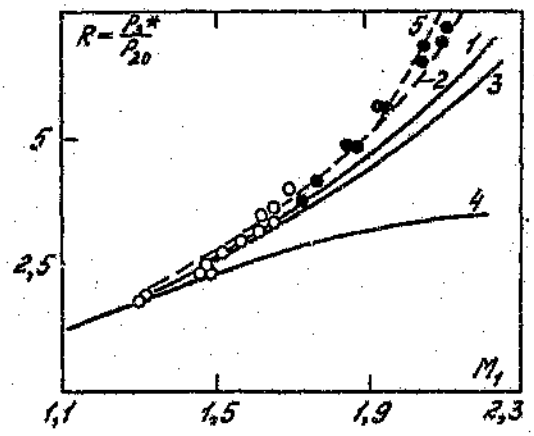


Figure 1.24 Variation of the coefficient of pressure increase at the rear shock tube wall covered by polyurethane foam : (1,3,5) - numerical simulation, (2,5) - experimental [32]

The previous models, firstly the model with the absence of heat exchange (adiabatic model - curve(4)) and secondly the model that assumed thermal equilibrium (equilibrium model - curve (3)) are shown for comparison.

It can be seen that even taking into account the interphase heat exchange the calculated value of R when $M_1 \geq 2,1$ is less than the corresponding experimental values.

The results of the numerical and experimental investigation for the blast wave interaction with a polyurethane foam are shown in figure 1.25. The polyurethane foam had a density of $\rho_f = 25.0\ kg/m^3$ and a length of $d = 50$. The incident shock wave Mach number at the end of the shock tube was 1.7 and the initial pressure $P_f = 1$ bar. The solid lines represent the experimental pressure variation and the dotted curve (2) represents the pressure variation obtained from the numerical model. Curve (1) is the pressure time history from a pressure transducer mounted in the solid plate behind the foam. Curve (3) is for the same transducer, but with no foam in front of it.

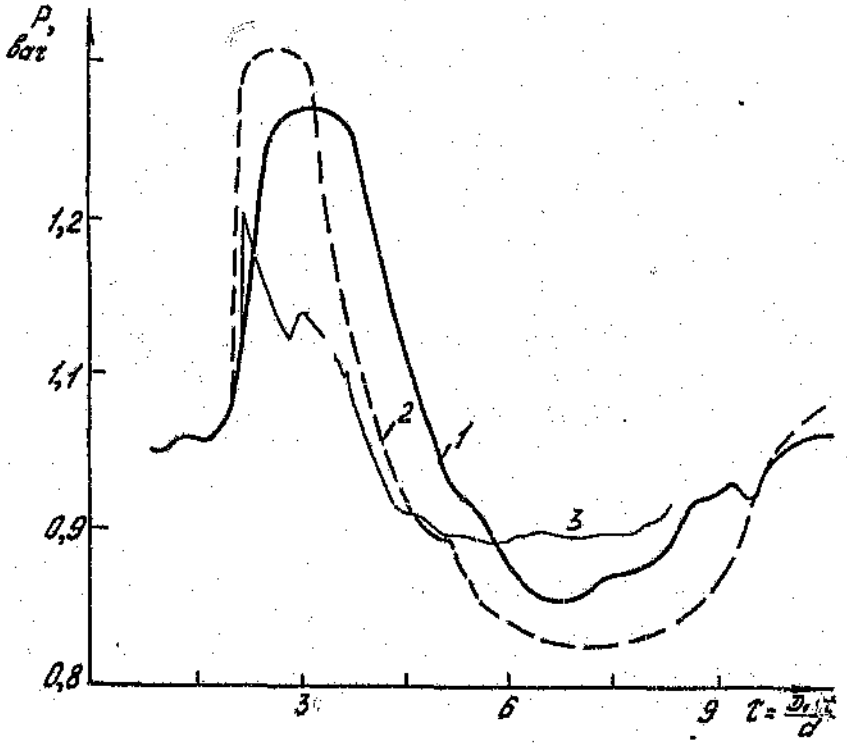


Figure 1.25 Experimental and numerical pressure time history of the solid plate covered with polyurethane foam after a weak blast wave reflection ; experimental - solid curve, computed - dotted curve [32]

Comparing curves (1) and (3) the presence of foam more than doubles the blast wave pressure on the solid wall.

Figure 1.26 shows the numerical and experimental variation of the coefficient of pressure increase at the wall (R) with incident Mach number (M_1) of a simulated blast wave. The solid curve represents the experimental values and the dotted curve the computed values.

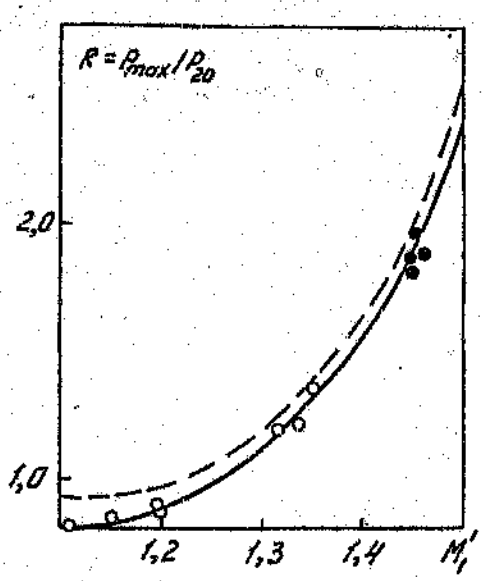


Figure 1.26 Variation of the coefficient of pressure increase at the rear shock tube wall covered by polyurethane foam, for blast wave reflection : solid curve - experimental data, dotted curve - computed data [32]

The presence of the foam on the solid plate does not cause any amplification of the back plate pressure with an incident blast wave number less than 1.2. Rayevsky et al. [32] stated that this effect was caused by two forces, firstly the reflection of the rarefaction wave from the boundary of the foam and secondly, inertia losses due to gas filtration from the foam.

1.3 Objectives

Determination and identification of all the waves present in the interaction of a shock wave and a porous compressible foam.

Explanation of the pressure amplification phenomena seen behind the foam.

Evaluation of various theoretical analyses that have been published and claim to predict the shock wave parameters during the interaction of a shock wave and a porous compressible foam.

2 Theoretical Analysis

Three different theoretical solutions to the interaction of a shock wave and a porous material are presented. The first is based on the analysis by Monti.[30] The second and third analyses are based on the work carried out by Gel'fand et al. [20] and Gvozdeva et al. [22] respectively.

The notation used in this section has been standardised for all the theoretical analyses. Thus the equations in the original papers may have different symbols. Figure 2.1 shows the definition of the subscripts used throughout this section.

where *S* is the incident shock wave
SR is the reflected shock wave
ST is the shock wave transmitted into the foam.

The different regions in the gas are numbered 1 to 3, while the regions in the foam are numbered I to III.

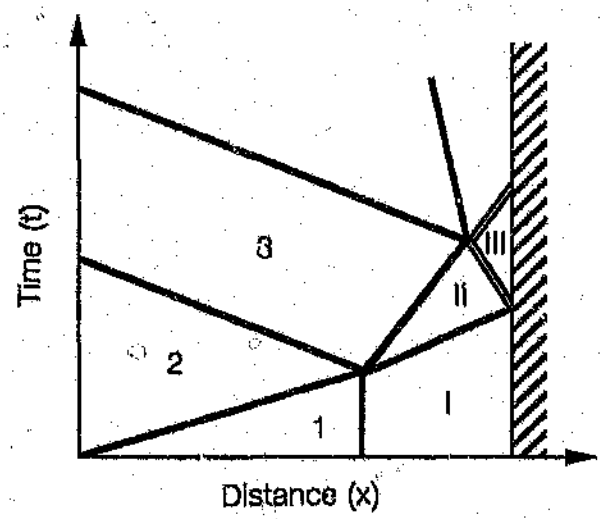


Figure 2.1 Shock wave interaction notation

2.1 Monti Analysis

Monti [30] developed a simple solution for the strength of the reflected and transmitted shock waves away from and into linear (Hooke Type) materials.

Starting with the Rankine Hugoniot equations which governing the propagation of normal, plane shock waves in continuous and isotropic media, one has the mass, momentum and energy equations (2.1) to (2.3). The subscripts 1 and 2 denote the conditions before and after the shock wave respectively.

$$\rho_1 V_S = \rho_2 (V_S - V_2) \tag{2.1}$$

$$P_{n1} + \rho_1 V_S^{\,2} = P_{n2} + \rho_2 (V_S - V_2)^2 \tag{2.2}$$

$$h_1 + \frac{V_S^{\,2}}{2} = h_2 + \frac{(V_S - V_2)^2}{2} \tag{2.3}$$

P_n is the stress in the medium normal to the shock wave front. For gases and liquids $P_n = P$, for solids $P_{n2} - P_{n1} = \sigma_x$, where x is the shock propagation direction. Thus equations (2.1) to (2.3) may be written as:

$$V_S = \frac{1}{\rho_1} \left[\frac{P_{n2} - P_{n1}}{v_1 - v_2}\right]^{1/2} \tag{2.4}$$

$$V_2 = [(P_{n2} - P_{n1}) (v_1 - v_2)]^{1/2} \tag{2.5}$$

$$h_2 - h_1 = \frac{1}{2} (P_{n2} - P_{n1}) (v_1 + v_2) \tag{2.6}$$

where v is the volume per unit mass.

For a perfect gas with constant heat capacity coefficients, one may write:

$$\frac{\rho 1}{\rho 2} = \frac{(1+n)P_1 + P_2}{P_1 + (1+n)P_2} \tag{2.7}$$

Where n is the number of internal degrees of freedom. ($n = 5$ for a biatomic gas)

Taking $M_S = \frac{V_S}{a_1}$, the conditions before and after the shock wave may be written as:

$$\frac{\rho 2}{\rho 1} = \frac{1+n}{1+\frac{n}{M_S{}^2}} \tag{2.8}$$

$$\frac{P_2}{P_1} = \frac{(2+n)M_S{}^2 - 1}{1+n} \tag{2.9}$$

$$\frac{V_2}{a_1} = \frac{n(M_S{}^2 - 1)}{(1+n)M_S} \tag{2.10}$$

Considering the one dimensional strain of the material, ($\eta y = 0$, $\eta z = 0$) one may write:

$$1 - \frac{v_2}{v_1} = 1 - \frac{L_2}{L_1} = \varepsilon x2 \tag{2.11}$$

where L denotes the length of a specimen of the solid material which varies as a function of the stress (σx). Defining an average stiffness modulus ($\pi 2$) by:

$$\sigma x2 = \varepsilon x2\, \pi 2 \tag{2.12}$$

Equations (2.4),(2.5) and (2.6) may be written in terms of $\pi 2$ as:

$$V_S = \left[\frac{\pi 2}{\rho 1}\right]^{1/2} \tag{2.13}$$

$$V_2 = \frac{\sigma x2}{\sqrt{\pi 2\,\rho 1}} = \varepsilon x2\, V_S \tag{2.14}$$

$$h_2 - h_1 = \sigma x2 \frac{V_1 + V_2}{2} = \frac{V_S^{\,2}}{2\rho_1} \varepsilon x2\,(2 - \varepsilon x2) \tag{2.15}$$

For the reflection of a weak shock wave from a material Monti [30] assumed the waves present were the ones shown in figure 2.2. *S* is the incident shock wave and *ST* and *SR* are the transmitted and reflected shock waves respectively. D represents the front face of the medium.

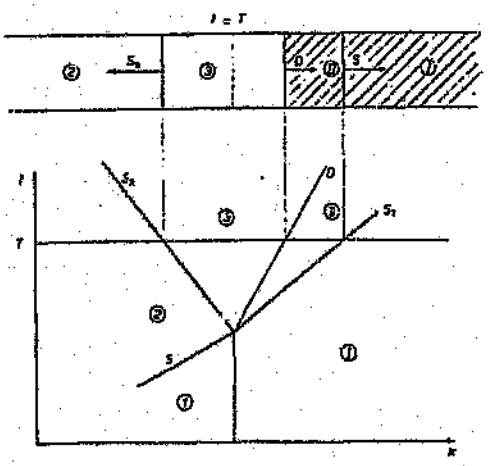


Figure 2.2 Shock wave motion as a function of time for a shock wave striking a discontinuity surface [30]

By assuming that no other waves are present, the velocity and pressure behind the reflected shock wave must be equal to the velocity and pressure behind the shock transmitted wave. That is:

$$P_3 = P_{nII} \tag{2.16}$$

$$V_3 = V_{II} \tag{2.17}$$

Monti [30] takes the Mach number (M) of the shock wave as a measure of its intensity (I):

$$M_S = \frac{|V_S|}{a_1} \equiv I_S \tag{2.18}$$

$$M_{SR} = \frac{|V_{SR}|}{a_2} \equiv I_R \tag{2.19}$$

The intensity of the transmitted shock wave may thus be written as:

$$\frac{P_{nII}}{P_{nI}} = \frac{P_{nII}}{P_1} \equiv I_T \tag{2.20}$$

The pressure P_3 behind the reflected shock wave may be written as:

$$P_3 = P_1 \left(\frac{P_2}{P_1}\right)\left(\frac{P_3}{P_2}\right)$$

$$P_3 = P_1 \frac{(2+n)\,M_S{}^2 - 1}{(1+n)} \frac{(2+n)\,M_{SR}{}^2 - 1}{(1+n)} \tag{2.21}$$

Note: equation (2.21) is incorrectly shown in Monti's [30] publication.

Similarly the gas velocity behind the reflected shock SR can be written as:

$$V_3 = V_2 - \left|\,\Delta V_R\,\right| = a_1 \left[\frac{V_2}{a_1} - \frac{a_2}{a_1}\frac{|\,\Delta V_R\,|}{a_2}\right] \tag{2.22}$$

ΔV_R is the velocity "induced" by the reflected shock wave as a function of M_S and M_{SR}, equation (2.22) becomes:

$$V_3 = \frac{n}{n+1} a_1 \left[\frac{M_2{}^2 - 1}{M_S} - \right.$$

$$\left. \frac{M_{SR}{}^2 - 1}{M_{SR}} \frac{\left[(n + M_S{}^2) \left[(2+n) M_S{}^2 - 1 \right] \right]^{1/2}}{(1+n) M_S} \right] \quad (2.23)$$

The pressure P_{nII} and the velocity V_{II} may be written in terms of the transmitted shock intensity (I_T), by assuming one dimensional strain as done in equations (2.13) to (2.15), as:

$$P_{nII} = P_1 \frac{P_{nII}}{P_{nI}} \quad (2.24)$$

$$V_{II} = P_2 \frac{\frac{P_{nII}}{P_{nI}} - 1}{\sqrt{\rho_I \pi_{II}}} \quad (2.25)$$

Substituting equations (2.21), (2.23), (2.24) and (2.25) into (2.16) and (2.17) yields:

$$\frac{n}{1+n} \left[\frac{M_S{}^2 - 1}{M_S} - B \frac{M_{SR}{}^2 - 1}{M_{SR}} \right] =$$

$$M \left[\frac{(2+n) M_S{}^2 - 1}{(1+n)} \frac{(2+n) M_{SR}{}^2 - 1}{(1+n)} - 1 \right] \quad (2.26)$$

where

$$B = \frac{\left[(n + M_S{}^2) \left[(2+n) M_S{}^2 - 1 \right] \right]^{1/2}}{(1+n) M_S} \quad (2.27)$$

$$m = \frac{P_1}{a_1} \frac{1}{\sqrt{\rho_I \pi_{II}}} \quad (2.28)$$

m is the material deformation parameter. For an elastic solid m is:

$$m = \frac{\rho_1}{\rho I} \frac{a_1}{V_S \gamma} \tag{2.29}$$

where

$$\gamma = 1 + \frac{2}{n} \tag{2.30}$$

Given a force - deformation curve for a foam material in one dimensional stress conditions Monti [30] defines an average stiffness modulus as:

$$\Theta = \frac{f_{xII}}{\epsilon_{xII}} \tag{2.31}$$

where f_x is the force per unit area

Using Θ, the material deformation parameter may be written as:

$$m = \frac{P_1}{a_1} \frac{1}{\sqrt{\rho I \, \Theta II}} \tag{2.32}$$

Rearranging equation (2.26) in terms of M_{SR} one obtains:

$$A\, M_{SR}^{\,3} + B\, M_{SR}^{\,2} + C\, M_{SR} + D = 0 \tag{2.33}$$

where

$$A = m \frac{2 + n}{n} \frac{(2 + n)\, M_S^{\,2} - 1}{1 + n} \tag{2.34}$$

$$B = - D \tag{2.35}$$

$$C = - \left[\frac{M_S^{\,2} - 1}{M_S} + \frac{m}{n} \left[(1 + n) + \frac{(2 + n)\, M_S^{\,2} - 1}{(1 + n)} \right] \right] \tag{2.36}$$

Thus having a force - deflection curve for the porous material and knowing the initial conditions of the incident shock wave, it is possible to calculate the strength of the reflected and transmitted shock waves into and away from the porous material.

2.2 Gel'fand et al Analysis

Gel'fand [20] developed a set of equations to predict the strength of the reflected shock wave originating from the interaction of a shock wave and a porous medium.

The analysis was based upon the model developed by Rudinger [30] In which he assumed that a two phase medium could be regarded as a pseudogas with an equivalent adiabatic exponent (Γ) and a speed of sound (a_f). Gel'fand applied this assumption to porous media. The adiabatic exponent and speed of sound for the porous media is given by equations (2.37) and (2.38) respectively

$$\Gamma = \frac{\gamma\,(1 + \eta\,\delta)}{1 + \gamma\,\eta\,\delta} \tag{2.37}$$

$$a_f = \left[- \frac{\Gamma\, a_1{}^2}{\gamma\,(1+\eta)\,(1-e_0)^2} \right]^{1/2} \tag{2.38}$$

where

$$\delta = \frac{c_f}{c_1} \tag{2.39}$$

$$\eta = \frac{\rho_f}{\rho_1} \tag{2.40}$$

where c is the specific heat capacity (J/kg)

e_0 is the volume fraction of foam in the porous sample (kg/m^3)

Gel'fand determined the Mach number of the transmitted shock wave using equation (2.41)

$$M_{ST} = \left[\frac{\frac{P_3}{P_1}(\Gamma + 1) + (\Gamma - 1)}{2\Gamma} \right]^{1/2} \tag{2.41}$$

By assuming that the pressures and velocities across the gas - foam interface were equal, Gel'fand derived equations (2.42) to (2.44)

$$P_2 - P_1 = \rho_1 V_S u_2 \tag{2.42}$$

$$P_3 - P_2 = \rho_2 (V_{SR} + u_2) (u_3 - u_2) \tag{2.43}$$

$$P_3 - P_1 = \rho_I V_{ST} u_3 \tag{2.44}$$

Equations (2.45) to (2.48) are derived from the Rankine Hugoniot equations ((2.1) to (2.3)) and relate the conditions before and after the normal shock waves.

$$P_2 = P_1 [\frac{(2 + n) M_S^{\,2} - 1}{1 + n}] \tag{2.45}$$

$$P_3 = P_2 [\frac{(2 + n) M_{SR}^{\,2} - 1}{1 + n}] \tag{2.46}$$

$$\rho_2 = \rho_1 [\frac{1 + \mu \frac{P_1}{P_2}}{\mu + \frac{P_1}{P_2}}] \tag{2.47}$$

The speed of sound in region 2 is calculated using equation (2.48).

$$a_2 = (\frac{\gamma P_2}{\rho_2})^{1/2} \tag{2.48}$$

The velocities of the incident (S), reflected (SR) and transmitted (ST) shock waves are given by:

$$V_S = M_S a_1 \tag{2.49}$$

$$V_{SR} = M_{SR} a_2 - u_2 \tag{2.50}$$

$$V_{ST} = M_{ST} a_I \tag{2.51}$$

Combining equations (2.43) and (2.50) equation (2.52) is obtained.

$$P_3 - P_2 - \rho_2 M_{SR} a_2 (u_3 - u_2) = 0 \qquad (2.52)$$

Substituting u_3 (2.44), u_2 (2.42), a_2 (2.48), ρ_2 (2.47), P_3 (2.46) and P_2(2.45) into equation (2.52), an equation is obtained in terms of M_{SR} and the incident shock wave parameters. This equation may be numerically solved to obtain the reflected shock wave Mach number.

2.3 Gvozdeva et al Analysis

Gvozdeva et al. [22] developed an analytic method for calculating the shock wave parameters in a porous medium, after a shock wave has struck the front face. The shock wave parameters include the strength and velocity of the transmitted shock wave and the maximum pressure on the solid wall behind the foam. In the work published by Korobeinikov [28] the equations were rederived in greater detail. Errors have been found in both papers.

The analytic solution is based on the assumption that the elasticity of the porous medium is only dependent on the pressure of the gas in the pores. The speed of sound in the porous medium is calculated assuming that the gas in the pores is adiabatically compressed.

$$a_f = \left[\frac{a_1}{\alpha (1 - \alpha) \frac{\rho_{of}}{\rho_1}} \right]^{1/2} \qquad (2.53)$$

where α is the volume fraction of air in the foam (porosity coefficient)
ρ_{of} is the density of the solid material in the foam

Simultaneously solving equations (2.1), (2.2) and (2.3) the expression for the Rankine Hugoniot curve is obtained.

$$U_1 - U_2 = \left(\frac{P_2 + P_1}{2} \right) \left(\frac{1}{\rho_1} - \frac{1}{\rho_2} \right) \qquad (2.54)$$

Assuming there is no heat exchange between the gas and the foam phases, the internal energy of the foam is equal to the internal energy of the gas inside the foam pores.

$$U = \frac{1}{\gamma - 1} \frac{P \alpha}{\rho} \qquad (2.55)$$

Neglecting the compressibility of the solid foam phase, the porosity coefficients before and after the shock wave are related by:

$$\alpha_{II} = 1 - (1 - \alpha_I)\frac{\rho_{II}}{\rho_I} \tag{2.56}$$

Substituting the internal energy of the material before and after the shock wave (2.55) and the porosity coefficients (2.56) into equation (2.54), one obtains.

$$\frac{\rho_{II}}{\rho_I} = \frac{\frac{P_{II}}{P_I}(\gamma + 1) + (\gamma - 1)}{\frac{P_{II}}{P_I}(\gamma + 1 - 2\alpha_I) + (2\alpha_1 + \gamma - 1)} \tag{2.57}$$

Equation (2.57) is used to determine an expression for the velocity of the shock wave travelling in the foam (V_{ST})

$$V_{ST} = \left[\frac{P_I}{\rho_I}\left(\frac{P_{II}}{P_I} - 1\right)\frac{\rho_{II}}{\rho_{II} - \rho_I}\right]^{1/2} \tag{2.58}$$

The transmitted shock wave Mach number is given by:

$$M_{ST} = \frac{V_{ST}}{a_I} \tag{2.59}$$

Using the balance of momentum equation for the incident and reflected shock waves, equation (2.60) is obtained

$$P_{III} = \frac{(3\gamma - 1)\frac{P_{II}}{P_I} - (\gamma - 1)}{(\gamma - 1)\frac{P_{II}}{P_I} + (\gamma + 1)} \tag{2.60}$$

Knowing M_{SR}, assuming $P_3 = P_{II}$ and substituting equations (2.45), (2.46), (2.58) and (2.57) into (2.60) the Mach number of the transmitted shock wave may be calculated.

3 Experimental Facilities

3.1 Shock Tube

The shock tube used is the one originally designed by Skews [37] in 1965. The shock tube consists of a compression chamber, expansion chamber and test section. The compression chamber is separated from the expansion chamber by two diaphragms. The various components are shown in figure 3.1

A shock wave is produced by pressurizing the compression chamber to a pressure above that in the expansion chamber and bursting the diaphragm. The shock wave travails down the expansion chamber and into the test section at supersonic velocity. By evacuating the test section and expansion chamber it is possible to produce a shock wave traveling at speeds up to Mach 5.

The compression chamber is 2 m in length and the expansion chamber 5 m long. There are two diaphragm holders, the first was the only one used in the current experimentation. The test section is located in a glass window housing. The window housing is enclosed by two circular plate glass windows.

Extensive modifications were made to enlarge and modernize the shock tube, the primary reason being to increase the internal cross section from 76.2 mm by 50.8 mm to 76.2 mm by 76.2 mm. To do this the entire tube after the second diaphragm had to be rebuilt.

3.1.1 Expansion Chamber

The internal cross-section of the compression and expansion chamber is round. This is changed to square via a round to square transition piece. A new round to square section was manufactured to accommodate the larger internal cross-section.

Due to the nature of shock wave flow it is imperative that the inside of the tube be as smooth as economically possible. Thus a large proportion of the machining and drilling was done using a N-C machine.

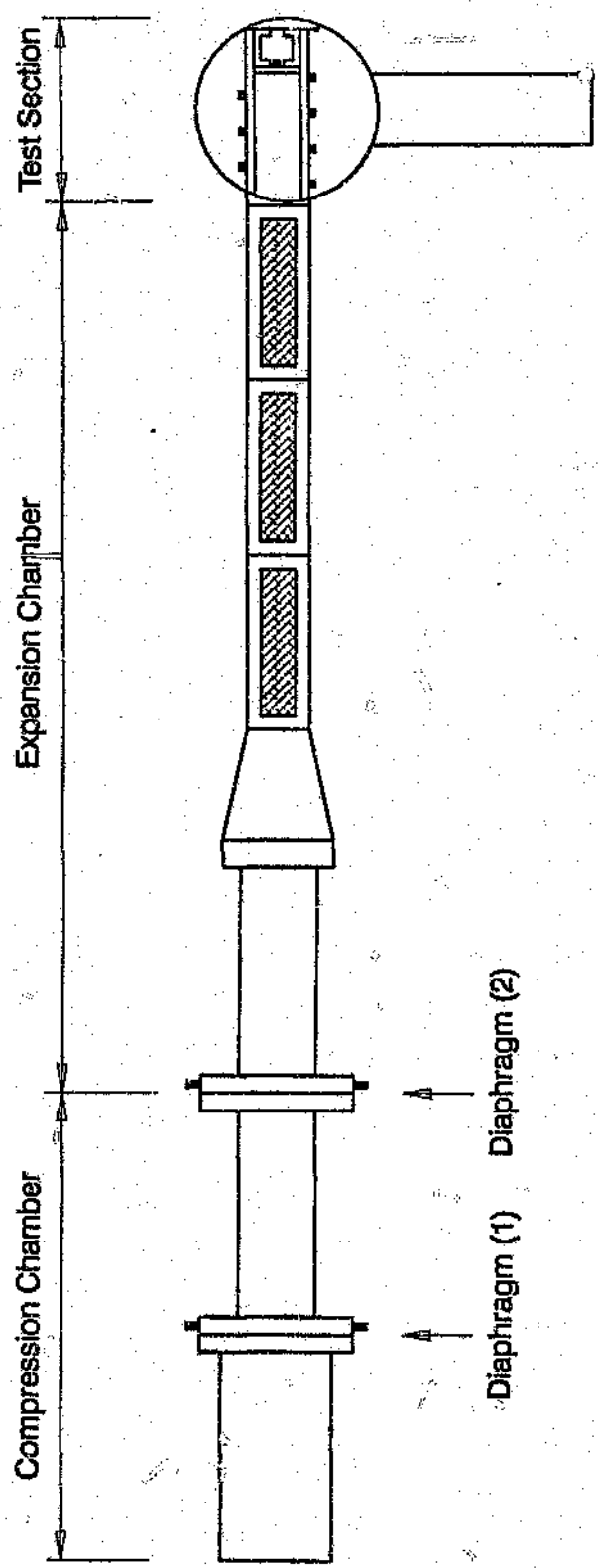


Figure 3.1 Shock tube

The square tube consists of three sections of four flat plates bolted together, part of a section is shown in figure 3.2. The original tube had an internal cross-section of 3" by 2", thus only two sides of the square section had to be manufactured. It must be noted that the original tube was manufactured using imperial units.

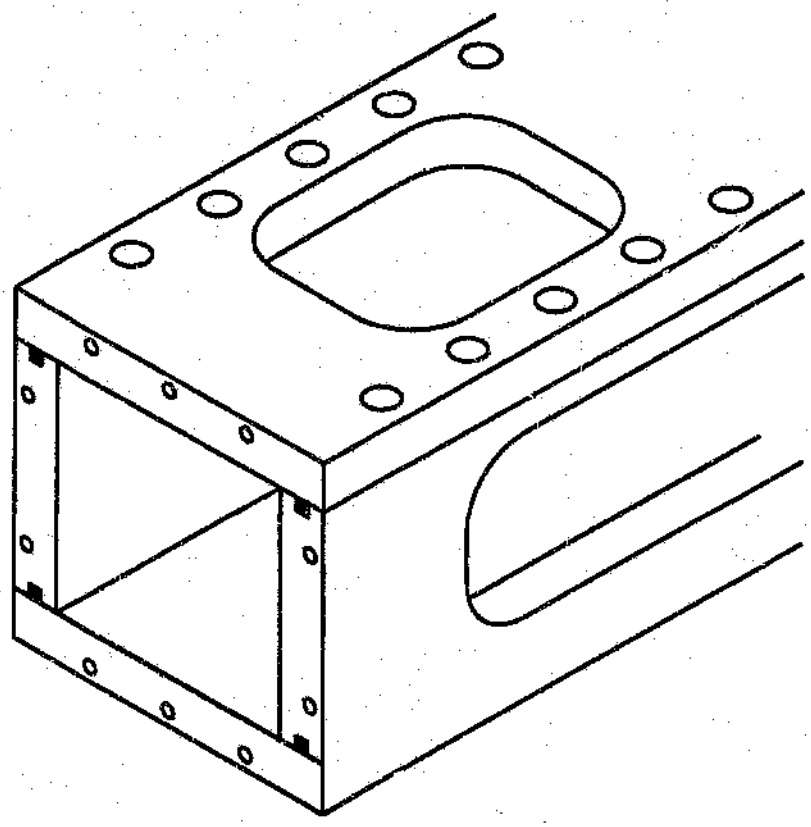


Figure 3.2 Square tube

The original square tube sections were held together by metal pins and bolts. The primary function of the pins was to ensure that when the plates were assembled that they were at right angles to one another.

When the original tube was manufactured the adjoining sections were clamped together and then the holes for the pins drilled. The accuracy between holes may not have seemed important at the time. But now that a new side had to be made to get the required accuracy for the pins to serve their function, each hole would have to be measured, aligned and drilled individually. Considering that there are approximately 240 holes and that this would preclude the use of the N-C machine, thus increasing the manufacturing time ten fold. It was decided to replace the pins with bolts.

Moving to a metric bolt and increasing the size of the bolt, the imperial bolt holes as well as the pin holes were retapped. For the bolts a larger tolerance between holes, as compared with the pin holes could be allowed, thus the plate could be manufactured using the N-C machine.

However there was nothing to ensure that the flat plates would be assembled correctly. Figure 3.3 shows the square block template of which two were manufactured. The block corresponds to the size of the tube. By placing one template at each end of the square tube and tightening the bolts in a sequence as not to incorrectly stress the bolts, the square tube was assembled with each side 90 degrees to the adjacent one. To remove the square template the hammer handle was used to force the template out of the tube.

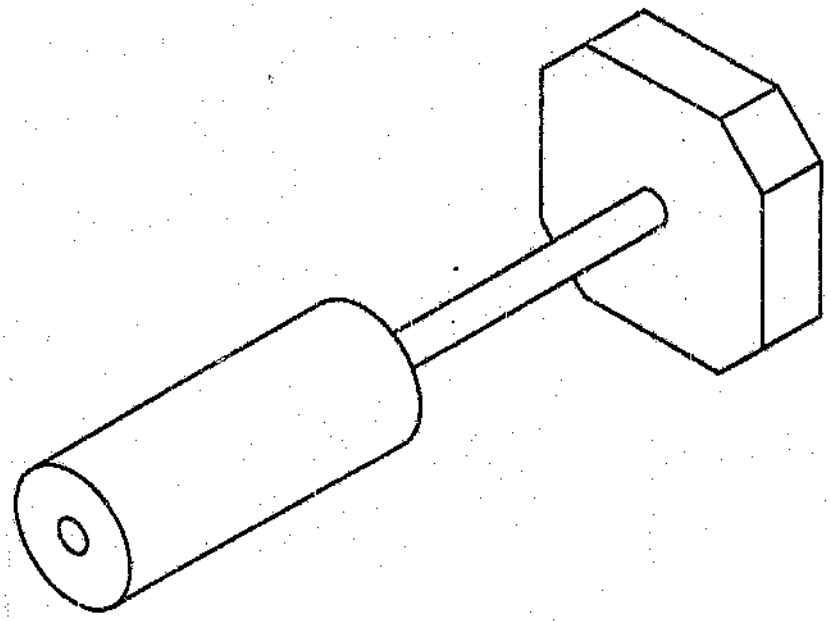


Figure 3.3 Square block template

The square section is sealed by four seals which run down its length, housed in the vertical sides. Two transducers were mounted in the square tube to record the time it took a wave to travel between them and hence accurately calculate the incident and reflected shock wave Mach number.

Between each square section and adjoining components a flange is located. The flange (figure 3.4) has a seal on each side circling the square cross-section. Thus as the components of the tube are bolted together the flanges seal the butting sections.

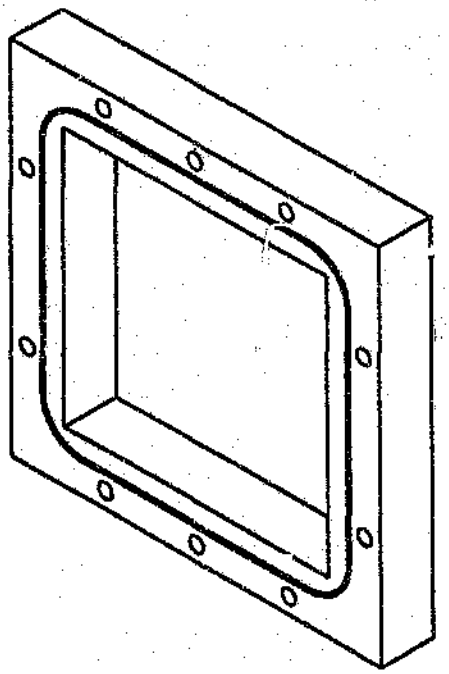


Figure 3.4 Sealing flange

3.1.2 Test Section

The original housing for the test section had been designed in such a way as to allow different shaped test sections to be inserted into the glass window housing. It was possible to enlarge the opening in the glass window housing and thus accommodate the larger tube cross-section.

The new test section is shown in figure 3.5. The original test section was manufactured from one block of material. To reduce manufacturing costs the test section was made in three parts, the circular face and the two flat plates. The flat plates were welded onto the circular face and the face then machined.

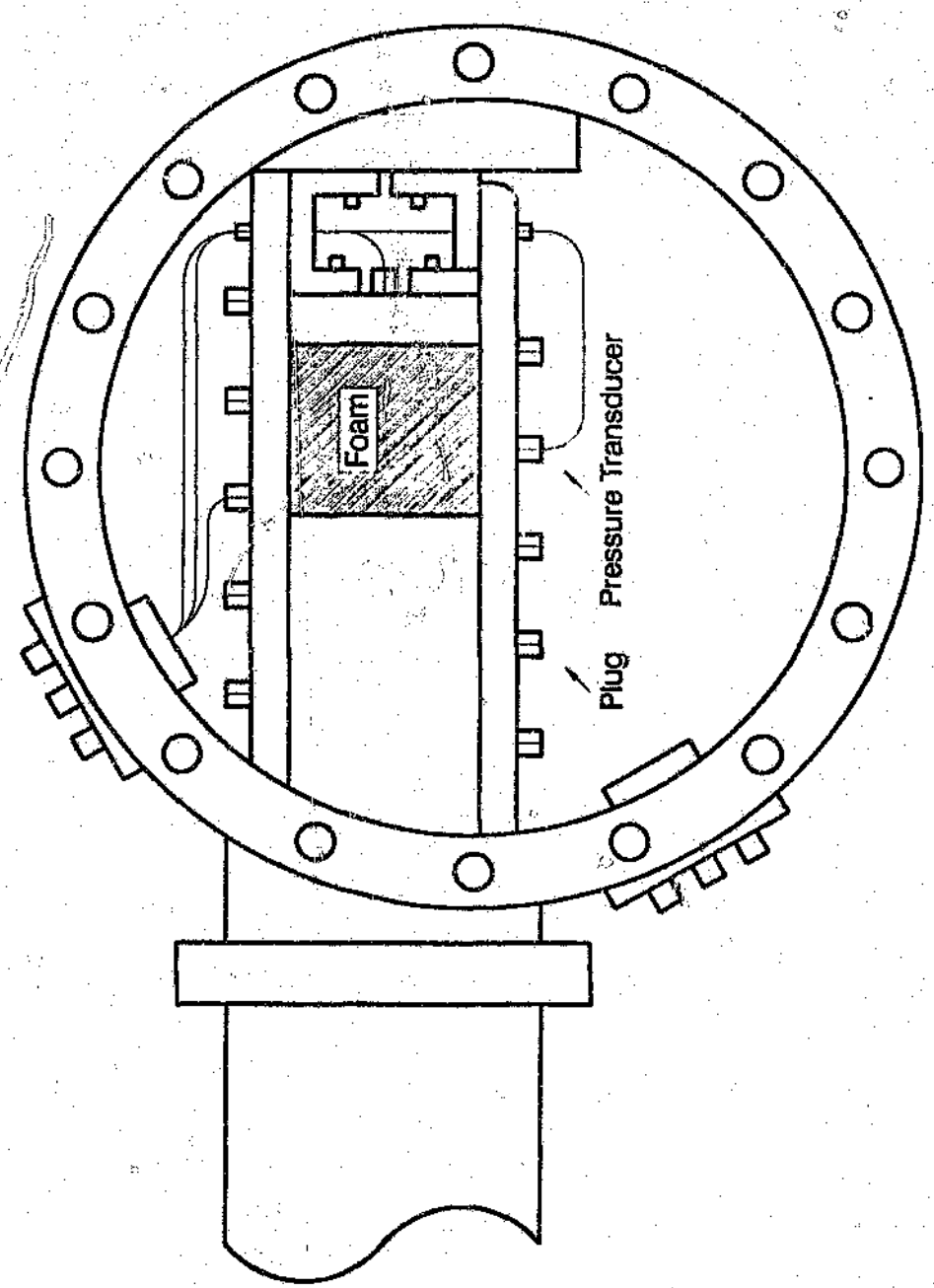


Figure 3.5 Test section

A seal located on the circumference of the circ.. face seals the test section.

Along the top and bottom of the test section are mounting positions for the transducers. In total there are nine, positioned 20 mm apart. Brass bolts were manufactured, to close the mounting positions which were not in use.

During the first few tests runs with the new test section, the parallel plates began to open. It was clear that they had to be secured to the rear of the glass window housing. This was done in conjunction with the mounting of the back plate (figure 3.6).

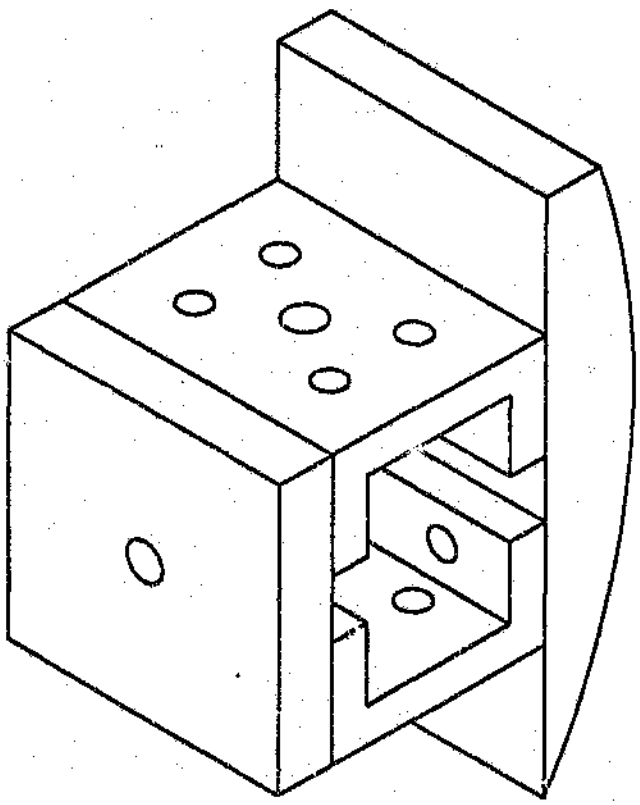


Figure 3.6 Back plate assembly

The back plate was mounted as close to the end of the test section as possible, to allow maximum view of the test specimen and flow field in front of it. A mounting position for a transducer was located in the centre of the back plate. The wires from the transducer in the back plate as well as those mounted in the bottom plate are taken through holes in the back plate assembly and test section parallel plates. These wires are then combined

with those from the transducers on the top plate and taken through a sealed polycarbonate plug in the glass window housing.

3.1.3 Diaphragm Bursting System

The needle used to rupture the diaphragm is driven by compressed air. The original circuit is shown in figure 3.7. To burst the diaphragm a toggle switch is closed which activates a magnetic valve, opening the air supply to the needle. Switching on the 220 V mains caused a voltage spike which activated the trigger PC board, resulting in the argon jet timing unit being bypassed and the argon lights flashed as the diaphragm burst

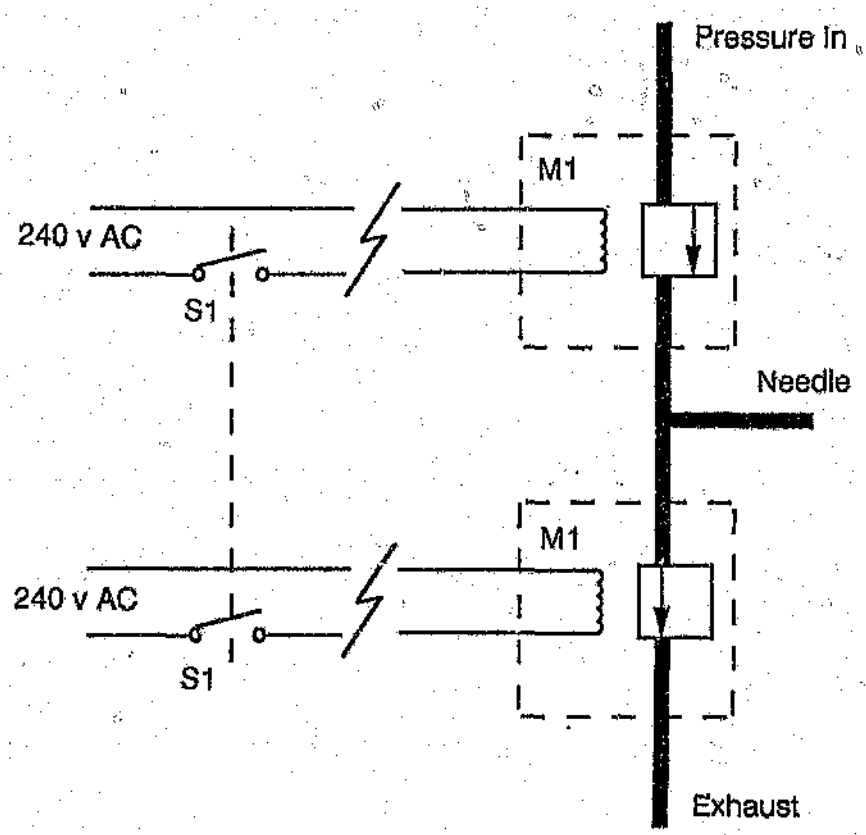


Figure 3.7 Diaphragm breaker circuit diagram 1

Various spark suppression circuits were tried until the one shown in figure 3.8 did not trigger the argon lights. The logic behind the circuit is that the toggle switch which is close to the argon lights is only switching 24V, which drives a relay at the other end of the shock tube to switch the 220 V mains. This together with varistors across the 220 V and 24 V supplies reduced the voltage spike enough for it not to interfere with the triggering of the argon lights at the required time.

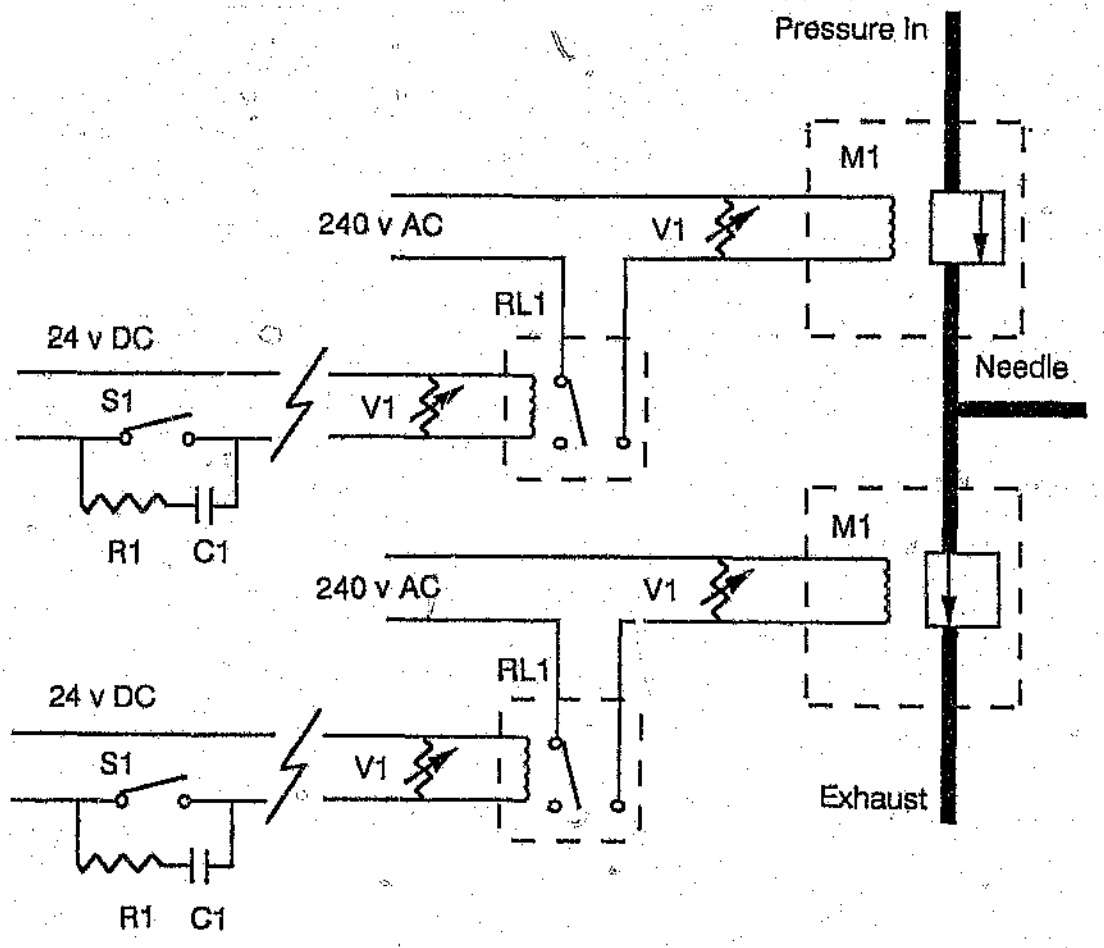


Figure 3.8 Diaphragm breaker circuit diagram 2

Table 3.1 Suppression circuit components

Components		
Type	**Qty**	**Description**
C1	2	Capacitor
M1	2	Magnetic pneumatic valve
R1	2	Resistor
S1	2	Single pole toggle switch
V1	2	Varistor

3.2 Schlieren System

A simple schlieren system is shown in figure 3.9. It consists of:

1 point light source
2 lenses
3 knife edge
4 photographic plate.

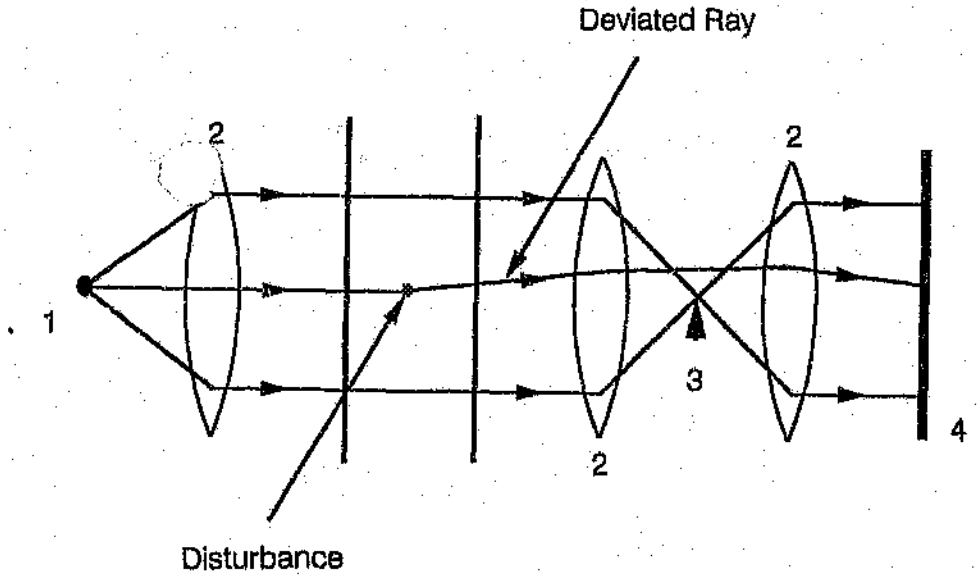


Figure 3.9 Simple schlieren system

The point source produces collimated light which is made parallel by the first lens. The light passes through the test section of the shock tube and the second lens focuses the light onto a photographic plate.

The sensitivity of the system may be adjusted but normally the knife edge is set so that only half of the light illuminates the photographic plate. A density variation in the shock tube which results in a refractive index gradient normal to the knife edge and optical axis will deviate the light ray which passed through it. Depending on the direction, the light will bypass or be blocked by the knife edge. This results in the darkening or lighting of the image of the shock tube. Thus the schlieren photograph is sensitive only to density gradients in one plane, that is perpendicular to the knife edge.

Schlieren systems can become more complex with the increasing number of mirrors and lenses required to accommodate the layout of the various shock tubes, but the basic principles remain the same.

3.2.1 Schlieren Layout

The schlieren system is set up as in figure 3.10 with the following components:

1 Shock tube test section
2 Argon jet light source
3 Parabolic mirrors
4 Knife edge and lens assembly
5 Photographic plate
6 Argon jet timing unit
7 Optical light sensor
8 Personal computer

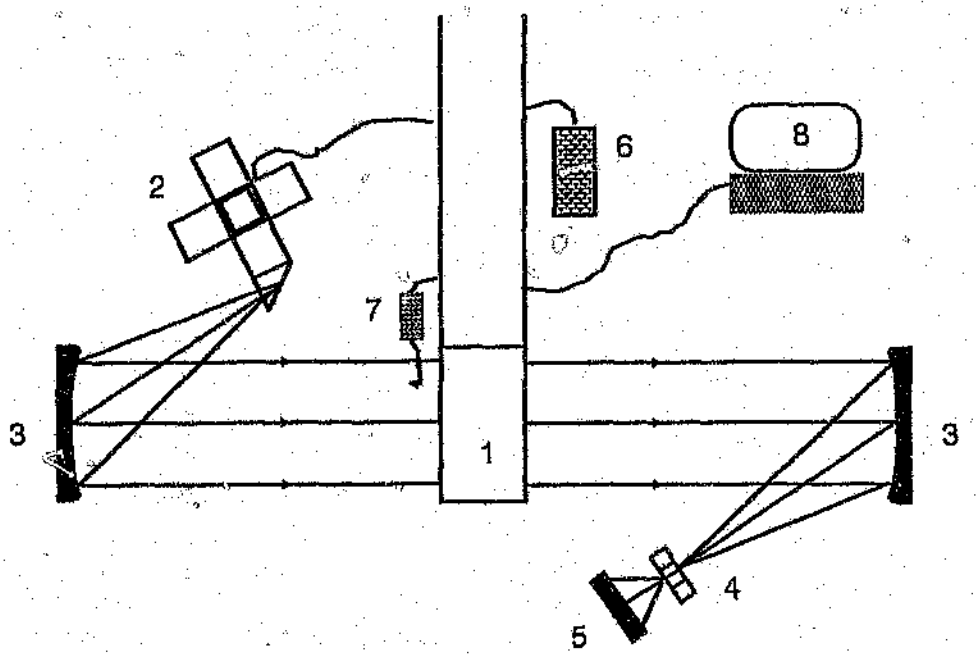


Figure 3.10 Schlieren layout

3.2.2 Argon Jet Light Source

The argon jet light source supplies a flash of duration of 0.3 microseconds. This is created by passing argon through a spark gap, across which is 10 kV. A pilot spark initiates the short and a flash is produced.

There are five individual light sources mounted on a stand which may be triggered at different times.

The main components of the light source are:

- storage capacitor
- trigger pc board
- spark gap
- test light
- focus lenses
- pilot spark initiator
- adjustable slit.

The general layout of the light source may be seen in figure 3.11

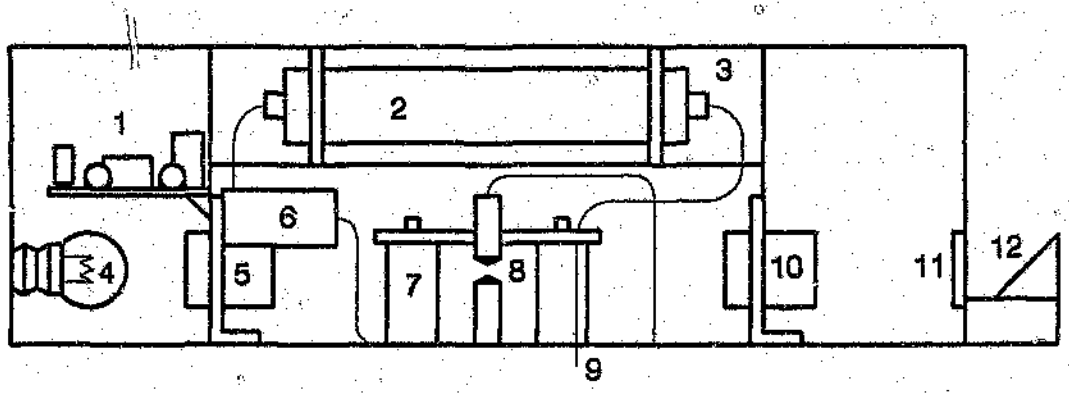
To operate the light source four power supplies are required, namely:

- 10 kV supply
- 300 V DC supply
- 24 V DC supply
- 12 V AC supply

A number of modifications were made to the original light source to improve its reliability and allow more accurate control.

The original unit had four storage capacitors which were connected in parallel, these were replaced by a single larger capacitor (15 kV 0.05 μf). This capacitor could no longer fit inside the original housing, thus an external polycarbonate box was manufactured. Tin foil is placed over the box. The polycarbonate provides the insulation and the tin foil the isolation for the capacitor. This insures that one light source does not trigger another.

A trigger pc board was manufactured to allow the interface between the light source and a new timing unit.



1 Trigger pc board
2 High voltage storage capacitor
3 Ploycarbonate insulator box
4 Alignment lamp
5 First lens
6 Transformer coil
7 Spacers
8 Spark electrodes
9 Argon gas input
10 Second lens
11 Adjustable slit
12 Plane mirror

Figure 3.11 Argon jet light source

Light source adjustments

To increase the light intensity of the flash, the spark gap is increased. This requires an increase in voltage and argon flow rate. The nominal settings are:

- spark gap ± 12 mm

- voltage 8,5 kV
- argon flow rate ± 2 cm of water.

The adjustable slits may be widened to increase the light intensity but if too wide will produce an uneven flash.

To ensure that the test light simulates the argon flash the lens at the rear must focus the test light into a sharp vertical beam positioned at the centre of the spark gap.

The front lens is used to focus the flash into a sharp vertical beam positioned on the adjustable slits.

3.2.3 Argon Jet Timing Unit

The timing unit consists of five separate channels which control the time at which the individual argon lights flash. The unit requires an input voltage to start the timing sequence. The time interval between the start voltage and the flash of the light source may be set using digital push button counters. The counters operate in the range 0 to 9999 microseconds in intervals of one microsecond.

The initial shock wave passing a pressure transducer is used to start the timing sequence. The output of the transducer amplifier is connected to the start pc board. This pc board sends a TTL pulse to the argon jet timing unit to start the timing sequence once the output from the transducer amplifier reaches a certain threshold. The threshold voltage may be set by altering the potentiometer mounted on the start pc board. This threshold voltage should be set at a minimum of 1 V to reduce the chance of interference and thus accidental triggering.

The output of the transducer amplifier tends to rise while not in use, this rise may cause the light to trigger incorrectly. To insure that this does not happen a toggle switch is use to ground the amplifier at the start of each test.

The argon jet timing unit grounds a 5 V supply which is connected to a light source, this activates the Trigger pc board and starts the flash. Figure 3.12 shows the schematic layout of the argon jet light system from the pressure transducer to the light flash.

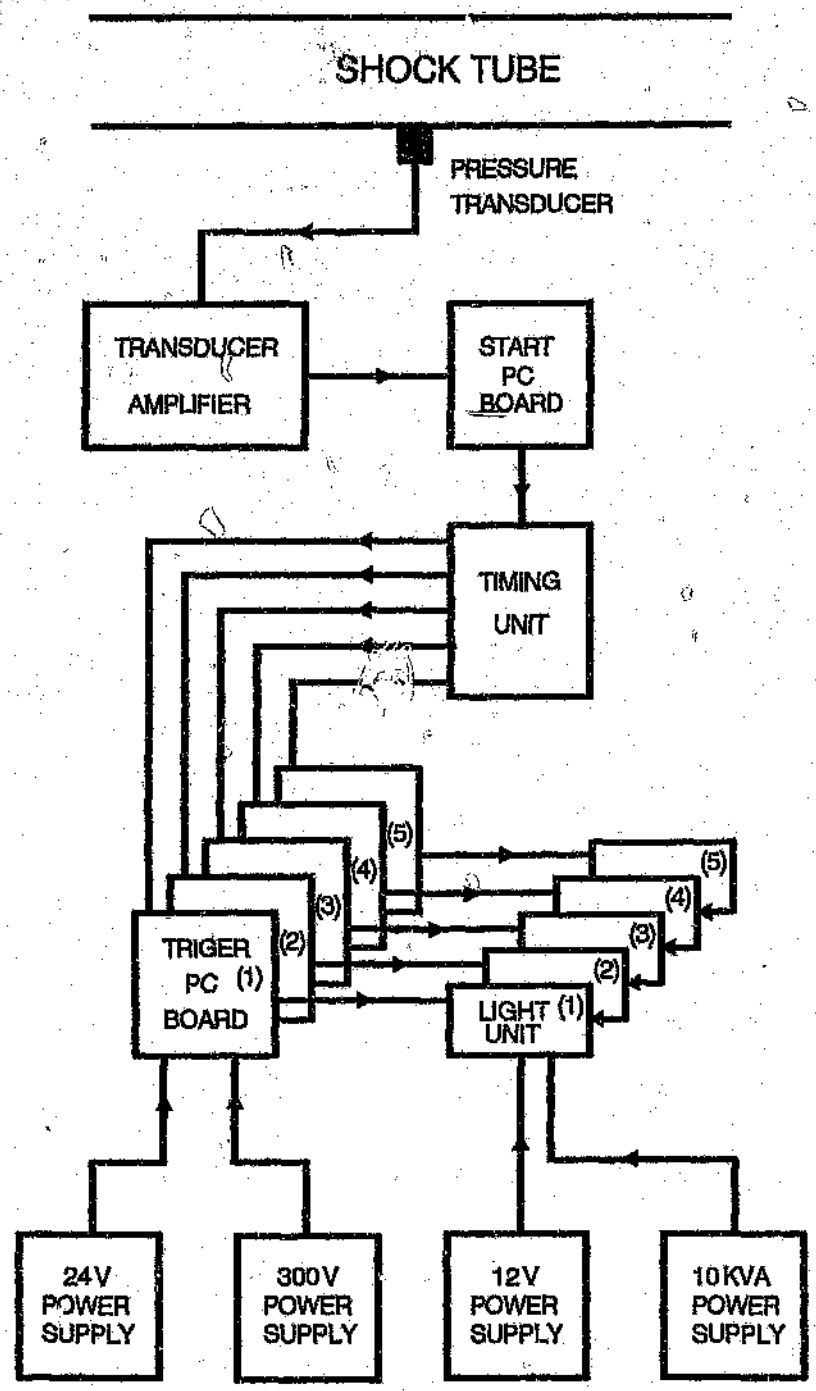


Figure 3.12 Argon jet light system layout

3.2.4 Optical Light Sensor

To check that the light source triggered at the correct time an optical light sensor was built. The light sensor uses a light sensitive transistor to pick up the light, it then sends a voltage pulse to the computer data acquisition system.

The sensitivity of the sensor may be varied using two pc board mounted potentiometers. The photo transistor has a limited angle of vision, thus it must be directly in line with the light that is to be read. The optical light sensor requires two power supplies, namely:

- 9V DC supply
- 15V DC supply

3.3 Foam

Two different foams were selected to cover a range of cell size structures and foam compressibility. The foams are shown in plate 3.1. The one on the left is a polyether foam having a density of 32.5 kg/m^3. The other foam is a polyester foam having a density of 38 kg/m^3, this foam is conventionally used as an acoustic absorber.

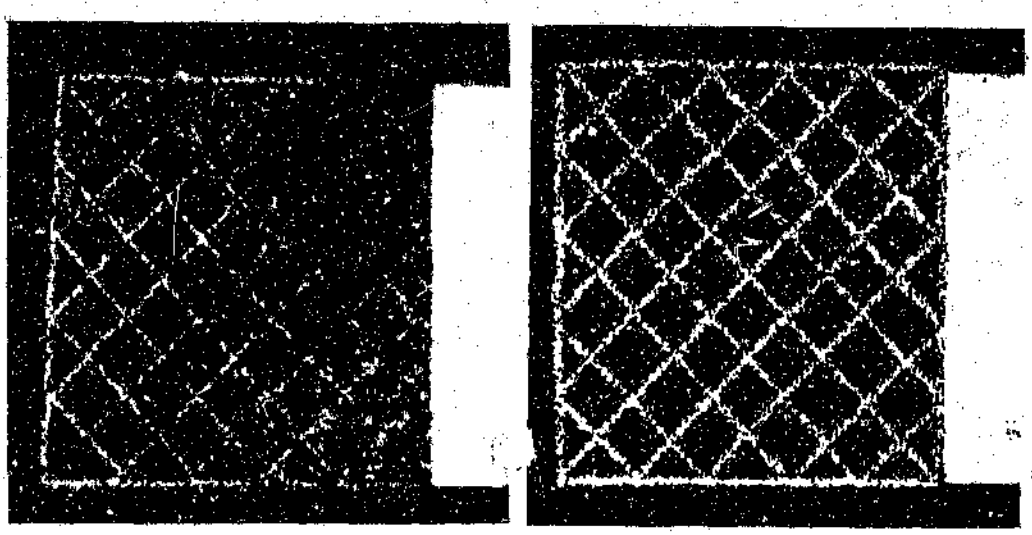


Plate 3.1 Polyether and polyester foam

The height and width of the foam is 77 mm ±1 mm, thus there is an interference fit between the foam and the boundaries of the shock tube. Other researchers have opted for an air gap between the foam and the shock tube boundaries. The reasons for choosing an interference fit are dealt with in section 5.6.

The length of all foam specimens tested was kept to 70 mm ± 1 mm. The volume fraction of foam was calculated to be 0.05 ± 0.02.(Atkins [1])

3.4 Instrumentation

3.4.1 PCB 113A21 Pressure Transducers

The PCB piezoelectric pressure transducers have been specifically designed for use in shock tubes. The PCB 113A21 transducer consist of quartz slides, an insulator and a metal housing. When a pressure is applied to the quartz crystals they produce an electric charge. Thus by converting the charge to a voltage the pressure applied to the transducer is found.

The PCB transducers come with their own mounting sleeve, allowing the face of the pressure transducer to fit flush with the wall of the shock tube.

The PCB 113A21 has a measuring range of 250 psi (1700 kPa) and a linearity of 1 %. Further specifications are given in Appendix A.The transducers have been calibrated in the shock tube, a description of this is found in Appendix B.

3.4.2 PCB 482A10 Line Power Supply

The PCB 482A10 Line Power Supply powers the PCB range of piezoelectric pressure transducers. If further amplification of the pressure transducer signal is required, the line power supply has this facility. (× 10, × 20)

The specifications for the PCB 482A10 are given in Appendix A.

3.5 Computer Hardware

3.5.1 XT Portable Personal Computer

The computer used in the acquisition of the data from the two pressure transducers located in the expansion chamber was a Protec Turbo 10. The Protec has the following specifications:

- 640 K of RAM
- twin floppy disk drives 360 K
- Processing speed of 4 MHz, changeable to 10 MHz
- IBM colour graphics card / mono Hercules graphics card.

3.5.2 AT Personal Computer

The pressure transducers in the test section were linked to the Protec AT. The AT has the following specifications:

- 640 K RAM
- one floppy disk drive 360 K, two hard drives (20 Mb, 40 Mb)
- Processing speed of 16 MHz
- IBM colour graphics card / mono graphics card
- maths coprocessor.

3.5.3 ISC-16 Hardware System

The ISC-16 hardware system consists of:

- 16 channel analog to digital converter card

- external instrument interface.

To operate the ISC-16 data acquisition system the ISC-16 card is placed in one of the computers expansion slots. The external instrument interface which is connected to the computer, collects data from the line power supplies.

The ISC-16 data acquisition system requires the host computer to have the following specifications:

- minimum of 256 K RAM
- IBM color standard graphics card
- graphics monitor.

3.6 Computer Software

3.6.1 ISC-16 Scope Driver

The Computerscope ISC-16 scope driver software together with the analog to digital converter card allows a personal computer to operate as a digital storage oscilloscope. The input data (up to 16 channels) is stored in the computers memory and displayed as a time sequence plot.

The program consists of two screens, an operating menu and a graphic display. While in the operations menu the following procedures may be executed:



- loading the data from a file
- saving the data to a file
- modifying the system parameters
- erasing a data file
- exiting from the system.

The system parameters which may be set include:

- the input channels activated
- the name of each channel
- the format of the input (analog or digital)
- the vertical gain sensitivity
- the sample period (minimum sample period 1 s with one input channel activated, 2 s with two channels activated, etc.)
- the amount of data collected (buffer size, maximum of 64 K).

After a test has been run and the data is stored in the computer's memory, the graphic display may be analyzed and modified as follows:

- the graph or part of, displayed on the screen may be shifted to the left or right
- the graph may be displayed as one dot per data point or a smooth curve
- the horizontal and vertical scale may be changed to compress or expand the graph
- with the aid of two vertical cursors, the vertical and horizontal values of the curves may be displayed in volts and seconds respectively. The Computerscope will display the vertical axes in any predefined units.

All the Computerscope operations are performed using simple key inputs, for these keys and more detailed information consult the computerscope manual. (12)

3.6.2 ISC - 16 Mass Storage Scope Driver

The ISC - 16 Mass Storage Scope Driver is similar to the ISC - 16 Scope Driver but it has the following additional features:

- larger data storage capacity
- data store in two formats, firstly as two Computerscope files with the extension *.DAT and *.PRM and secondly as a ASCII file with the extension *.ASC.

4 Experimentation

4.1 Procedure

1. Switch on the PCB line power supplies at least an hour before commencing test. This will allow power supplies to stabilize.

2. Remove one glass window and clean both. Insert foam test specimen into shock tube, ensuring that the foam is not compressed. Refit glass window.

3. Insert diaphragm and seal shock tube. Close valves labelled PRELOAD 1, RELEASE and PRELOAD 2, RELEASE. Open valves labelled PRELOAD 1, LOAD and PRELOAD 2, LOAD. This will activate a pneumatic locking system , sealing the shock tube.

4. Set the required time interval for each light channel.

5. Boot up computers.

6. Enter "ISC-16", thus loading the Computerscope Data Acquisition system.

   Note. This program will not run on an AT computer. The Protec AT used for data acquisition was fitted with a switch at the rear to change its performance from an AT to a XT. The program also requires a colour card. The Protec AT has two graphics cards, a Hercules card and a colour card. The Hercules card is normally operational. To activate the colour card enter "MODE CO80". To return to the Hercules card enter "MODE MONO". The portable Protec also has two cards. A switch on the side is used to select the required graphics card.

7. Set the system parameters.

8. Depress the "V" key to gain access to the Computerscope graph display mode.

9. Activate the single sweep mode of the Computerscope data acquisition system by simultaneously pressing the "CTRL" and "S" keys.

10. Check Schlieren system alignment.

    (a) Switch on test light.
    WARNING The test light must not be left on for more than two minutes as it heats up the trigger pc board and might destroy it.

    (b) The first mirror must project a circular beam of light which covers the test section. It must then shine onto the second mirror illuminating its entire diameter.

    (c) The vertical beam of light falling on the knife edges must be focused.

    (d) The image of the test section shown on the photographic plate must be in focus.

11. Rotate film holder to a portion of the film that has not been exposed.

12. Stick test number to glass window.

13. Evacuate expansion chamber.

    (a) Close valve labelled ATMOS.

    (b) Open valves labelled TUBE, PANEL and PUMP.

    (c) Start vacuum pump.

    (d) The required vacuum is set by adjusting the TUBE valve.

14. Adjust Argon flowrate to approximately 20 mm of water.

15. Ground timer transducer.

16. Test light source flash, ensuring that all channels are triggering.

17. Pressurize compression chamber.

    (a) Close valve labelled ATMOS .

    (b) Open valves SUPPLY and LOAD 1.

(c) By closing LOAD 1 the pressure in the chamber may be seen on a pressure gauge. Thus LOAD 1 is kept open until the air in the compression chamber reaches the required pressure.

18. Ground timer transducer.

19. Darken room.

20. Open film plate.

21. Activate the diaphragm breaker.

22. Close film plate.

23. The lights may now be switched on.

24. Open the ATMOS valve to depressurise the shock tube.

25. Switch off vacuum pump.

26. The Computerscope should now display the recorded data, to save this data depress the "F1" key, the "S" key and enter the data file name.

27. Return to the graph display mode by depressing the "V" key.

28 Simultaneously depress the "CTRL" and "V" keys, The vertical cursors will be displayed on the screen. Depress the "R" key, then "2" and move the cursor to the first sharp rise in pressure (voltage) of channel 2 using the arrow keys. Depress the "L" key, then "1" and move the cursor to the first sharp rise in pressure of channel 1. The time displayed under "RT - LT:" is the interval between the shock wave passing the first and second transducer. Record this time.

29. Develop the Polaroid film.

(a) Move camera control arm to P (Process).

(b) Withdraw film and start timing the development process.

(c) After the required time (60 seconds) separate the print from the negative and remove paper masks.

(d) Immerse the negative in a solution of 18 % sodium sulphite for a minute.

(e) Coat the print with the anti scratch and fade solution.

(f) Wash negative in water and hang up to dry.

30. Unlock the shock tube by closing the valves PRELOAD 1 LOAD and PRELOAD 2 LOAD and opening valves PRELOAD 1 RELEASE and PRELOAD 2 RELEASE.

31. Ensure that the shock tube in completely depressurised then open the diaphragm section.

32. The test section windows may now be removed and cleaned ready for the next test.

4.2 Path Photographs

To determine how different parts of the foam were moving while it was being tested a new experimental concept was explored. If a series of reflective diagonal lines were painted on the foam and photographs taken, the path of foam particles could be tracked. Hence the name path photographs. The argon jet light sources were available but far more light was required for the path photographs, than was for the schlieren photographs. Using half the standard schlieren optical layout and a 35 mm camera (figure 4.1) the problem of obtaining enough light was tackled.

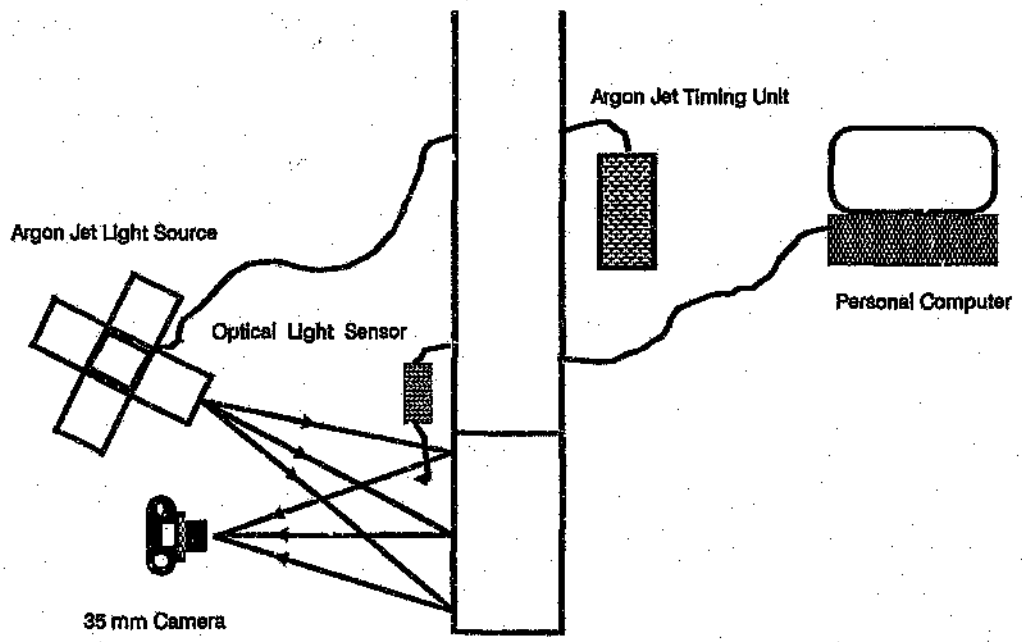


Figure 4.1 Part of the standard optical setup for schlieren photographs

The first attempt to solve the insufficient light problem was to trigger all five of the argon jet light sources at the same time. There was still not enough light. It soon became apparent that a high ASA rated film was required and the ESCOM photographic lab was contacted for their advice. They had previous experience with low level light photography and recommend a 1000 ASA color reversal film. The film was developed as if it were color negative film and development times pushed to the equivalent of a 6400 ASA film. The

technique of development is said to enhance the contrast of the film. An image was obtained, but it was not of any experimental value.

The problem was tackled from a different angle, rather than to increase the light from the light source or the film ASA, the portion of light reflected was increased. Various different types of reflective paints were tried. These included; white and silver metallic spray paint, a mixture of varnish and aluminium filings, varnish and glitter. A 0.5mm silver metallic pen was found to be the most reflective and easiest to use. This alone did not solve the problem.

Finally after a number of different configurations the path photographs were obtained using the experimental layout in figure 4.2 together with the following adjustments to the argon jet light sources:

The spark gap was opened as far as possible, being limited by the maximum voltage of the 10 kV supply.

The vertical slits at the front of each light source were opened as wide as possible.

The right angled mirror was removed from the front of the argon jet light stand.

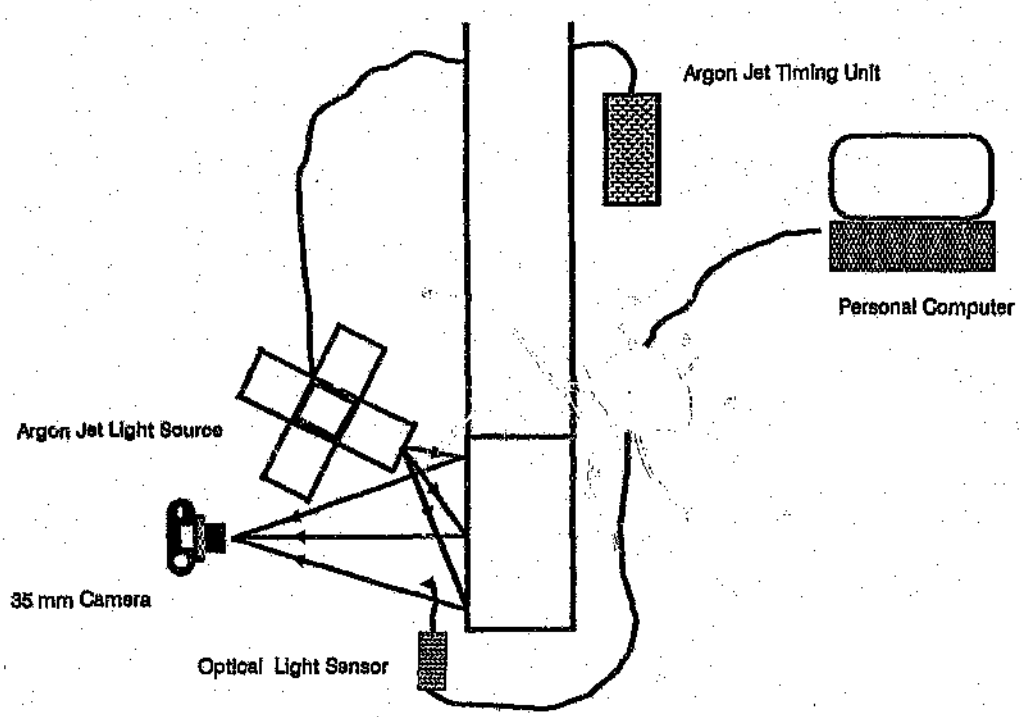


Figure 4.2 Optical equipment layout for path photographs

All five light sources were trigged simultaneously, meaning that only one photograph per test run could be obtained.

4.3 Observations

The observations for each test are listed in table 4.3. Each test was given an identifying name, which also serves as the name under which the data is stored. The list below explains what each digit in the eight digit file name represents:

digit 1	(letter)	object in shock tube
digit 2	(number)	density of object
digit 3	(letter)	further object specifications
digit 4 5	(number)	incident Mach number
digit 6 7	(number)	test number
digit 8	(letter)	pressure transducer positions.

For "digit 1" there are two possibilities ;

F	Foam
P	Solid wall.

For "digit 2" the densities are represented as follows:

1	32.5 kg/m^3	Polyether Foam
2	38.0 kg/m^3	Polyester Foam

Table 4.1 lists the various foam sizes and configurations tested, represented by "digit 3". Two different sizes of cross-section were tested, one such that the foam touched the sides of the shock tube, the other so that there was a gap of 2.1 mm $\pm$0.1 mm between the foam and the walls. Tests were run using foam, which had various sides sealed with cling rap, a clear thin plastic. Figure 4.3 shows a foam specimen with each face numbered. The shaded regions in table 4.1 indicated which sides of the foam were sealed.

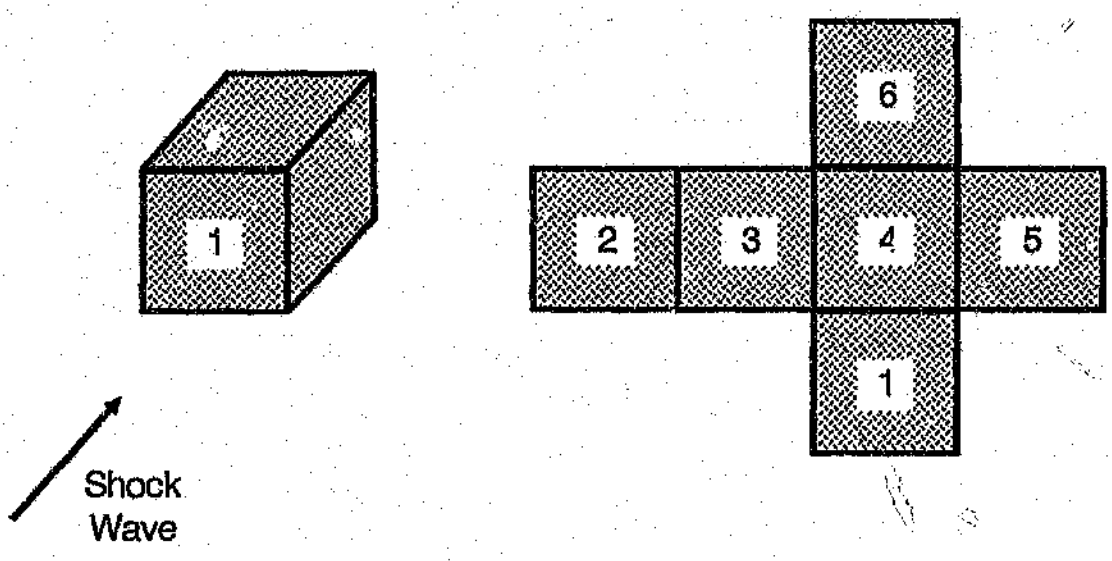


Figure 4.3 Foam sides

Table 4.1 Foam specifications

Digit 3	Foam size (mm)			Sealed Sides					
	X	Y	Z	1	2	3	4	5	6
A	76.2	76.2	70						
B	76.2	76.2	70	■					
C	76.2	76.2	70	■	■	■	■	■	
D	76.2	76.2	70		■	■	■	■	■
E	76.2	76.2	70	■	■	■	■	■	■
F	76.2	76.2	70		■	■	■	■	
G	72	72	70						
H	72	72	70		■	■	■	■	

Table 4.2 and figure 4.4 indicate what transducer positions were used for various tests. Four transducers were available to be used in the test section. The numbers 1 to 4 represent specific transducers:

1 SN4815
2 SN4816
3 SN4818
4 SN5218

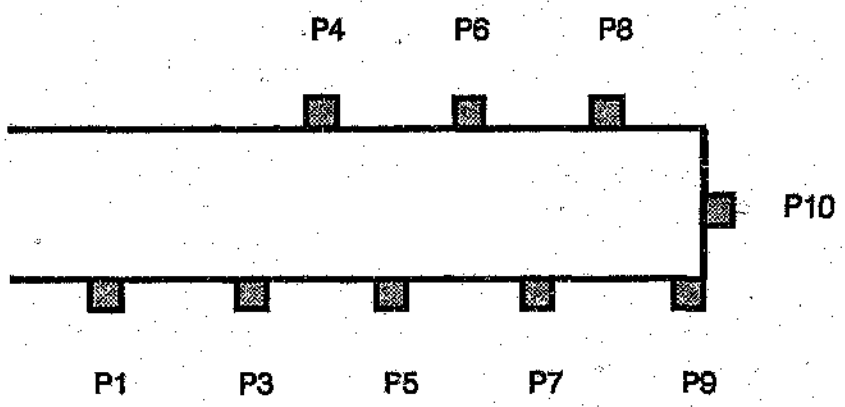


Figure 4.4 Transducer positions in the test section of the shock tube.

Two transducers were located in the square tube section of the expansion chamber. The first transducer (SN 4817) mounted 620.5 mm ahead of the second transducer (SN 5219).

The "L" seen in the transducer position P1 indicates that this transducer was used to trigger the light sources and thus no pressure record was obtained from it.

Table 4.2 Transducer Positions

Digit 8	Transducer positions								
	P1	P3	P4	P5	P6	P7	P8	P9	P10
A	1			3	2				4
B	L		2	3			4		
C	1	3					2		4

Digit 8	Transducer positions								
	P1	P3	P4	P5	P6	P7	P8	P9	P10
D	1		2					3	4
E	L		2	3					4
F	L		2					3	4
G	L	3					2		4
H	L			3	2				4
I	1				2	3			4
J	L		2			3			4
K	1	3	2						4

The second column of table 4.3 is the photograph number, the prefix "S" representing a schlieren photograph and "P" a 35mm photograph. The next four columns house the time settings that were used to trigger the light sources. The atmospheric pressure and the compression chamber pressure are recorded in the next two columns. Finally the time taken for the incident shock wave to travel between the two transducers located outside the test section is shown in the last column. For tests F1A1601b to F1A1607b the distance between the transducers was 20 mm, while for the rest it was 320.5 mm.

4.4 Data Processing

The data from the piezoelectric transducers were recorded using two Computerscope data acquisition boards. One connected to a portable XT and one to an AT computer, the latter acquisition board being a new version which has a number of new features.

After each test the data is saved on disk, the XT Computerscope saves the data in two files with the following extensions; .DAT and .PRM. The PRM file contains information about the Computerscope settings e.g. number of data channels recorded, sample rate, etc. The DAT file contains the voltage from the pressure transducers, stored as a number in the range 0 to 4096, where 0 represents -10 volts and 4096 represents 10 volts.

The data file is formatted in such a way that it can not be imported to Lotus. So a program was written which uses both files to create an ASCII file containing the actual transducer voltage.

The latest Computerscope has the ability to create an ASCII file containing the voltage from its main menu.

The data was manipulated using Lotus 123. The pressure transducers were calibrated in the shock tube. A detailed description of this may be found in Appendix B. The pressure recorded by the transducers may be calculated using equations 4.1 to 4.6

$$P = Patm + 297.7Vc \quad \text{SN4815} \quad (4.1)$$

$$P = Patm + 309.2Vc \quad \text{SN4816} \quad (4.2)$$

$$P = Patm + 252.4Vc \quad \text{SN4817} \quad (4.3)$$

$$P = Patm + 266.9Vc \quad \text{SN4818} \quad (4.4)$$

$$P = Patm + 266.9Vc \quad \text{SN5218} \quad (4.5)$$

$$P = Patm + 260.9Vc \quad \text{SN5219} \quad (4.6)$$

Where

- Vc voltage (mv)
- Patm atmospheric pressure (Pa)

- SN transducer serial number.

Table 4.3 Porous compressible foam tests

File Name	Photo No	Timing Unit Settings				Atmos-pheric Pressure (KPa)	Bursting Pressure (psi)	Shock Time (μs)
		T1	T2	T3	T4			
		(μs)						
F1A1601B		195	217	239	261	82.49	30	40
F1A1602B	S 3.1	195	217	239	261	82.49	30	40
F1A1603B	S 3.2	283	305	328	350	82.49	30	40
F1A1604B		372	394	416	438	82.49	30	40
F1A1605B	S 3.3	372	394	416	438	82.49	30	40
F1A1606B	S 3.4	460	482	504	526	82.49	30	40
F1A1607B	S 4	829	1197	1397	1685	82.49	30	40
F1A1601E	S 79	1240	1280	1320	1360	82.50	30	
F1A1601F	S 79	620	680	740	800	82.50	30	620
F1A1602F		620	680	740	800	82.50	25	635
F1A1501F	S 80	620	680	740	800	82.50	25	648
POO1501F	S 81	101	202	404	505	82.50	25	644
F1A1502F	S 82	380	440	500	560	82.40	25	
F1A1503F		860	920	980	1040	82.40	25	646
F1A1504F	S 83	860	920	980	1040	82.40	25	646
F1A1505F	S 84	1100	1160	1220	1280	82.40	25	646
F1A1506F	S 85	1340	1400	1460	1520	82.40	25	
F1A1507F	S 86	1580	1640	1700	1760	82.40	25	646
	S 87	1820	1880	1940	2000	82.59	25	670
F1A1508F	S 87	1820	1880	1940	2000	82.59	25	670
F1A1603F						82.59	28	632
F1A1604F						82.59	27	640
F1A1509F						82.59	26	654
F1A1510F						82.59	26.8	640

File Name	Photo No	Timing Unit Settings				Atmos-pheric Pressure (KPa)	Bursting Pressure (psi)	Shock Time (μs)
		T1	T2	T3	T4			
		(μs)						
F1A1511F	S 88	1820	1880	1940	2000	82.59	26.8	646
F1A1512F	S 89	2060	2120	2180	2240	82.59	26.8	642
F1A1501G						82.55	25	644
F1A1502G						82.55	25	646
F1A1503G						82.55	25	650
F1A1504G	S 90	2300	2360	2420	2480	82.55	25	640
F1A1501A	S 91	2540	2600	2660	2720	82.55	25	648
F1A1502A						82.55	25	640
F1A1503A						82.55	25	642
F1A1501I						82.55	25	648
F1A1502I						82.55	25	646
F1A1503I						82.55	25	642
F1A1504I						82.55	25	648
F1A1505I						82.55	25	650
F1A1506I						82.50	25	646
	S 92	2780	2840	2900	2960	82.50	25	
F1A1501E						82.85	25	650
S1A1501E						82.85	25	648
P011501E						82.87	25	668
F2A1501E	S 92	380	440	500	560	82.87	26	656
F2A1502E	S 93	380	440	500	560	82.87	26	676
F2A1601E	S 94	380	440	500	560	82.87	27	636
F2A1503E	S 95	620	680	740	800	82.87	26.5	654
F2A1602E	S 96	860	920	980	1040	82.87	27	638
F2A1504E	S 97	1100	1160	1220	1280	82.87	26.5	642

File Name	Photo No	Timing Unit Settings				Atmos-pheric Pressure (KPa)	Bursting Pressure (psi)	Shock Time (μs)
		T1	T2	T3	T4			
		(μs)						
F2A1505E	S 98	1340	1400	1460	1520	82.50	26	656
F2A1506E	S 99	1580	1640	1700	1760	82.50	26.5	644
F2A1507E	S 1	1820	1880	1940	2000	82.50	26.5	642
F2A1508E	S 2	2060	2120	2180	2240	82.50	26.5	6[illegible]0
F2F1509E	S 3	1340	1400	1460	1520	83.10	26.5	642
F2B1510E	S 4	1340	1400	1460	1520	83.10	26.5	648
F2B1603E	S 5	860	920	980	1040	83.10	26.5	636
F2B1511E	S 6	380	440	500	560	83.10	26	648
F2C1501E	S 7	1340	1460	1580	1820	82.75	26.5	648
F2D1501E	S 8	1340	1460	1580	1820	82.75	26.5	650
F2E1501E	S 9	1340	1460	1580	1820	82.75	26.5	644
F2F1501E	S 10	1340	1460	1580	1820	82.75	26.5	644
F2A1512E	P 6	250	250	250	250	82.90	26.5	648
F2A1604E	P 9	350	350	350	350	82.90	26.5	638
F2A1513E	P 10	450	450	450	450	82.54	26.5	652
F2A1514E	P 11	450	450	450	450	82.54	26.5	670
F2A1515E	P 12	250	250	250	250	82.54	26.5	644
F2A1516E	P 13	550	550	550	550	82.54	26.5	646
F2A1517E	P 14	650	650	650	650	82.54	26.5	642
F2A1518E	P 15	750	750	750	750	82.54	26.5	642
F2A1519E	P 16	850	850	850	850	82.54	26.5	642
F2A1520E	P 17	950	950	950	950	82.54	26.5	650
F2A1521E		250	250	250	250	83.60	26.5	654
F2A1522E		350	350	350	350	83.60	26.5	660
		450	450	450	450	83.60	27.5	

File Name	Photo No	Timing Unit Settings (μs)				Atmospheric Pressure (KPa)	Burst Pressure (psi)	Shock Time (μs)
		T1	T2	T3	T4			
F2A1523E		550	550	550	550	83.60	27.5	636
F2A1524E		650	650	650	650	83.60	27	646
F2A1525E		750	750	750	750	83.60	27	646
F2A1526E		850	850	850	850	83.60	27	658
F2A1527E		950	950	950	950	83.60	27	644
F2A1528E	P 3	260	260	260	260	83.11	27	650
F2A1529E	P 4	260	260	260	260	83.11	27.1	654
F2A1530E	P 5	320	320	320	320	83.11	27.5	650
F2A1531E	P 9	380	380	380	380	82.87	28	646
F2A1532E	P 10	440	440	440	440	82.87	28	640
F2A1533E	P 11	500	500	500	500	82.87	28	640
F2A1534E	P 12	560	560	560	560	82.87	28	642
F2A1535E	P 13	620	620	620	620	82.87	28	646
F2A1536E	P 14	680	680	680	680	82.87	28	646
F2A1537E	P 15	740	740	740	740	82.87	28	646
F2A1538E	P 16	800	800	800	800	82.87	28	642
F2A1539E	P 17	860	860	860	860	82.87	28	642
F2A1540E	P 18	920	920	920	920	82.87	28	642
F2A1541E	P 19	980	980	980	980	82.87	28	642
F2A1542E	P 20	1040	1040	1040	1040	82.87	28	640
F2A1543E	P 21	1100	1100	1100	1100	82.87	28	642
F2A1544E	P 22	1160	1160	1160	1160	82.87	28	642
F2A1545E	P 23	1220	1220	1220	1220	83.40	28	640
F2A1546E	P 24	1280	1280	1280	1280	83.40	28	648

File Name	Photo No	Timing Unit Settings				Atmos-pheric Pressure (kPa)	Bursting Pressure (psi)	Shock Time (μs)
		T1	T2	T3	T4			
		(μs)						
F2A1547E	P 25	1340	1340	1340	1340	83.40	28	670
F2A1548E	P 26	1340	1340	1340	1340	83.40	28	642
F2A1549E	P 27	1400	1400	1400	1400	83.40	28	636
F2A1550E	P 28	380	380	380	380	83.40	28	642
F2A1551E	P 29	500	500	500	500	83.40	28	666
F2A1552E	P 30	680	680	680	680	83.40	28	652
F2A1553E	P 31	860	860	860	860	83.40	28	658
F2A1554E	P 32	1040	1040	1040	1040	83.40	28	642
F2A1555E	P 33	560	560	560	560	83.40	28	642
F1A1502E	P 4	260	260	260	260	82.92	28	642
F1A1503E	P 5	320	320	320	320	82.92	28	670
F1A1504E	P 6	320	320	320	320	82.92	28	646
F1A1505E	P 7	380	380	380	380	82.92	28	674
F1A1506E	P 8	380	380	380	380	82.92	28	642
F1A1507E	P 9	440	440	440	440	82.92	28	636
F1A1508E	P 10	500	500	500	500	82.92	28	646
F1A1509E	P 11	560	560	560	560	82.92	28	640
F1A1510E	P 12	620	620	620	620	82.92	28	642
F1A1511E	P 13	680	680	680	680	82.92	28	636
F1A1512E	P 14	740	740	740	740	83.11	28	670
F1A1513E	P 15	740	740	740	740	83.11	28	638
F1A1514E	P 16	800	800	800	800	83.11	28	642
F1A1515E	P 17	860	860	860	860	83.11	28	648
F1A1516E	P 18	920	920	920	920	83.11	28	656
F1A1517E	P 19	980	980	980	980	83.11	28	650

File Name	Photo No	Timing Unit Settings				Atmos-pheric Pressure (KPa)	Bursting Pressure (psi)	Shock Time (μs)
		T1	T2	T3	T4			
		(μs)						
F1A1540J						83.40	28	662
F1A1541J						83.40	28.5	636
F1A1518E	P 20	1040	1040	1040	1040	83.11	28.2	642
F1A1519E	P 21	1100	1100	1100	1100	83.11	28.2	664
F1A1520E	P 22	1100	1100	1100	1100	83.11	28.2	664
F1A1521E	P 23	1100	1100	1100	1100	83.11	28.2	654
F1A1522E	P 24	1160	1160	1160	1160	83.11	28.5	660
F1A1523E	P 25	1160	1160	1160	1160	83.11	29	648
F1A1524E	P 26	1220	1220	1220	1220	83.11	29	656
F1A1525E	P 27	1280	1280	1280	1280	83.11	29.5	668
F1A1526E	P 28	1280	1280	1280	1280	83.11	30	632
F1A1527E	P 29	1280	1280	1280	1280	83.11	29	634
F1A1528E	P 30	1340	1340	1340	1340	83.11	28.5	666
F1A1529E	P 31	1400	1400	1400	1400	83.11	29	648
F1A1530E	P 32	680	680	680	680	83.11	29	638
F1A1531E	P 33	740	740	740	740	83.11	28.5	638
F1A1532E	P 34	920	920	920	920	83.11	28	642
F1A1533E	P 35	1100	1100	1100	1100	83.11	28	642
F1A1534E	P 36	1220	1220	1220	1220	83.11	28	660
F1A1535E						83.40	28	686
F1A1536E						83.40	29	656
F1A1537E						83.40	29.5	630
F1A1538J						83.40	29.5	634
F1A1539J						83.40	29	632
F1A1542J						82.59	28.5	640

File Name	Photo No	Timing Unit Settings				Atmos-pheric Pressure (KPa)	Bursting Pressure (psi)	Shock Time (μs)
		T1	T2	T3	T4			
		(μs)						
F1A1513D						82.59	28.5	640
P021502D						82.59	28.5	644
F1A1514D						82.59	28.5	644
F1A1505C						82.59	28.5	664
F1A1506C						82.59	28.5	642
P021501C						82.59	28.5	636
F1A1504A						82.43	28.5	668
F1A1505A						82.43	28.5	640
P021501A						82.43	28.5	636
F2A1501A						82.43	28.5	646
F2A1502A						82.43	28.5	646
P021502A						82.43	28.5	650
F2A1501C						82.43	28.5	666
F2A1502C						82.43	28.5	642
F2A1501D						82.43	28.5	668
F2A1502D						82.43	28.5	644
F2A1501K						82.43	28.5	674
F2A1502K						82.43	28.5	646
F2G1501J	P 3	500	500	500	500	83.57	28.5	638
F2G1502J	P 4	680	680	680	680	83.57	28	640
F2G1503J	P 5	680	680	680	680	83.57	28	646
F2G1504J	P 6	800	800	800	800	83.57	28	640
F2G1505J	P 7	1040	1040	1040	1040	83.57	28	654
F2G1506J	P 8	1220	1220	1220	1220	83.57	28	642
F2G1507J	P 9	1220	1220	1220	1220	83.57	28	632

File Name	Photo No	Timing Unit Settings (μs)				Atmospheric Pressure (KPa)	Bursting Pressure (psi)	Shock Time (μs)
		T1	T2	T3	T4			
F2G1508J	P 10	1040	1040	1040	1040	83.57	28	644
F2G1509J	P 11	500	500	500	500	83.57	28	640
F2H1501J	P 12	500	500	500	500	83.57	28	668
F2H1502J	P 13	680	680	680	680	83.57	28	630
F2H1503J	P 14	800	800	800	800	83.57	28	638
F2H1504J	P 16	1040	1040	1040	1040	83.57	28	664
F2H1506J	P 17	1220	1220	1220	1220	83.57	28	670
F2H1507J	P 18	1220	1220	1220	1220	83.57	28	634
F2H1507J		500	500	500	500	83.57	28	658
F2H1508J	P 19	500	500	500	500	83.57	28	644
F2H1509J	P 20	800	800	800	800	83.57	28	642
F2H1510J	P 21	1040	1040	1040	1040	83.57	28	636
F2H1511J	P 22	680	680	680	680	83.57	28	670
F2H1512J	P 23	680	680	680	680	83.57	28	640

5 Results and Discussion

5.1 Pressure Variation

This section contains the presentation of the pressure records and what was obtained from them, this includes:

- pressure traces
- pressure contour plots.

Four pressure transducers were available to record the pressure variation in the test section. Figure 5.1 shows the different mounting positions for the transducers. Various tests were run with the transducers in different positions until a trace was obtained for each transducer position. Thus the pressure history before, alongside and behind the foam was obtained.

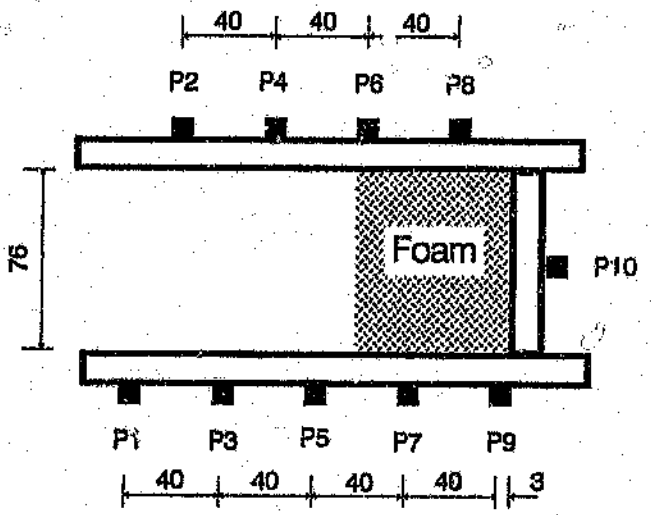


Figure 5.1 Transducer positions in the test section

The first set of results are for the interaction of an incident shock wave of Mach number 1.4 with 70 mm of polyether foam having a density of 32.5 kg/m^3.

Figure 5.2 is the pressure record obtained from a transducer in position P1. The incident shock wave passes the transducer at time = 0 μs, this origin for the time scale is kept throughout the report, for all the graphs, photographs and programs, unless otherwise stated. Thus if a photograph was taken at 200 μs, this means that 200 μs after the incident shock wave passed the transducer in position P1 the photograph was taken.

The incident shock wave strikes the foam, a wave is transmitted and a shock wave is reflected. The reflected shock wave passes the transducer and causes the second rise in pressure. The reflected shock wave is travelling at Mach 1.172. The next rise in pressure is a compression wave. Figures 5.3 to 5.5 are the pressure traces from transducers in positions P3, P4 and P5, they all show the incident and reflected shock wave and compression wave.

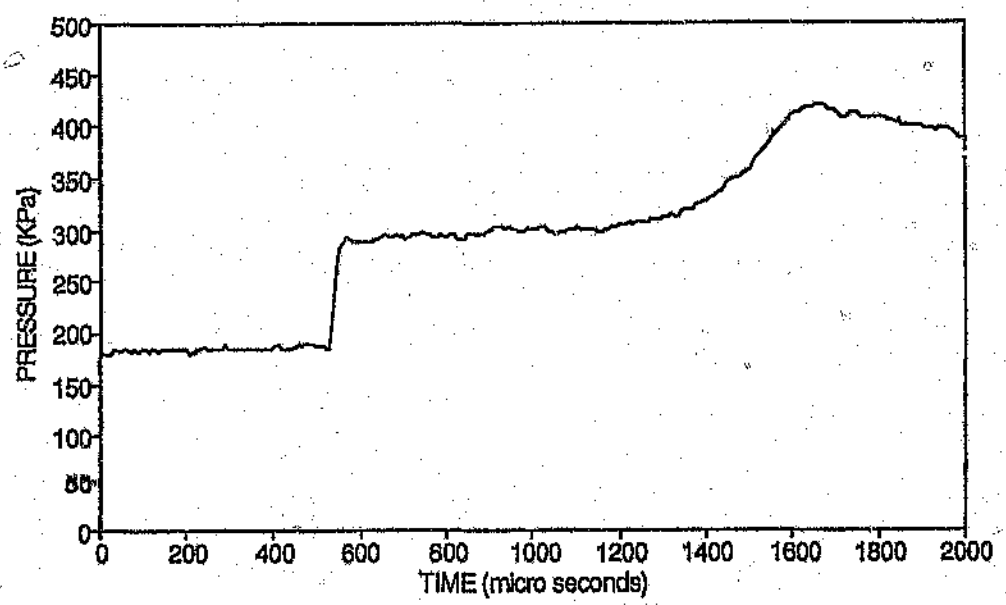


Figure 5.2 Pressure variation at P1, 70 mm of polyether foam, incident shock wave Mach number 1.4

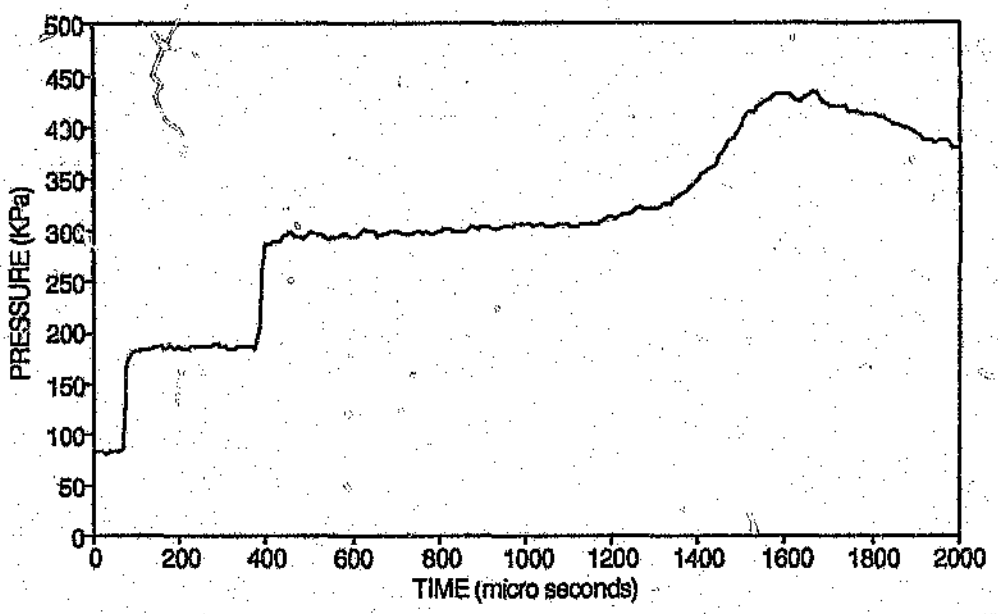


Figure 5.3 Pressure variation at P3, 70 mm of polyether foam, incident shock wave Mach number 1.4

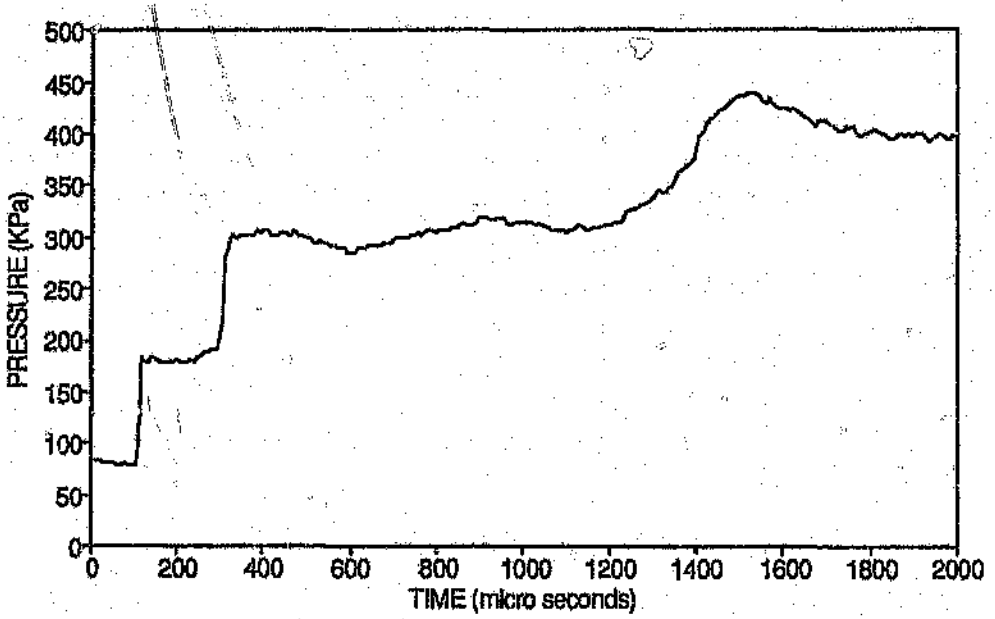


Figure 5.4 Pressure variation at P4, 70 mm of polyether foam, incident shock wave Mach number 1.4

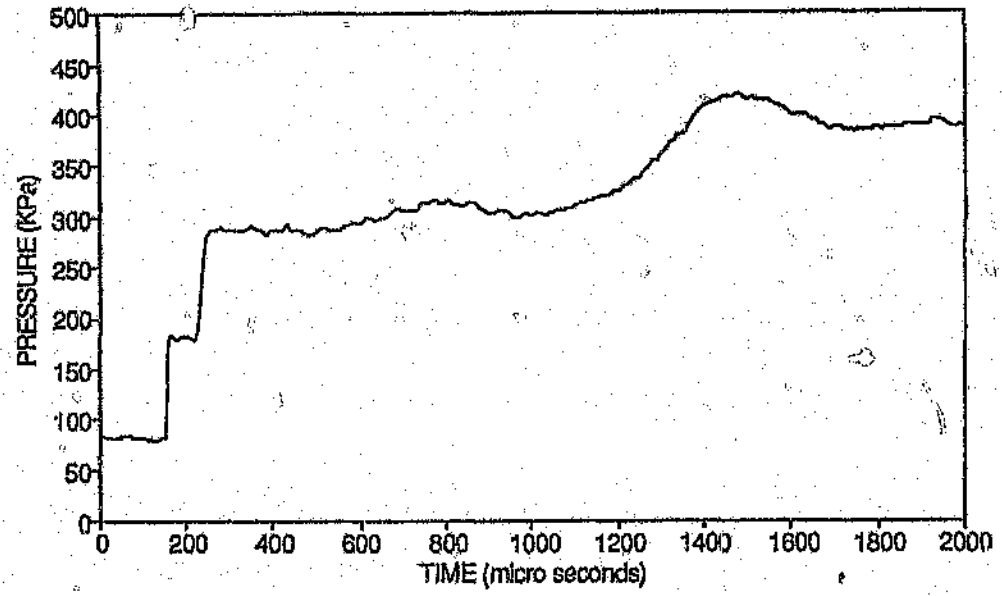


Figure 5.5 Pressure variation at P5, 70 mm of polyether foam, incident shock wave Mach number 1.4

Figures 5.6 to 5.8 are the pressure traces from the transducers in positions P6, P7, P8. It must be assumed that the foam moves after the incident shock wave strikes the foam, thus it is not clear which parts of the traces represent the pressure in the foam. It is reasonable to assume that the first compression wave is one which is travelling through the foam and the last compression wave is the one which has been seen in previous graphs.

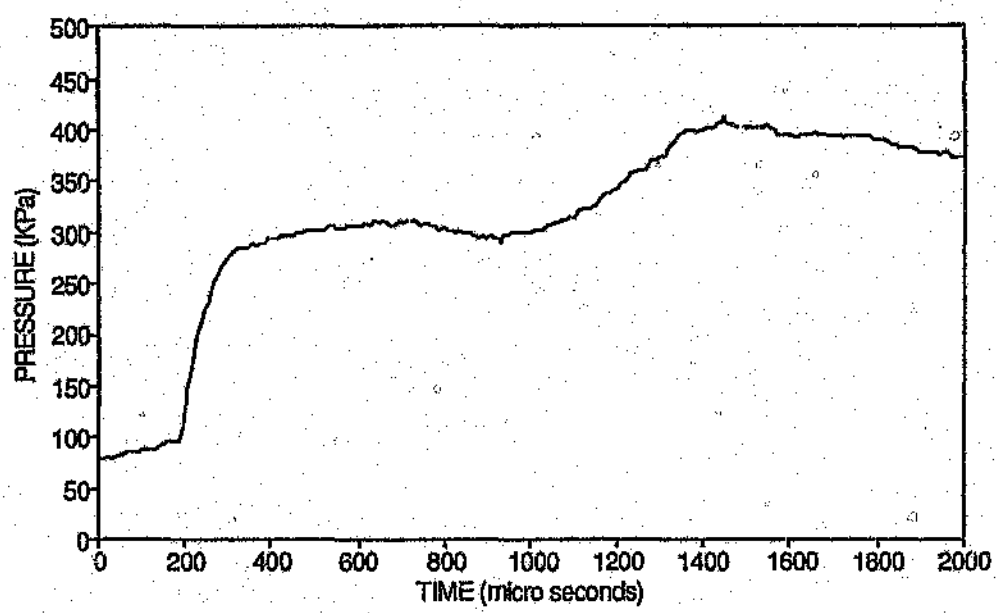


Figure 5.6 Pressure variation at P6, 70 mm of polyether foam, incident shock wave Mach number 1.4

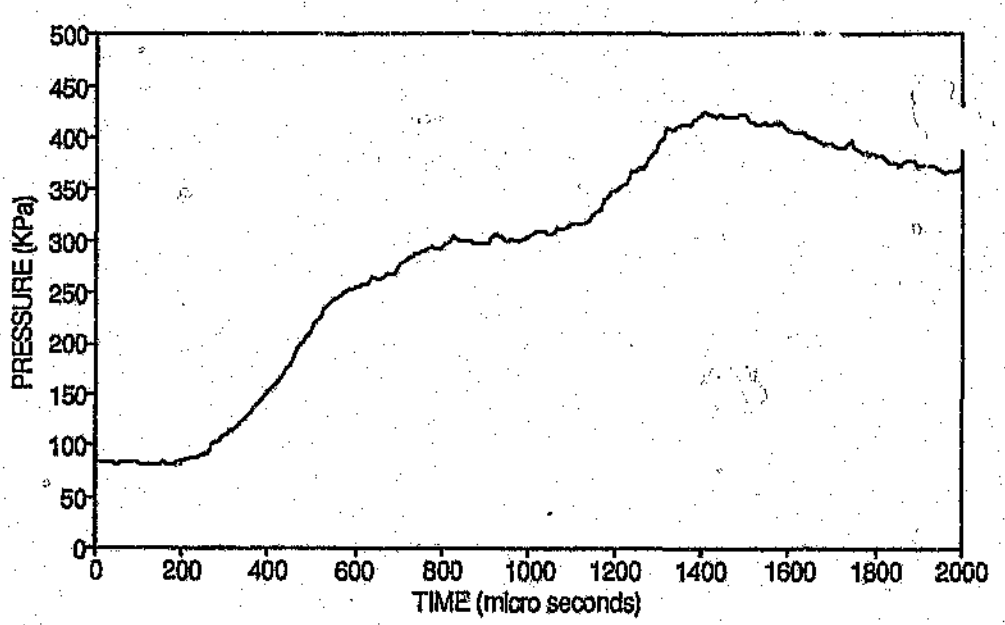


Figure 5.7 Pressure variation at P7, 70 mm of polyether foam, incident shock wave Mach number 1.4

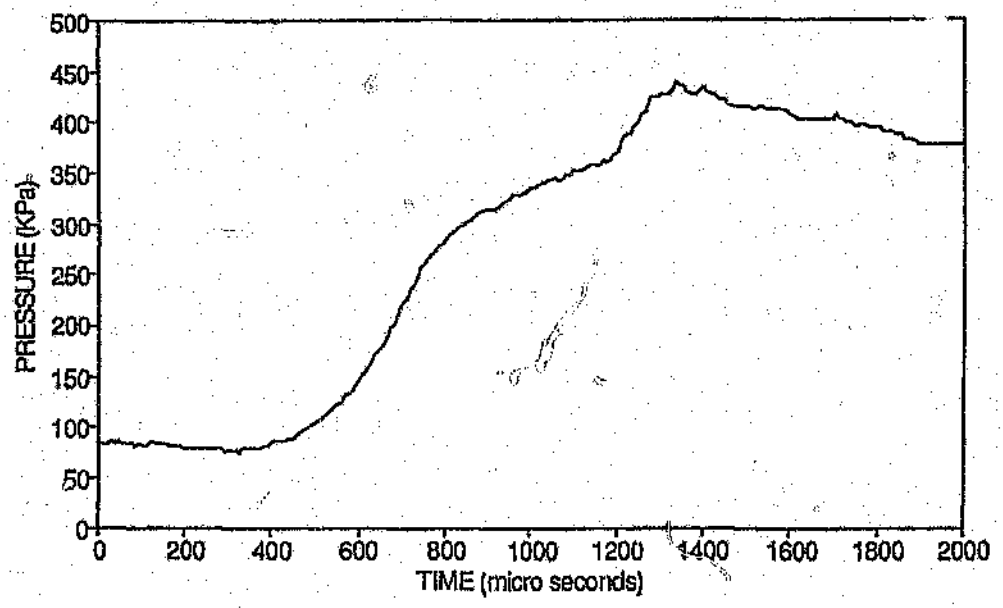


Figure 5.8 Pressure variation at P8, 70 mm of polyether foam, incident shock wave Mach number 1.4

Figures 5.9 to 5.10 are pressure traces from transducers in positions P9 and P10 respectively. The pressure variation has changed completely. Figure 5.10 shows the extremely high pressure that is reached at the rear of the foam, considering that the strength of the incident shock wave is only 100 kPa and the pressure is amplified up to 750 kPa. Various precautions and different tests were run to ensure that the pressure measured at the rear of the foam was as a result of gas pressure and not mechanical interference.

To interpret the different wave interactions throughout the test section a pressure contour plot (figure 5.11.) was constructed using all the information from each pressure trace. The initial position of the front face of the foam before the incident shock wave strikes it is shown as a dotted line. The poor resolution of this plot is a feature of the computer package that was available and not a feature of the data. The movement of the incident (S_I)and reflected shock wave (S_R) can clearly be seen. So too can the compression wave (C_1) travelling through the foam. However it is not immediately clear what is causing the other waves, further information regarding the the movement of the foam is required.

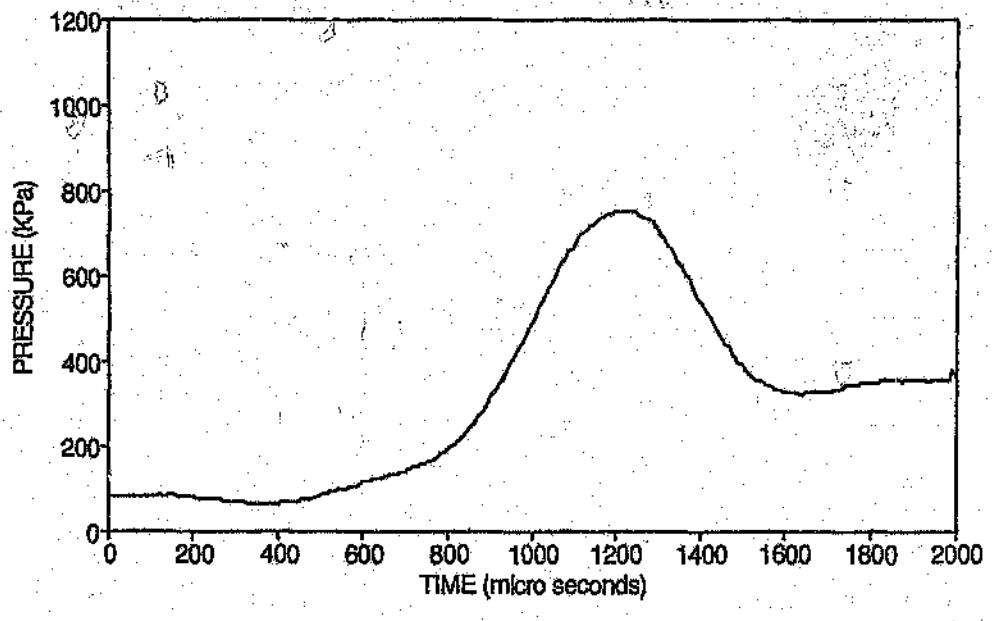


Figure 5.9 Pressure variation at P9, 70 mm of polyether foam, incident shock wave Mach number 1.4

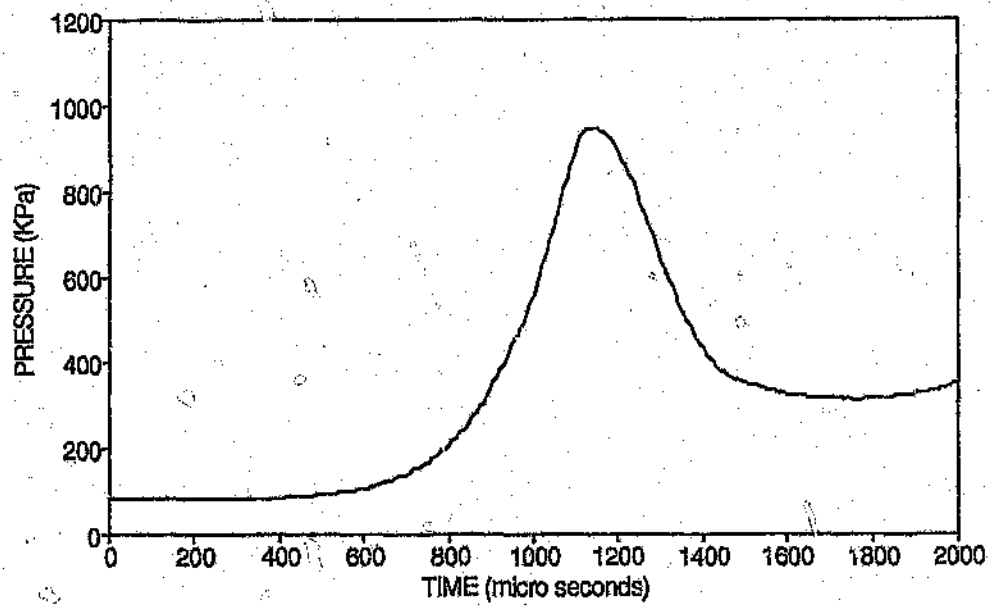


Figure 5.10 Pressure variation at P10, 70 mm of polyether foam, incident shock wave Mach number 1.4

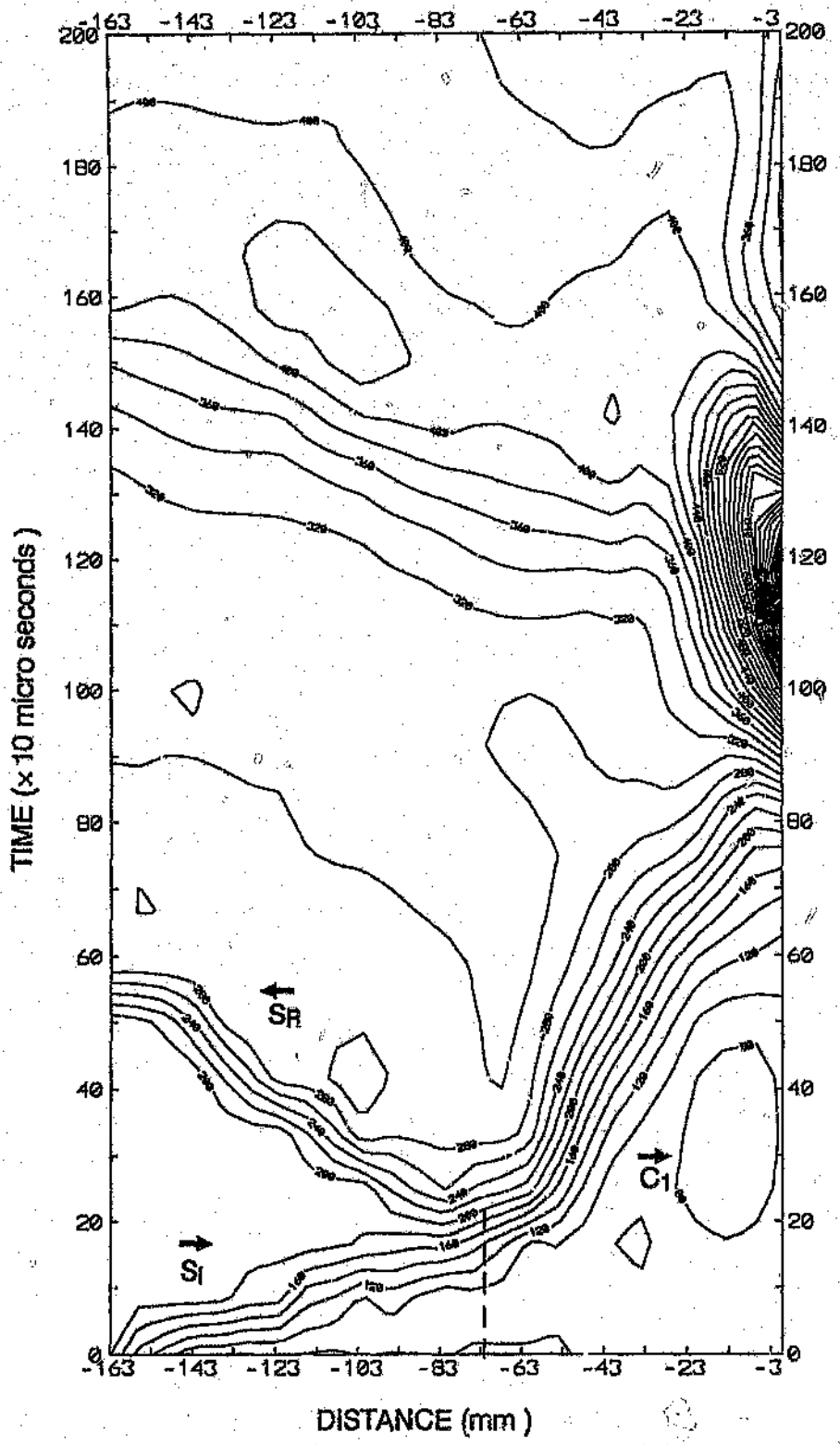


Figure 5.11 Pressure contour plot, 70 mm of polyether foam, incident shock wave Mach number 1.4

Tests were run on another foam, namely a polyester foam having a density of 38 kg/m^3. The tests were carried out using the same initial Mach number as the previous foam. A full set of pressure traces over the entire test section were obtained. These may be found in appendix C. The pressure traces are very similar to those for the polyether foam. The only large difference was the peak pressure recorded behind the foam, at 1200 KPa.

The pressure traces were combined to obtain a pressure contour plot. (figure 5.12). The initial position of the front face of the foam is represented by a dotted line. The waves and wave interactions are basically the same as the previous foam. The reflected shock wave Mach number is 1.180. Once again more information regarding the foam movement is required before a detailed explanation of exactly what is physically happening may be made.

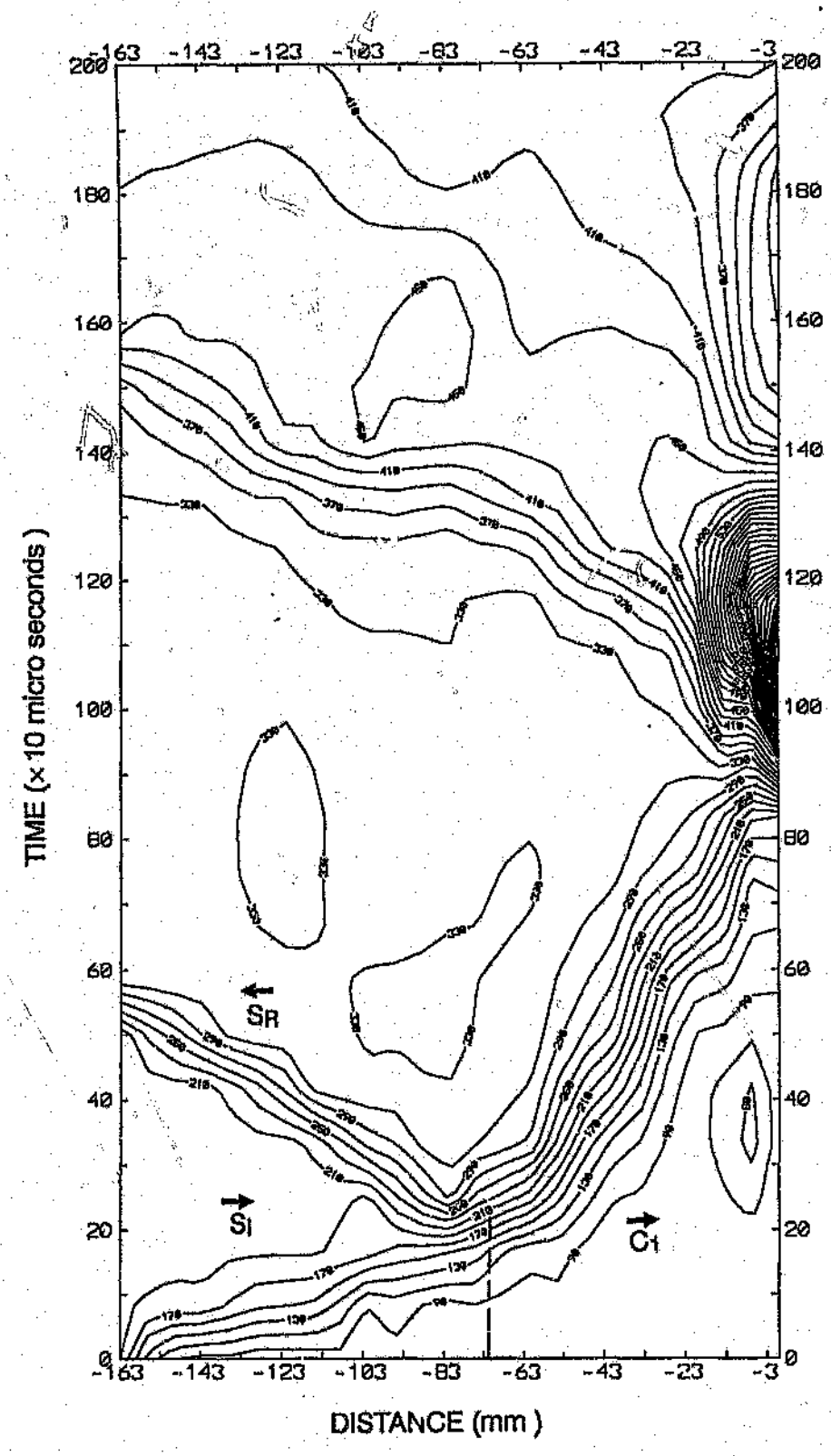


Figure 5.12 Pressure contour plot, 70 mm of polyester foam, incident shock wave Mach number 1.4

5.1.1 Reflected Shock Wave

Two transducers were located in the expansion chamber of the shock tube, upstream of the test section. These transducers were primarily used to accurately calculate the speed of the incident and reflected waves. This was done by determining the time taken for the shock waves to travel between the two transducers.

The rate at which data can be recorded by the Computerscope data acquisition system is dependent on the number of data channels being recorded. Thus to obtain the most accurate calculation of the speed of the shock waves, only the two transducers in the expansion chamber were linked to the portable Computerscope. This gave a maximum sample rate of 500 kHz.

The pressure variation recorded by the two transducers located in the expansion chamber (positioned 620.5 mm apart) during the interaction of a shock wave having a Mach number of 1.426 and 70 mm of polyether foam is shown in figure 5.13 (File F1A1511F). It must be noted that the zero time datum used for the graphs of the pressure variation from the two transducers in the expansion chamber is not the same as the one used throughout the rest of the report.

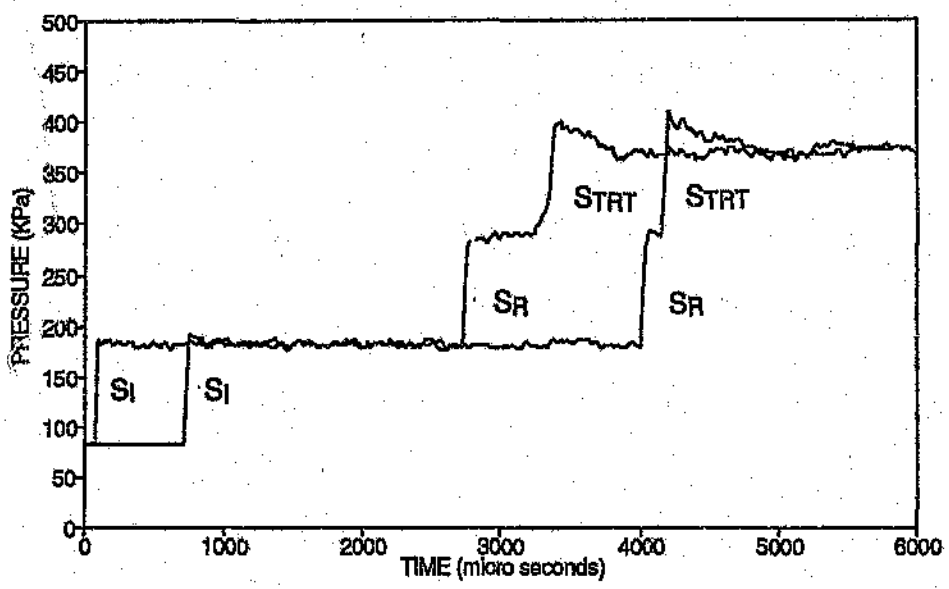


Figure 5.13 Pressure variation in the expansion chamber 70 mm of polyether foam, incident shock wave Mach number 1.426

Analyzing the first curve in figure 5.13 it can be seen that the first rise in pressure is as a result of the incident shock wave passing the transducer. The second rise in pressure is the shock wave that was reflected from the front face of the foam. Recalling figure 5.3 which was the pressure variation in the test section for the same experiment, it can be seen that the compression wave that was recorded in the test section has steepened and now further up the shock tube has become a shock wave.

Comparing the two curves in figure 5.13 it can be deduced that the shock wave S_{TRT}, originally from the compression wave is travelling faster than the the shock wave S_R which was reflected from the front face of the foam, which in fact must be the case since a shock wave travels at subsonic speed relative to the gas behind it and at supersonic speed relative to the gas ahead of it. Further up the shock tube the shock wave S_{TRT} will interact with the shock wave S_R.

Figure 5.14 is the pressure variation recorded by the transducers in the expansion chamber for the interaction of an incident shock wave having a Mach number of 1.426 and 70 mm of polyester foam.(File F2A1501H) This pressure trace exhibits the same characteristics as the trace for the shock wave interacting with the polyether foam.

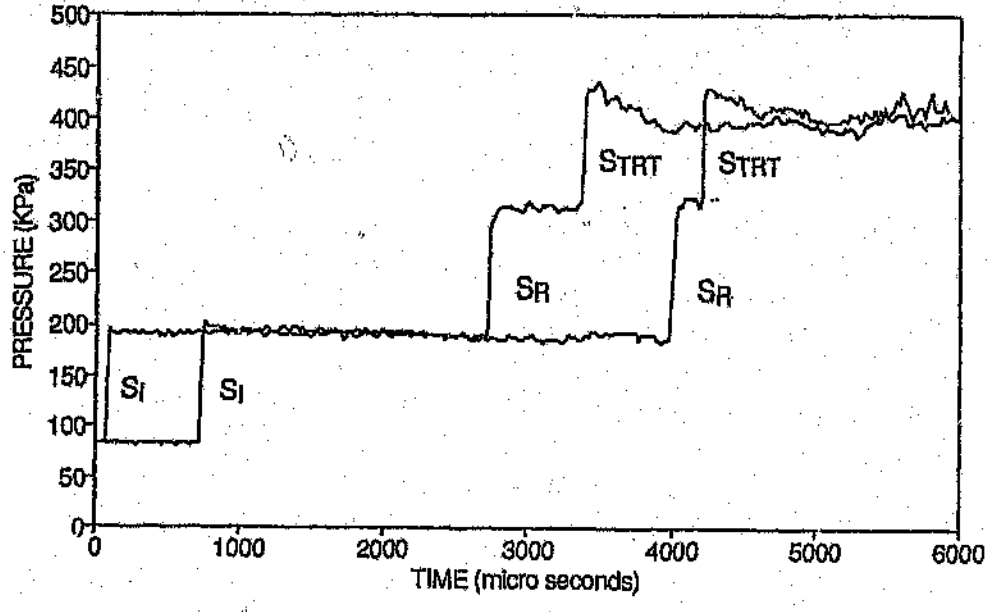


Figure 5.14 Pressure variation in the expansion chamber 70 mm of polyester foam, incident shock wave Mach number 1.426

Figure 5.15 is the interaction of a shock wave having a Mach number of 1.429 and 70 mm of polyether foam. (F1A1511E) The shock waves are propagating faster than the waves in figure 5.15 and the transducer (T12) records the results of the S_{TRT} shock overtaking the S_R shock wave.

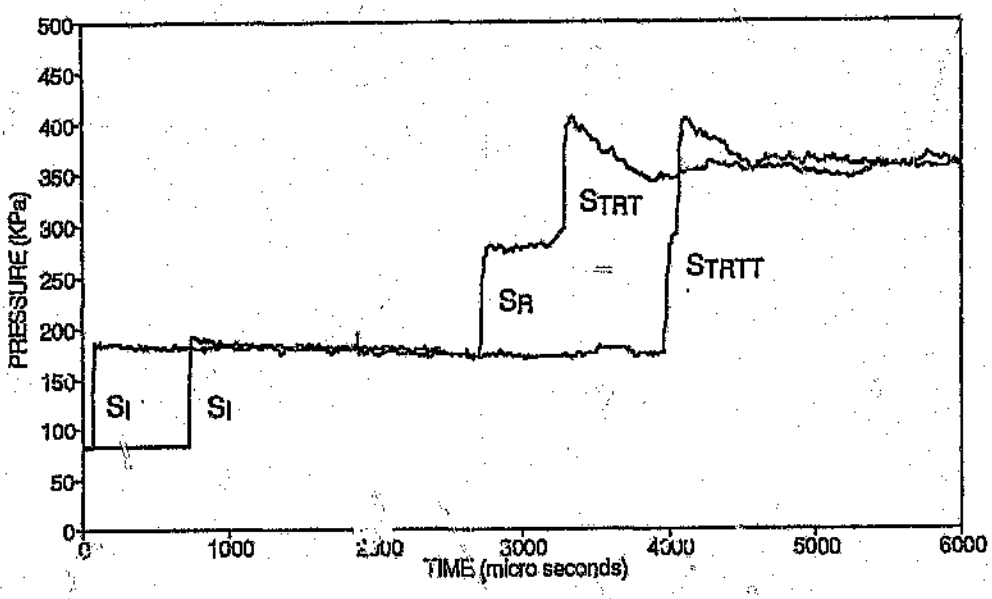


Figure 5.15 Pressure variation in the expansion chamber 70 mm of Polyether foam, incident shock wave Mach number 1.449

The shock wave overtaking and the position of transducers T11 and T12 are shown in the figure 5.16. Shock wave S_{TRT} overtakes S_R and a transmitted shock wave S_{TRTT} is formed, while a centered rarefaction wave R_2 is reflected. S_{TRT}, S_R and S_{TRTT} can clearly be seen in the pressure trace figure 5.15, but the rarefaction wave R_2 is not as easy to locate. There is also a rarefaction wave R_1 arising from the foam interaction which will catch up with S_{TRT}. The effect of R_1 on S_{TRT} is also present in the pressure traces.

For all the tests conducted it was required that the incident shock wave Mach number be kept constant, the required Mach number was taken as 1.426. The majority of the tests were within ± 6 percent of this value. With the present control system for the compression chamber pressure, ± 6 percent was the least practical scatter in the incident shock wave Mach number that could be obtained. Considering that the incident shock wave Mach number could only be measured to within ± 3 percent, a scatter of ± 6 percent is acceptable.

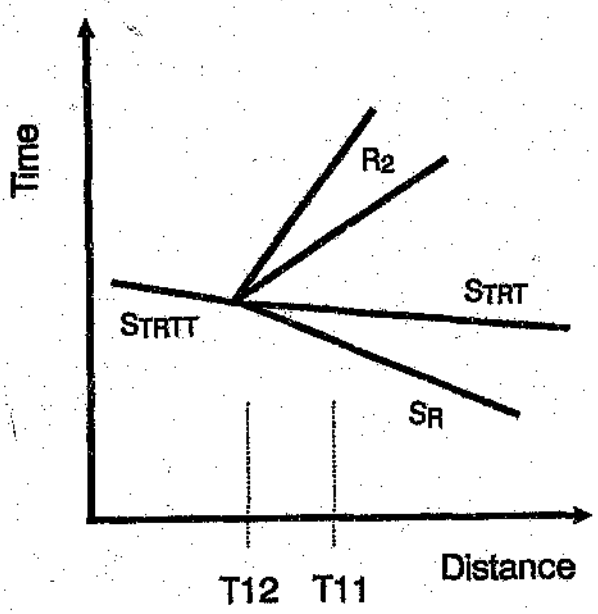


Figure 5.16 Intersection of shock waves

A few tests were outside the ±6 percent range and the results from them were not used to construct the pressure contour plots or for any comparative photographic analysis. To reduce the scatter in the incident shock wave Mach number for different tests a new compression chamber pressure control system and a data recording device, having a sample rate of more than 500 kHz would be required.

Table 5.1 gives the reflected shock wave Mach numbers for the range of incident shock wave Mach numbers that were obtained during the testing of the polyether foam. The results from the testing of the polyester foam are listed in table 5.2

Table 5.1 Reflected shock waves from polyether foam.

File Name	Incident Shock Mach Number (M_S)	Reflected Shock Mach Number (M_{SR})
F1A1511E	1.449	1.192
F1A1603F	1.458	1.199
F1A1502G	1.426	1.180
F1A1511F	1.426	1.172

File Name	Incident Shock Mach Number (M_S)	Reflected Shock Mach Number (M_{SR})
F1A1511E	1.449	1.192
F1A1508F	1.375	1.177
F1A1503E	1.375	1.159

Table 5.2 Reflected shock waves from polyester foam.

File Name	Incident Shock Mach Number (M_S)	Reflected Shock Mach Number (M_{SR})
F2A1523E	1.449	1.198
F2A1549E	1.449	1.204
F2A1501K	1.426	1.180
F2A1525E	1.426	1.178
F2A1547E	1.375	1.168
F2A1551E	1.348	1.164

The variation of the reflected shock wave Mach number with the incident shock wave Mach number is shown in figure 5.17. The scatter band of the incident shock wave Mach number that was considered acceptable for comparative analysis is represented by region A.

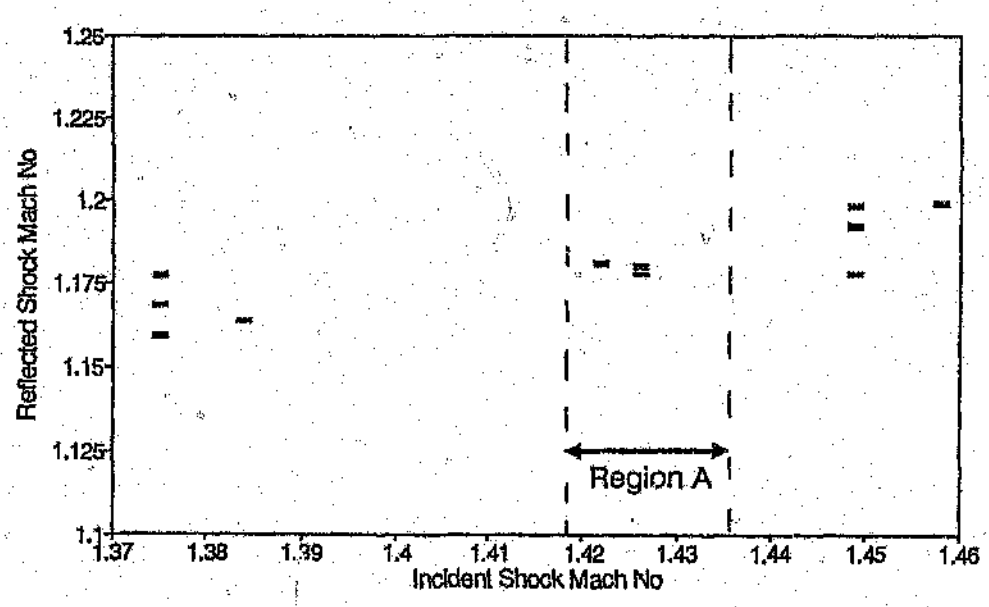


Figure 5.17 Reflected shock wave Mach number variation with incident shock wave Mach number

5.1.2 Rear Wall Pressure

A curious phenomena of the shock wave foam interaction is the high pressure recorded behind the foam, on the solid back plate. The coefficient of pressure increase (R) is defined as the ratio of the maximum pressure recorded behind the foam and the pressure behind a shock wave reflected from a solid wall. The rear wall pressure for the polyether foam and polyester foam are listed in tables 5.3 and 5.4 respectively.

Table 5.3 Rear wall pressure polyether foam

File Name	Incident Shock Mach Number (M_S)	Rear Wall Pressure (P_{III}) (Pa)	Coefficient of Pressure Increase (R)
F1A1537E	1.462	1264400	3.11
F1A1603F	1.457	1224100	3.05
F1A1539E	1.457	1041540	2.6
F1A1511F	1.426	929440	2.52
F1A1502G	1.426	947860	2.57
F1A1502I	1.426	915290	2.48
F1A1536E	1.404	1033800	2.97
F1A1508F	1.375	631050	1.97
F1A1535E	1.343	657200	2.25

Table 5.4 Rear wall pressure polyester foam

File Name	Incident Shock Mach Number (M_S)	Rear Wall Pressure (P_{III}) (Pa)	Coefficient of Pressure Increase (R)
F2A1501K	1.448	1197940	3.06
F2A1502K	1.448	1201940	3.07
F2A1504E	1.444	1183530	3.05
F2A1516E	1.435	1130150	2.99
F2A1502E	1.426	1174450	3.18
F2A1601E	1.426	1059950	2.87
F2A1603E	1.417	1023390	2.84

File Name	Incident Shock Mach Number (M_S)	Rear Wall Pressure (P_{III}) (Pa)	Coefficient of Pressure Increase (R)
F2A1520E	1.366	985490	3.15
F2A1602E	1.362	946520	3.06

Figure 5.18 shows the coefficient of pressure increase variation with incident shock wave Mach number for the polyester and polyether foams. The denser foam generally has a higher coefficient of pressure increase. Due to the small range of incident Mach numbers, little can be said about the coefficient of pressure increase variation with incident Mach number.

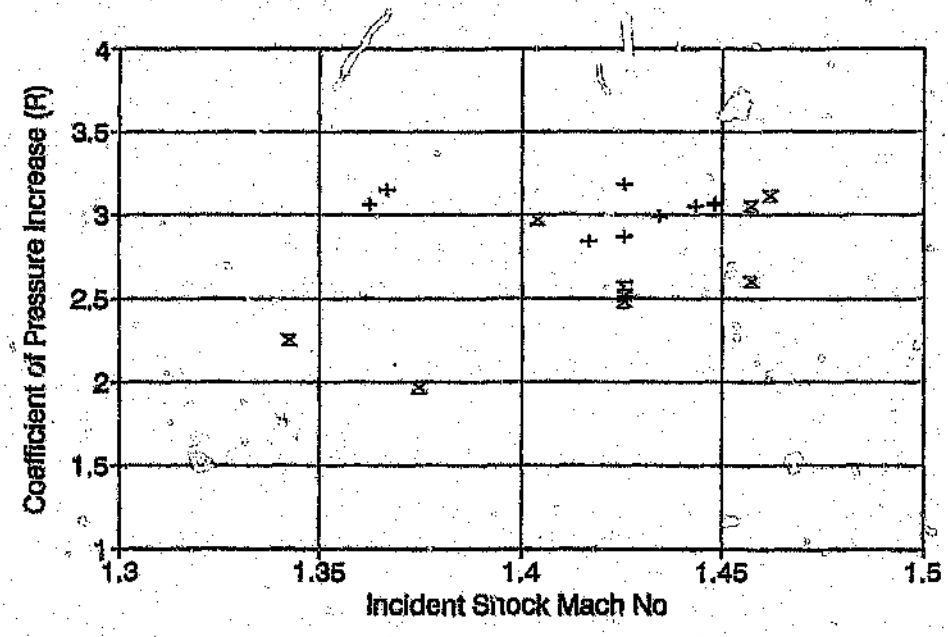


Figure 5.18 Coefficient of pressure increase variation with incident shock wave Mach number

5.2 Schlieren Photographs

This section contains the presentation of the schlieren photographs and the information that was obtained from them, this includes:

- schlieren photographs
- sound wave tracking
- measurement of photographs
- x-t diagram for the foam movement.

To obtain a complete picture of the interaction of a shock wave with a foam material, a full set of schlieren photograph were taken for each foam, starting with the first photograph just before the incident shock wave struck the foam and each successive photograph 60 μs after the previous one, until the foam temporarily comes to rest, before the reflected rarefaction wave generated at the bursting of the diaphragm enters the test section.

The first set of photographs shown are for the interaction of an incident shock wave of Mach number 1.4 with 70 mm of polyether foam having a density of 32.5 kg/m^3.

Plate 5.1 shows the shock wave just before it strikes the foam. It can be seen that the shock is completely planar. Plate 5.2 is after the incident shock wave has struck the foam and now the reflected shock wave can be seen travelling back down the tube. The reflected wave is also planar.

The next photograph plate 5.3 shows a number of other waves present besides the reflected shock wave. These are sound waves, which can be produced when a shock wave passes a protrusion or disturbance on the walls of the shock tube. To ensure that this was the case, and that these waves were not coming from or had anything to do with the foam a program was written, to establish possible sources of disturbances.

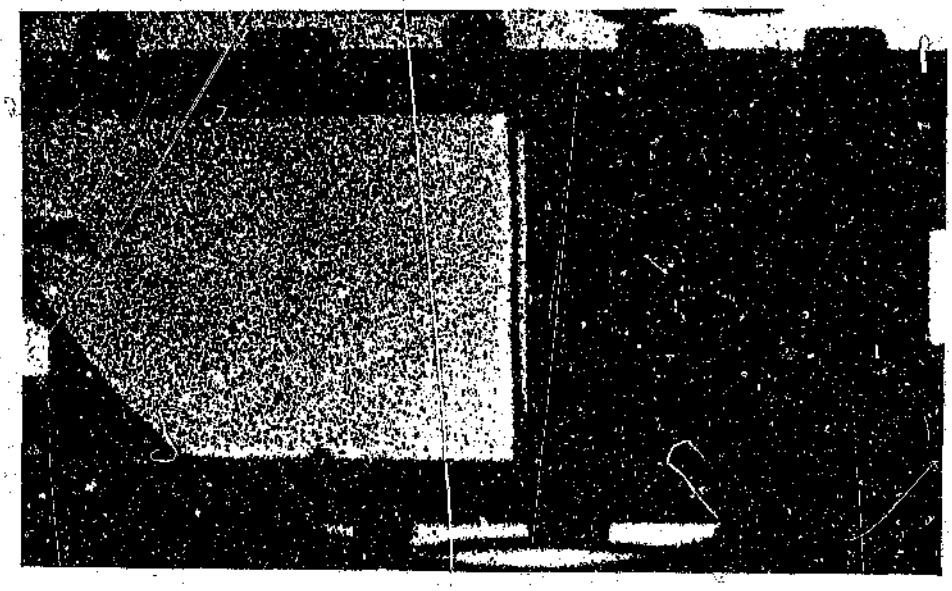


Plate 5.1 Schlieren photograph, polyether foam, density 32.5 kg/m^3, time 195 μs

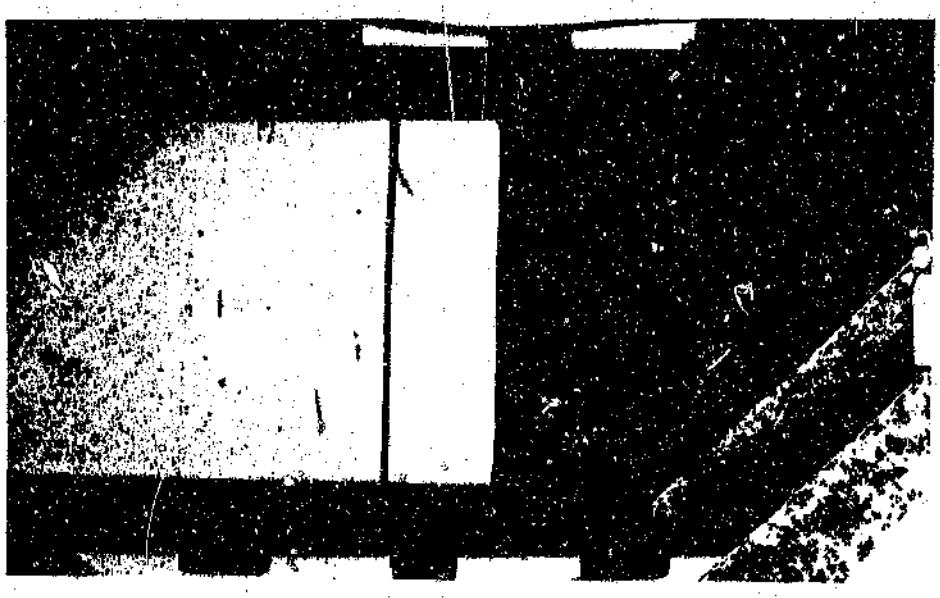


Plate 5.2 Schlieren photograph, polyether foam, density 32.5 kg/m^3, time 261 μs

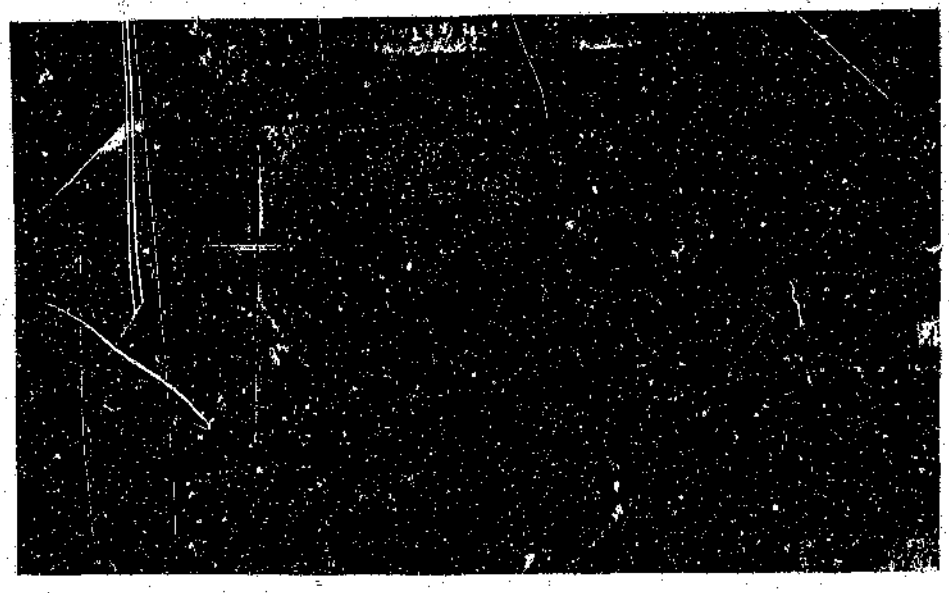


Plate 5.3 Schlieren photograph, polyether foam, density 32.5 kg/m^3, time 380 μs

The program titled "Reflected sound wave propagation" calculates the sound wave pattern as seen in the test section window at a certain time as a result of a disturbance, such as a small step in the joints of the shock tube. A listing and detailed description of the program may be found in appendix E.

To determine what was causing the sound waves in plate 5.3 the program requires the following information:

- Incident shock wave Mach number - 1.4
- pressure ahead of the incident shock - 82550 Pa
- temperature ahead of the incident shock - 301 K
- time the photograph was taken - 380 μS
- number of vertical grid points - 11.

Figure 5.19 shows the sound wave pattern obtained from the program as a result of a disturbance, namely a flange joining two sections of the shock tube. The sound waves are of the same shape and in the same position as the ones in the photograph. The flange was loosened and realigned, which removed the disturbance and thus the sound wave from later photographs. Other disturbances were found but not all could be removed, most were as a result of slight inaccuracies in the manufactured components.

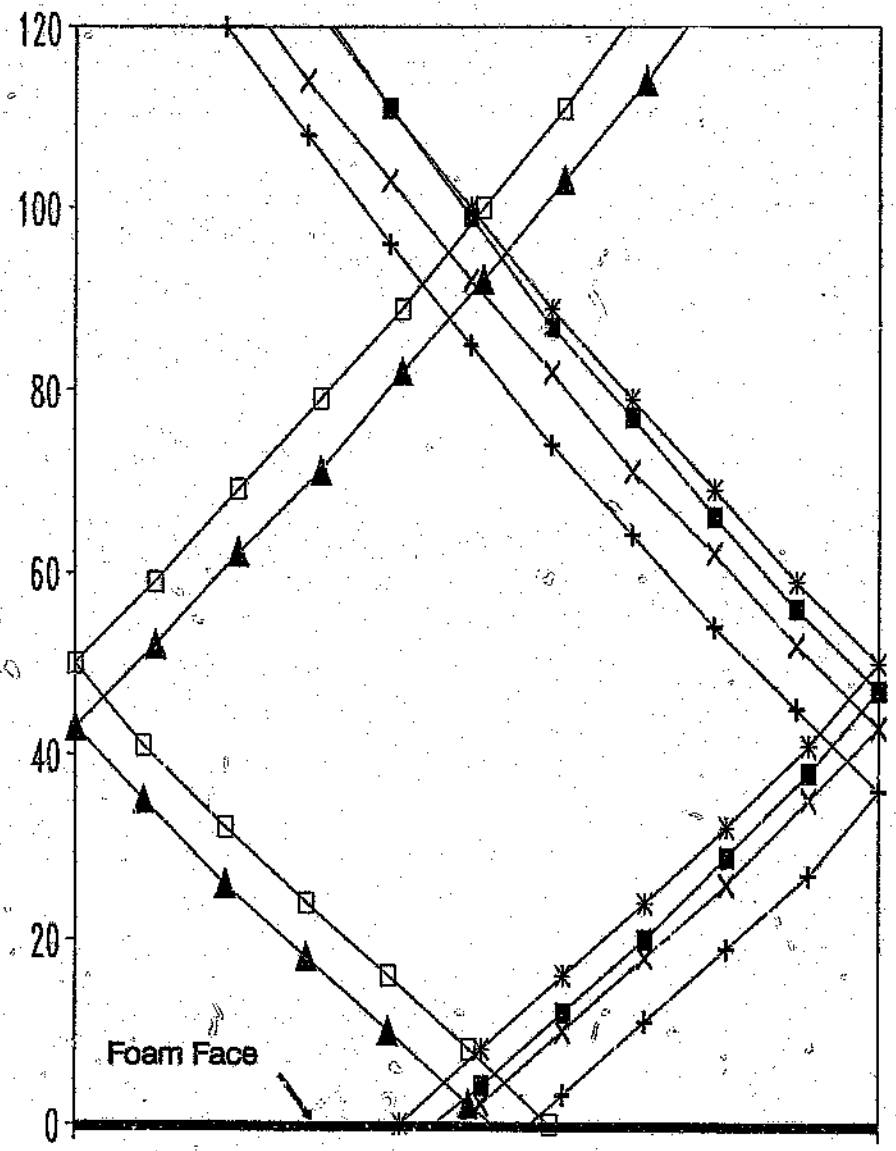


Figure 5.19 Sound wave pattern

In future photographs in which it was unclear if the waves were sound waves caused by disturbances in the shock tube, the program Reflected Sound Wave Propagation was used to clarify this.

Plate 5.4 was taken at 1100 μs, the foam has almost reached its maximum compression, but still there is no sign of gas escaping from the foam. There are slight bulges of foam at the corners, which brings up the question of the one dimensionality of the experiment. This question is dealt with in section 5.6

The next photograph (Plate 5.5) taken 60 μs after the previous one, shows the first sign of gas coming out of the foam. The foam is still being compressed.

Plate 5.6, taken at 1340 μs shows the emergence of a wave or gas front, which for now will be referred to as a surface discontinuity. The surface discontinuity does not touch the walls of the shock tube, but rather curls around on itself next to the wall. The gas front is continuing to move.

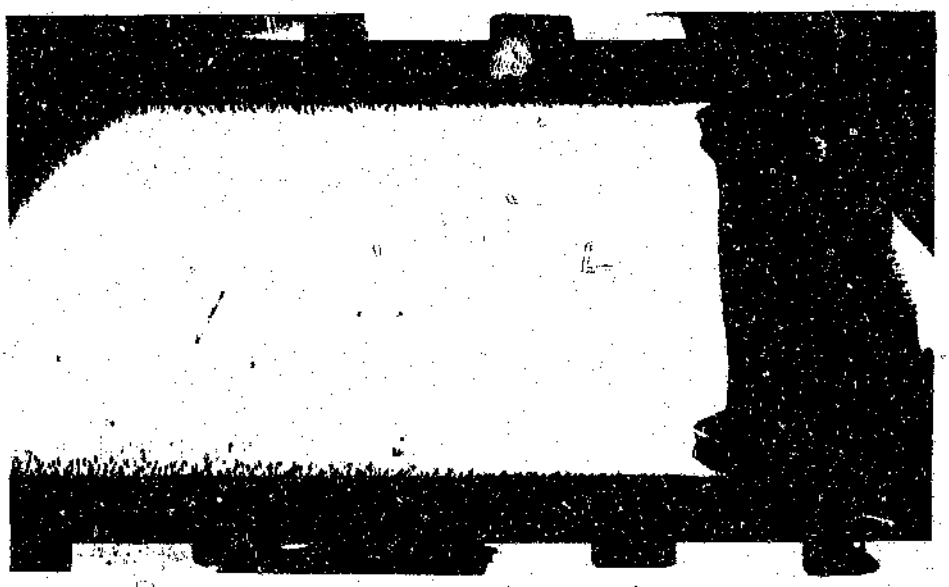


Plate 5.4 Schlieren photograph, polyether foam, density 32.5 kg/m^3, time 1100 μs

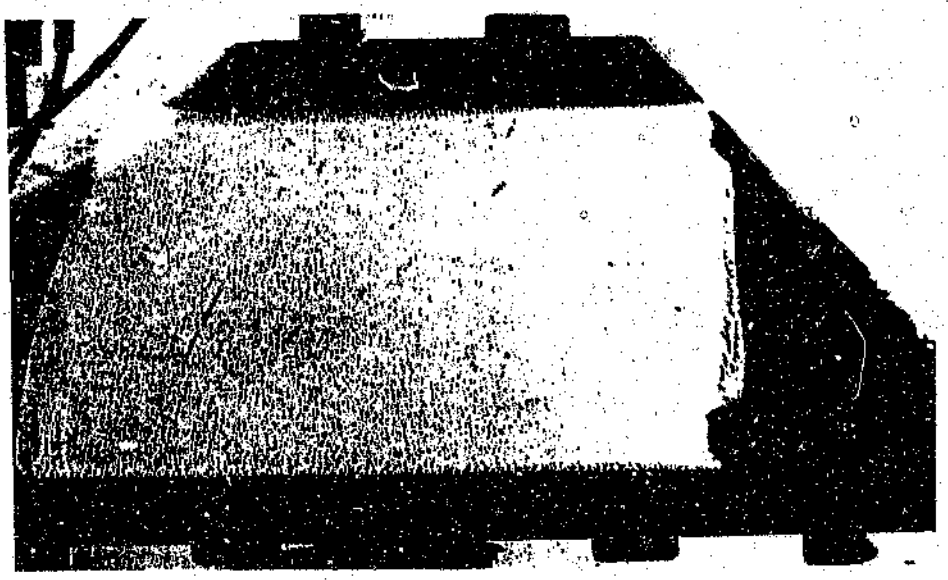


Plate 5.5 Schlieren photograph, polyether foam, density 32.5 kg/m^3, time 1160 μs

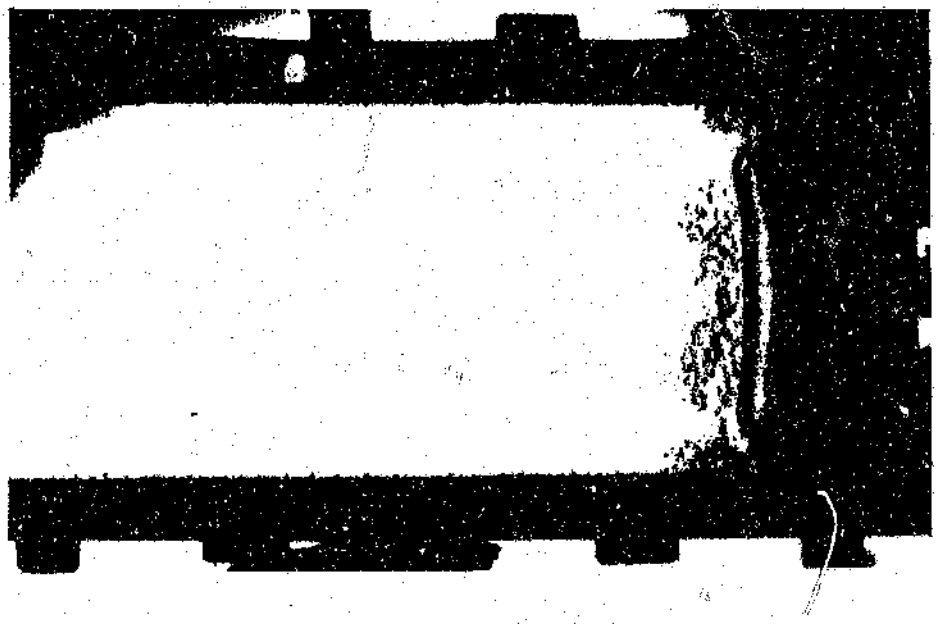


Plate 5.6 Schlieren photograph, polyether foam, density 32.5 kg/m^3, time 1340 μs

Plate 5.7 taken at 1580 μs confirms that the surface discontinuity and gas front are remaining stationary.

At the time plate 5.8 was taken (1880 μs) the surface discontinuity had disappeared. The foam has now also come to rest.

Plates 5.1 to 5.8 are selected schlieren photographs which illustrate the different phenomena seen in the interaction of the shock wave with the foam. The complete set of photographs may be seen in appendix F.

The schlieren photographs for the intersection of a shock wave and polyester foam are shown in appendix F.

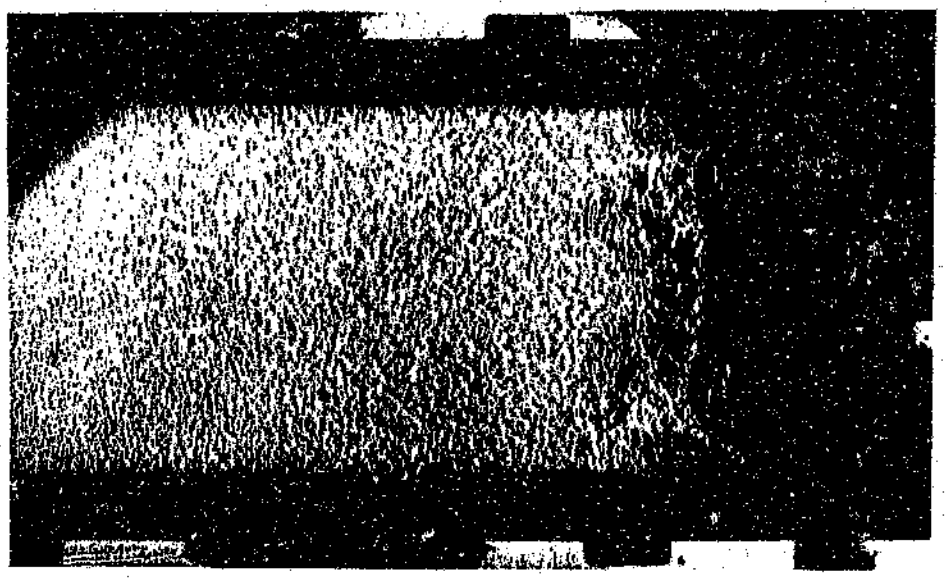


Plate 5.7 Schlieren photograph, polyether foam, density 32.5 kg/m^3, time 1580 μs

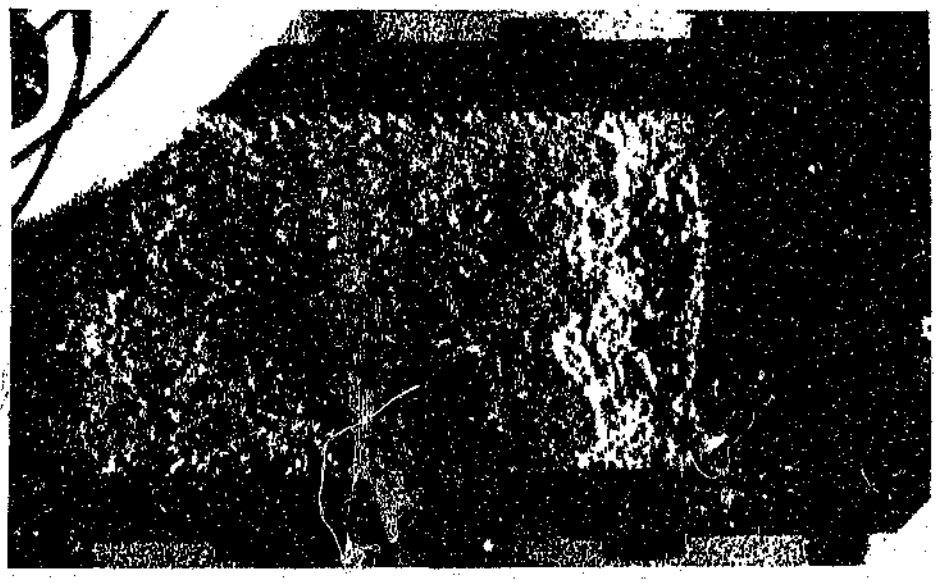


Plate 5.8 Schlieren photograph, polyether foam, density 32.5 kg/m^3, time 1880 μs

The position of the shock waves, foam, gas front and surface discontinuity were measured for each photograph. An enlarger which projected the image of the negative on to a ground glass screen, having a cartesian vernier system was used to measure the photographs.

A program was written which converted the data obtained from the cartesian vernier system to the distance between the phenomena and the back plate of the shock tube. The listing and detailed description of the program titled "Photograph Conversion" is given in Appendix D.

Figure 5.20 shows the typical points that were chosen to represent the different phenomenon in the photographs. Five points along the foam front, contact surface and gas front, and three points on the shock waves were measured. The points measured for the foam position did not include any close to the walls, thus only measuring the one dimensional effect of the foam front.

Once the measured photographic data had been converted using the Photograph Conversion program, the points representing each phenomena were averaged to obtain one point. These results for both foams may be found in table 5.5.

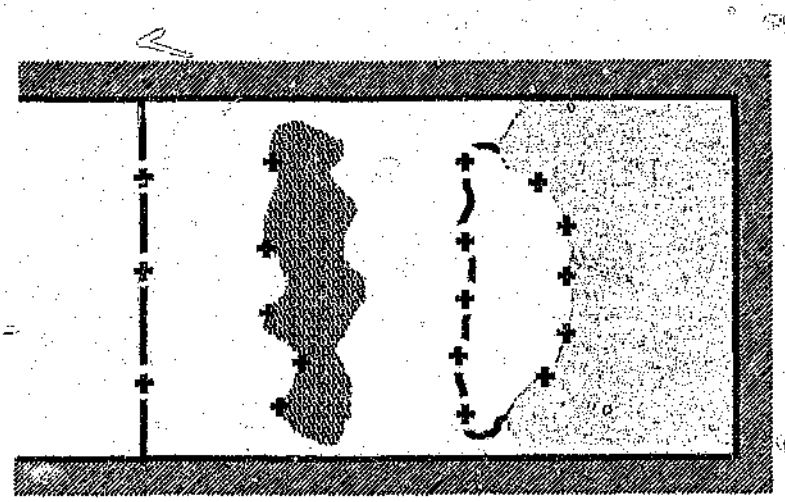


Figure 5.20 Photograph measurement

Table 5.5 Foam and gas motion

Time (μS)	Polyether Foam (mm)			Polyester Foam (mm)		
	Foam	Gas Front	Contact Surface	Foam	Gas Front	Contact Surface
0	70.0			70.0		
200	70.0			70.0		
380	67.4			61.5		
440	64.3			60.2		
500	62.2			55.7		
560	57.6			55.0		
620	53.6			51.6		
680	49.9			50.2		
740	48.2			45.6		
800	42.1			46.4		
860	39.1			34.5		
920	35.3			32.4		
980	32.5			28.8		
1040	27.1			27.4		

Table 5.5 (Cont.) Foam and gas motion

Time (μS)	Polyether Foam (mm)			Polyester Foam (mm)		
	Foam	Gas Front	Contact Surface	Foam	Gas Front	Contact Surface
1100	29.5			23.6		
1160	23.2	26.8		23.5		
1220	22.1	29.0		19.9		
1280	15.4	30.4	20.6	18.6	17.7	
1340	16.0	36.8	23.7	13.4	31.2	21.3
1400	17.5	39.3	25.8	16.6	36.2	20.9
1460	20.8	45.9	28.6	20.5	38.9	23.1
1520	18.8	45.1	27.8	21.2	42.8	26.1
1580	21.6	49.2	30.2	22.7	44.5	26.8
1640	21.9	49.8	29.9	25.8	46.8	28.7
1700	26.3	54.3	33.4	27.1	46.6	29.6
1760	25.6	53.4	32.7	28.7	53.4	32.7
1820	27.9	55.4	32.9	27.7	52.8	
1880	28.3	57.4		28.1	52.5	
1940	30.4	57.1		28.4	52.5	
2000	28.7	56.1		29.0	54.0	
2060	30.0	56.3		28.9	52.6	
2120	30.6	60.7		29.1	53.9	
2180	31.6	54.2		29.2	54.1	
2240	30.7	55.3		30.6	57.5	
2300	30.1	57.6				
2360	31.0	56.8				
2420	31.4	56.4				
2480	29.9	57.1				
2540	31.2	56.7				
2600	32.1	56.3				
2660	31.7	56.0				
2720	31.1	58.7				

It must be noted that depending upon which way the foam front is moving the photograph shows different sections of the foam. In figure 5.21 (a) the foam is being compressed and due to the friction on the walls the centre of the foam (dotted line) is compressed further than the side (solid line). Thus from a photograph the position of the side of the foam would be measured. However if the foam were expanding (figure 5.21 (b) the reverse would be true and the position of the centre of the foam would be measured from a photograph. It has been assumed that this effect will not greatly affect the accuracy of the movement of the foam front and no attempt has been made to compensate for this effect. It can be seen from the photographs taken when the foam is expanding that the bulge in the center is small, which adds confidence to the validity of the assumption.

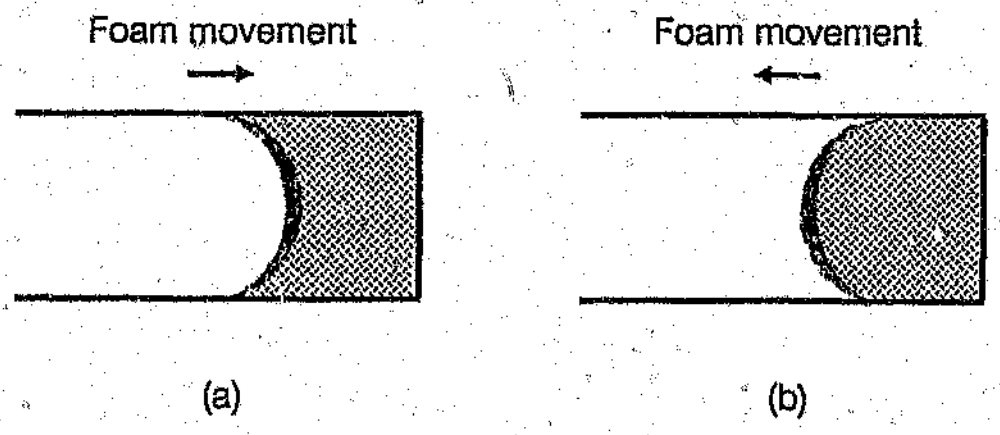


Figure 5.21 Foam face movement

Figure 5.22 is a distance time graph for the movement of the front face of the polyether foam. The motion of the contact surface and gas front are also shown. The incident shock wave struck the foam at 200 μs then after the initial foam acceleration the foam front compresses at a constant velocity.

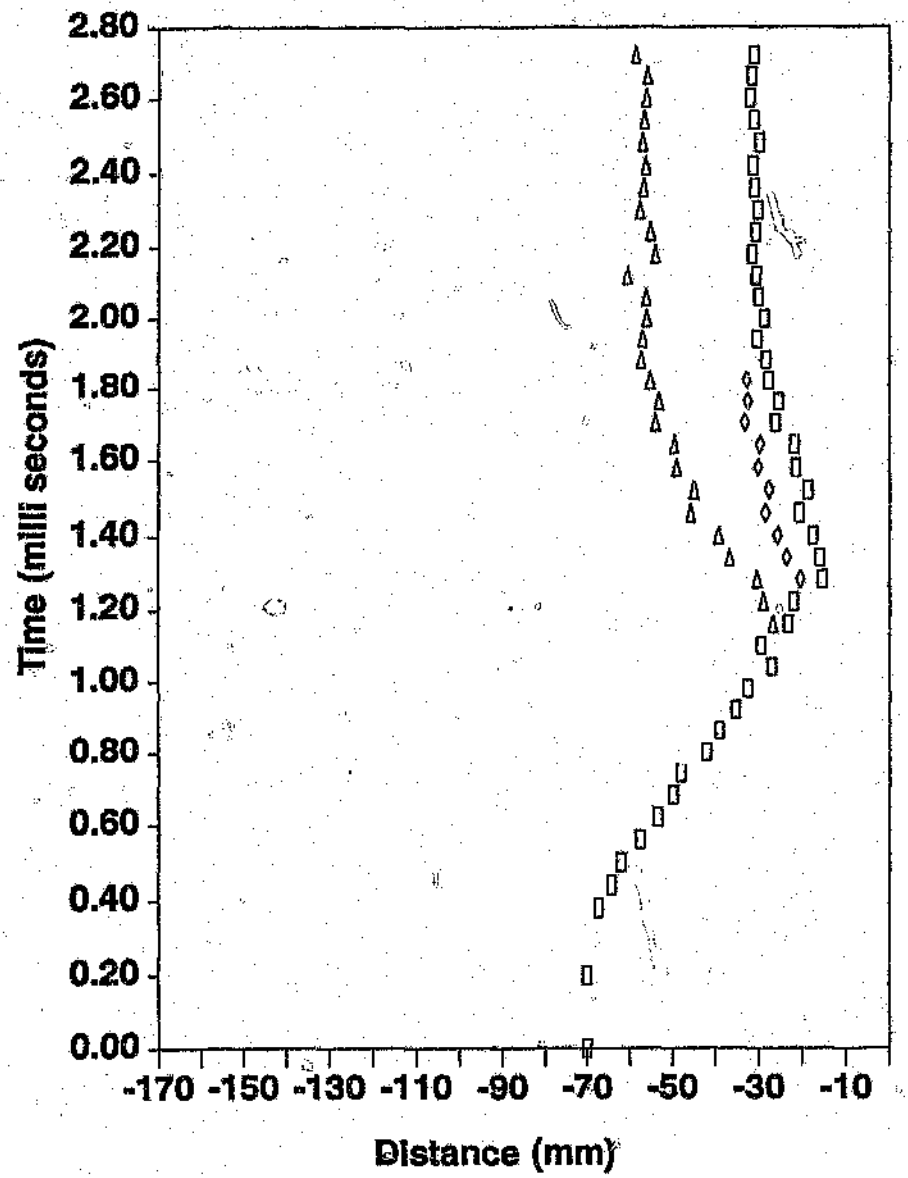


Figure 5.22 Motion of polyether foam (square - foam, triangle - gas, diamond - contact surface)

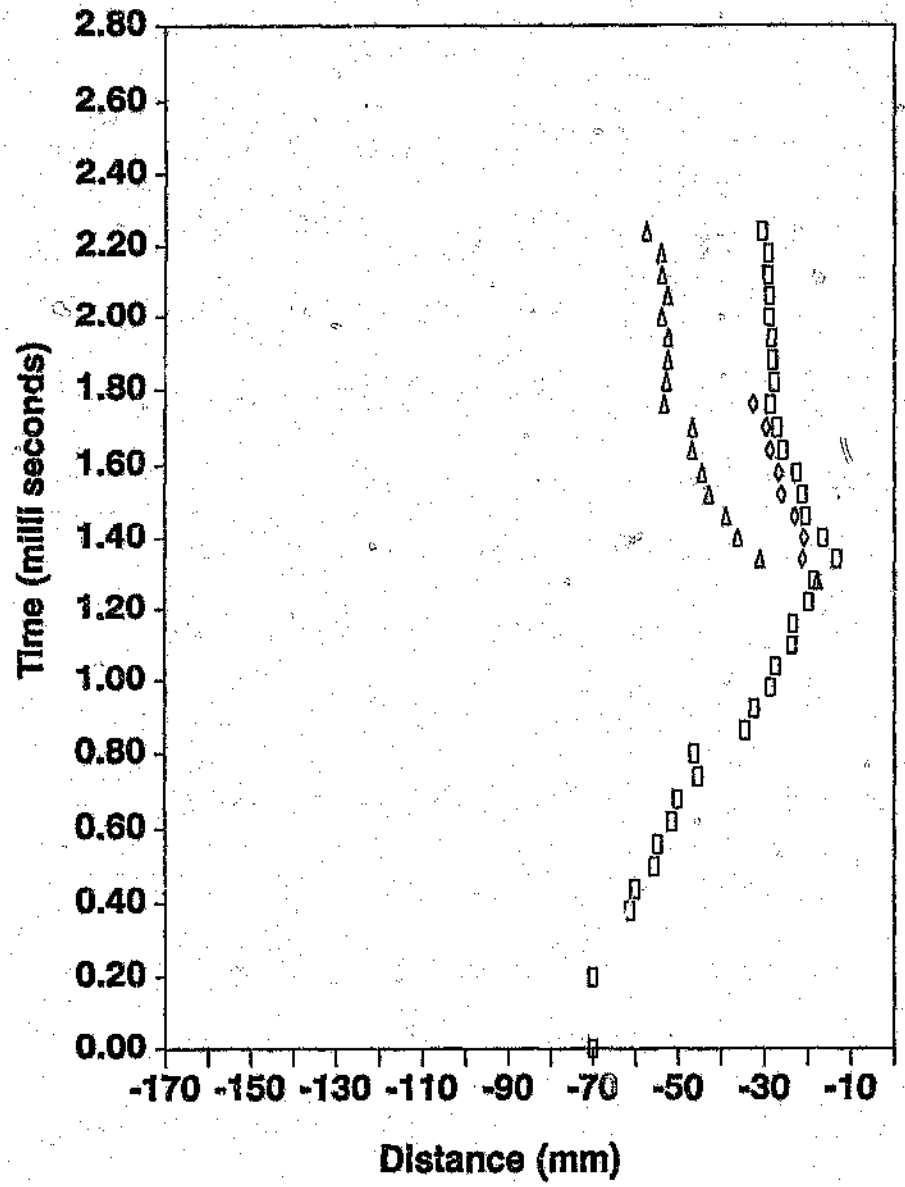


Figure 5.23 Motion of polyester foam (square - foam, triangle - gas, diamond - contact surface)

5.3 Path Photographs

This section contains the path photographs and the information that was obtained from them, this includes:

- path photographs
- measurement of photographs.
- particle paths

To determine how the foam moved as it was being compressed path photographs of the foam were taken. A series of diagonal lines forming squares were drawn on the foam using a silver metallic pen. The argon jet light sources were used to illuminate the foam, while the shutter of a 35 mm camera was left open and the photograph taken.

Certain modifications were made to the argon jet light sources and all five were flashed simultaneously, to obtain sufficient light for the photographs. A detailed description of the experimental layout is given in section 4.2. Since all five light sources had to be triggered at once, only one photograph could be obtained per test.

Full sets of path photographs were taken for both foams. The photographs were taken at the same time as the schlieren photographs, (60 μs interval) to allow a direct comparison between the results obtained.

The following six photographs are part of the set taken during tests on 70 mm of polyester foam having a density of 38 kg/m^3. The incident shock wave Mach number is once again 1.4

Plate 5.9 was taken before the incident shock wave struck the foam. The position of the diagonal lines when the foam is not loaded may be seen.

In plate 5.10, taken at 440 μs the foam has been compressed to 61mm. From the position of the intersection points of the lines and the distortion of the squares, the location of a wave travelling in the foam may be seen. Only the front section of the foam is compressed indicating that the foam is not compressed uniformly.

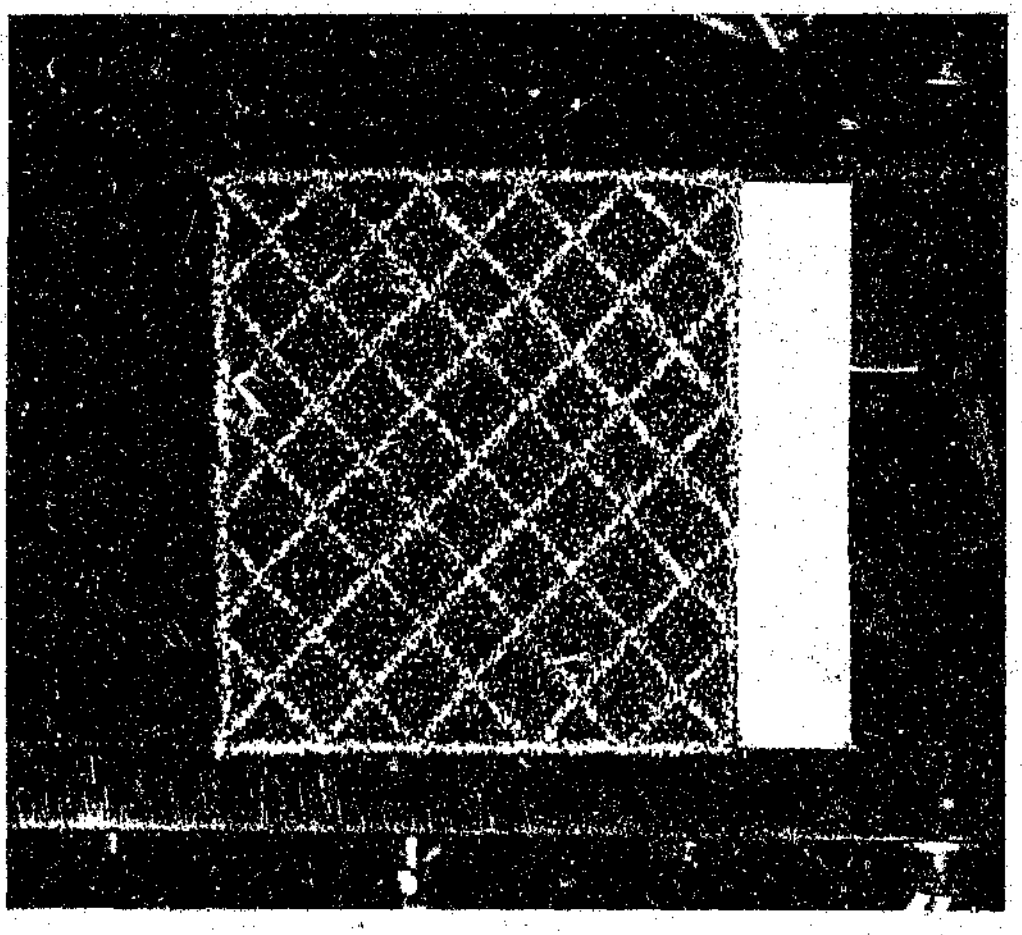


Plate 5.9 Path photograph,polyester foam, density 38 kg/m^3, time 0 μs

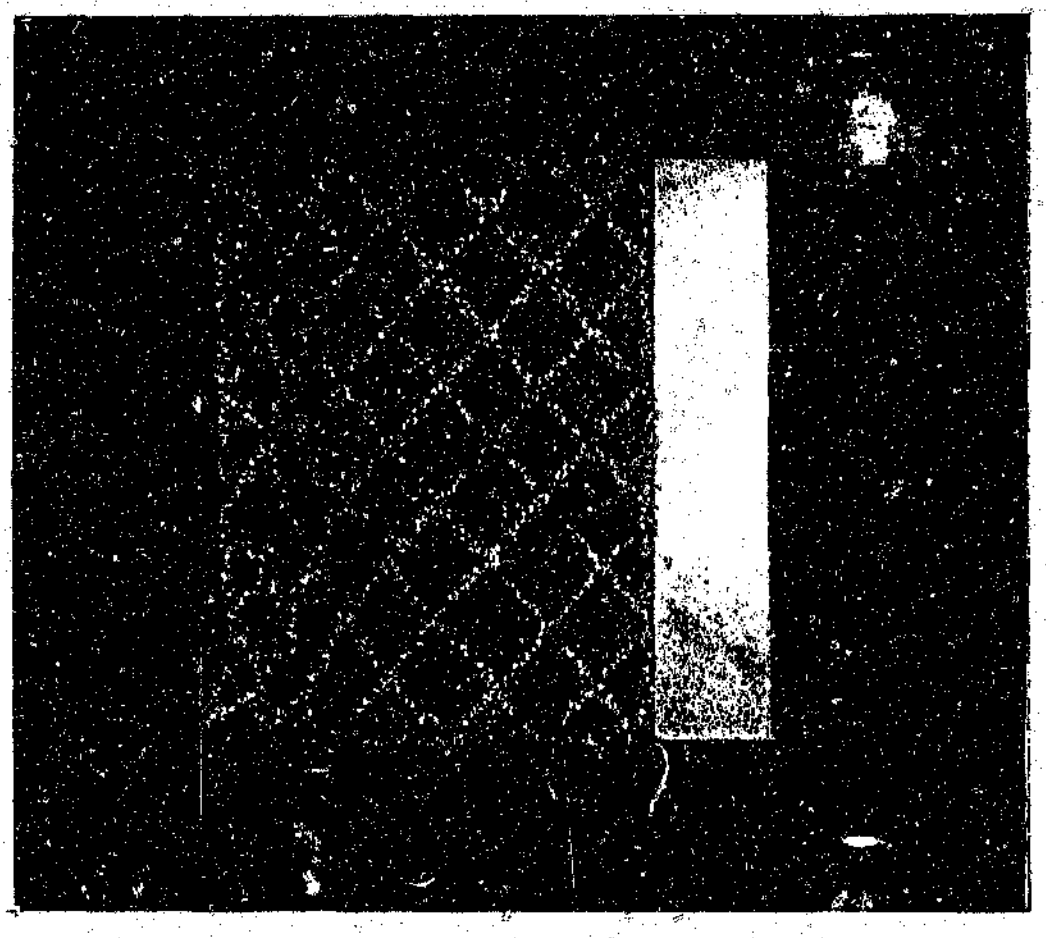


Plate 5.10 Path photograph,polyester foam, density 38 kg/m^3, time 440 μs

Plate 5.11 was taken at 800 μs, the foam length being 41 mm. The wave in the foam can clearly be seen, located in the center of the reduced foam length. The front of the foam has began to expand again. The rear half of the foam has not yet been affected, confirming that the foam is not compressed uniformly.

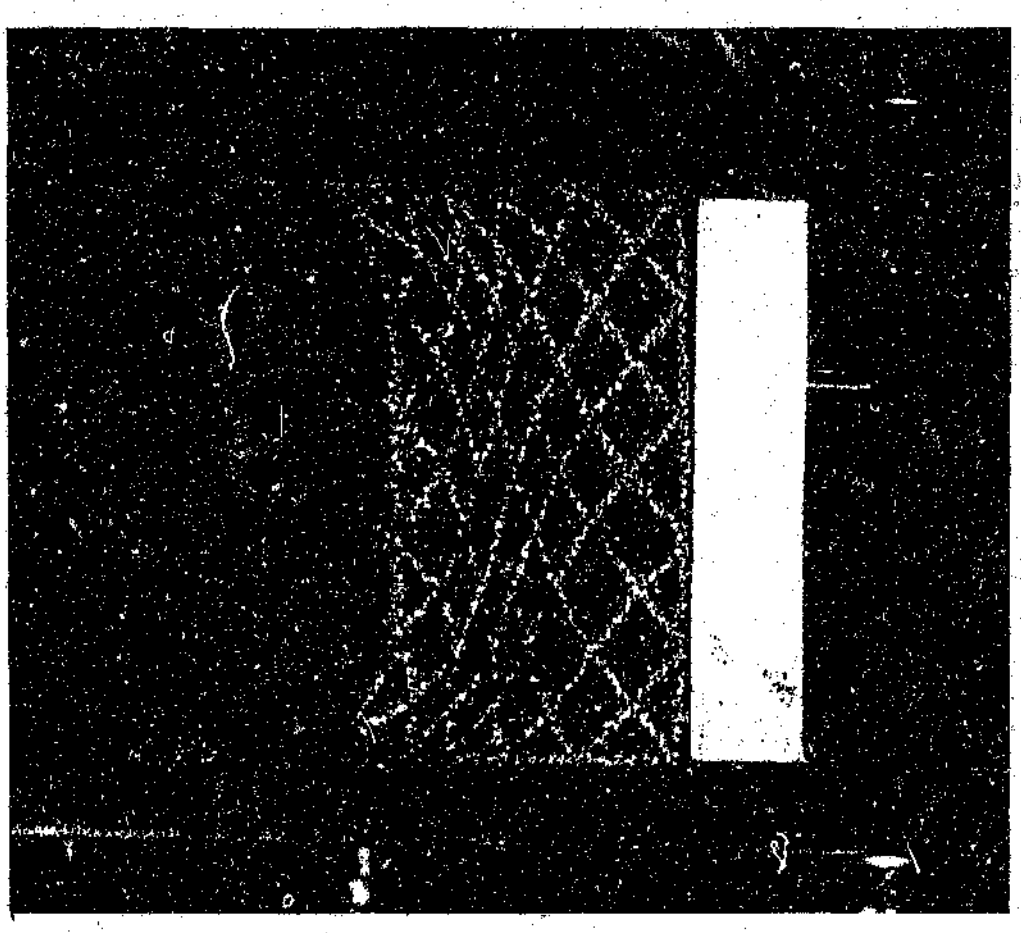


Plate 5.11 Path photograph,polyester foam, density 38 kg/m^3, time 800 μs

Plate 5.12 taken at 1040 μs shows the foam compressed to a length of 27 mm. The wave has travelled right through the foam. The two dimensional corner effects have become noticeable as the foam lifts of the wall. This is the last photograph that results could be measured from as after this the lines became indistinct. It must be noted that the centre section of the front face of the foam is essentially plane.

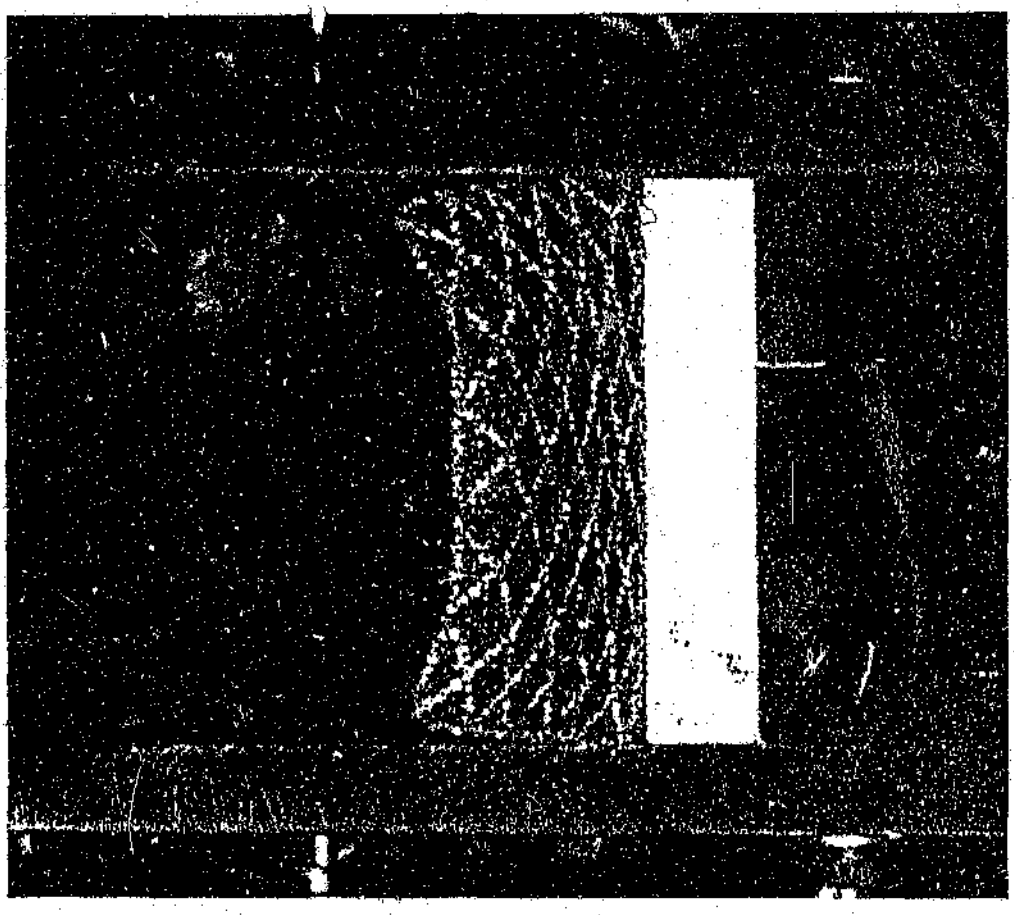


Plate 5.12 Path photograph,polyester foam, density 38 kg/m^3, time1040 μs

Plate 5.13, taken at 1400 μs, the foam passed its maximum compression and is now expanding. The difference between the centre and the side of the foam can clearly be seen, resulting from the two dimensional effects, which once again have been ignored. A full set of path photographs may be seen on the contact prints shown in Appendix G.

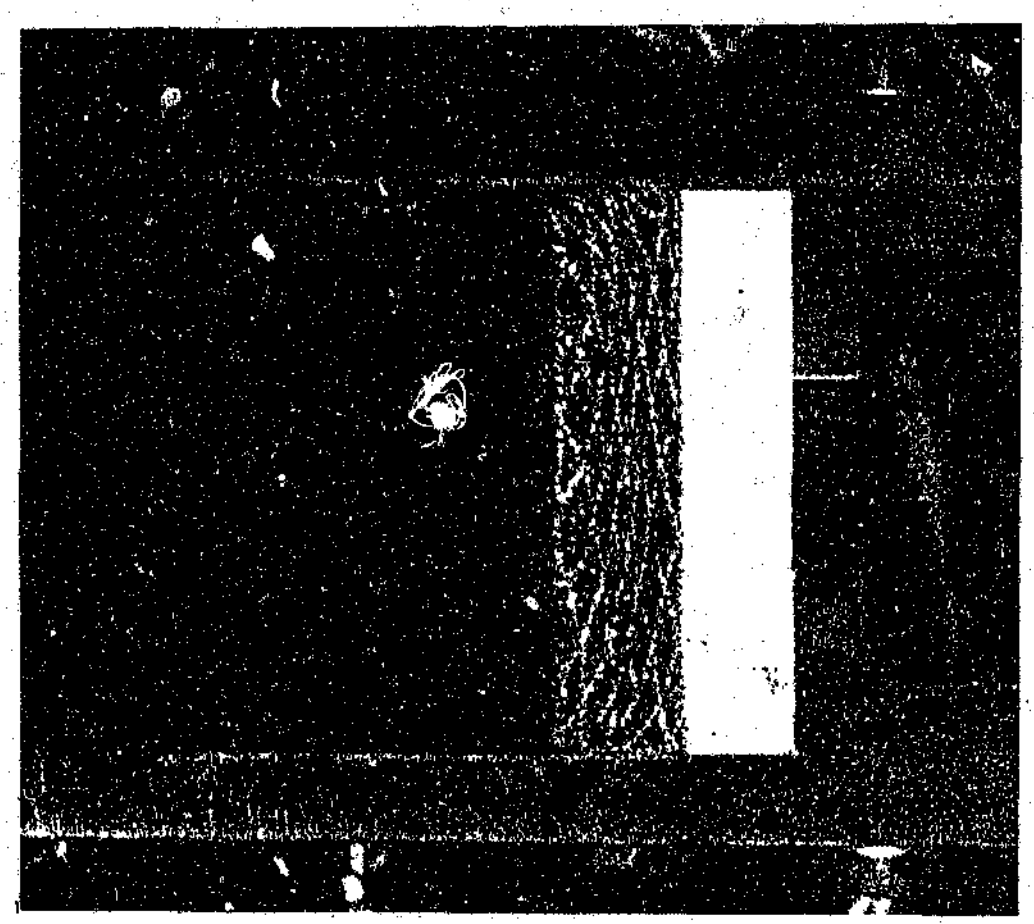


Plate 5.13 Path photograph,polyester foam, density 38 kg/m^3, time1400 μs

Plate 5.14 is a photograph taken at 440 μs during the testing of the polyether foam, having a density of 32.5 kg/m^3, the incident Mach number being 1.4. The wave in the foam can again be seen and all the basic phenomena that have occurred with the previous foam occur with this one. A contact print of the full set of path photographs may be seen in Appendix G.

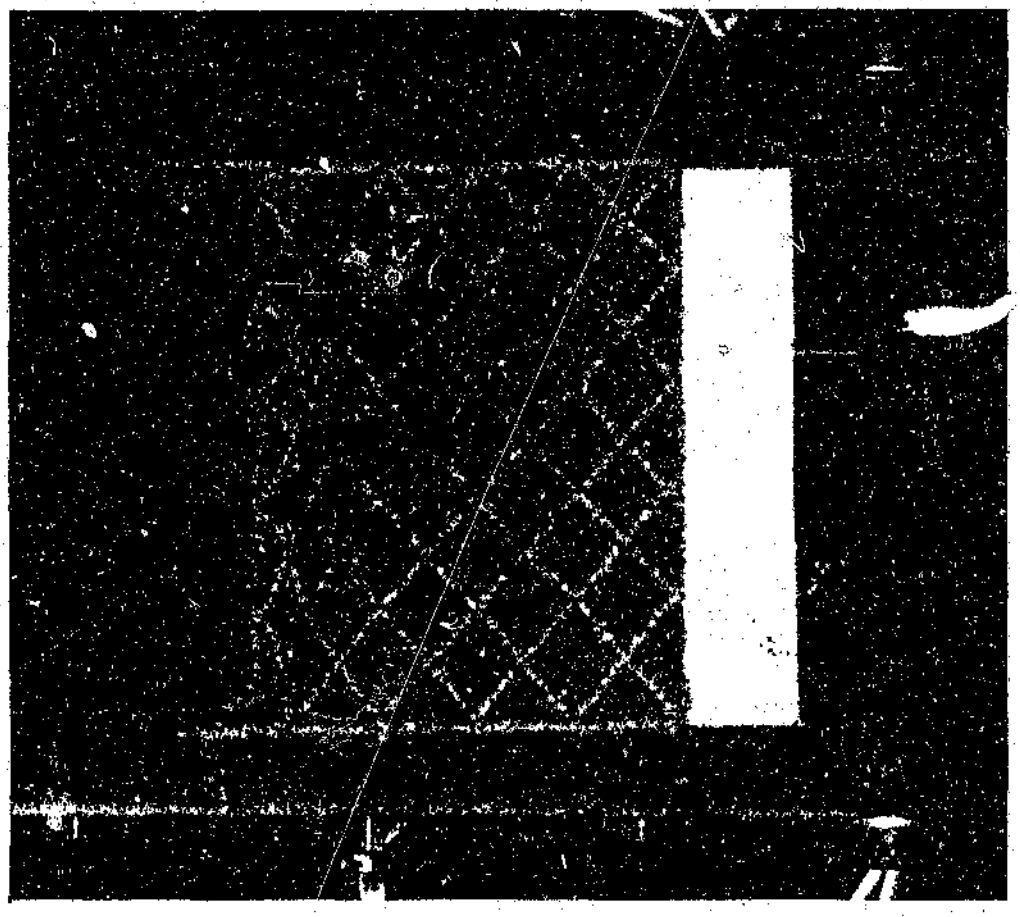


Plate 5.14 Path photograph,polyether foam, density 32.5 kg/m^3, time 440 μs

To ensure that the horizontal motion of the foam was analyzed and the two dimensional corner effects did not influence the results, only the position of certain intersection points were measured.

Figure 5.24 show the diagonal lines drawn on the foam. The inter section points that are circled are the only ones that were measured. The position of each point was measured directly from the print, the data scaled to the correct size and the points in the same vertical plane averaged. Thus from an entire set of photographs the path of ten different particles were tracked, hence the name path photographs.

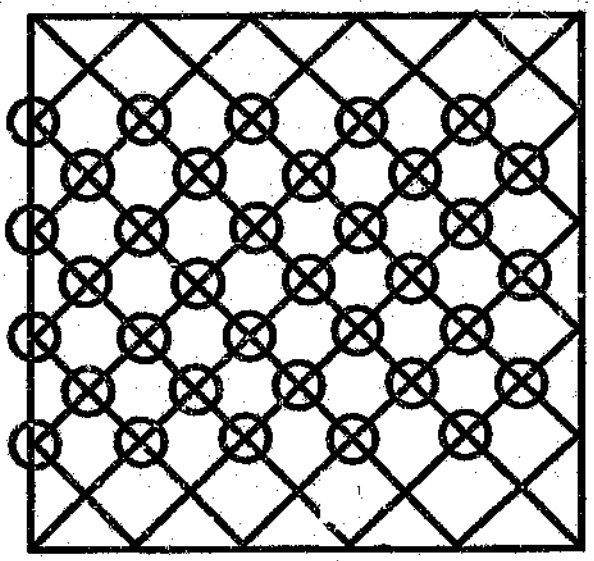


Figure 5.24 Diagonal lines for Path photographs.

5.3.1 Foam Skeleton Wave

Figure 5.25 shows the path of ten particles of polyester foam during the compression stage after the incident shock wave struck the foam. After the initial acceleration the particles travel at constant velocity. The particle paths identify a wave propagating through the skeleton material of the foam.

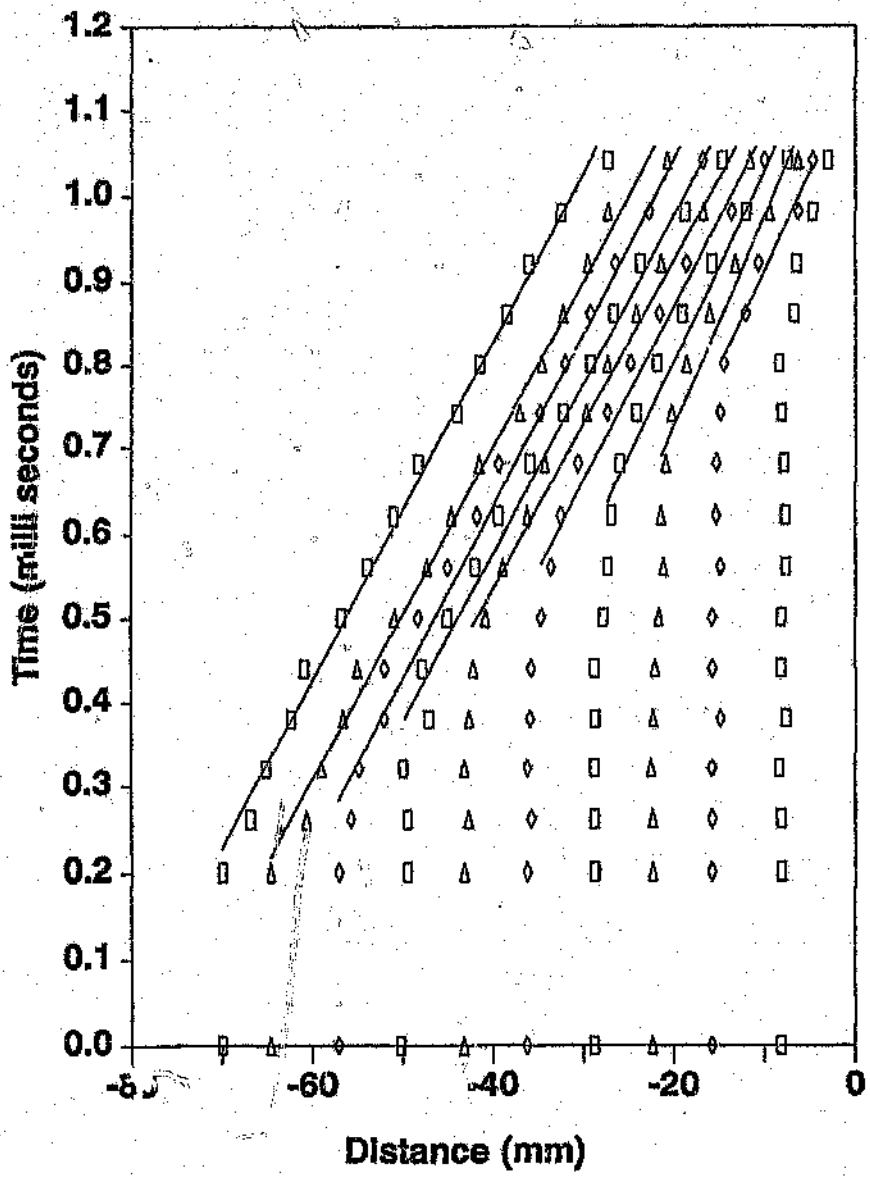


Figure 5.25 Particle paths, polyester foam
38 kg/m^3 M_I = 1.4

To analyses the motion of the particle paths, two straight lines were fitted through each set of particle points. The first straight line (curve A) represents the undisturbed foam. The second curve (curve B) represents the motion of the particle. The equations of the curves representing the particle motion of the foam are in table 5.6.

The intersection of a curve A and a curve B is the point at which that particle of foam begins to move. The intersection point for each group of curves is given in table 5.6.

Table 5.6 Polyester foam particle path equations

x position (mm)	Equation ($y = mx + c$)		Intersection point (μs)
	Slope (m)	Intercept (c)	
-15.8	23.01	1141.1	777.8
-22.3	25.15	1226.2	665.4
-28.8	22.51	1252.0	603.7
-36.2	20.65	1281.5	534.0
-43.2	19.36	1309.9	473.5
-49.5	19.88	1372.7	388.6
-57.2	20.38	1447.1	281.4
-64.6	19.71	1490.0	216.7
-70.0	19.75	1616.4	233.9

Figure 5.26 shows each of the intersection points, through which a straight line has been fitted. This line represents the motion of the wave front in the skeleton of the foam material. The slope of this curve is the velocity of propagation of the wave travelling through the skeleton material. For the polyester foam the wave propagating through the skeleton material at 89 m/s.

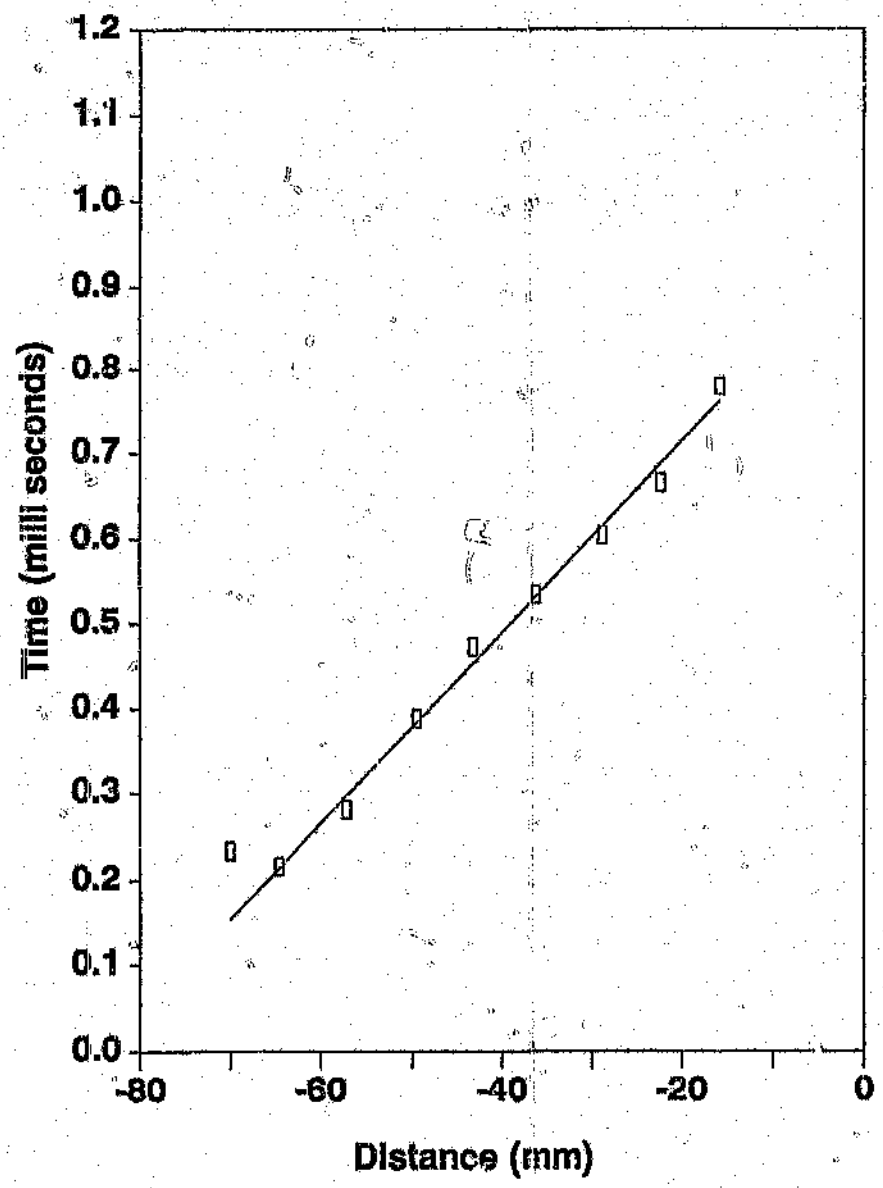


Figure 5.26 Polyester foam face motion

The same method of analysis was applied to the polyether foam. The particle paths for the polyether are shown in figure 5.27, behaving in a similar manner to the polyester foam. Once again it is possible, from the particle paths, to identify a wave propagating through the skeleton material of the foam.

The equations of the curves representing the particle motion of the polyether foam (curve B) and the intersection points of curves A and B are shown in table 5.7.

Table 5.7 Polyether foam particle path equations

x position (mm)	Equation ($v = mx + c$)		Intersection point (μs)
	Slope (m)	Intercept (c)	
-14.9	37.13	1362.8	
-21.9	31.77	1431.3	735.5
-28.9	27.48	1430.4	665.1
-35.8	22.88	1429.8	610.7
-42.4	22.53	1475.3	520.0
-49.2	22.13	1519.5	430.7
-56.1	21.26	1540.0	347.3
-63.1	20.48	1563.9	271.6
-70.0	20.37	1660.2	234.3

Figure 5.28 shows the motion of the wave front in the skeleton of the polyether foam. This wave is propagating through the skeleton material at 90 m/s.

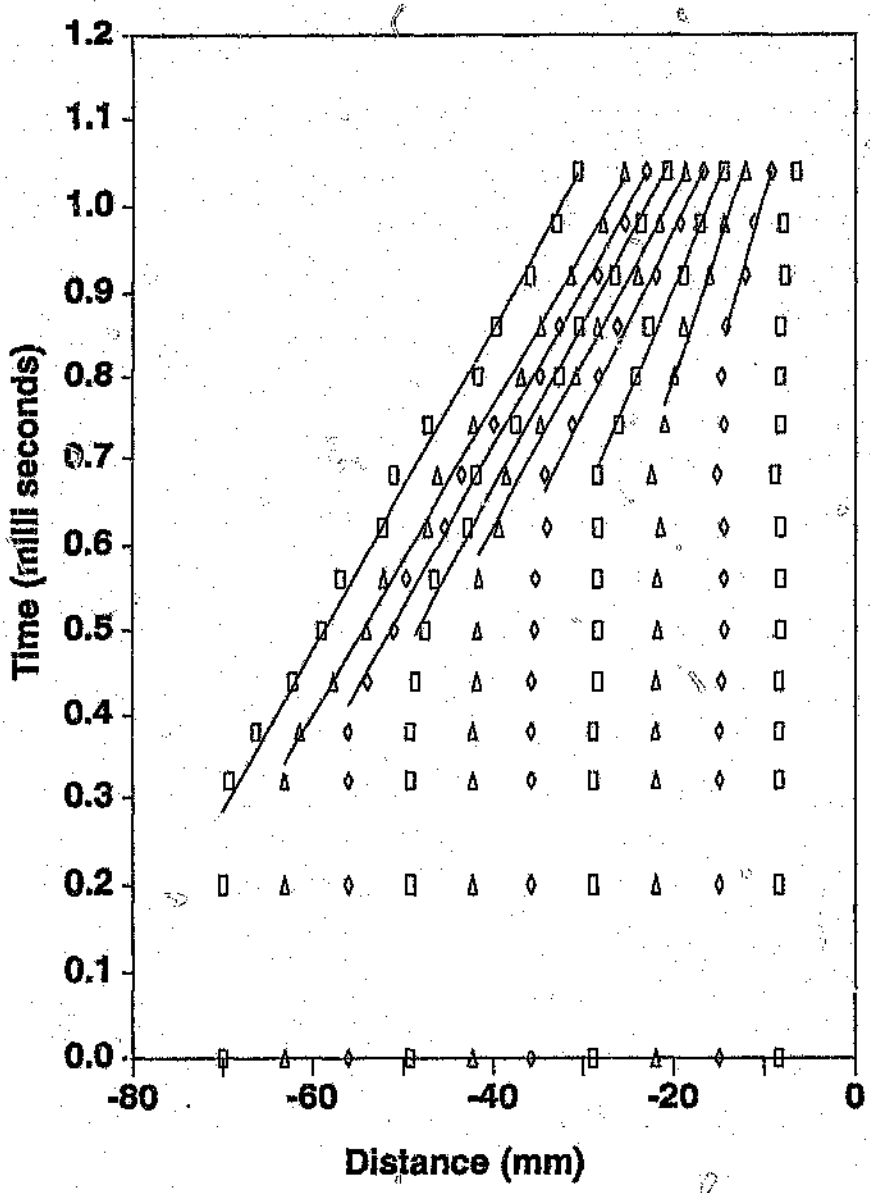


Figure 5.27 Particle paths, polyether foam 32.5 kg/m^3 M ; = 1.4

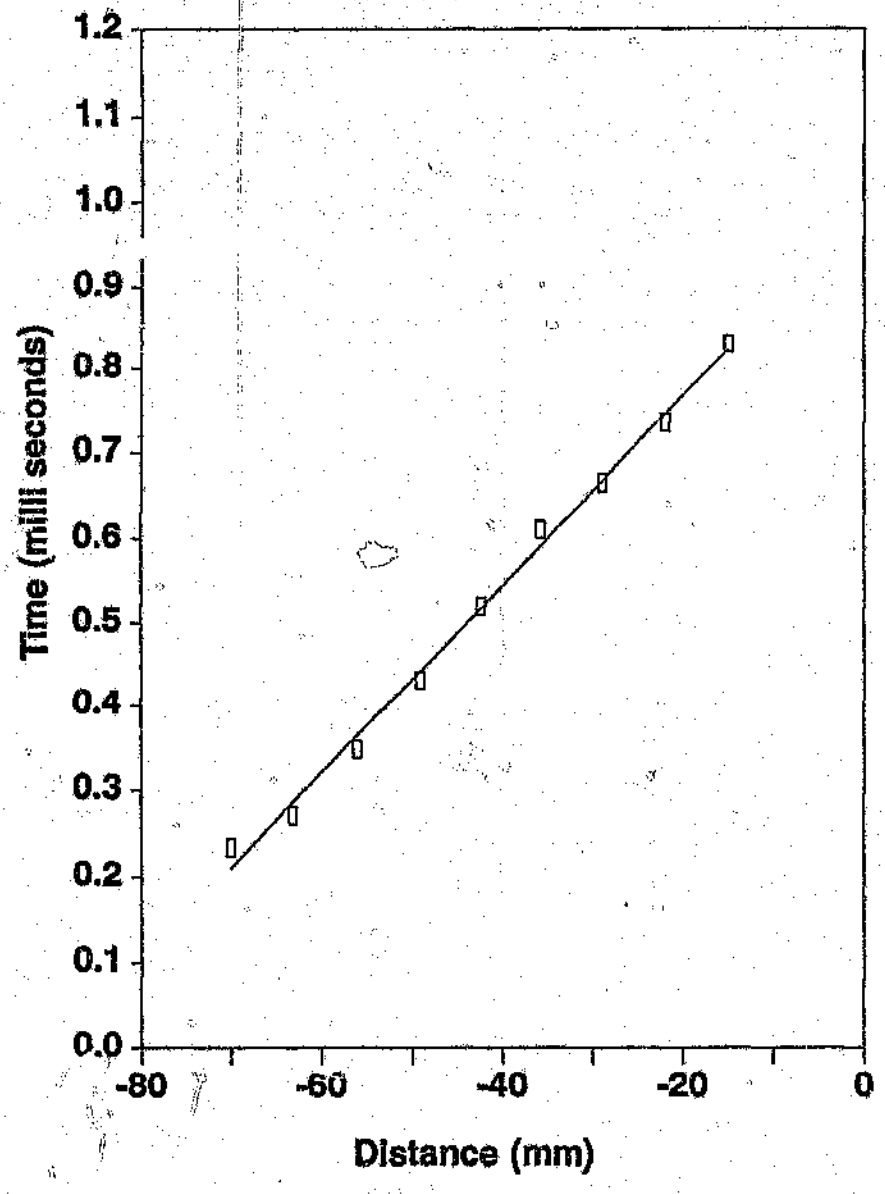


Figure 5.28 Polyether foam face motion

Figure 5.29 is the path of the front face of the polyester foam as calculated using the schlieren photographs (crosses) and the path photographs (squares). The average absolute error is 5.2 percent.

The velocity of the front face of the polyester foam is 54 m/s. This is the average of the velocities obtained using the path photographs and the schlieren photographs.

Figure 5.30 is the path of the front face of the polyether foam as calculated using the schlieren photographs (crosses) and the path photographs (squares). The average absolute error is 5.2 percent.

The velocity of the front face of the polyether foam is 58 m/s. This is the average of the velocities obtained using the path photographs and the schlieren photographs.

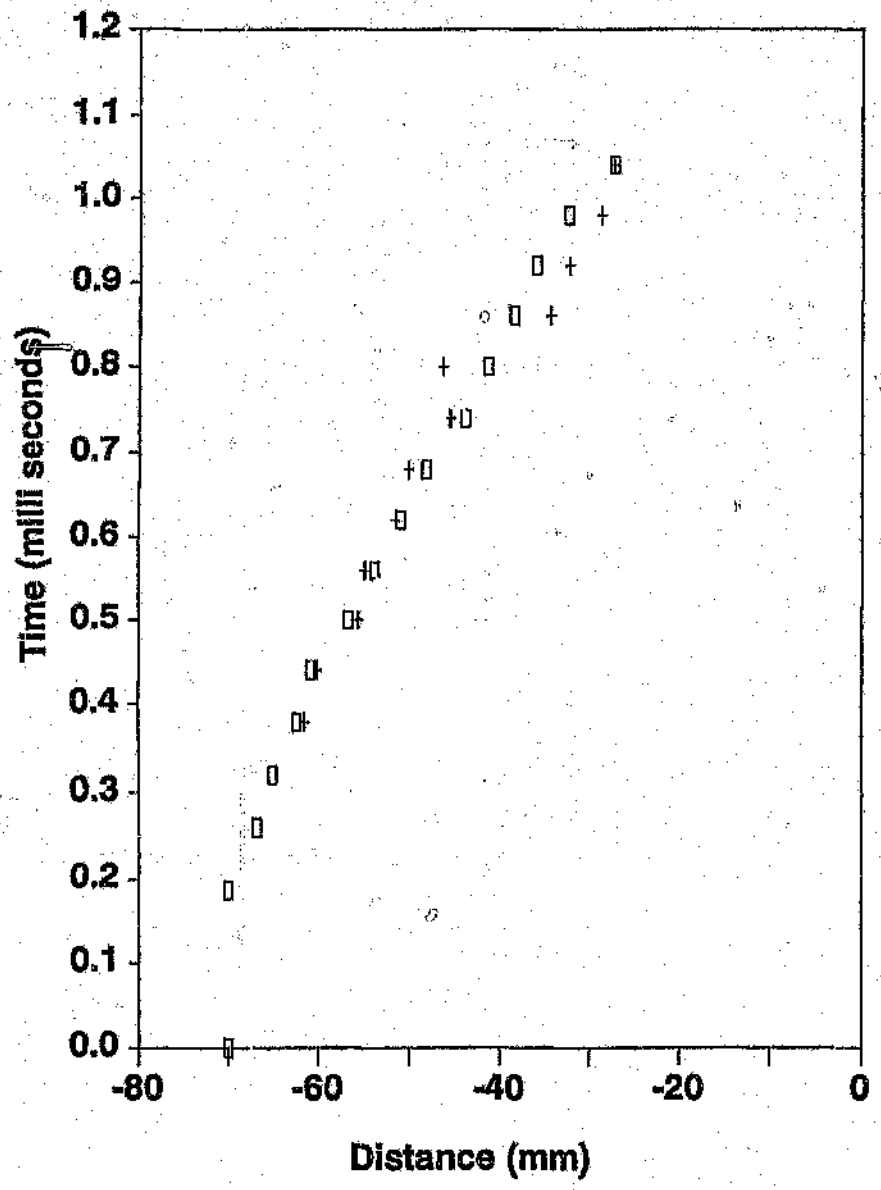


Figure 5.29 Polyester foam face motion, schlieren photographs (crosses) path photographs (squares)

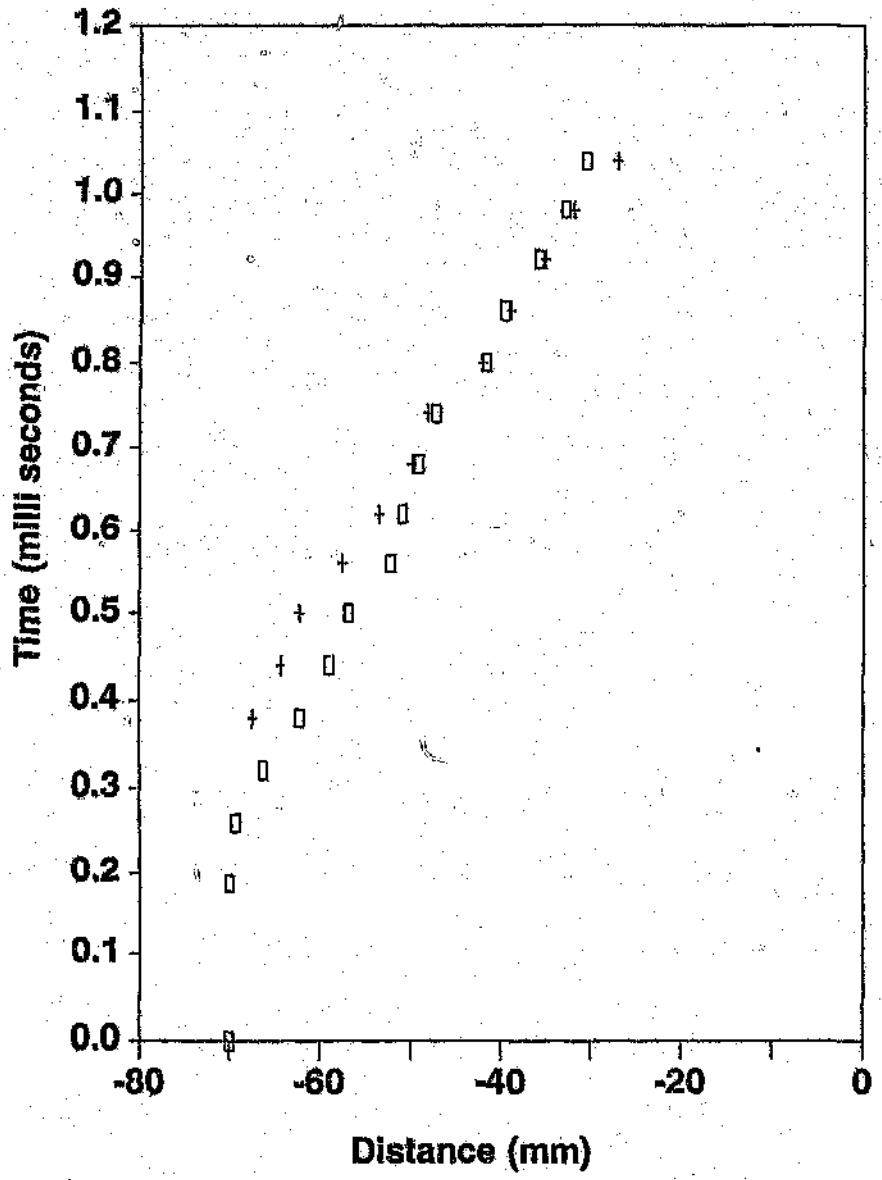


Figure 5.30 Polyether foam face motion, schileren photographs (crosses) path photographs (squares)

5.3.2 Transmitted Compression Wave

From the pressure contour plots figure 5.12 and 5.11 a gas compression wave was identified, travelling through the foam (transmitted compression wave) this wave having been generated after the incident shock wave struck the front face of the foam.

To compare the propagation of the transmitted compression wave and the foam skeleton wave a portion of the pressure contour plot (from figure 5.25) was superimposed upon the particle path plot (figure 5.25 .) This comparison, for the polyester foam is shown in figure 5.31.

The leading edge of the transmitted wave is travelling at 140 m/s. Recalling that the foam skeleton wave moved at 89 m/s, one can identify two distinct waves travelling "through" the foam.

The propagation of the transmitted wave and the foam skeleton wave in the polyether foam is compared in figure 5.32. The leading edge of the transmitted wave is travelling at 198 m/s. The foam skeleton wave traveled at 90 m/s, Once again one can identify two distinct waves travelling "through" the foam.

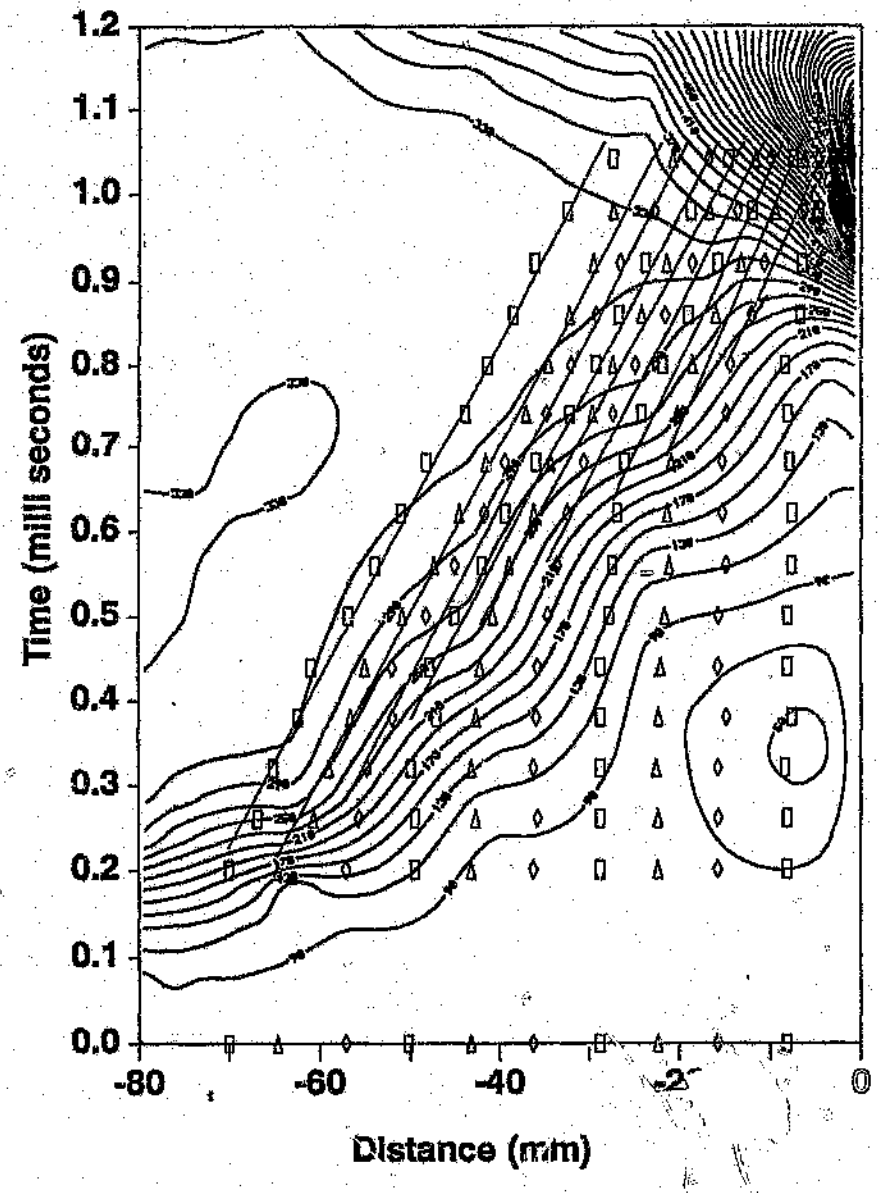


Figure 5.31 Transmitted compression wave and foam skeleton wave comparison, polyester foam 38 kg/m^3

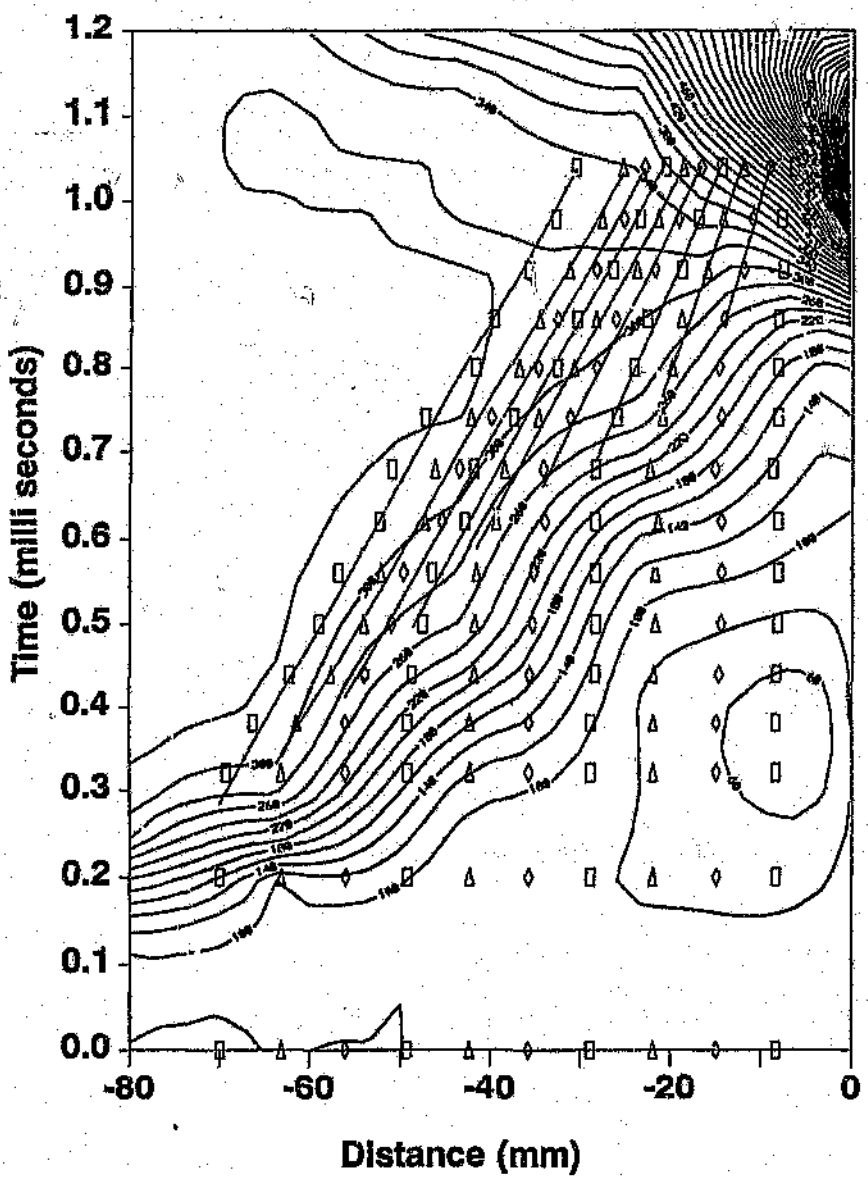


Figure 5.32 Transmitted compression wave and foam skeleton wave comparison, polyether foam 32.5 kg/m^3

5.4 Theoretical Analysis

5.4.1 Solid Wall Reflection

Figure 5.33 shows the interaction of a shock wave and a solid wall.

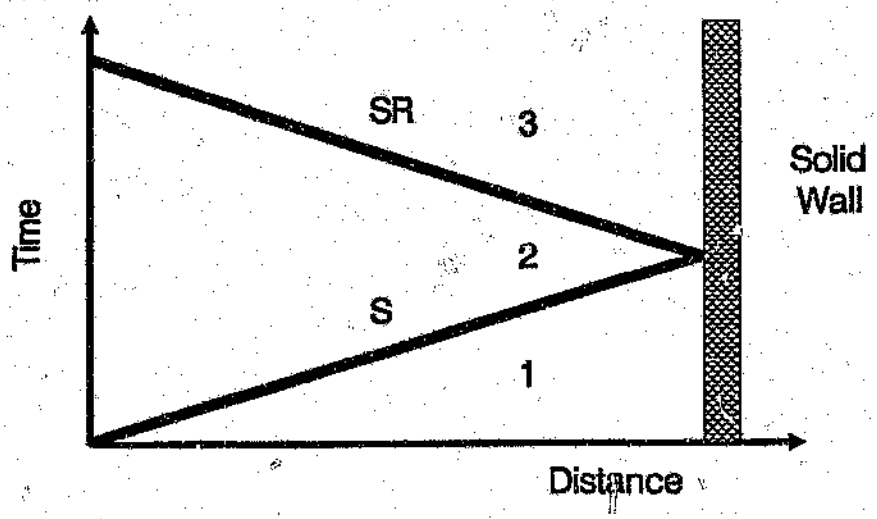


Figure 5.33 Shock wave interaction with a solid wall

Based on the following input conditions the standard normal shock wave equations were used to calculate the strength (P_3) and Mach number (M_{SR}) of the shock wave reflected from a solid wall, the results of which are listed in table 5.8.

$P_1 = 82\,566\ Pa$

$a_1 = 348\ m/s$

$\rho_1 = 0.955\ kg/m^3$

Table 5.8 Solid wall reflection

Incident Shock Mach Number (M_S)	Reflected Shock Mach Number (M_{SR})	Reflected Shock Pressure (P_3) (Pa)
1.449	1.389	392840
1.426	1.372	369440
1.375	1.332	320680

5.4.2 Monti's Theoretical Analysis

A detailed description of the theoretical analysis Monti [30] used to calculate the strengths of the reflected and transmitted shock waves was given in section 2.1.

The analysis is used to predict the reflected and transmitted Mach numbers for the polyester foam. These predicted results are compared to the experimental results obtained.

A compression test of the foam was required in order to determine its average stiffness modulus (Θ). The compression test equipment available is usually used to test materials much stiffer than the foam. The compression testers thus did not have the sensitivity required to test the foam. A manual static test was done by placing different weights on the foam and measuring its change in length. The static compression is shown in figure 5.34 as the variation of the force per unit area (f_x) with strain (εx).

Although the tests performed were simple in nature, the results obtained were repeatable. The force-deformation curve has three regions. (Monti [30] observed the same characteristics for the foam he tested.) The slope of the curve located in region C is taken as the average stiffness modulus (Θ), as defined by Monti. [30]

Based on the following input conditions the shock wave interaction parameters as proposed by Monti [30] were calculated, the results of which are shown in table 5.9.

$P_1 = 82\,566\ Pa$

$a_1 = 348\ m/s$

$\rho_1 = 0.955\ kg/m^3$

$\Theta = 51\,400\ N/m^2$

$N = 5$

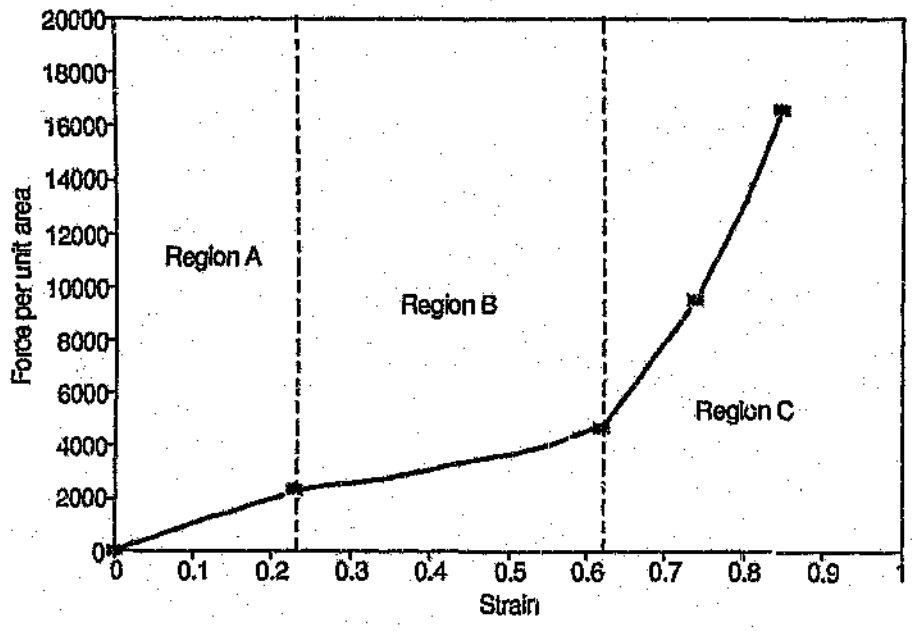


Figure 5.34 Experimental force-deformation curve for the polyester foam

Table 5.9 Results of Monti's [30] theoretical analysis

	Polyester foam ($\rho_1 = 38\ kg/m^3$)		Polyether foam ($\rho_1 = 32.5\ kg/m^3$)	
Incident Shock Mach Number (M_S)	Reflected Shock Mach Number (M_{SR})	Reflected Shock Pressure (P_3) (Pa)	Reflected Shock Mach Number (M_{SR})	Reflected Shock Pressure (P_3) (Pa)
1.449	1.151	259910	1.141	254700
1.426	1.148	249660	1.138	244700
1.375	1.139	226760	1.130	222865

The reflected shock wave Mach number and the pressure behind it were calculated over the range for which experimental results existed. A comparison between the experimentally recorded reflected Mach number and the Mach number calculated number using Monti's [30] analysis is shown in figure 5.35. The pressures behind the reflected shock waves are compared in figure 5.36, Monti's [30] analysis under predicts the reflected shock wave Mach number and the reflected shock wave pressure.

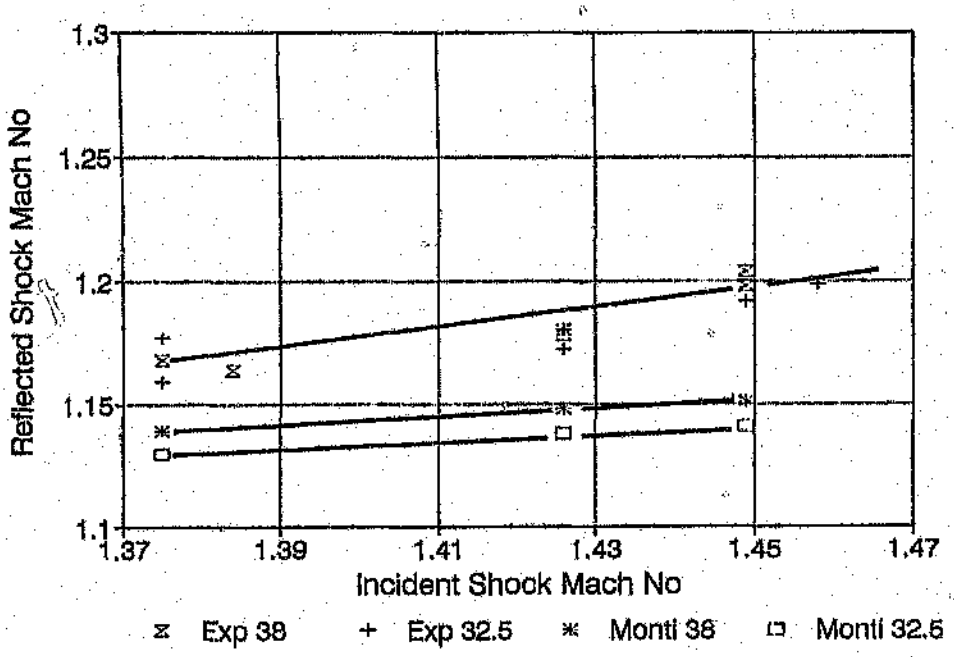


Figure 5.35 Reflected shock wave Mach number variation with incident shock wave Mach number, experimental and Monti's [30] theoretical results

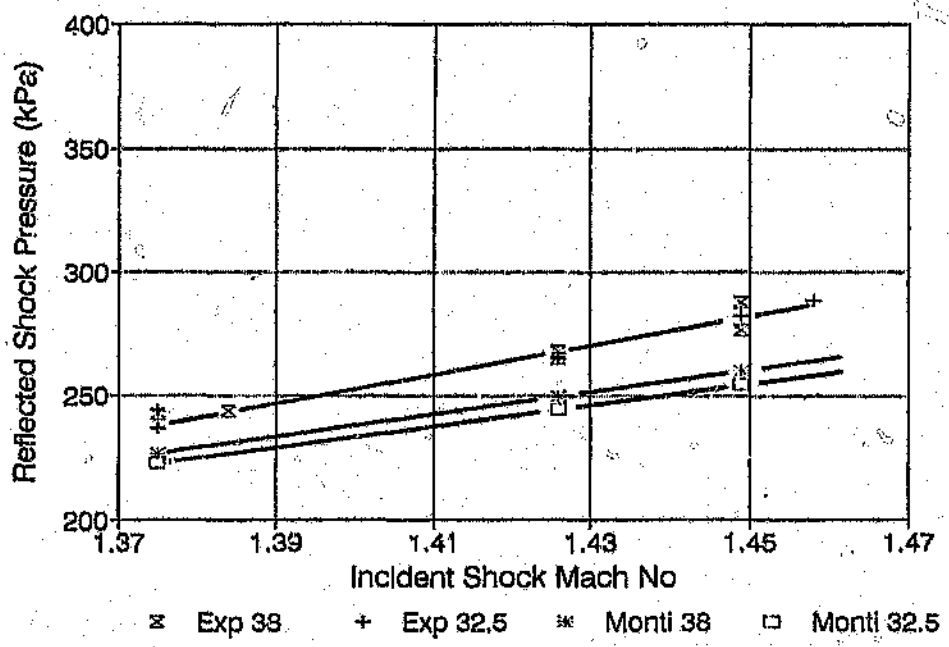


Figure 5.36 Reflected shock pressure variation with incident shock wave Mach number, experimental and Monti's [30] theoretical results

5.4.3 Gel'fand's Theoretical Analysis

A detailed description of the theoretical pseudo-gas analysis Gel'fand [20] used to calculate the strengths of the reflected and transmitted shock waves was given in section 2.2. The following input conditions were used to calculate the shock wave interaction parameters using the Gel'fand analysis:

$P_1 = 82\,566\ Pa$

$a_1 = 348\ m/s$

$\rho_1 = 0.955\ kg/m^3$

$c = 1200\ J/kg$

$c_1 = 1002\ J/kg$

$\varepsilon_l = 0.05$

The results of the interaction of a shock wave and a porous foam according to the Gel'fand analysis are listed in table 5.10.

Table 5.10 Results of Gel'fand's [20] theoretical analysis

	Polyester foam ($\rho_l = 38\ kg/m^3$ $a_l = 48.6\ m/s$)		Polyether foam ($\rho_l = 32.5\ kg/m^3$ $a_l = 52\ m/s$)	
Incident Shock Mach Number (M_S)	**Reflected Shock Mach Number (M_{SR})**	**Reflected Shock Pressure (P_3) (Pa)**	**Reflected Shock Mach Number (M_{SR})**	**Reflected Shock Pressure (P_3) (Pa)**
1.449	1.263	319150	1.254	314500
1.426	1.251	302350	1.243	298050
1.375	1.226	267000	1.218	263500

A comparison between the experimental results and Gel'fand's theoretical analysis for the reflected shock wave Mach number and the reflected shock wave strength are shown in figures 5.37 and 5.38 respectively

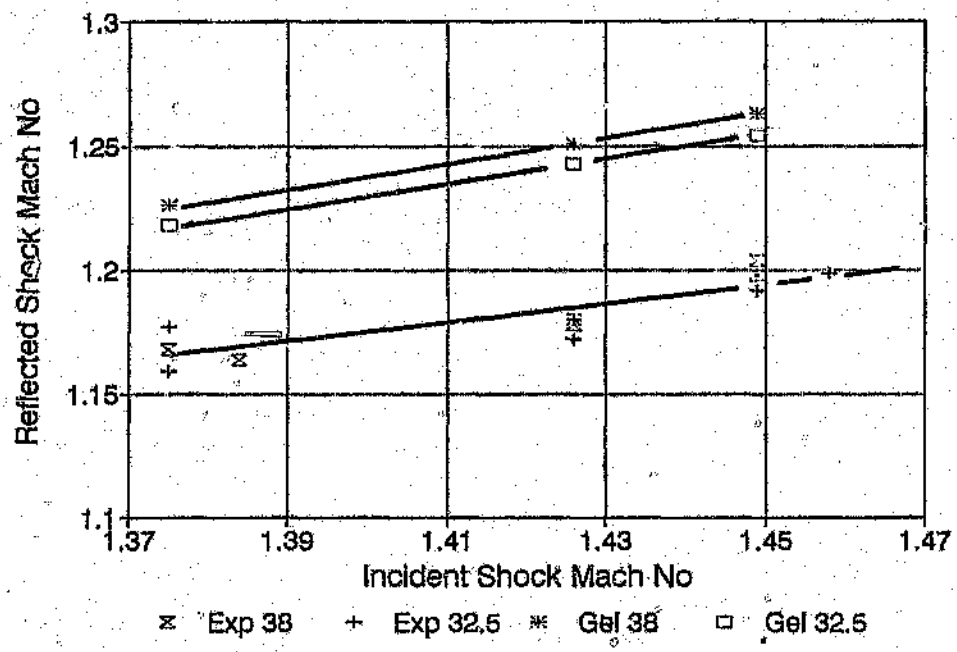


Figure 5.37 Reflected shock wave Mach number variation with incident shock wave Mach number, experimental and Gel'fand's [20] theoretical results

Gel'fand's analysis over predicts the reflected shock wave Mach number and the reflected shock wave pressure. The increase in experimental reflected shock wave Mach number as the incident Mach number increases (slope) is suitably predicted by Gel'fand's analysis, over the range of incident Mach numbers considered. The same holds true for the reflected shock wave pressure (figure 5.38.)

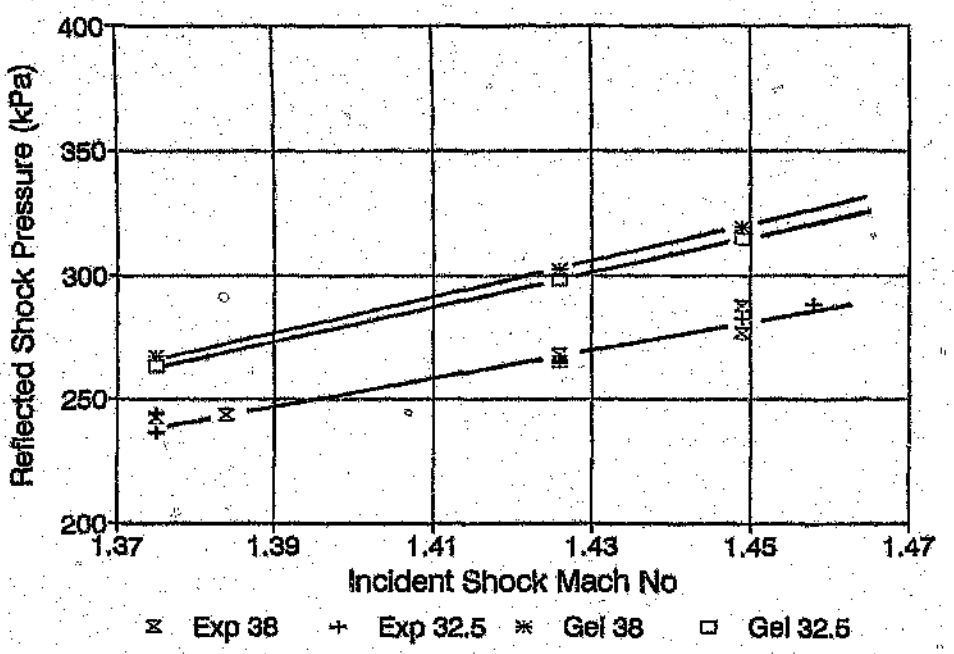


Figure 5.38 Reflected shock wave pressure variation with incident shock wave Mach number, experimental and Gel'fand's [20] theoretical results

Figure 5.39 and 5.40 show the reflected shock wave Mach number variation with incident shock wave Mach number from the experimental results, Monti [30] analysis, Gel'fand [20] analysis and solid wall interactions. Figure 5.39 is the shock wave interaction for the 70 mm of polyester foam, while figure 5.40 is for the polyether foam.

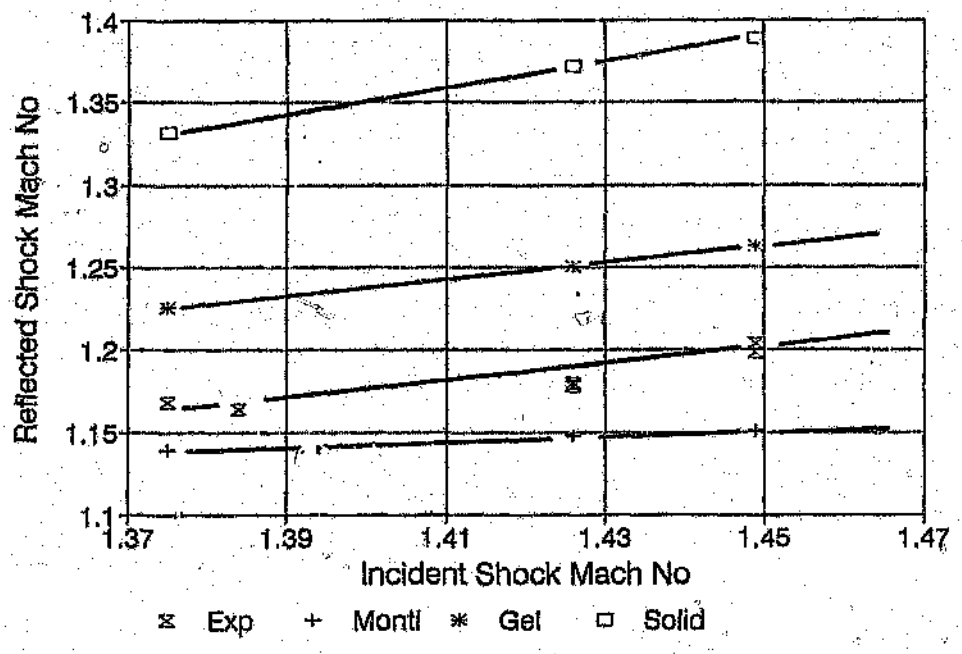


Figure 5.39 Reflected shock wave Mach number variation with incident shock wave Mach number, polyester foam

By placing a compressible foam in front of a solid surface it can be seen that the reflected shock wave Mach number has been reduced. The experimental reflected shock wave Mach number lies between the Mach number predicted by Gel'fand's analysis and and the Mach number predicted by Monti's analysis. These conclusions hold true for both foams tested.

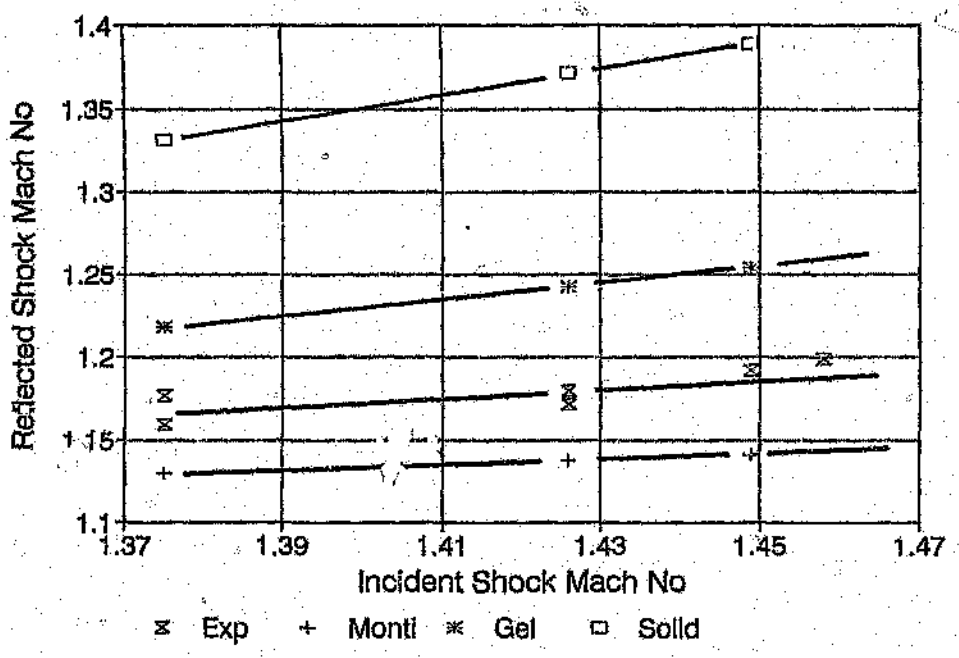


Figure 5.40 Reflected shock wave Mach number variation with incident shock wave Mach number, polyether foam

Figure 5.41 and 5.42 show the reflected shock wave pressure variation with incident shock wave Mach number from the experimental results, Monti [30] analysis, Gel'fand [20] analysis and solid wall interactions. Figure 5.41 is the shock wave interaction for the 70 mm of polyester foam, while figure 5.42 is for the polyether foam.

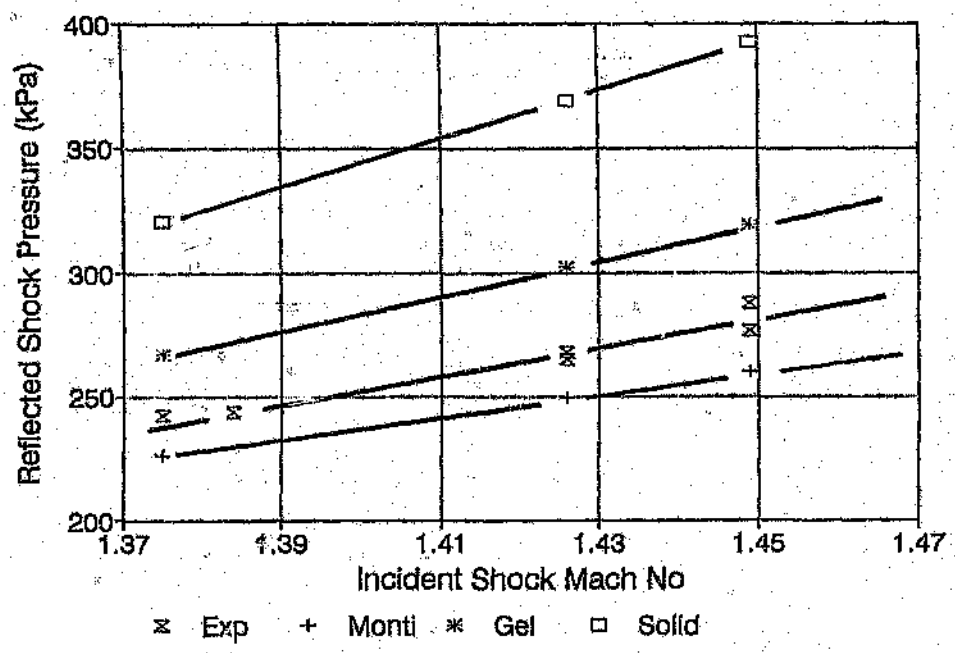


Figure 5.41 Reflected shock wave pressure variation with incident shock wave Mach number, polyester foam

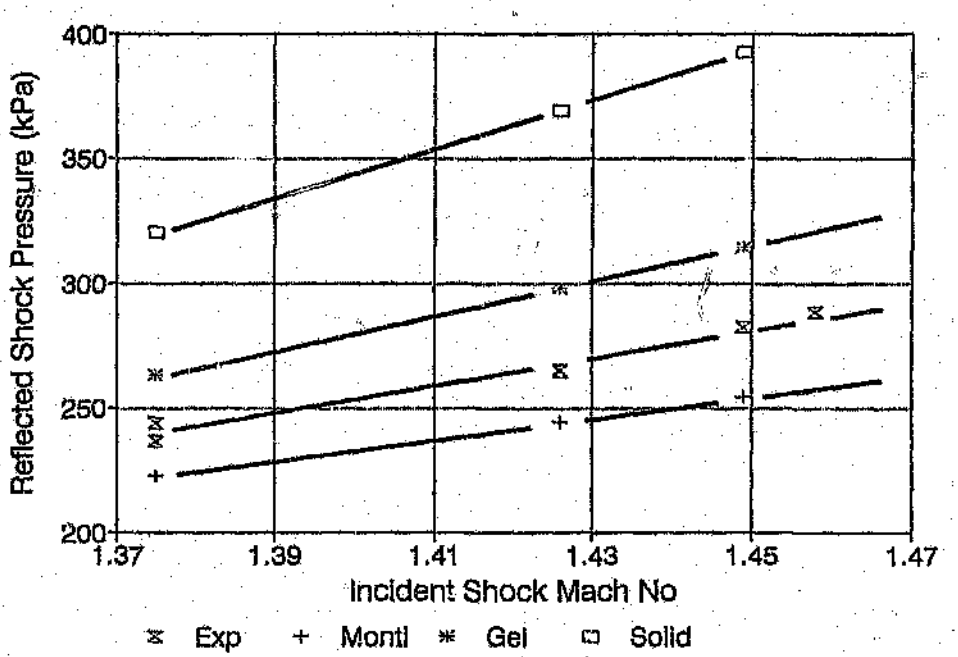


Figure 5.42 Reflected shock wave pressure variation with incident shock wave Mach number, polyether foam

5.4.4 Gvozdeva's Theoretical Analysis

A detailed description of the analytic method Gvozdeva [22] developed for calculating the shock wave parameters in a porous medium, after a shock wave has struck the front face is given in section 2.3.

The analysis requires the input of the Mach number of the reflected shock wave. The reflected shock wave Mach number may be calculated using either Monti's [30] or Gel'fand's [20] analysis. But for the purpose of the calculations to follow the experimentally measured reflected shock wave Mach number has been used.

The following input conditions were used to calculated the shock wave parameters in the porous medium.

$P_1 = 82\,566\ Pa$

$a_1 = 348\ m/s$

$\rho_1 = 0.955\ kg/m^3$

$N = 5$

$\alpha_l = 0.95$

Polyester foam $\rho_{ol} = 726\ kg/m^3$ for $\rho_l = 38\ kg/m^3$

Polyether foam $\rho_{ol} = 632\ kg/m^3$ for $\rho_l = 32.5\ kg/m^3$

The results of the interaction of a shock wave and a porous foam according to the Gvozdeva's analysis are listed in table 5.11 and table 5.12.

Table 5.11 Results of Gvozdeva's [22] theoretical analysis for polyester foam

Polyester foam ($\rho_1 = 38\ kg/m^3$ $a_1 = 52.3\ m/s$)				
Incident Shock Mach Number (M_S)	Reflected Shock Mach Number (M_{SR}) *	Transmitted Shock Mach Number (M_{ST}) (Pa)	Rear Wall Pressure (P_{III}) (Pa)	Coefficient of Pressure increase (R)
1.449	1.201	1.742	1067490	2.72
1.426	1.179	1.680	940870	2.55
1.375	1.168	1.603	794870	2.48

Table 5.12 Results of Gvozdeva's [22] theoretical analysis for polyester foam

Polyether foam ($\rho_1 = 32.5\ kg/m^3$ $a_1 = 62.1\ m/s$)				
Incident Shock Mach Number (M_S)	Reflected Shock Mach Number (M_{SR}) *	Transmitted Shock Mach Number (M_{ST}) (Pa)	Rear Wall Pressure (P_{III}) (Pa)	Coefficient of Pressure increase (R)
1.449	1.192	1.725	1038200	2.64
1.426	1.176	1.672	931920	2.52
1.375	1.168	1.600	794885	2.48

* - Experimental result

The coefficient of pressure increase variation with incident shock wave Mach number for the polyester foam is shown in figure 5.43. The experiments are compared to those obtained from Gvozdeva's [22] theoretical analysis. The coefficient of pressure increase for the polyester foam is under predicted by the Gvozdeva [22] analysis.

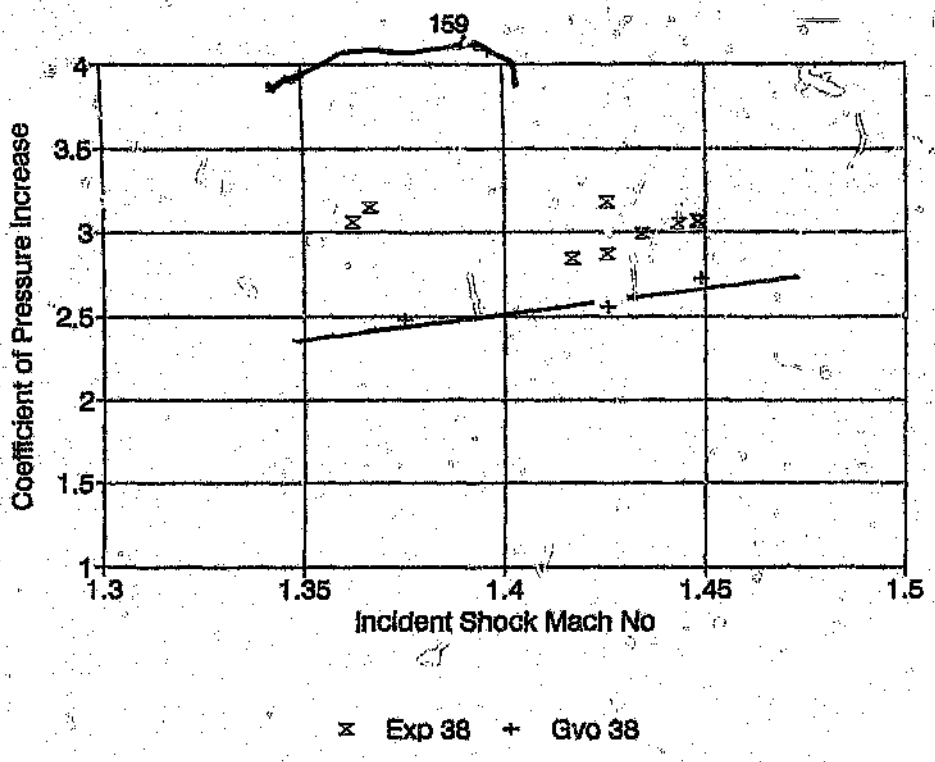
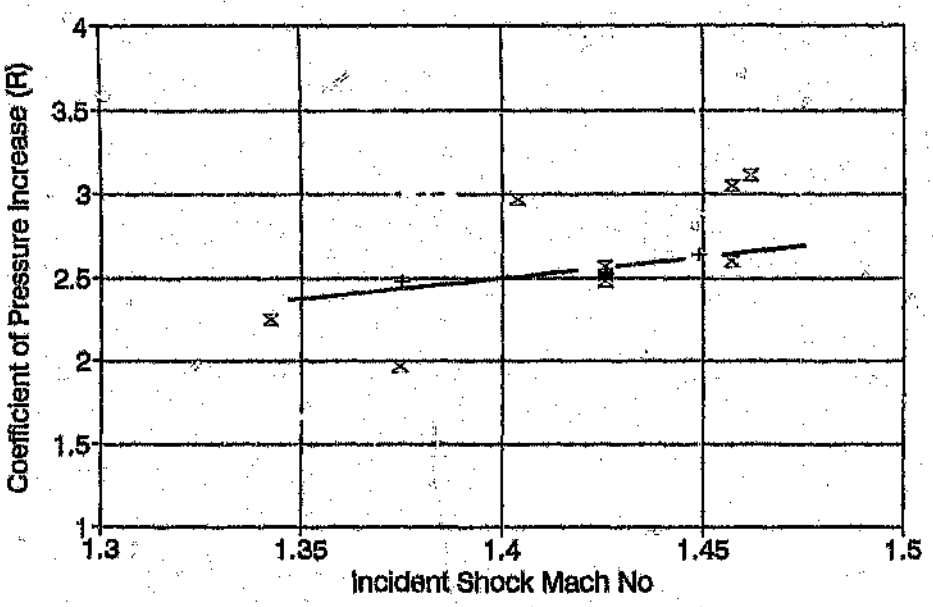


Figure 5.43 Coefficient of pressure increase variation with incident shock wave Mach number, polyester foam

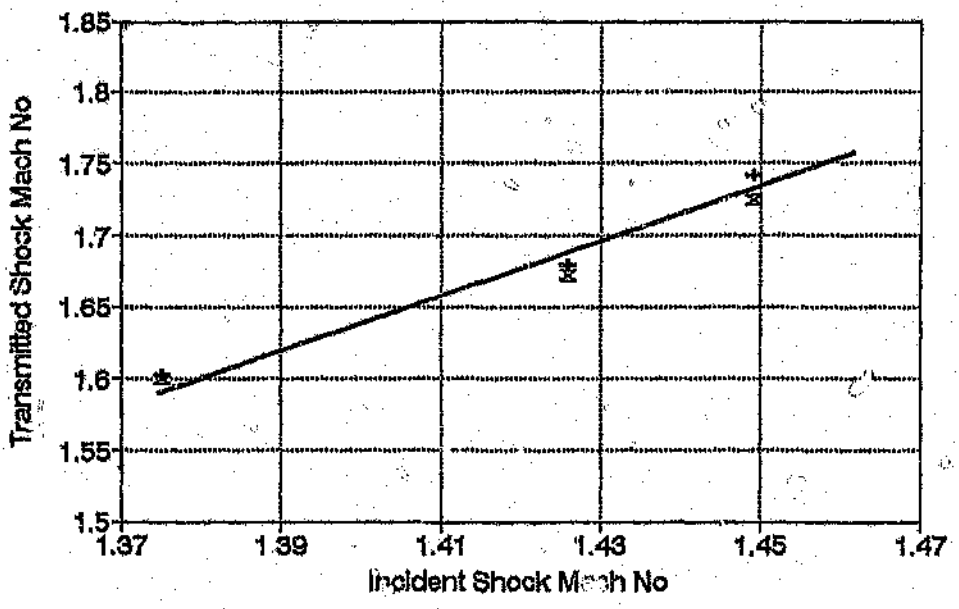
Figure 5.44 shows the results for the polyether foam, the predicted coefficient of pressure increase falls within the scatter of the experimental data. Thus for this range of incident Mach numbers and the two foams tested Gvozdeva's [22] theoretical analysis predicts the coefficient of pressure increase to within 20 percent.

The Mach number of the transmitted shock wave variation with incident Mach number according to Gvozdeva's [22] analysis is shown in figure 5.45.



⧖ Exp 32.5 + Gvo 32.5

Figure 5.44 Coefficient of pressure increase variation with incident shock wave Mach number, polyether foam



⧖ Gvo 32.5 + Gvo 38

Figure 5.45 Transmitted shock Mach number variation with incident shock wave Mach number (Gvozdeva's analysis)

5.5 Foam Model

The problem of understanding what physically happens when a shock wave strikes the front face of a compressible porous foam was tackled on three levels, namely;

- recording the pressure before, alongside and behind the foam
- schlieren photographs
- path photographs.

In this section the three sources of information will be considered and combined to formulate a physical model for the interaction of a shock wave and a compressible porous foam.

Combing the data from the pressure transducers, it was possible to construct pressure contour plots, figures 5.11 and 5.12. The schlieren photographs supplied information about the movement of the foam front face, a gas front and a contact surface, figures 5.22 and 5.23.

Superimposing the information obtained from the schlieren photographs and the pressure transducers, figure 5.46 and figure 5.47 were constructed. Analyzing the figures it is possible to identify the gas waves present in the shock wave, foam interaction. The incident shock wave strikes the front face of the foam (S_I), a shock wave is reflected (S_R), a compression wave(C_1) is transmitted into the foam and the front face of the foam begins to move. The transmitted compression wave strikes the solid back plate and is reflected from the back plate (C_2). During this time the foam is being compressed. The reflected compression wave (C_2) strikes the foam / air interface, a compression wave (C_3) is transmitted into the air and a rarefaction wave (R_1) is reflected back into the foam. The front face of the foam continues to be compressed. A gas front emerges from the front face of the foam, then a contact surface. The foam then begins to expand again, stabilizing at approximately 30 mm in length. It was shown that the gas front is gas leakage past the sides of the foam (Seitz and Skews [36]). It has been assumed that it does not significantly affect the one-dimensional nature of the flow along the centreline of the tube.

At the end of the test the foam did not return to its original length (70 mm.) The friction between the foam and the walls of the shock tube held the foam in a compressed position. When the foam was removed from the test section it returned to its original position, no permanent damage being done to its structure.

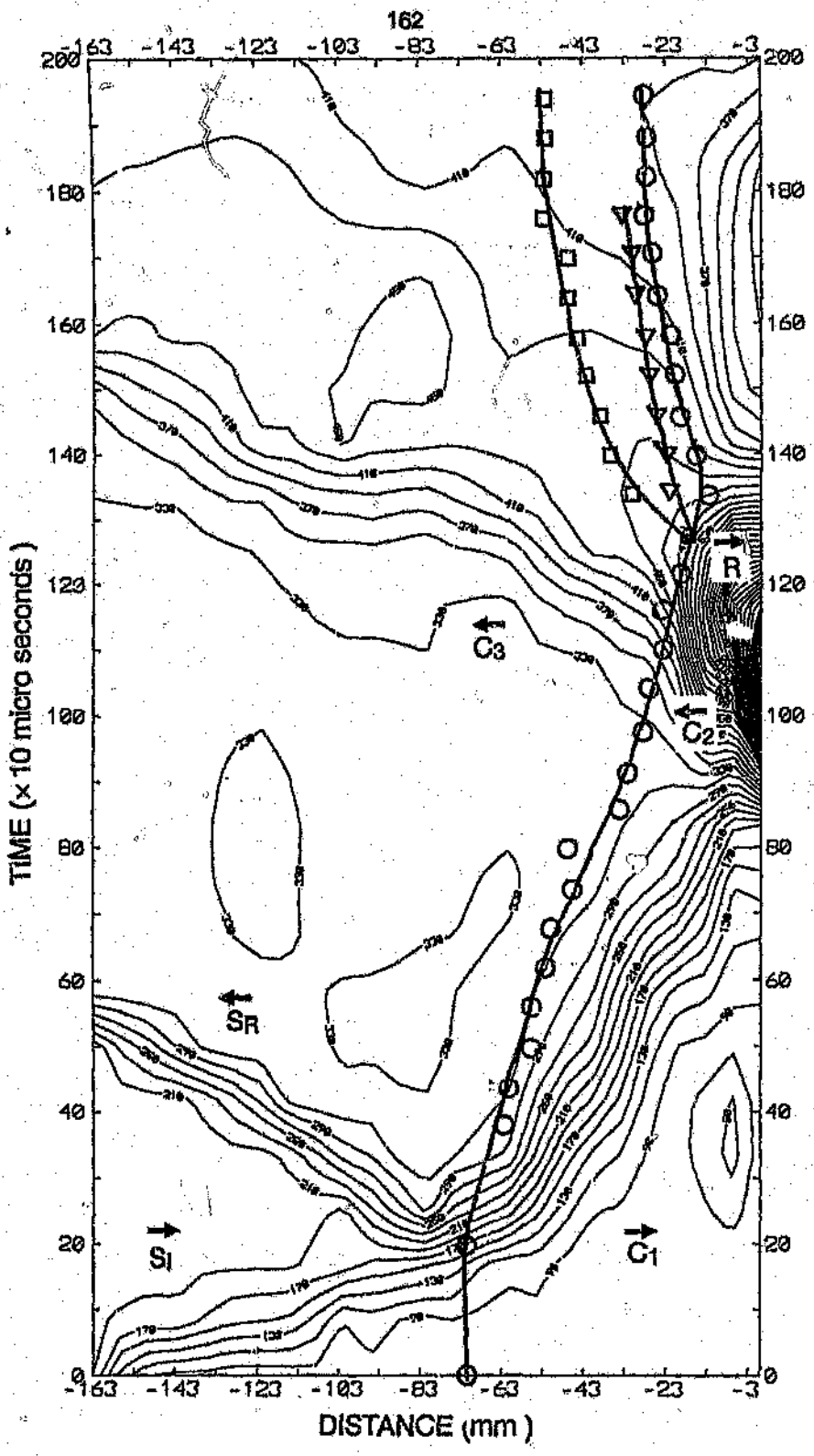


Figure 5.46 Pressure contour plot and motion of 70 mm of polyester foam, incident shock wave Mach number 1.4

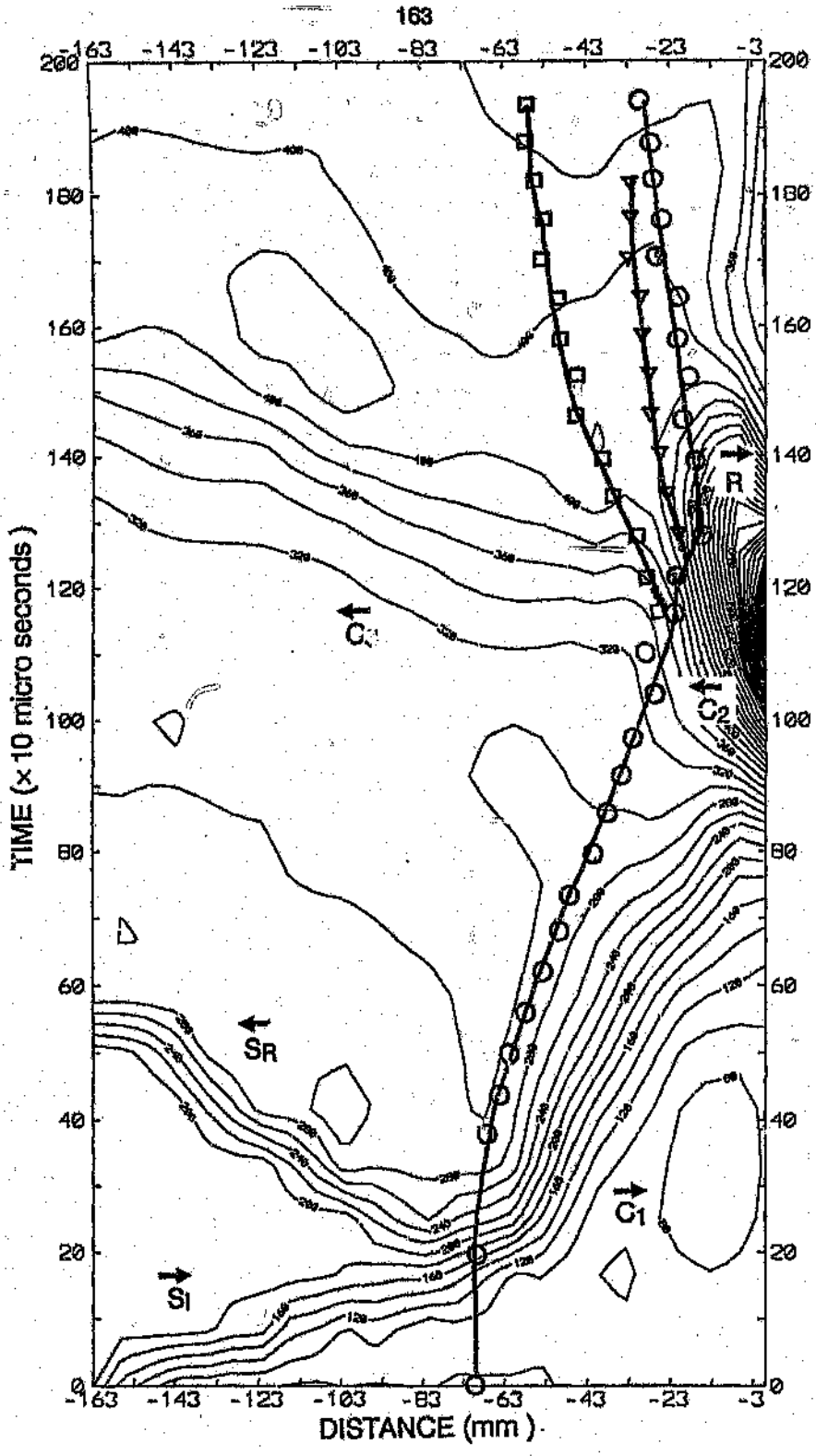


Figure 5.47 Pressure contour plot and motion of 70 mm of polyether foam, incident shock wave Mach number 1.4

A composite wave diagram (figure 5.48) was constructed for the polyether foam (Skews, Atkins and Seitz [38].) The particle path in the gas space was determined. It must be noted that the velocity in region 3 is almost the same as that of the foam front and the velocity in region 4 is approximately the same as that of the contact surface.

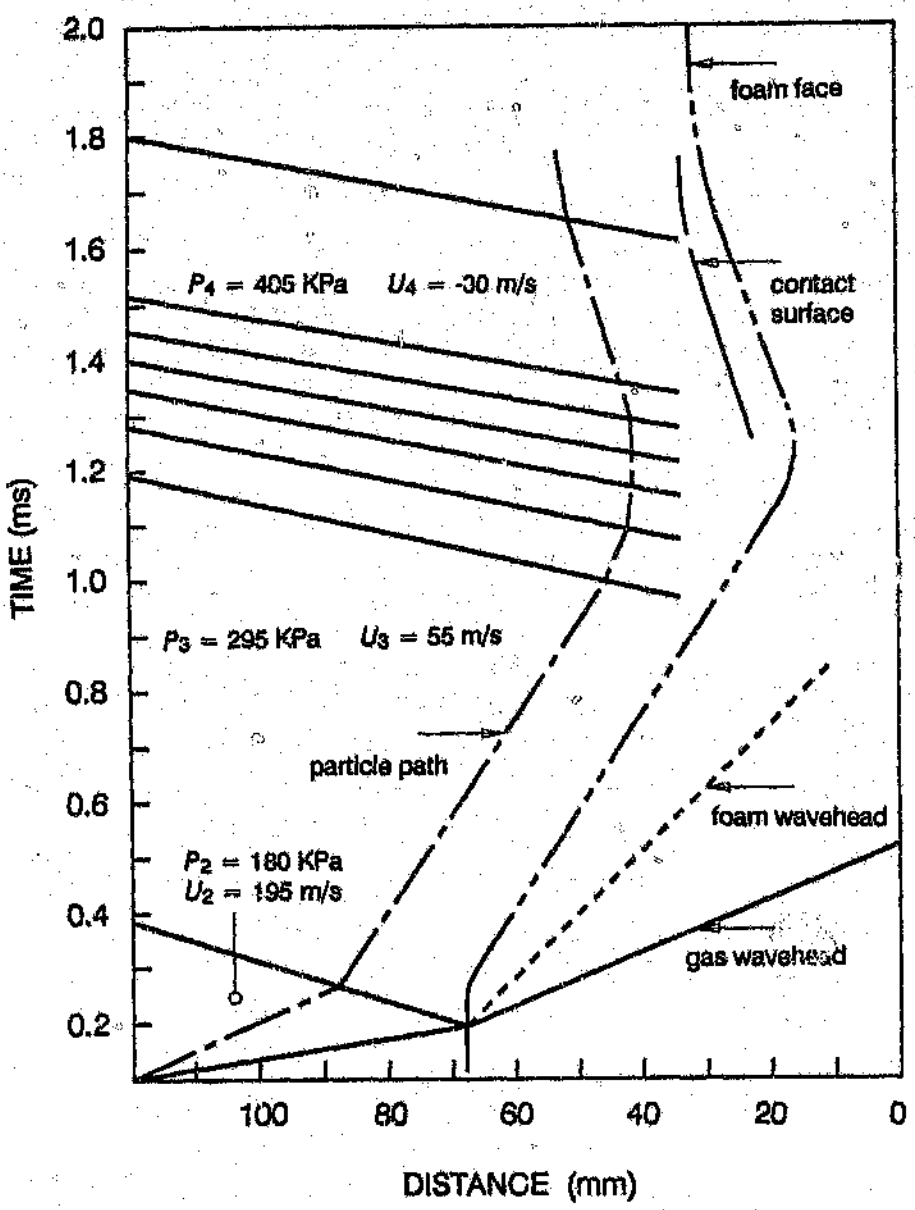


Figure 5.48 Composite wave diagram, polyether foam [38]

The path photographs provided the information on the movement of the particle paths in the foam (figures 5.25 and 5.27.) From this information it was possible to identify a wave propagating through the skeleton of the foam and to propose the following physical explanation of the large pressure recorded behind the foam.

It is proposed that the foam wave acts as an almost solid piston, trapping and compressing the gas in front of it. It is this mechanical action of the foam piston compressing the gas into a diminishing volume which causes the amplification of the pressure behind the foam. As the gas trapped inside the foam is compressed its temperature increases. This high pressure results in the gas being expelled out along the sides of the foam, followed by the contact surface (temperature discontinuity.)

To validate the mechanical piston theory a program was written to evaluate the foam face movement given the pressure distribution in the foam (appendix H.) Assuming isentropic compression the program calculates the position of the compressed foam boundary (piston) which would result in the mean of the measured pressure distribution. A description of the compressed foam boundary program, input conditions and a listing is given in appendix H.

The program calculates the mean pressure within the compressed foam boundary, the temperature of the gas within the boundary and the position of the boundary. The results for the polyester foam and polyether foam are given in tables 5.13 and 5.14 respectively.

Table 5.13 Path of the polyester compressed foam boundary

Time (μs)	Mean Pressure (Pa)	Distance (mm)	Temperature (K)
0	83974	69.7	303
20	84658	69.2	303
80	84073	68.8	303
140	82624	70.3	301
200	80958	71.4	299
260	80354	71.0	299
320	80412	71.4	299
380	85595	68.1	304
440	93875	63.7	312

Time (μs)	Mean Pressure (Pa)	Distance (mm)	Temperature (K)
440	93875	63.7	312
500	102187	60.3	320
560	110330	57.0	327
620	122836	53.1	337
680	141448	47.8	351
740	157808	44.5	362
800	174887	41.1	373
860	235422	33.3	406
920	420093	22.0	479
980	707847	15.2	556
1040	476329	20.2	407
1100	567036	17.8	522
1160	912519	12.6	598
1220	757936	14.5	567
1280	610636	16.8	533
1340	476913	20.1	497
1400	384408	23.4	467
1460	336115	25.8	450
1520	322752	26.6	445
1580	319212	26.8	443
1640	316675	26.6	442
1700	313161	26.8	441
1760	313435	27.0	441
1820	321229	26.7	444
1880	[illegible]	25.8	450
1940	361696	24.5	459

Time (μs)	Mean Pressure (Pa)	Distance (mm)	Temperature (K)
2000	387810	23.3	469

Table 5.14 Path of the polyether compressed foam boundary

Time (μs)	Mean Pressure (Pa)	Distance (mm)	Temperature (K)
24	83109	70.2	302
80	82824	69.7	301
144	83534	69.8	302
200	81850	70.9	300
264	81568	70.4	300
320	83708	69.6	302
384	87876	67.4	307
440	94189	63.8	313
504	105092	59.2	323
560	116742	55.1	332
624	133190	50.1	345
680	151315	45.8	358
744	177189	41.0	375
800	208163	36.4	392
864	280102	29.4	427
920	380117	23.7	466
984	507651	19.2	506
1040	647271	16.2	542
1104	800423	13.9	576
1160	839650	13.4	584
1224	798606	13.9	576

Time (μs)	Mean Pressure (Pa)	Distance (mm)	Temperature (K)
1280	714544	15.1	558
1344	599341	17.1	531
1400	499049	19.5	504
1464	412813	22.4	477
1520	363863	24.4	460
1584	336377	25.9	450
1640	328415	26.3	447
1704	327661	26.1	446
1760	338659	25.7	451
1824	346328	25.3	454
1880	352042	25.0	456
1944	356868	24.8	458
2000	364268	24.4	460

Figure 5.49 shows the calculated compressed foam boundary and the observed foam motion as recorded by the schlieren photographs for the polyester foam. For the first three quarters of the foam compression the compressed foam boundary theory accurately predicts the foam motion. The last portion of the foam compression deviates from the calculated position. The main reasons for this is that the measured foam position does not take into account the 3-D curvature of the front face of the foam, that is the position of the front face will actually be more compressed.

Once the foam begins to expand again the compressed foam boundary theory adequately describes the motion of the foam.

The calculated compressed foam boundary and the observed foam motion for the polyether foam is shown in figure 5.50. The same phenomena as in the previous foam are present.

It can thus be concluded that the high pressure on the rigid back plate is as a result of the mechanical action of the almost solid foam piston compressing the gas into a smaller volume. This pressure is further increased by the transmitted gas compression wave reflecting from the solid back plate.

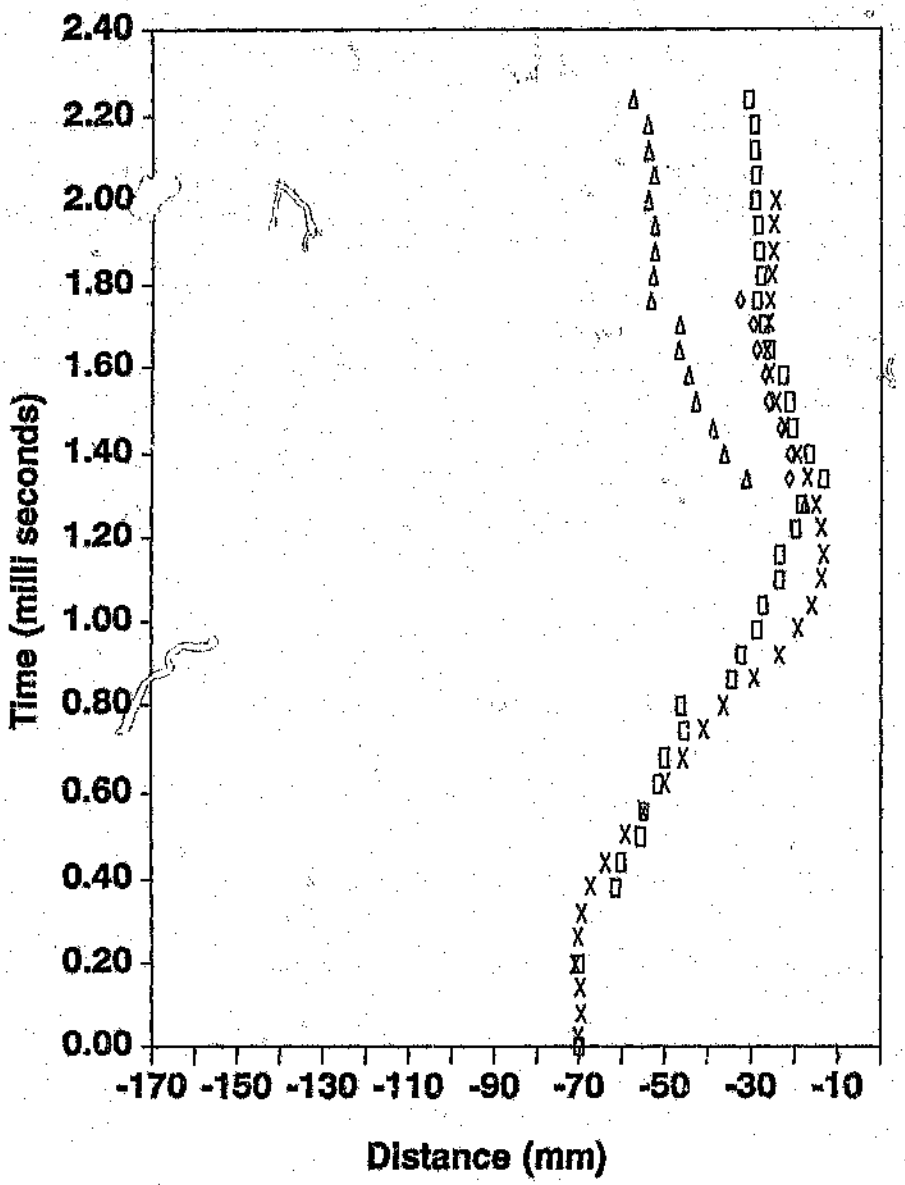


Figure 5.49 Motion of polyester foam (square - foam, triangle - gas, diamond - contact surface, x - calculated compressed foam boundary)

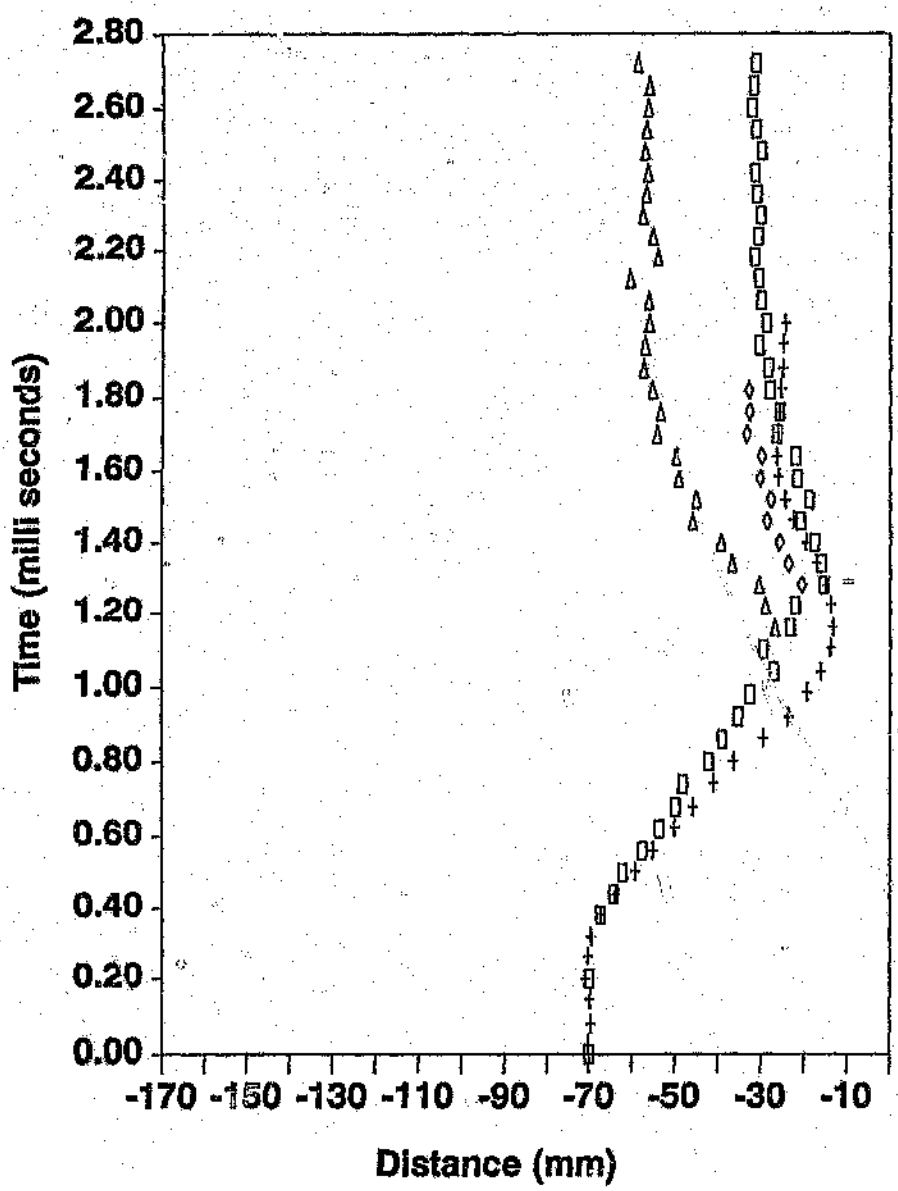


Figure 5.50 Motion of polyether foam (square - foam, triangle - gas, diamond - contact surface, x - calculated compressed foam boundary)

5.6 Two Dimensional Effects

There has been a debate in the literature as to the one dimensionality of the foam block with its sides touching the shock tube walls. It has been said that the friction between the foam surface and the shock tube walls alter the motion of the foam, and that it is better to reduce the foam size and to glue the foam block to the back plate so that there is a gap between the surface of the foam and the shock tube walls. To date there is no evidence in the literature as to which is the better test procedure for the interaction of a shock wave and a compressible foam material.

A series of tests were performed with a polyester foam block such that there was a 2.1 mm gap between the foam and the walls of the shock tube. A path photograph taken before the incident shock wave is shown in plate 5.15.

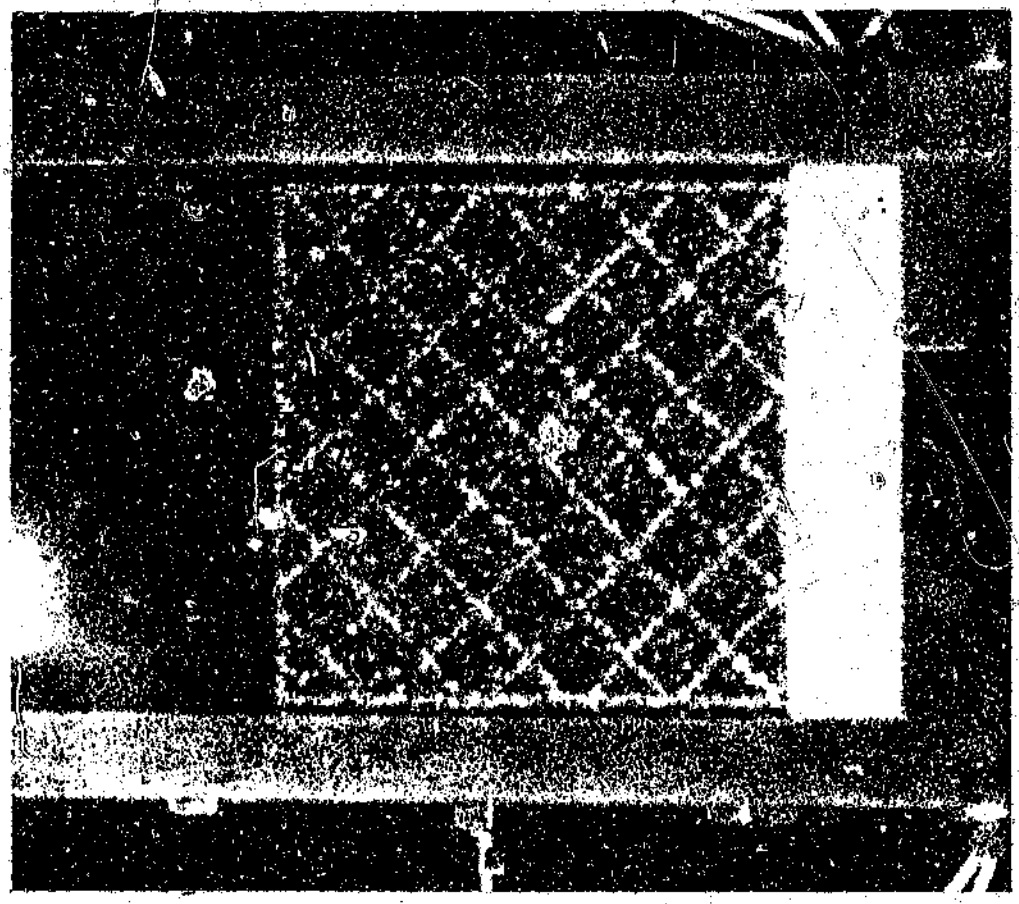


Plate 5.15 Path photograph,polyester foam, density 38 kg/m^3, (72 mm × 72 mm), time 0 μs

Plate 5.16 was taken 500 μs after the incident shock wave struck the front face of the foam. It can be seen that the foam begins to compress and that the compressed portion of the foam folds over and fills the original gap between the wall and the foam.

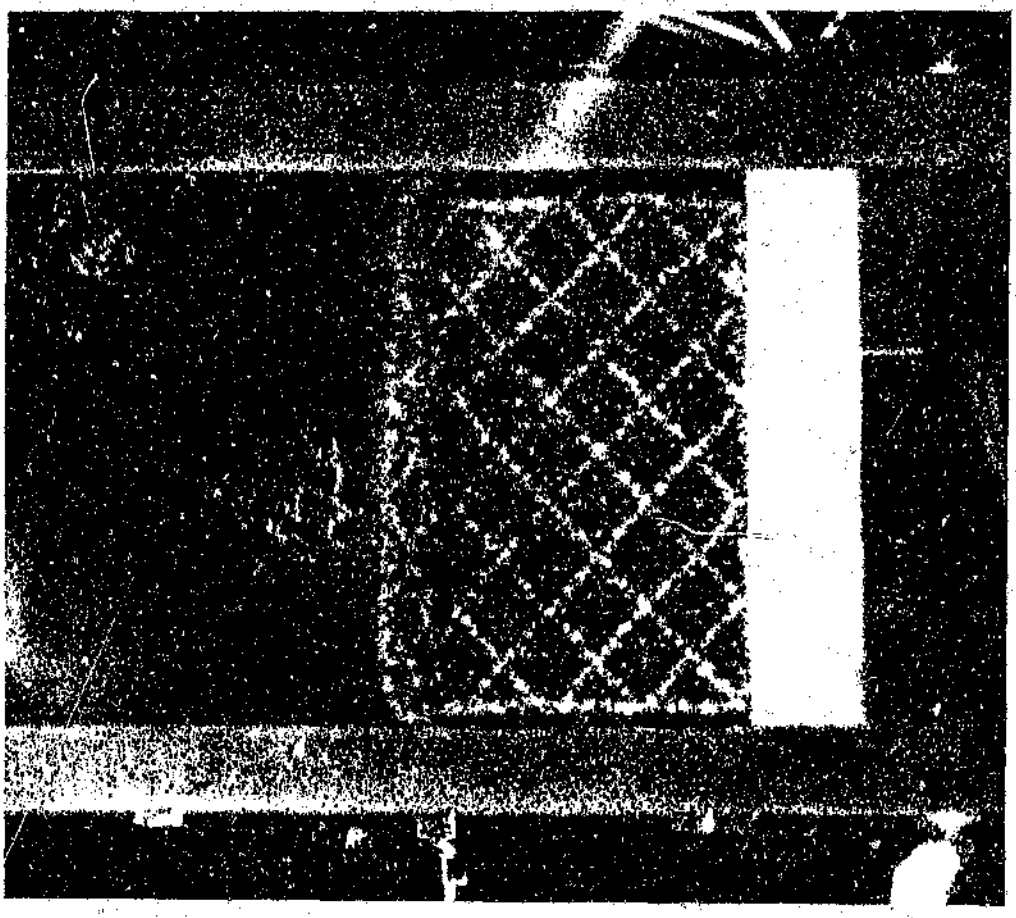


Plate 5.16 Path photograph,polyester foam, density 38 kg/m^3, (72 mm × 72 mm), time 500 μs

Plate 5.17 was taken 800 μs after the incident shock wave struck the front face of the foam. The foam that has been compressed fills the original air gap.

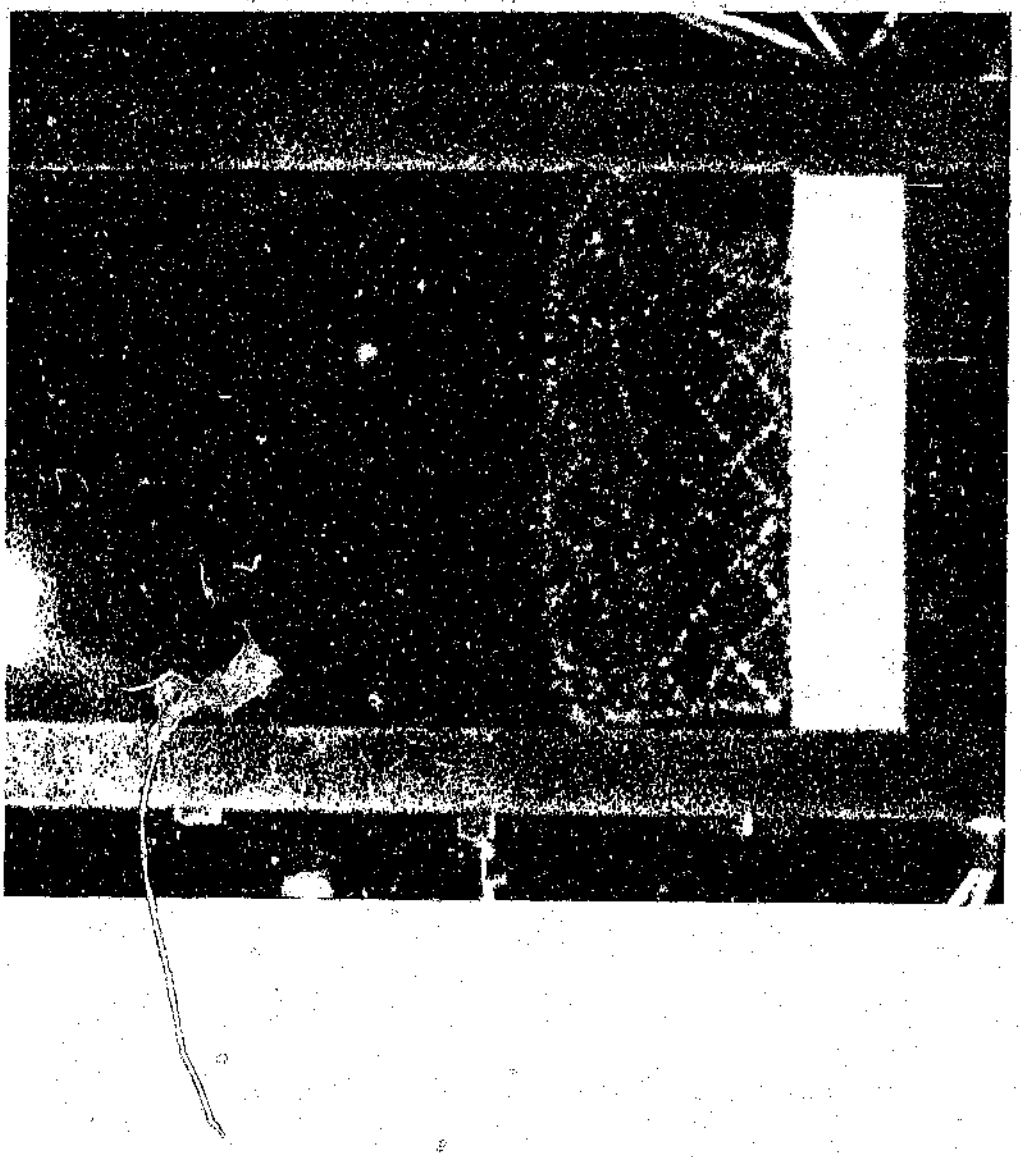


Plate 5.17 Path photograph,polyester foam, density 38 kg/m^3, (72 mm × 72 mm), time 800 μs

From these results it is the authors feeling that the foam behaves more one dimensionally with the foam material adjacent the shock tube walls, particularly as regards to the pressure measurement.

A series of tests were run with different sides of the polyester foam covered with cling rap (a flexible clear plastic), the idea being to quantify the transverse gas flow (side leakage.)

Plate 5.18 is a schlieren photograph taken 1340 μs after the incident shock wave struck the polyester foam. In this test all sides of the foam except the rear face of the foam was covered with cling rap. The compression wave that was transmitted into the air can be seen traveling away from the front face of the foam. The gas front can be seen emerging from the front face of the foam. The sides of the foam curve to the center of the shock tube as a result of the restricted foam movement imposed on it by the cling rap.

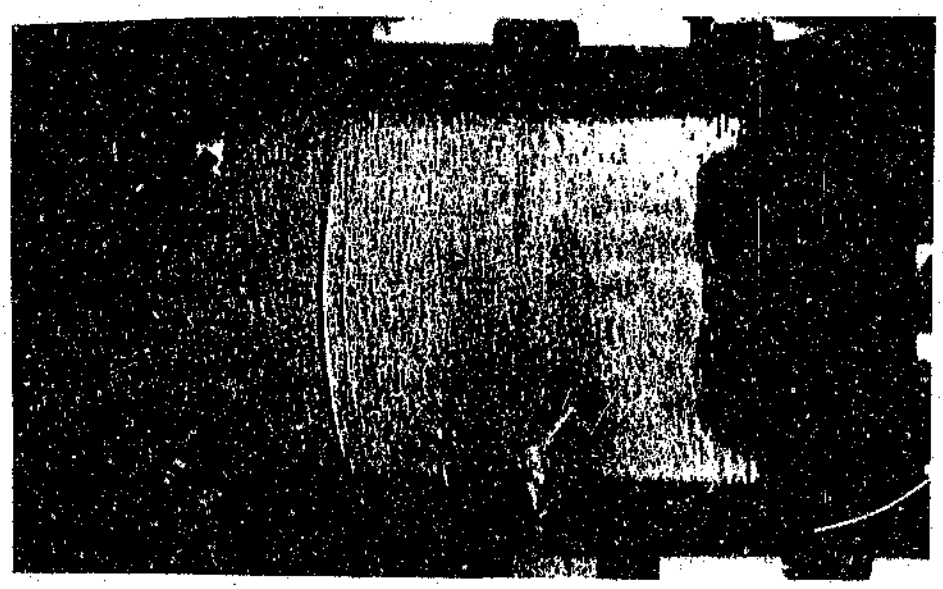


Plate 5.18 Schlieren photograph, polyester foam, density 38 kg/m^3, cling rap side, time 1340 μs

Different sides of the foam were covered and tests performed, a set of schlieren photographs of these tests are shown in appendix G. It is the author's opinion that due to the restricting nature of the cling rap on the foams motion this type of test adds another complicating factor to the shock foam interaction and a comprehensive set of tests of this nature would be required before any concrete conclusion concerning transverse gas flow could be

made. Further 3-D analysis of this nature is not within the scope of this research.



6 Conclusions

A series of tests in a shock tube were conducted on two compressible porous foams, a polyether (32.5 kg/m^3) and polyester (38 kg/m^3 .) The following sequence of events were identified taking place after an incident shock wave (S_I, Mach 1.426) struck the compressible porous foam:

- a shock wave (S_R, polyether Mach 1.176, polyester Mach 1.179) is reflected from the front face of the foam
- a gas compression wave (C_1, polyether 198 m/s, polyester 140 m/s) is transmitted into the foam
- the front face of the foam begins to move and the foam starts to be compressed (velocity of the front face of the foam, polyether 58 m/s, polyester 54 m/s)
- a foam compression wave (polyether 90 m/s, polyester 89 m/s) travels through the skeleton of the foam material
- an almost solid piston is formed by the gas compression wave, trapping and compressing the air in front of it into a smaller volume
- the transmitted gas compression wave (C_1) strikes the solid wall behind the foam and reflects back into the foam (C_2)
- the compression wave (C_2) strikes the air / foam interface, a compression wave (C_3) is transmitted into the air and a rarefaction wave is reflected back into the foam (R_1)
- a large pressure (polyether R = 2.55, polyester R = 3.09) builds up on the solid wall behind the foam, as a result of the mechanical action of the foam piston, aided by the compression waves C1 and C2
- the high pressure behind the foam results in gas leakage past the sides of the foam

- a contact surface emerges from the front face of the foam
- the foam reaches it maximum point of compression and begins to expand
- the contact surface is no longer visible
- all the gas has been expelled from the the foam
- the foam reaches a stable semi compressed state, approximately half it's original length
- the compression wave C_3 steepens and forms a shock wave (S_{TRT})
- shock wave S_{TRT} overtakes shock wave S_R, a transmitted shock wave S_{TRTT} is formed, while a centred rarefaction wave R_2 is reflected back towards the foam.

Between the range of incident Mach numbers 1.37 to 1.46 and the density range of compressible porous foams 32 to 38 kg/m^3 the following conclusions are drawn with regard to the theoretical predictions of Monti, Gel'fand and Gvozdeva:

- the experimental reflected shock wave Mach number lies between the values predicted using Gel'fand's analysis (upper limit) and Monti's analysis (lower limit)
- for an incident shock wave Mach number of 1.426 striking the polyether foam, Gel'fand's analysis over predicts the Mach number by 5.6 % and Monti's analysis under predicts the reflected Mach number by 3.2 %
- for an incident shock wave Mach number of 1.426 striking the polyester foam, Gel'fand's analysis over predicts the Mach number by 6.1 % and Monti's analysis under predicts the reflected Mach number by 2.6 %
- the coefficient of pressure increase as predicted by Gvozdeva's analysis for the polyether foam lies within the scatter of the experimental results

- the coefficient of pressure increase as predicted by Gvozdeva's analysis for the polyester foam is approximately 15 % lower than the experimental values.

References

[1] **Atkins M D (1987)** Shock Wave Interaction With Porous Materials Undergraduate Research Report, University of the Witwatersrand Johanesburg

[2] **Beavers G S, Sparrow E M (1969)** Non-Darcy Flow Through Fibrous Porous Media J. of Applied Mechanics December pp.711-714

[3] **Beavers G S, Matta R K (1972)** Reflection of Weak Shock Waves From Permeable Materials AIAA Journal Vol. 10 No. 7

[4] **Borisov A A, Gel'fand B E, Kudinov V M, Palamarchuk V V, Stepanov E I, Timofeev E I, Khomik S V (1978)** Shock Waves in Water Foams Acta Astronautica vol. 5 pp. 1027-1033

[5] **Campbell I J, Pricher (1958)** Shock Waves in a Liquid Containing Gas Bubbles Proc. R. Soc. London Ser. A. vol. 1235 pt.3 pp.534-545

[6] **Clarke J F (1983)** Regular Reflection of a Weak Shock Wave From a Rigid Porous Wall Q. JL. Mech. APPL. Math 37 pp.87-110

[7] **Clarke J F (1983)** Regular Reflection of a Weak Shock Wave From a Rigid Porous Wall; Some Additional Results Cranfield Inst. of Tech. COA Memo No 8225.

[8] **Clarke J F (1984)** Regular Reflection of a Weak Shock Wave From a Perforated Plug J. Engng Maths. vol. 18 pp. 335-349

[9] **Clarke J F (1984)** Regular Reflection of Weak Shock Waves From Absorbent Surfaces Proc. R. SOC. Lond. A 596, pp. 365-382.

[10] **Clarke J F (1985)** Effect of a Porous Surface on a Shock Wave Initially Normal to it Cranfield Inst. of Tech. COA Report, NFP85/15.

[11] **Cloutier M, Devereux F, Doyon P, Fitchett A, Heckman D, Moir L, Tardif L (1971)** Reflection of Weak Shock Waves from Acoustic Materials J. of the Acoustical Society of America. 50 pp.1393-1396

[12] **Computerscope ISC - 16 (1987)** Reference Manual RE Electronics Inc. Santa Barbra USA

[13] **Du Plessis J P, Masliyah J H (1988)** Mathematical Modeling of Flow Through Consolidated Isotropic Porous Media Transport in Porous Media 3 pp.145-161.

[14] **Emuanuel G, Jones J P (1966)** Compressible flow through a porous plate Aerospace Corporation TR-669(6240-20)-15

[15] **Fritz J N, Taylor J W (1966)** An Equation of State for Adiprene Foam and its Application in Producing Low Pressure-Long Time Pulses Los Alamos Scientific Laboratory Report LAMS-3400-MS

[16] **Frolov S M, Gel'fand B E, Medvedev S P, Tsyganov S A (1989)** Quenching of Shock Waves by Barriers and Screens 17 th International Symposium on Shock Tubes and Waves

[17] **Gel'fand B E, Gubanov A V, Kogarko S M, Timofeev A I (1974)** Passage of Shock Waves Through an Interface of Two-Phase Gas-liquid Media Izv. Akad. Nauk. Sssr, Mekh. Zhidk. Gaza. vol. 6 pp.58-65

[18] **Gel'fand B E, Gubin S A, Kogarko S M, Popov O E (1975)** Investigation of the Special Characteristics of Propagation and Reflection of Pressure Waves in a Porous Medium Fh. Prikl. Mekh. Tekl. FIZ. No 6, pp.74-77

[19] **Gel'fand B E, Gubanov A V, Timofeev A I (1982)** Peculiarities of Shock Wave Propagation in Foams Fizika Goreniya I Vzryva Vol. 17 No. 4 pp. 129-136

[20] **Gel'fand B E, Gubanov A V, Timofeev A I (1983)** Interaction of Shock Waves in Air with a Porous Screen Izv. An Sssr, Mzhg, No 4, pp.79-84

[21] **Guy T B (1973)** Attenuation of Reflecting Shock Waves in a Duct with Absorbent Lining J. of Sound and Vibration. 29(4) pp.501-503

[22] **Gvozdeva L G, Faresov Yu M (1985)** Calculating the Parameters of Steady Shock Waves in Porous compressible media Zh. Tekh. Fiz. vol. 55 pp.773-775

[23] **Gvozdeva L G, Faresov Yu M, Brossard J, Charpentie N (1987)** Normal Shock Reflection on Compressible Material Prog. Astron. Aeron. vol.106 pp.155-165

[24] **Gvozdeva L G, Lyakhov V N, Raevskii D K, Faresov Yu M (1987)** Shock Wave Propagation in a Gas and a Porous Medium Fizika Goreniya I Vzryva, Vol.23 No. 4 pp. 125-129

[25] **Henderson L F (1988)** On the Refraction of Longitudinal Waves in Compressible Media Lawrence Liverore Natural Laboratory UCRL-53853

[26] **Henderson L F (1989)** On the Refraction of Shock Waves J. Fluid Mech. vol.198 pp.365-386

[27] **Henderson L F,Gvozdeva L G, Syam R, Virgona R J (1989)** Refraction of a Normal Shock Wave From Nitrogen into Polyurethane Foam 17 th International Symposium on Shock Tubes and Waves

[28] **Korobeinikov V P (1989)** Unsteady Interaction of Shock and Detonation Waves in Gases Hemisphere Corporation New York

[29] **Mazor G, Ben-Dor G, Mond M, Igra O (1987)** Shock Wave Formation in a Suddenly Compressed Rubber Rod AIAA Journal, vol. 25, No 1. pp.116-119

[30] **Monti R (1970)** Normal Shock Wave Reflection On Deformable Solid Walls Meccanica vol. 5 pp. 285-296 S32. 593: 532. 529 Plenum.

[31] **Morioka S, Matsui G (1975)** Pressure - Wave Propagation through a Separated Gas - Liquid Layer in a Duct J. of Fluid Mech. vol. 70 part 4 pp.721-731.

[32] **Rayevsky D K, Gvozdeva L G, Faresov Yu, Brossard J, Bailly P (1989)** Reflection of Shock and Explosion Waves from Surfaces covered with Layers of Polyurethane Foam Explosion conference 1989

[33] **Rudinger G (1965)** Some Effects of Finite Particle Volume on the Dynamics of Gas-Particle Mixtures AIAA Journal vol. 3 No 7 pp.1217-1222.

[34] **Savu G, Trifu O (1984)** Porous Airfoils in Transonic Flow. AIAA Journal, vol. 22, No 7, pp.989-991

[35] **Savu G, Trifu O (1985)** Numerical Prediction of the Aerodynamic Behaviour of Porous Airfoils J. Spacecraft Vol. 22 No. 6

[36] **Seitz M W, Skews B W (1991)** Three-dimensional effects in the study of shock wave loading of porous compressible foams 18 th International Symposium on Shock Waves, Sendal Japan

[37] **Skews B W (1966)** Shock Wave Diffraction PhD Thesis, University of the Witwatersrand Johanesburg

[38] **Skews B W, Atkins M D, Seitz M W (1991)** Gas dynamic and physical behaviour of compressible porous foams struck by a weak shock wave18 th International Symposium on Shock Waves, Sendal Japan

[39] **Sommerfeld M (1985)** The Unsteadiness of Shock Waves Propagating Through Gas-Particle Mixtures Experiments in Fluids. vol. 3 pp.197-206

[40] **Stupochenko Ye V, Loscv S A, Osipov A I (1967)** Relaxation in Shock Waves Springer - Verlag New York.

[41] **Van Wijngaarden (1972)** One-Dimensional flows of liquids containing small gas bubbles Ann. Rev. Fluid Mech. vol.4 pp.369- 396

[42] **Voskoboinikov M, Gel'fand E Z, Gubin S A, Kogarko M, Popov O E (1976)** Utilization of Liquid - Gas Bubble Mixtures for the Transfer of Shock Wave Disturbances Fizlheskil Zhurnal vol.31 pp.674-677

[43] **Weaver P M, Pratt N H (1989)** Experimental Study of Shock Structure in Aqueous Foams and the Unsteady Shock Emergence at the Foam/Air Boundary 17 th International Symposium on Shock Tubes and Waves

Appendix A

A.1 Transducer Specifications

Performance specifications for the 113A21 PCB pressure transducer:

Range	50 psi
Maximum pressure	3000 psi
Resolution	0.01 psi
Sensitivity	20 mV/psi
Resonant frequency	500 KHz
Discharge constant	1 s
Low frequencies response	0.5 Hz
Linearity	1%
Output impedance	100 ohms
Acceleration sensitivity	0.002 psi/g
Temperature coefficient	0.03 %/F
Temperature range	-100 to 275 F
Weight	6 gm
Excitation / constant current	13 to 28

A.2 Power Supply Specifations

Performance specifications for the 482A10 PCB line power supply

Sensor excitation	2 to 20
Voltage to CC regulator	+24 V
Voltage gain	1; 10; 20
Coupling time constant	10
Frequency response	0.5 to 200K Hz
Output impedance	2 ohms
Output noise	0.5
Output current	± 10 mA
Output voltage	± 10 V
Weight	2 lb.

Appendix B

B.1 Pressure Transducer Calibration

The PCB piezoelectric pressure transducers were calibrated in the shock tube. Two transducers located upstream of the test section, 620,5 mm (Δd) apart were used to measure the time (Δt) it took for the incident shock wave to travel between them. From the time, the velocity of the shock wave and hence the pressure (P_2) behind it could be calculated. Knowing the pressure behind the incident shock wave the transducers in the test section were calibrated.

Equations B.1 to B.5 were used to determine the sensitivity of the transducers.

$$V_I = \frac{\Delta d}{\Delta t} \tag{B.1}$$

$$a_1 = \sqrt{\gamma R T_1} \tag{B.2}$$

$$M_I = \frac{V_I}{a_1} \tag{B.3}$$

$$P_2 = P_1 \left[\frac{2\gamma M_I^2}{\gamma+1} - \frac{\gamma-1}{\gamma+1}\right] \tag{B.4}$$

$$S = \frac{P_2 - P_1}{v_I} \tag{B.5}$$

Where:

- S sensitivity (Pa/mv)
- v_I average voltage (mv).

To calibrate transducer SN 4815 tests F1A1502H, F1A1503H and F1A1504I were used. Table B.1 shows the parameters of the calibration.

Table B.1 Calibration of transducer SN 4815

File	F1A1502H	F1A1503H	F1A1504I
CH2	CH2	CH2	CH3
P_1 (Pa)	82550	82550	82530
T_1 (K)	301	301	301
t (Us)	640	640	640
v_i (mv)	344.3	343.1	333.0
a_1 (m/s)	347.8	347.8	347.8
V_i (m/s)	500.8	499.2	494.8
M_i	1.44	1.44	1.42
P_2 (Pa)	185800	184600	180900
S (Pa/mv)	300.0	297.5	295.5

Combining the three tests the sensitivity for transducer SN 4815 is :

$$S = \frac{300.0 + 297.5 + 295.5}{3}$$

$$= 297.7 \ \ Pa/mv$$

The manufactures state that the transducers have a 1% linearity, thus only one calibration point is required. Table B.2 lists the sensitivity of the transducers used in the test section.

Table B.2 Transducer sensitivity

Transducer	Sensitivity (Pa/mv)
SN 4815	297.7
SN 4816	309.2
SN 4817	282.4
SN 4818	266.9

Table B.2 cont. Transducer sensitivity

Transducer	Sensitivity (Pa/mv)
SN5218	266.9
SN5219	260.9

Appendix C

C.1 Pressure Traces

Figures C.1 to C.9 are the pressure traces along the test section for the shock wave interaction with the polyester.

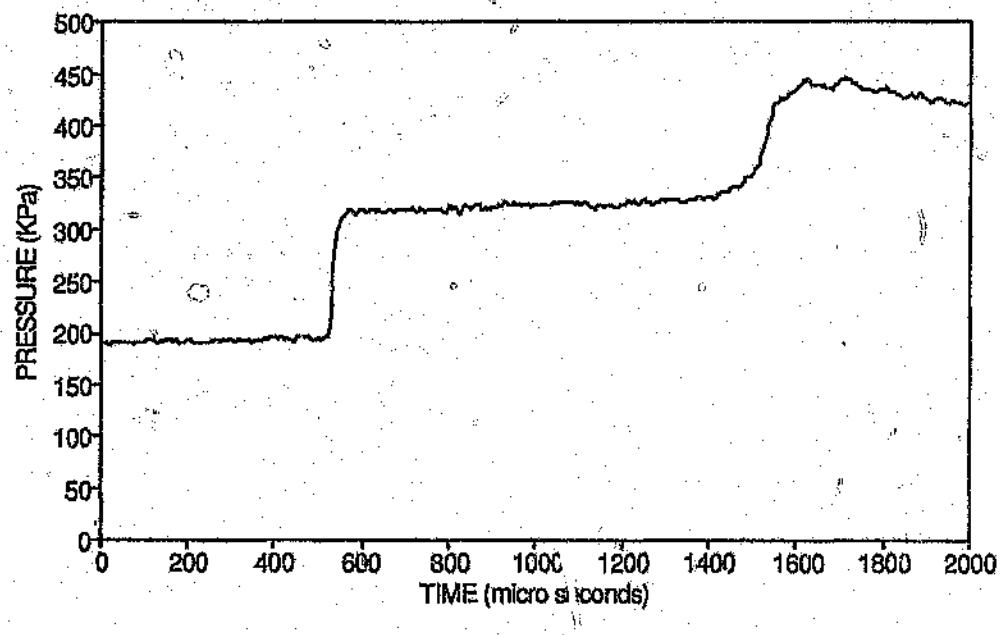


Figure C.1 Pressure variation at P1, 70 mm of polyester foam, incident shock wave Mach number 1.4

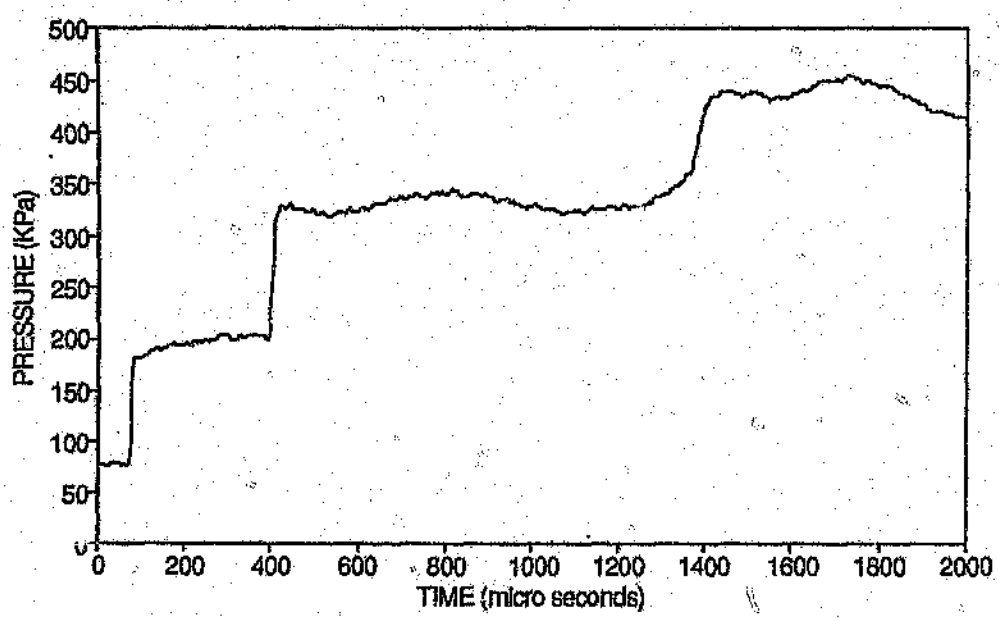


Figure C.2 Pressure variation at P3, 70 mm of polyester foam, incident shock wave Mach number 1.4

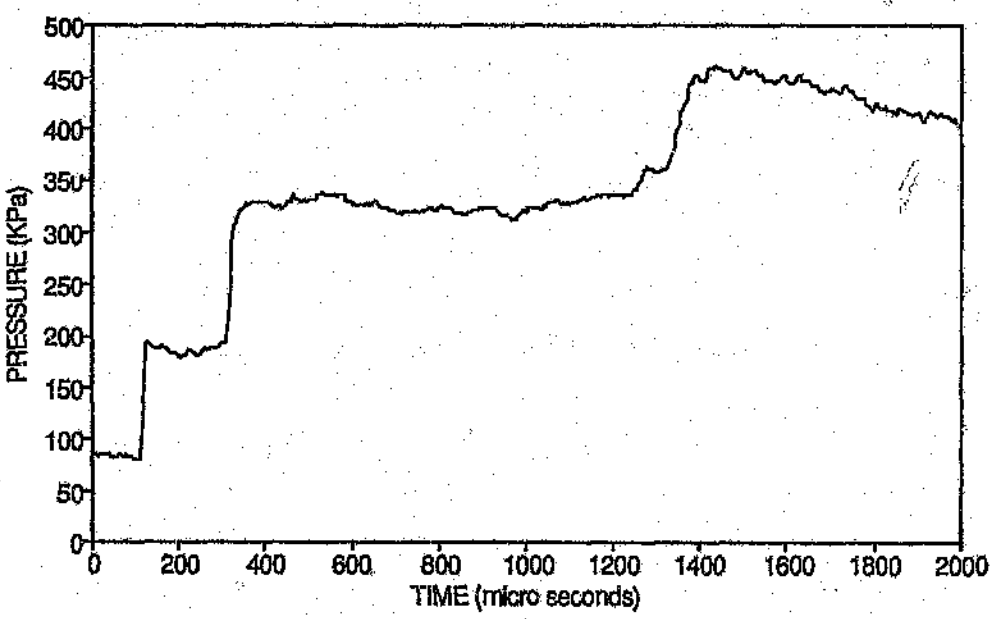


Figure C.3 Pressure variation at P4, 70 mm of polyester foam, incident shock wave Mach number 1.4

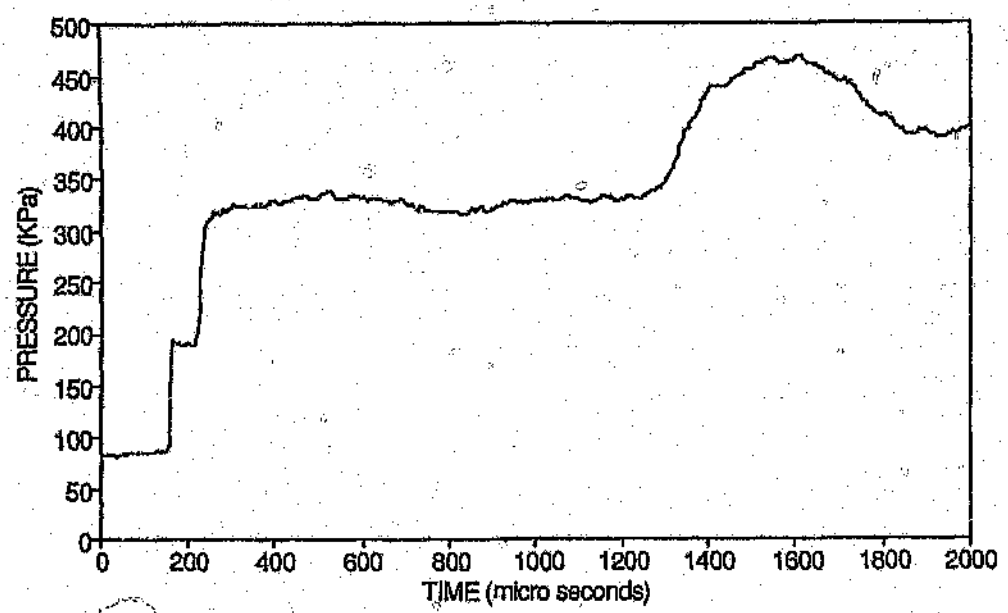


Figure C.4 Pressure variation at P5, 70 mm of polyester foam, incident shock wave Mach number 1.4

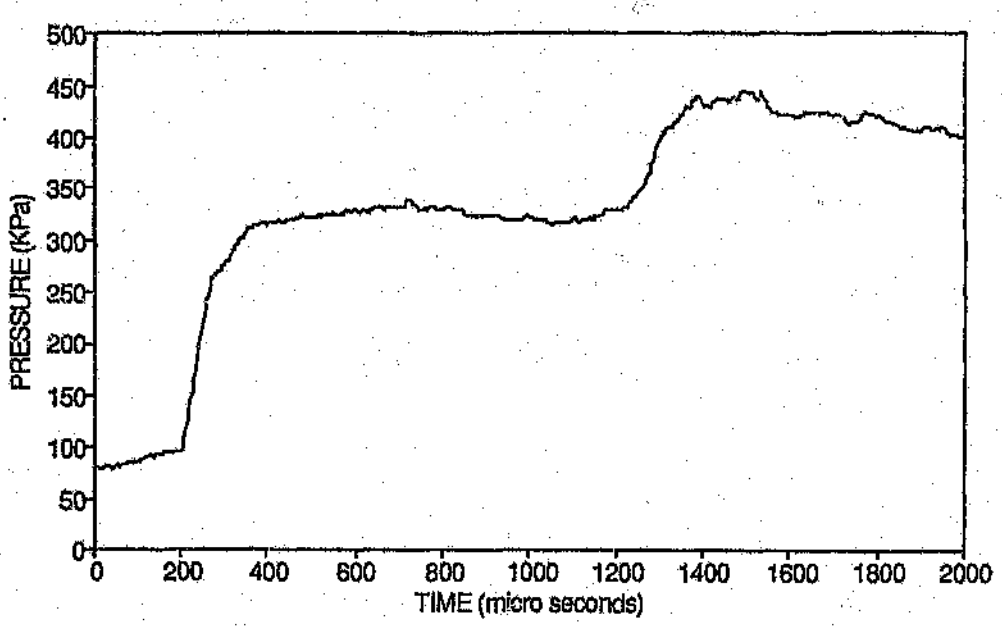


Figure C.5 Pressure variation at P6, 70 mm of polyester foam, incident shock wave Mach number 1.4

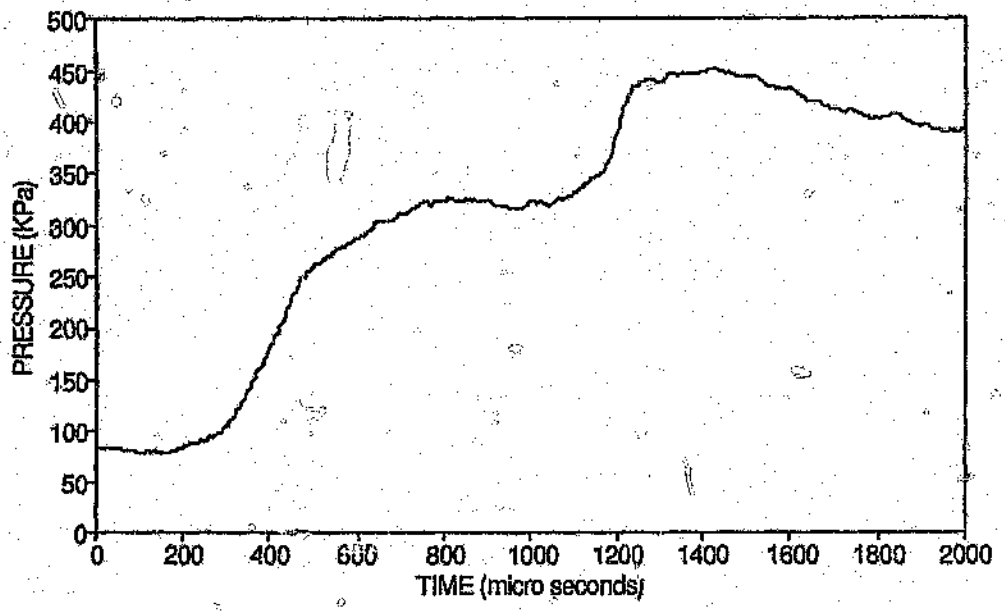


Figure C.6 Pressure variation at P7, 70 mm of polyester foam, incident shock wave Mach number 1.4

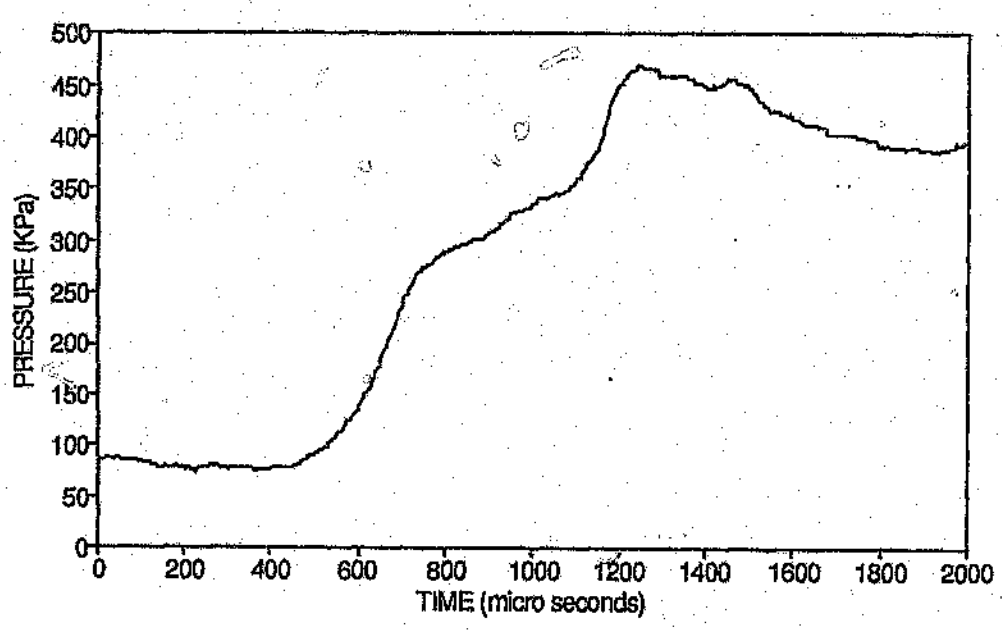


Figure C.7 Pressure variation at P8, 70 mm of polyester foam, incident shock wave Mach number 1.4

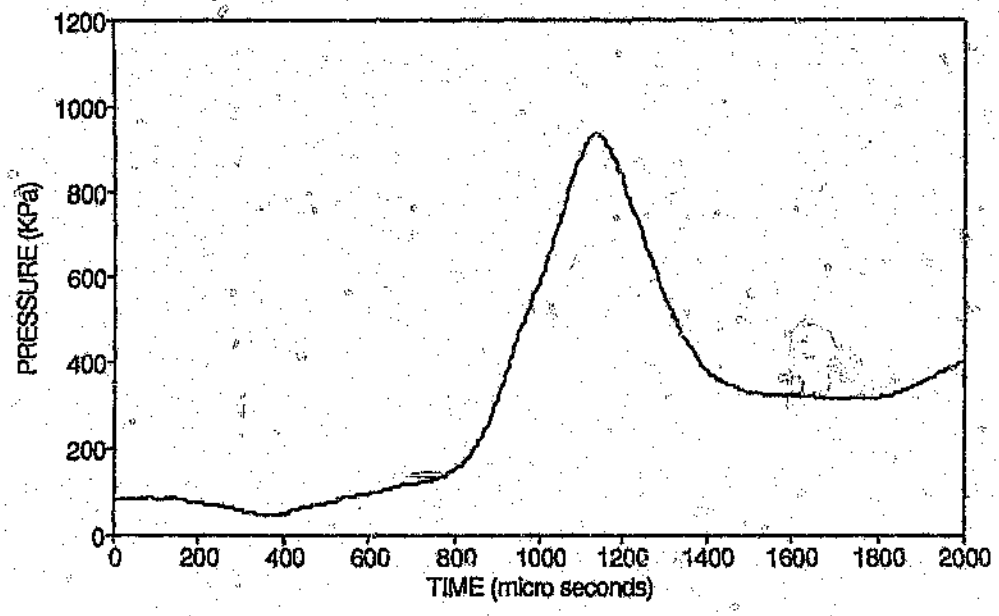


Figure C.8 Pressure variation at P9, 70 mm of polyester foam, incident shock wave Mach number 1.4

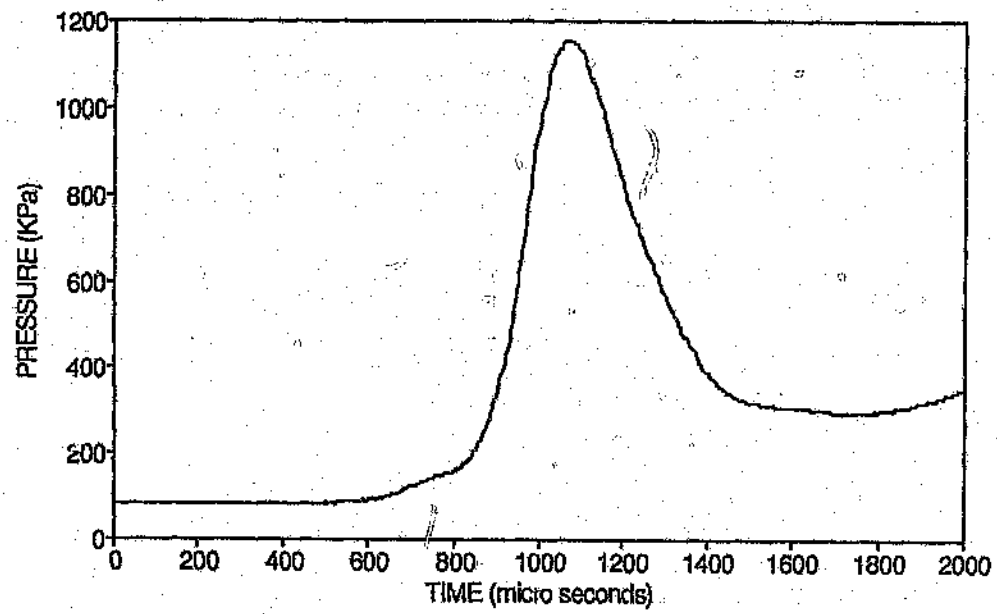


Figure C.9 Pressure variation at P10, 70 mm of polyester foam, incident shock wave Mach number 1.4

Appendix D

D.1 Program Photograph Conversion

Description

The program translates, rotates and scales data that was measured from negatives using a cartesian vernier system.

Input

The following information is supplied to the program via the keyboard:

- number of photograph data points
- coordinates of data point (X,Y)
- actual distance between data point (X_2,Y_2) and the back plate of the shock tube.

The program requires three specific data points to be entered first,in a certain order. They are shown in figure D.1. The second point (X_2 ,Y_2), must be located on the top wall of the shock tube. Further the distance between (X_2

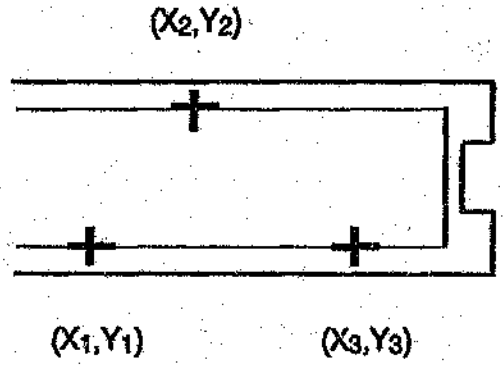


Figure D.1 Shock tube test section

,Y_2) and the back plate must be known. Point one (X_1,Y_1) is on the bottom of the shock tube to the left of (X_2 ,Y_2). Point three (X_3 ,Y_3) is on the bottom of the shock tube to the right of (X_2 ,Y_2).

Operation

The first data point becomes the origin of the new axes system, which is rotated to get the x axis parallel to the top and bottom shock tube walls. The data is then scaled to the correct size using a magnification factor. This factor is calculated using the first three data points and knowing the distance between the top and bottom walls. The origin of the axes system is shifted to the base of the back plate of the shock tube and the distances to the left shown as positive. Thus a X coordinate is the distance between the back plate and its point.

Output

The output file PHOTO.PRN contains:

- data point number
- input coordinates (X,Y)
- transformed coordinates (X,Y).

```
C
C                    PHOTOGRAPH CONVERSION
C
C     Program to translate, rotate and scale data that was measured
C     from negatives using a cartesian vernier system
C
      DOUBLE PRECISION X(30),Y(30),R(30),THETA(30),ALFA,
      MAG1,MAG2,MAG,DIST1,DIST2,ERROR,XX(30),YY(30)
      INTEGER INUM,IC,IORIG,IAXIS,PT1,PT2,PT3,PT4
      OPEN(10,FILE='PHOTO.PRN',STATUS='OLD')
C
C     Read in data measured from photograph
C
      WRITE(*,400)
400   FORMAT(1X,'ENTER Number of photograph data points')
      READ(*,*) INUM
      DO 10 I=1,INUM
      WRITE(*,410) I
410   FORMAT(1X,'ENTER Data point number ',I3,'  X,Y')
      READ(*,*) XX(I),YY(I)
10    CONTINUE
      WRITE(*,420)
420   FORMAT(1X,'ENTER Distance between data point 2 and back
      plate')
      READ(*,*) KNOX
C
C     Translate the axes to get a point at the origin
C
      PI=3.14159
      IORIG=1
      DO 20 I=1,INUM
      X(I)=XX(I)-XX(IORIG)
      Y(I)=YY(I)-YY(IORIG)
20    CONTINUE
C
C     Rotate the axes to get a point on the Y axis
C
      DO 30 I=1,INUM
      R(I)=SQRT(X(I)**2+Y(I)**2)
      IF(X(I).EQ.0.0)THEN
      THETA(I)=0.0
      ELSE
      THETA(I)=ATAN(ABS(Y(I)/X(I)))
      IF(X(I).GE.0.0.AND.Y(I).GE.0.0)THETA(I)=THETA(I)
      IF(X(I).LT.0.0.AND.Y(I).GT.0.0)THETA(I)=PI-THETA(I)
      IF(X(I).LT.0.0.AND.Y(I).LT.0.0)THETA(I)=PI+THETA(I)
      IF(X(I).GE.0.0.AND.Y(I).LT.0.0)THETA(I)=2*PI-THETA(I)
      END IF
```

```
30      CONTINUE
        IAXIS=3
        ROTATE=THETA(IAXIS)
        DO 40 I=1,INUM
        THETA(I)=THETA(I)-ROTATE
40      CONTINUE
        DO 50 I=1,INUM
        X(I)=R(I)*COS(THETA(I))
        Y(I)=R(I)*SIN(THETA(I))
50      CONTINUE
C
C       Calculate the magnification factor of the data
C
        A=SQRT((X(1)-X(2))**2+(Y(1)-Y(2))**2)
        B=SQRT((X(2)-X(3))**2+(Y(2)-Y(3))**2)
        C=SQRT((X(1)-X(3))**2+(Y(1)-Y(3))**2)
        ALPHA=ACOS((B**2+C**2-A**2)/2/B/C)
        Z=B*SIN(ALPHA)
        MAG=76.2/Z
        DO 60 I=1,INUM
        X(I)=X(I)*MAG
        Y(I)=Y(I)*MAG
60      CONTINUE
C
C       Transfer origin to base of back plate
C
        SHIFT=KNOX+X(2)
        WRITE(10,200)
200     FORMAT(1X,'Number  Input Data   Output Data')
        WRITE(10,210)
210     FORMAT(8X,'X',6X,'Y',9X,'X',5X,'Y')
        WRITE(10,220)
220     FORMAT(1X)
        DO 70 I=1,INUM
        X(I)=-(X(I)-SHIFT)
        WRITE(10,230)I,XX(I),YY(I),X(I),Y(I)
230     FORMAT(1X,I3,4(F6.1,2X))
70      CONTINUE
        STOP
        END
```

Appendix E

E.1 Program Reflected Sound Wave Propagation

Description

The program calculates the sound wave pattern as seen in the test section window at a certain time as a result of a disturbance.

Input

The following information is supplied to the program ia the keyboard:

- incident shock mach number
- pressure ahead of incident shock wave (Pa)
- temperature ahead of incident shock wave (K)
- time of photograph (μS)
- number of vertical grid points.

Operation

The parameters describing the incident shock wave and the time at which the photograph was taken are entered. The conditions ahead of and behind the incident shock wave are calculated using the normal shock wave equations.

The program contains the position of all the possible disturbances that might produce a sound wave. These consist of all the joints and transducers in the shock tube.

Figure E.19 shows the equations that govern the prorogation of sound waves. Where a_0, a_1 are the speeds of sound in front of and behind the shock respectively, M the Mach number of the shock, u_1 the speed of gas behind the shock and t the time. The program uses the equations to calculates the

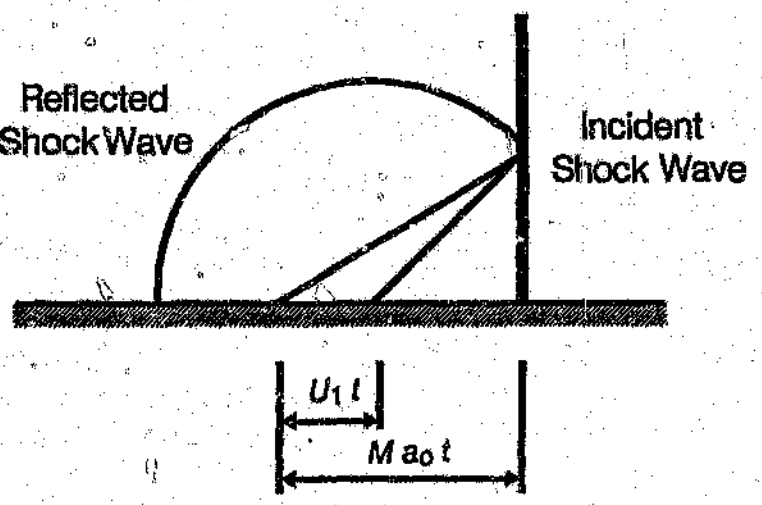


Figure E.1 Reflected sound wave propagation

shape and position of each sound wave system that would be seen in the test section at a certain time.

Output

The output file WAVE.PRN contains:

- disturbance number (Di)
- coordinates of the sound waves (Xi,Yi).

```
C
C                REFLECTED SOUND WAVE PROPAGATION
C
C       Program to calculate the propagation of a reflected sound wave
C       as a result of a disturbance
C
        REAL DX(45),DY(45),TX(45),RAD(45),CENT(45),
       &X(45,25,30),Y(45,25,30),M0,M1,MS
        INTEGER JS(42)
        OPEN(10,FILE='WAVE.PRN',STATUS='OLD')
        WRITE(6,200)
200     FORMAT(1X,'ENTER Incident shock Mach number')
        READ(*,*)MS
        WRITE(6,210)
210     FORMAT(1X,'ENTER Pressure ahead of incident shock wave (Pa)')
        READ(*,*)P0
        WRITE(6,220)
220     FORMAT(1X,'ENTER Temperature ahead of incident shock wave
        (K)')
        READ(*,*)T0
        WRITE(6,230)
230     FORMAT(1X,'ENTER Timing unit setting for photograph (micro
        sec)')
        READ(*,*)TP
        WRITE(6,240)
240     FORMAT(1X,'ENTER Number of vertical grid points')
        READ(*,*)N
C
C       Calculation of variables across the shock
C
        GAMA=1.4
        R=287.1
        CONST1=(GAMA-1.0)/2
        CONST2=(GAMA-1.0)/(GAMA+1.0)
        CONST3=(2.0*GAMA)/(GAMA-1.0)
        CONST4=(2.0*GAMA)/(GAMA+1.0)
        A0=SQRT(GAMA*R*T0)
        RO0=P0/R/T0
        M0=MS
        P1=P0*(CONST4*(M0**2)-CONST2)
        T1=T0*((1.0+(CONST1*M0**2))*((CONST3*M0**2)-1.0))/(M0*
        *2*(CONST3 +CONST1))
        M1=SQRT((M0**2+(CONST3/GAMA))/(CONST3*M0**2-1.0))
        A1=SQRT(GAMA*R*T1)
        RO1=P1/R/T1
        VS=MS*A0
        V1=A0*((P1/P0-1.0)/(GAMA*SQRT(1.0+1.0/CONST4*(P1/P0-1.
        0))))
```

```
C
C     Disturbance distances from back plate in (mm)
C
      DW=3.0
      DX(1)=-5.0+DW
      DY(1)=0.0
      DX(2)=5.0+DW
      DY(2)=0.0
      DX(3)=15.0+DW
      DY(3)=76.2
      DX(4)=25.0+DW
      DY(4)=76.2
      DX(5)=35.0+DW
      DY(5)=0.0
      DX(6)=45.0+DW
      DY(6)=0.0
      DX(7)=55.0+DW
      DY(7)=76.2
      DX(8)=65.0+DW
      DY(8)=76.2
      DX(9)=75.0+DW
      DY(9)=0.0
      DX(10)=85.0+DW
      DY(10)=0.0
      DX(11)=95.0+DW
      DY(11)=76.2
      DX(12)=105.0+DW
      DY(12)=76.2
      DX(13)=115.0+DW
      DY(13)=0.0
      DX(14)=125.0+DW
      DY(14)=0.0
      DX(15)=135.0+DW
      DY(15)=76.2
      DX(16)=145.0+DW
      DY(16)=76.2
      DX(17)=155.0+DW
      DY(17)=0.0
      DX(18)=165.0+DW
      DY(18)=0.0
      DX(19)=277.5+DW
      DY(19)=0.0
      DX(20)=277.5+DW
      DY(20)=76.2
      DX(21)=287.5+DW
      DY(21)=0.0
      DX(22)=287.5+DW
      DY(22)=76.2
```

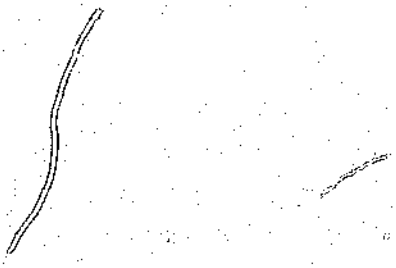
```
      DX(23)=405.2+DW
      DY(23)=76.2
      DX(24)=422.2+DW
      DY(24)=76.2
      DX(25)=426.2+DW
      DY(25)=76.2
      DX(26)=445.2+DW
      DY(26)=76.2
      DX(27)=765.2+DW
      DY(27)=76.2
      DX(28)=782.2+DW
      DY(28)=76.2
      DX(29)=788.2+DW
      DY(29)=76.2
      DX(30)=805.2+DW
      DY(30)=76.2
      DX(31)=922.1+DW
      DY(31)=0.0
      DX(32)=922.1+DW
      DY(32)=76.2
      DX(33)=932.1+DW
      DY(33)=0.0
      DX(34)=932.1+DW
      DY(34)=76.2
      DX(35)=1568.3+DW
      DY(35)=0.0
      DX(36)=1568.3+DW
      DY(36)=76.2
      DX(37)=1578.3+DW
      DY(37)=0.0
      DX(38)=1578.3+DW
      DY(38)=76.2
      DX(39)=2213.7+DW
      DY(39)=0.0
      DX(40)=2213.7+DW
      DY(40)=76.2
      DX(41)=2223.7+DW
      DY(41)=0.0
      DX(42)=2223.7+DW
      DY(42)=76.2
C
C     Calculation of sound wave pattern as seen in test section window
C     at time TP, as a result of a disturbance at DX(I),DY(I)
C
      IIS=0
      DO 10 I=1,42
      KKK=0
      IF(DY(I).EQ.0.0)THEN
```

```
      KKK=1
      ELSE
      KKK=2
      END IF
      D=DX(I)-163
      TX(I)=D/1000.0/VS+TP/1.0E6
      CENT(I)=V1*TX(I)*1000.0
      RAD(I)=A1*TX(I)*1000.0
C
C     Calculation of the starting point on the curve
C
      IF(D.GT.0.0)THEN
      DO 20 J=1,25
      IF(J.NE.1)THEN
      X(I,J,1)=X(I,J-1,N)
      Y(I,J,1)=Y(I,J-1,N)
      ELSE
      X(I,J,1)=RAD(I)
      Y(I,J,1)=DY(I)
      END IF
C
C     Calculation of sound wave coordinates
C
      IF(Y(I,J,1).LT.0.01)THEN
      M=2.0
      ELSE
      M=1.0
      END IF
      YC=SQRT(RAD(I)**2-X(I,J,1)**2)
      DO 30 K=2,N
      Y(I,J,K)=Y(I,J,1)+(-1)**(M)*(K-1)*(76.2/(N-1.0))
      Z=Y(I,J,1)-Y(I,J,K)
      IF(KKK.EQ.2)Z=(RAD(I)**2-(YC+(-1)**(J+1)*Z)**2)
      IF(KKK.EQ.1)Z=(RAD(I)**2-(YC+(-1)**J*Z)**2)
      JJ=0
      IF(Z.LT.0.0)THEN
      X(I,J,K)=0
      JJ=1
      GO TO 30
      ELSE
      ENDIF
      X(I,J,K)=SQRT(Z)
30    CONTINUE
      IF(JJ.EQ.1) GO TO 40
      XTEST=DX(I)-X(I,J,1)-CENT(I)-DS
      IF(XTEST.GT.200)GO TO 40
20    CONTINUE
      ELSE
```

Appendix F

F.1 Schlieren Photographs

Plates F.1 to F.9 are the schlieren contact prints of the tests conducted. The time at which each photograph was taken may be found using the S number and table 4.3.



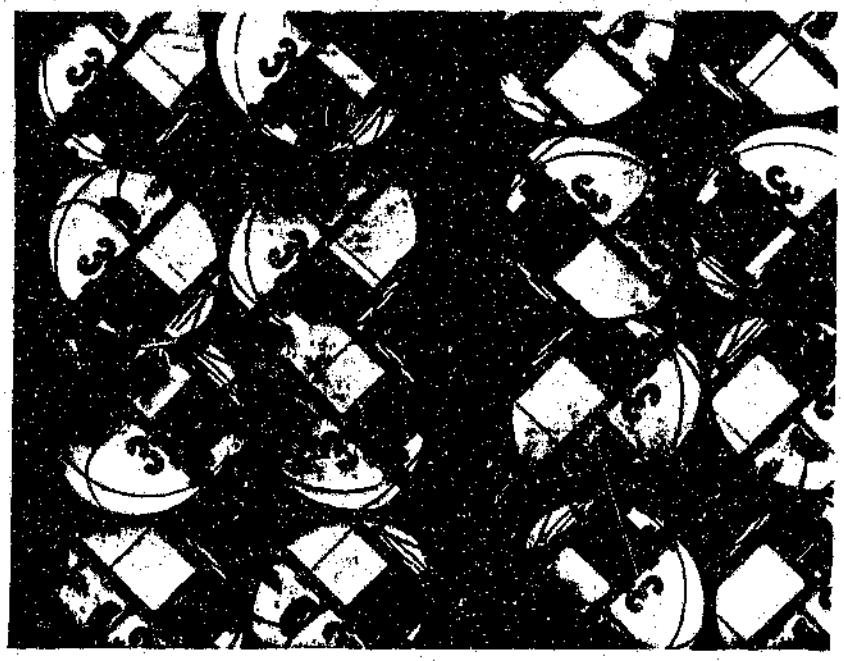


Plate F.1 Schlieren photographs, polyether foam, density 32.5 kg/m^3, (S3.1 to S3.4)

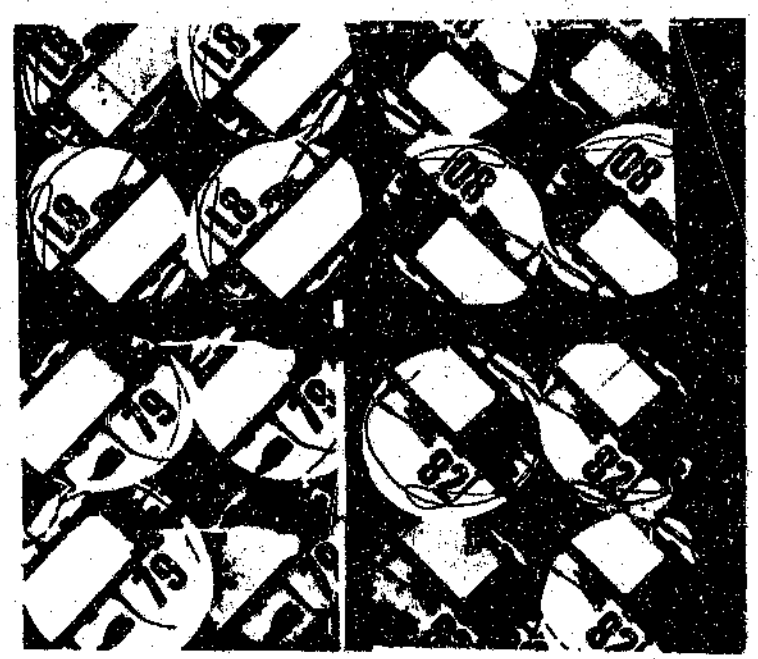


Plate F.2 Schlieren photographs, polyether foam, density 32.5 kg/m^3, (S79 to S82)

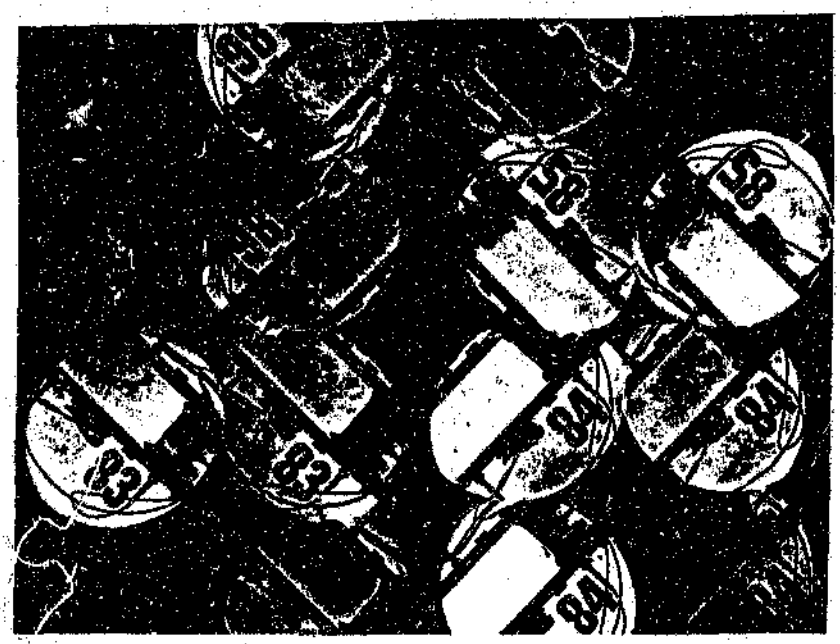


Plate F.3 Schlieren photographs, polyether foam, density 32.5 kg/m^3, (S83 to S86)

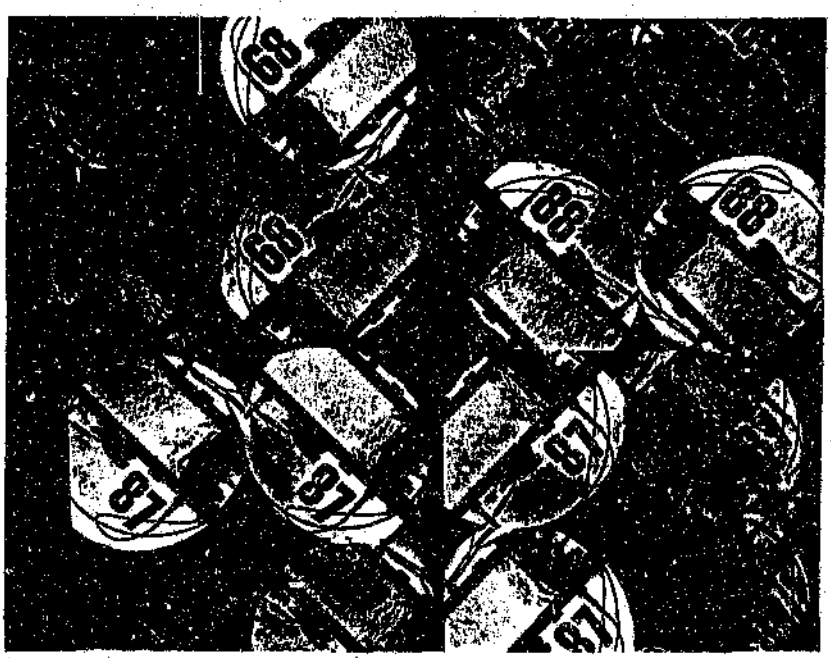


Plate F.4 Schlieren photographs, polyether foam, density 32.5 kg/m^3, (S87 to S89)



Plate F.5 Schlieren photographs, polyester foam, density 38 kg/m^3, (S90 to S93)

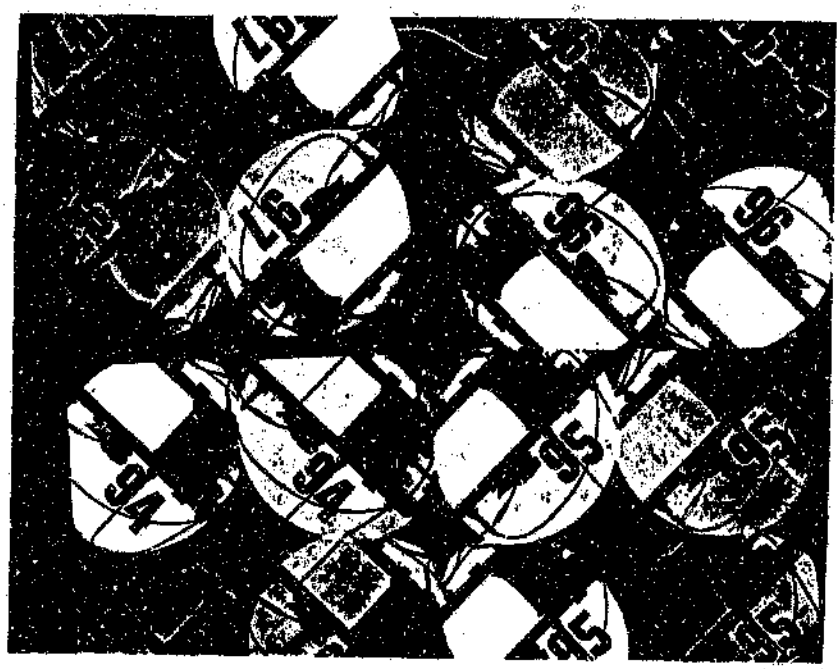


Plate F.6 Schlieren photographs, polyester foam, density 38 kg/m^3, (S94 to S97)

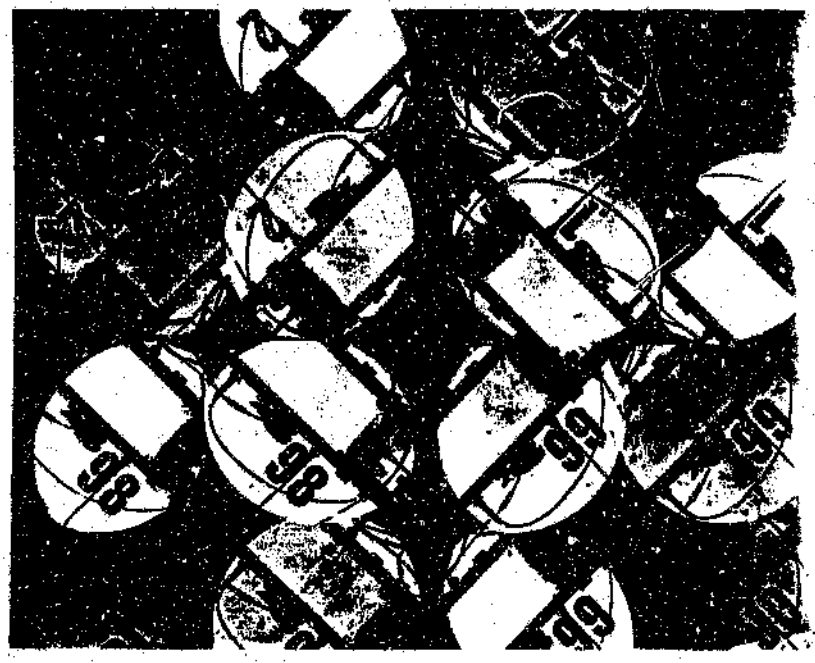


Plate F.7 Schlieren photographs, polyester foam, density 38 kg/m^3, (S98 to S2)

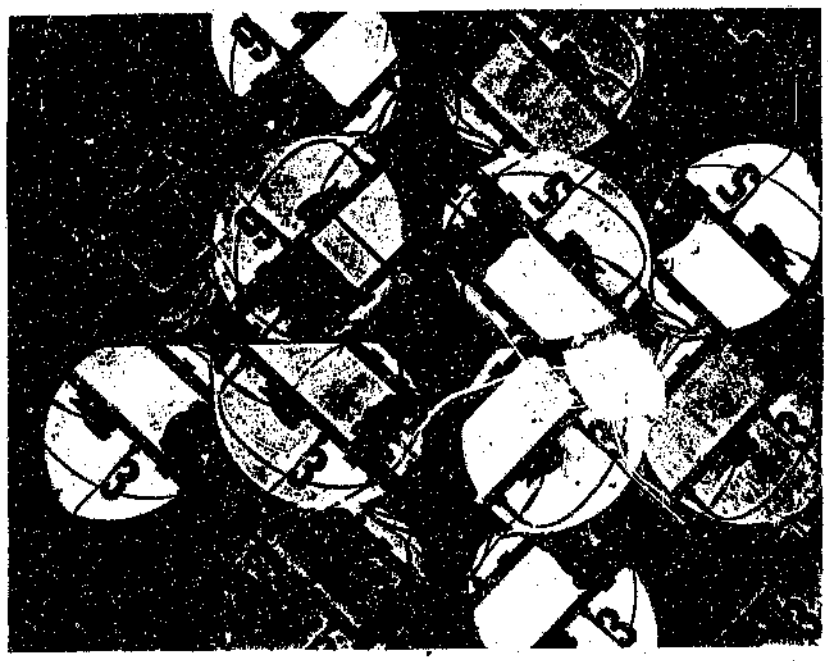


Plate F.8 Schlieren photographs, polyester foam, density 38 kg/m^3, (S3 to S6)

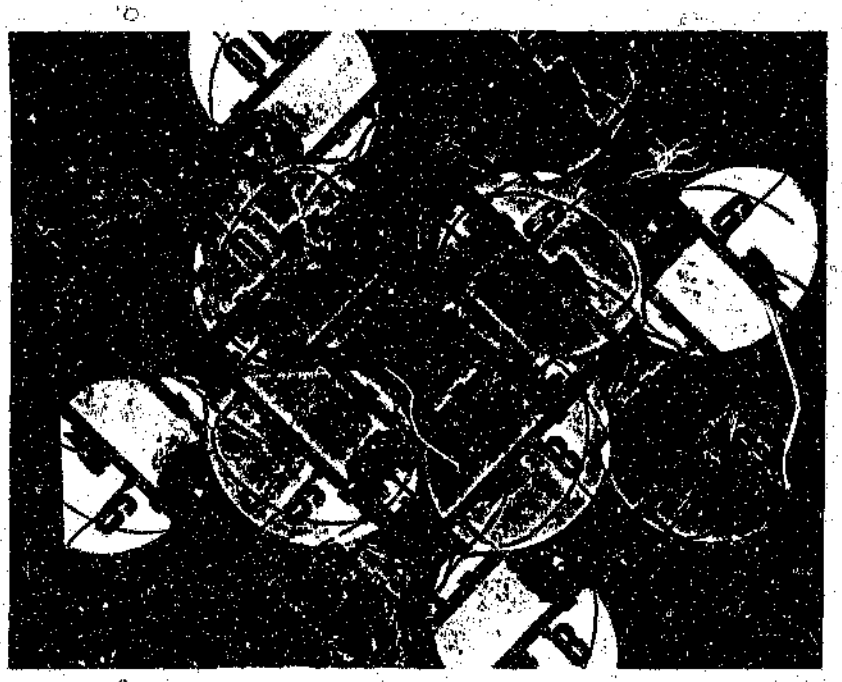


Plate F.9 Schlieren photographs, polyester foam, density 38 kg/m^3, (S7 to S10)

Appendix G

G.1 Path Photographs

Plates G.1 to G.7 are the path contact prints of the tests conducted. The time at which each photograph was taken may be found using the P number and table 4.3.

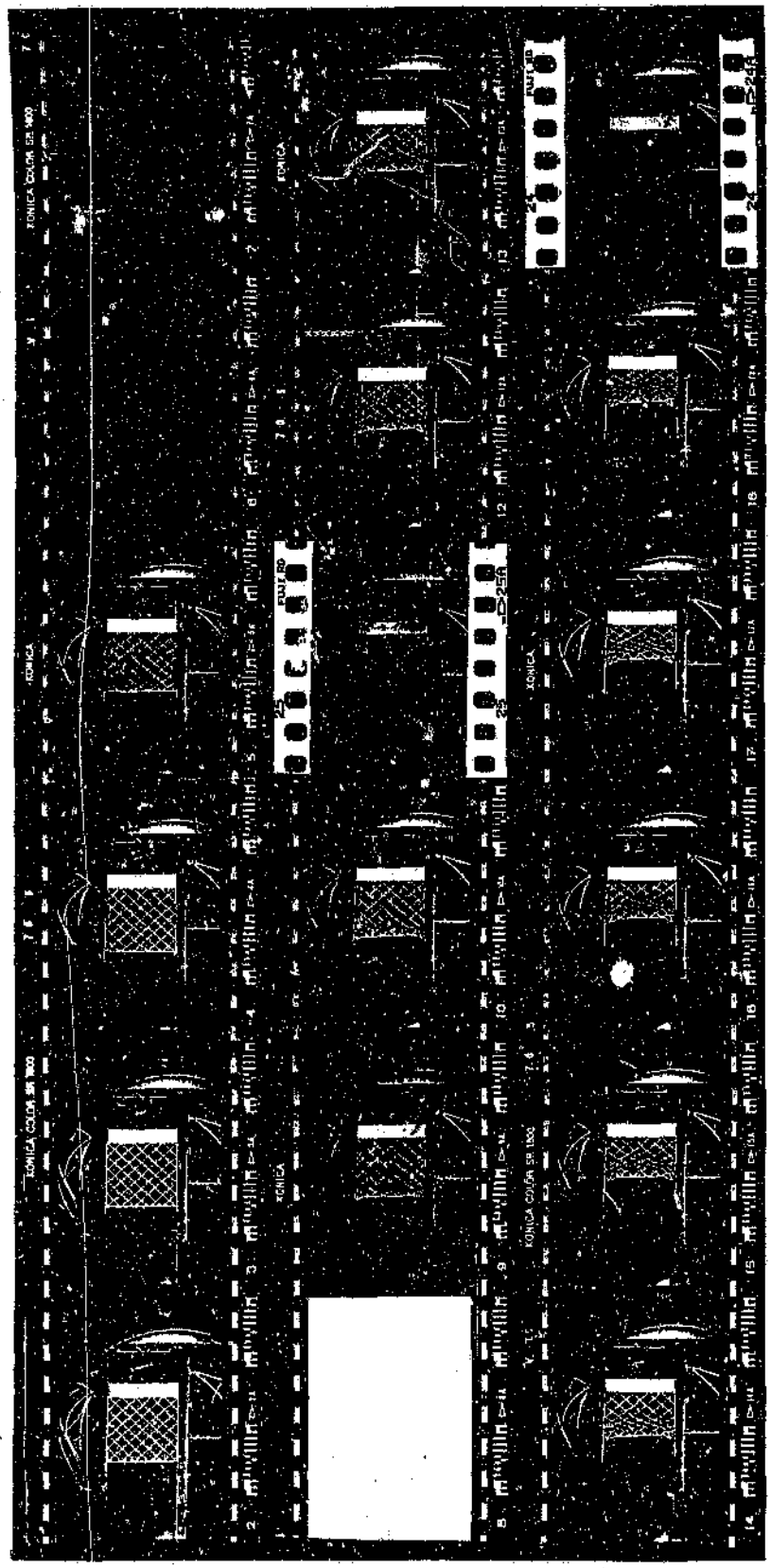


Plate G.1 Path photographs, polyester foam, density 38 kg/m^3, (P2 to P19)

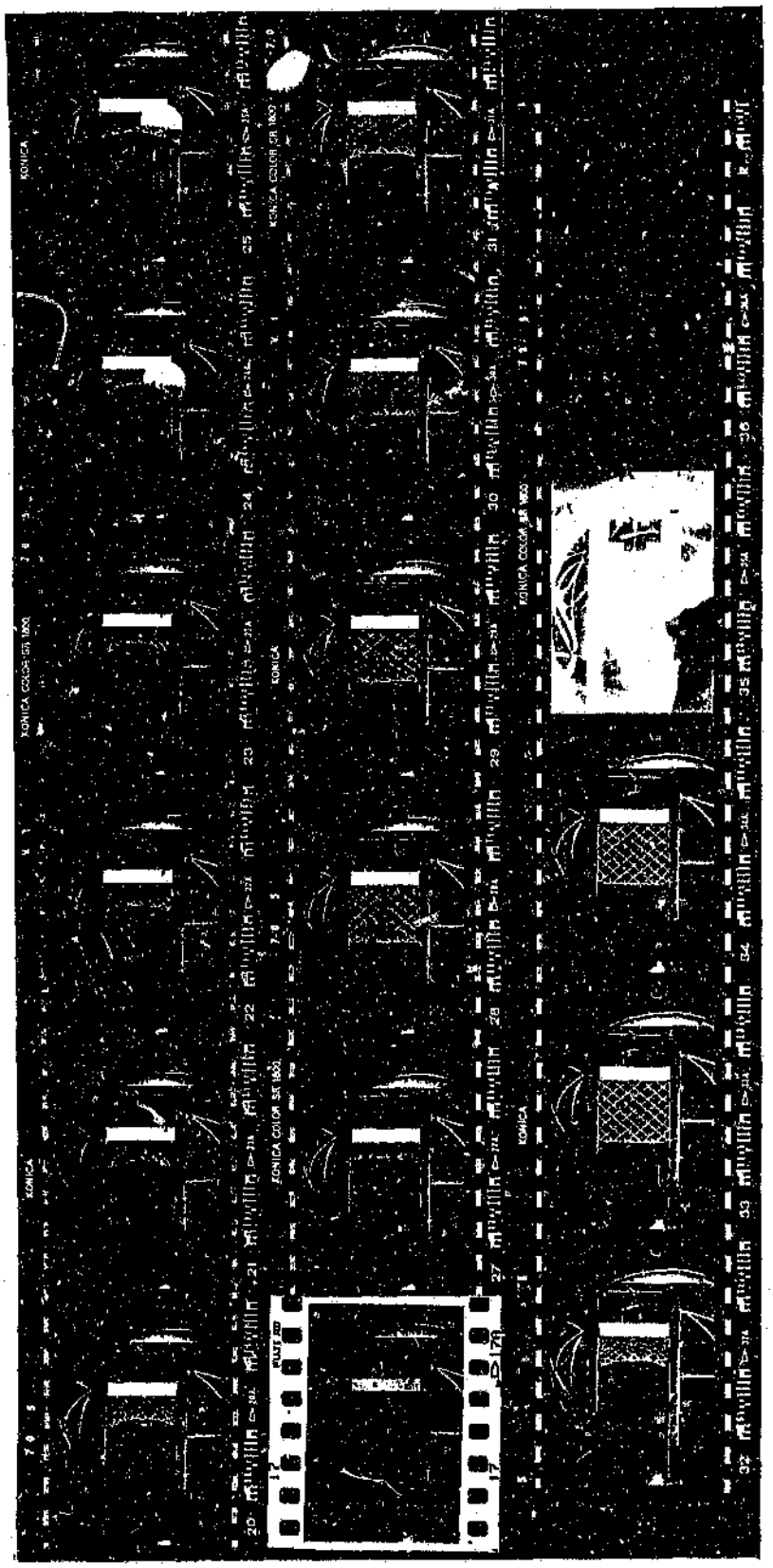


Plate G.2 Path photographs, polyester foam, density 38 kg/m^3, (P20 to P35)

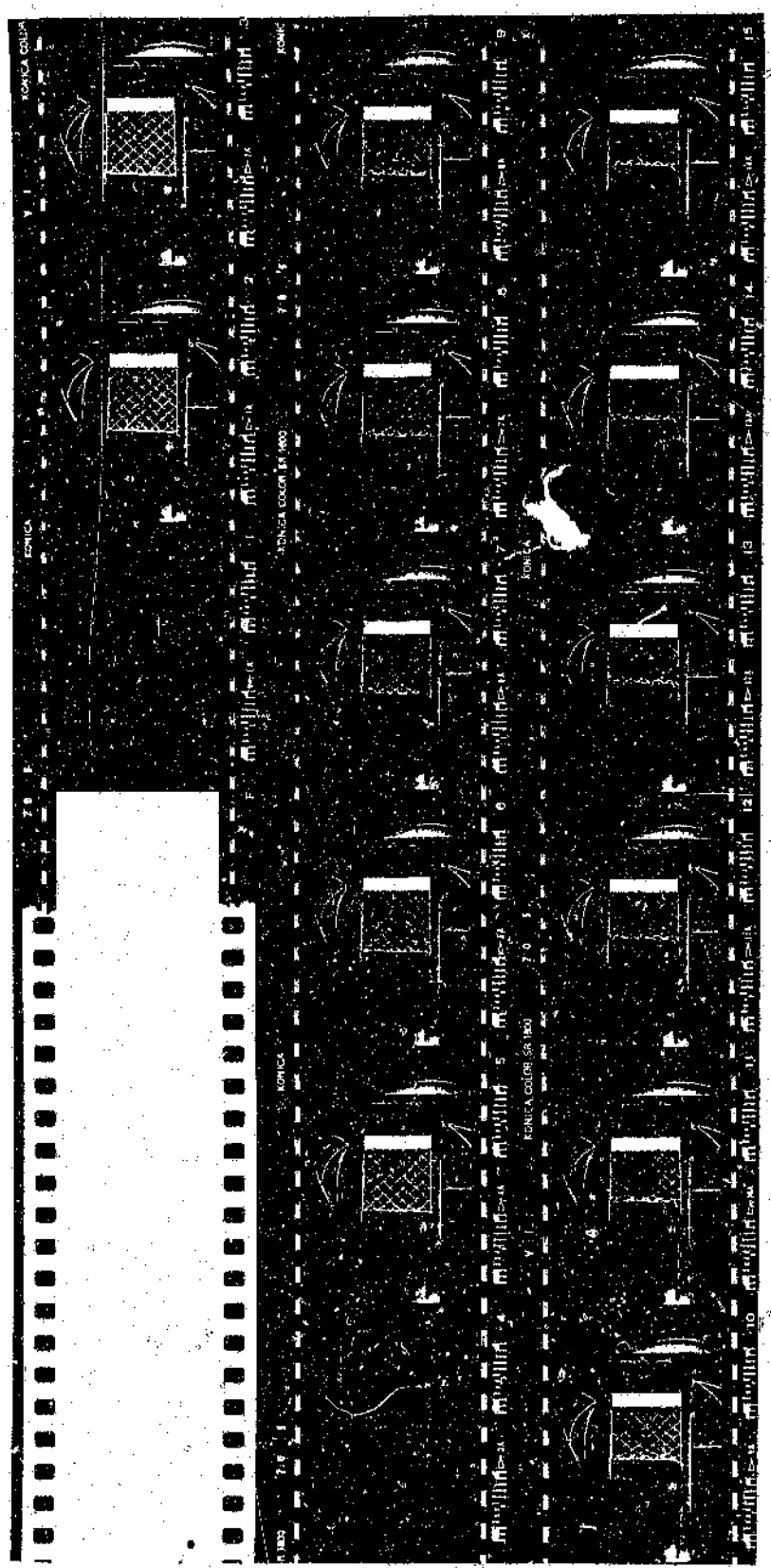


Plate G.3 Path photographs, polyether foam, density 32.5 kg/m^3, (P1 to P14)

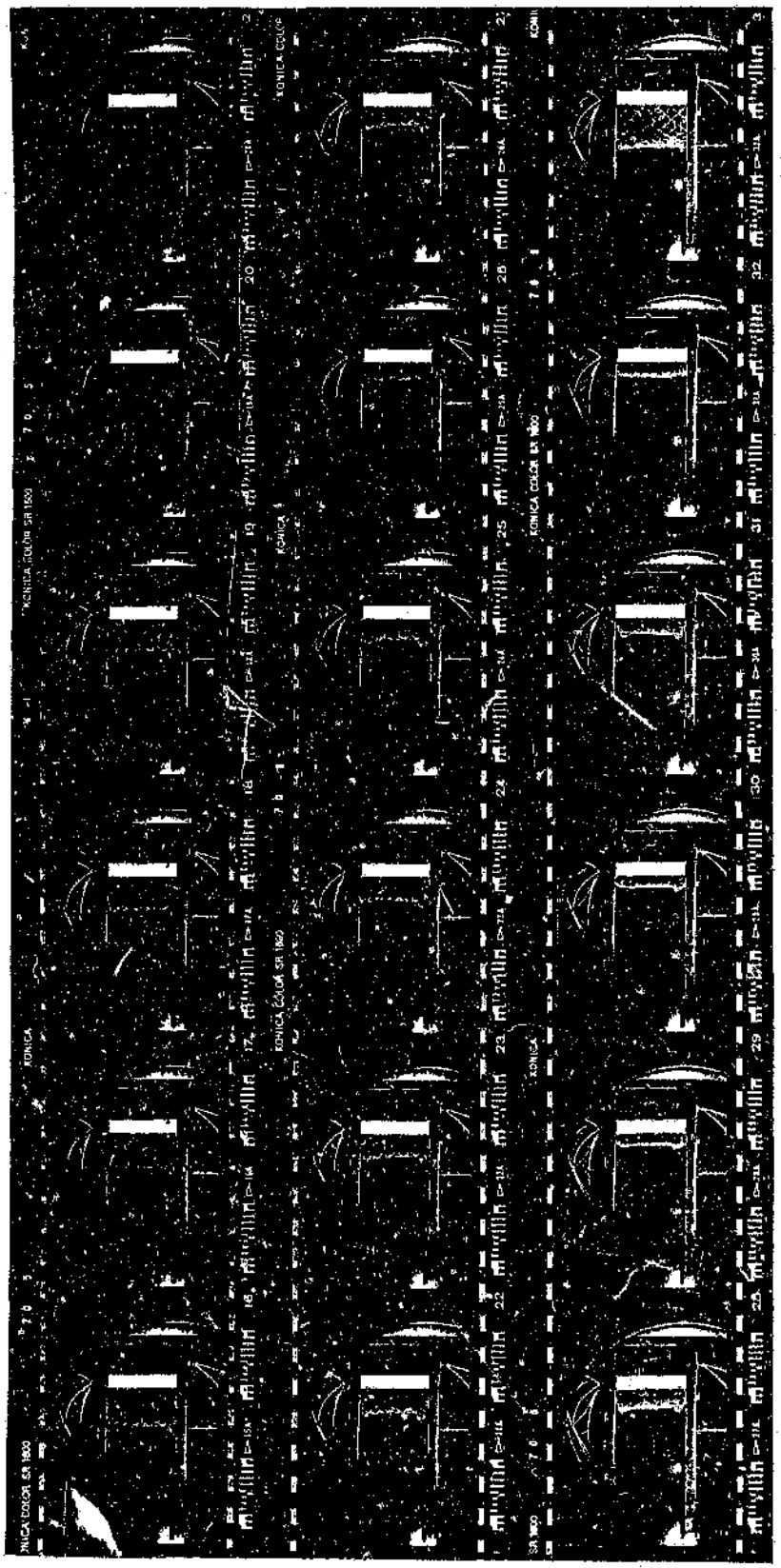


Plate G.4 Path photographs, polyether foam, density 32.5 kg/m^3, (P15 to P32)

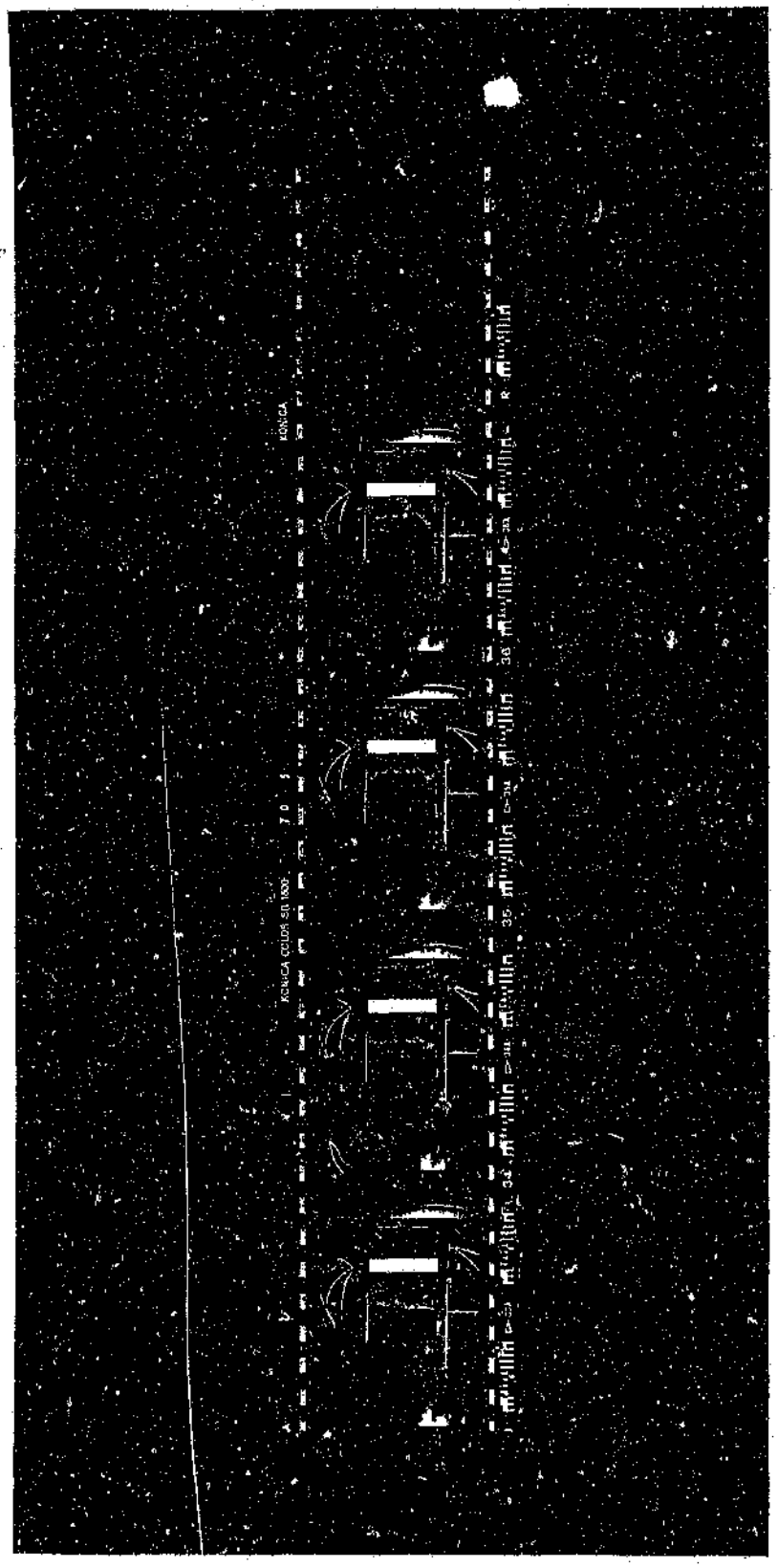


Plate G.5 Path photcgraphs, polyether foam, density 32.5 kg/m^3, (P33 to P36)

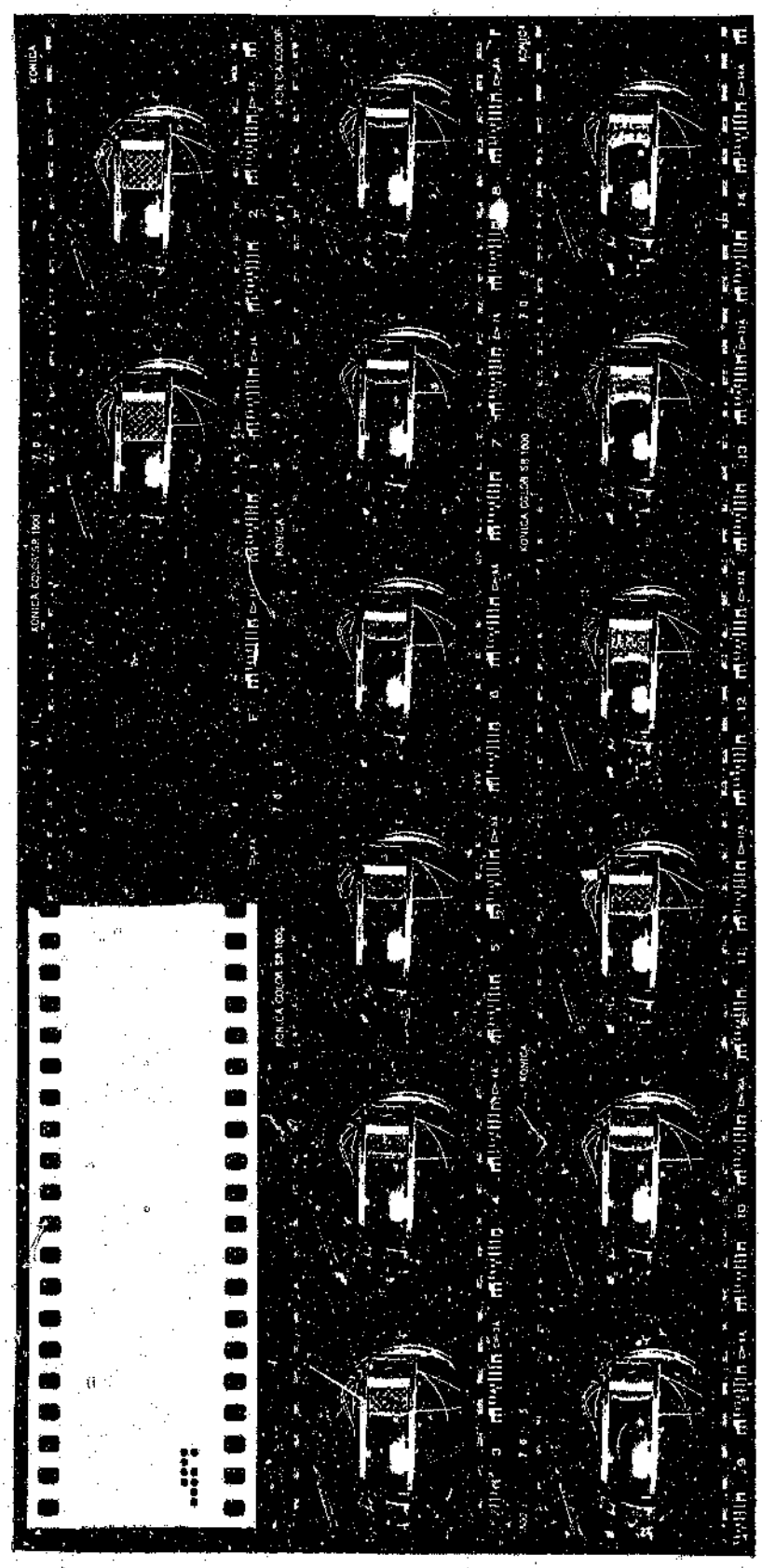


Plate G.6 Path photographs, polyester foam, density 38 kg/m^3, (72 mm × 72 mm), (P1 to P14)

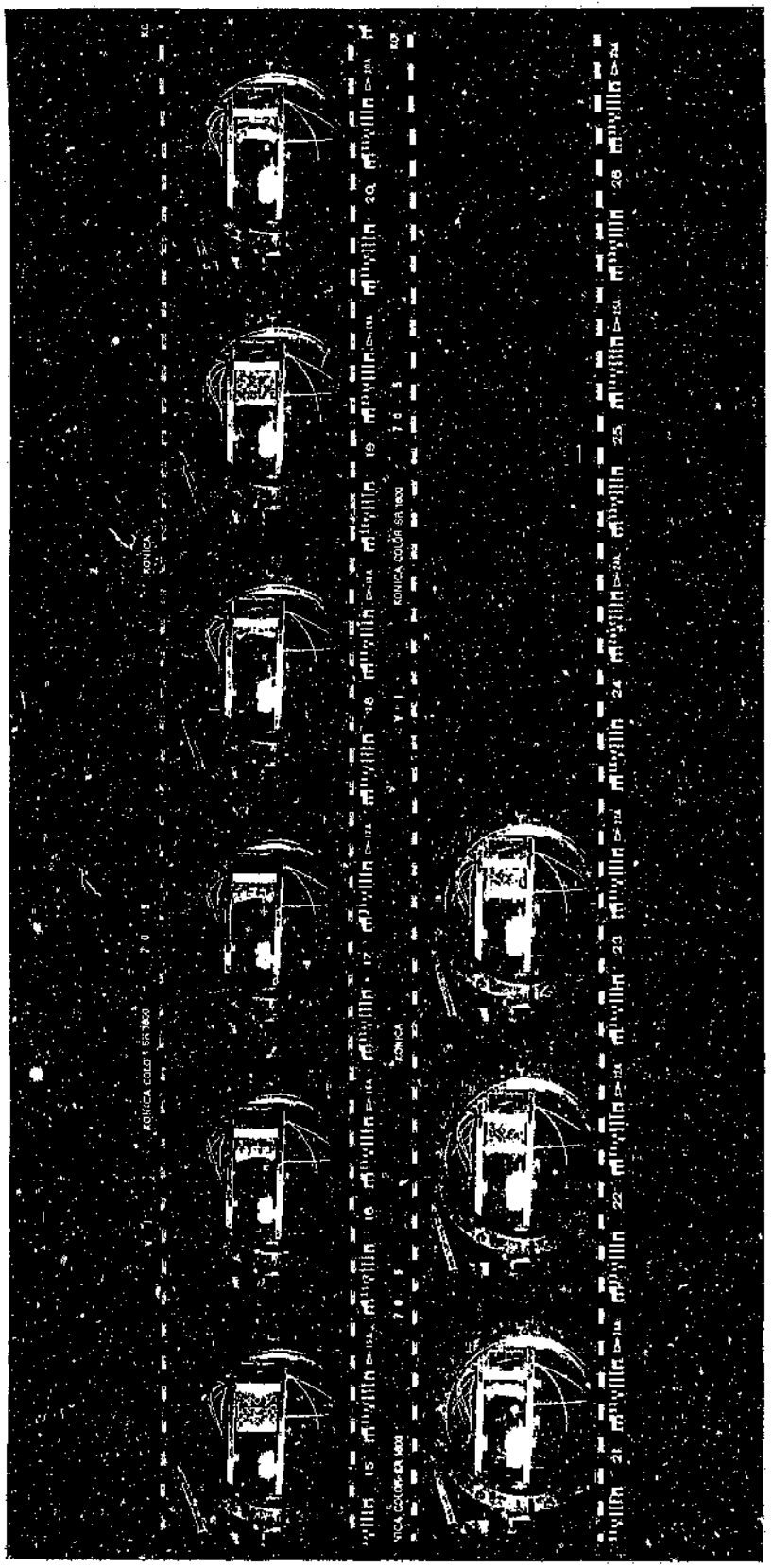


Plate G.7 Path photographs, polyester foam, density 38 kg/m^3, (72 mm × 72 mm), (P15 to P26)

Appendix H

H.1 Program Compressed Foam Boundary

Description

The program calculates the path of the compressed foam boundary given a pressure distribution history. Assuming issentropic compression.

Input

An input file named PRESSURE.IN containing position of the transducers (X_i), time (T_i) and pressure (P_i) is required. This file must be in the following format.

X_6 X_5 X_4 X_3 X_2 X_1
T_1 P_5 P_4 P_3 P_2 P_1
T_{1+1} P_5 P_4 P_3 P_2 P_1
ect.

The pressure recorded by the five pressure transducers alongside the polyester foam is listed in table H.1. The pressure recorded alongside the polyether foam is listed in table H.2.

Table H.1 Pressure recorded along side the polyester foam (input for the compressed foam boundary program)

Time (*m s*)	Pressure (Pa) *x = 63 mm*	Pressure (Pa) *x = 43 mm*	Pressure (Pa) *x = 23 mm*	Pressure (Pa) *x = 3 mm*	Pressure (Pa) *x = 0 mm*
0	81620	83957	87334	82890	83884
20	[illegible]	83957	88922	83957	83884
80	85747	81823	85747	86626	82817
140	92096	81823	80033	85292	83884
200	95271	83957	78446	79154	83884

Time ($m\,s$)	Pressure (Pa) $x = 63\ mm$	Pressure (Pa) $x = 43\ mm$	Pressure (Pa) $x = 23\ mm$	Pressure (Pa) $x = 3\ mm$	Pressure ( ) $x = 0\ mm$
260	243844	94365	81620	68746	82817
320	288924	116515	78446	53001	82817
380	313686	162149	76858	50333	85219
440	316861	218190	80033	63409	82817
500	321305	260088	92096	76485	86554
560	324480	276900	112097	91963	89222
620	327655	291311	152415	103705	96963
680	330829	305455	217495	116515	115379
740	332417	319865	270194	127189	141268
800	329242	323868	290511	153075	160752
860	324480	325203	301305	223527	232548
920	324480	319865	313686	371904	431922
980	320036	317197	330829	536292	849087
1040	316861	319865	343210	701748	1125329
1100	320036	330273	360354	889353	1123994
1160	322893	348687	401941	914171	955847
1220	330829	416470	460990	770865	760476
1280	372735	441021	462577	605410	611813
1340	417497	442356	457815	468508	483967
1400	431465	449027	448609	382578	387617
1460	434640	447693	454640	344684	331568
1520	439402	443690	437815	328939	316088
1580	422259	431948	422259	323868	309415
1640	425434	420206	411465	322534	304344
1700	419084	412467	403529	319865	297672
1760	417497	405795	399084	319865	296337

Time ($m\,s$)	Pressure (Pa) $x = 63\ mm$	Pressure (Pa) $x = 43\ mm$	Pressure (Pa) $x = 23\ mm$	Pressure (Pa) $x = 3\ mm$	Pressure (Pa) $x = 0\ mm$
1820	415910	404728	391148	325203	303010
1880	406703	398056	389560	343349	312084
1940	406703	391652	387973	371904	328899
2000	400354	394053	394322	400725	349717

Table H.2 Pressure recorded along side the polyether foam (input for the compressed foam boundary program)

Time ($m\,s$)	Pressure (Pa) $x = 63\ mm$	Pressure (Pa) $x = 43\ mm$	Pressure (Pa) $x = 23\ mm$	Pressure (Pa) $x = 3\ mm$	Pressure (Pa) $x = 0\ mm$
24	81283	82553	83823	83633	83633
80	85410	82553	83823	83633	82566
144	91759	81486	83823	86302	82566
200	113347	82553	79696	82566	83633
264	246682	94028	78109	76161	82566
320	283825	116178	76521	69757	83633
384	280174	144999	81283	67088	83633
440	296206	173554	88585	74827	88970
504	300968	217853	105728	87636	95375
560	304143	245340	125728	104716	102046
624	307318	258416	161602	122862	115121
680	307318	267490	201602	138341	134601
744	307318	286971	254301	161825	165822
800	304143	293642	283825	194382	206116
864	296206	300047	305730	262165	285636
920	293349	306452	316524	349430	380900

Time (*m s*)	Pressure (Pa) *x = 63 mm*	Pressure (Pa) *x = 43 mm*	Pressure (Pa) *x = 23 mm*	Pressure (Pa) *x = 3 mm*	Pressure (Pa) *x = 0 mm*
984	297794	301381	332080	460445	515123
1040	307318	307786	342873	572261	686972
1104	316524	315792	352080	679274	912457
1160	333667	328602	358429	736650	942344
1224	353667	356089	386366	753462	843344
1280	369223	380907	425097	727309	698713
1344	393985	409461	437478	637643	539673
1400	400017	421203	432716	535968	432935
1464	404779	419869	415573	432958	366490
1520	403192	413464	412716	367844	348345
1584	395573	413464	411128	335285	331266
1640	393985	403057	401604	327280	322194
1704	393985	392649	406366	332618	316857
1760	393985	387312	397160	349430	313121
1824	387636	376904	389223	357436	316857
1880	381604	376904	381604	358770	324862
1944	375255	370499	378429	358770	335269
2000	372398	371567	378429	362506	347010

The following information is supplied to the program via the keyboard:

- number of pressure records
- atmospheric pressure (Pa)
- atmospheric density (kg/m^3)
- percentage difference between successive iterations acceptable for determining the compressed foam path.

Operation

At each time internal the program assumes a starting point for the position of the compressed foam boundary (CFB) X_I. The mean pressure within that portion of the foam is calculated using the pressure recorded by the transducers assuming isentropic compression ie.

$$V P^{\frac{1}{\gamma}} = constant$$

the position X_{I+1} of the CFB is calculated using the mean pressure and the pre shock conditions. If the percentage difference between X_I and X_{I+1} is not within a certain value X_{I+1} becomes X_I and the calculation procedure is repeated. When the required accuracy is obtained the CFB at the next time interval is calculated.

Output

The output file PATH.OUT contains:

- time (μs)
- mean pressure (Pa)
- compressed foam boundary position (mm)
- mean temperature (K).

```
$STRICT
$DEBUG
C
C                    COMPRESSED FOAM BOUNDARY
C
C       Program to calculate the path of the compressed foam boundary
C       given a pressure distribution history. Assuming isentropic
C        compression.
C
        DOUBLE PRECISION X(10),P(10),C(10)
        INTEGER TIME
        OPEN(10,FILE='PRESSURE.IN',STATUS='OLD')
        OPEN(12,FILE='PATH.OUT',STATUS='OLD')
        WRITE(6,400)
400     FORMAT(1X,'ENTER Number of Pressure Records')
        READ(*,*) N
        WRITE(6,410)
410     FORMAT(1X,'ENTER Atmospheric pressure (Pa)')
        READ(*,*) PATM
        WRITE(6,420)
420     FORMAT(1X,'ENTER Atmospheric density (kg/m^3)')
        READ(*,*) RHO
        WRITE(6,430)
430     FORMAT(1X,'ENTER Percentage difference between successive',/
       &,7X,'iterations acceptable for piston path')
        READ(*,*) ACY
C
        READ(10,200) X(6),X(5),X(4),X(3),X(2),X(1)
200     FORMAT(1X,6(F7.3,1X))
        WRITE(12,440)
440     FORMAT(12X,'Mean',19x,'Mean')
        WRITE(12,450)
450     FORMAT(3X,'Time',3X,'Pressure',3x,'Distance',3x,'Temperature')
        WRITE(12,460)
460     FORMAT(4X,'uS',7X,'Pa',9X,'mm',11X,'K')
        WRITE(12,470)
470     FORMAT(1X)
C
C       Calculation of mean pressure
C
10      READ(10,210) TIME,P(6),P(5),P(4),P(3),P(2),P(1)
210     FORMAT(1X,I5,1X,6(F7.3,1X))
        IF (XX.EQ.0) THEN
          XX = 0.030
        ELSE
          XX=XC
        END IF
        IT = 0
```

```
      N = N-1
      CALL LSTSQ(X,P,C)
20    PAVG = C(1)*XX+C(2)*XX**2/2+C(3)*XX**3/3
      PAVG = (PAVG +C(4)*XX**4/4+C(5)*XX**5/5)/XX*1000
C
C     Calculation of the path of the compressed foam boundary
C
      T = (PAVG**(0.4/1.4)*(PATM)**(1.0/1.4))/287.1/RHO
      XC = (PATM)**(1.0/1.4)*0.07/PAVG**(1.0/1.4)
      DIFF = ABS((XC-XX)/XX*100)
      IF (DIFF.LT.ACY) GOTO 50
      IF (XC.LT.XX) THEN
       XX = XC + (XX-XC)/2
      ELSE
       XX = XC - (XX-XC)/2
      END IF
      IT = IT+1
      IF (IT.GT.50) THEN
       WRITE(6,480)
480    FORMAT(1X,'NOT CONVERGING')
       STOP
      END IF
      GOTO 20
C
C     Store results
C
50    D=XX*1000
      WRITE(12,490) TIME,PAVG,D,T
490   FORMAT(1X,I6,4X,F7.0,5X,F4.1,9X,F4.0)
      IF (N.GT.0) GOTO 10
      STOP
      END
C
C     This subroutine fits a polynomial to a set of data points
C
      SUBROUTINE LSTSQ(X,Y,C)
      DOUBLE PRECISION X(10),Y(10),C(10),A(10,11),XN(10)
      MF = 4
      N = 6
5     MFP1 = MF+1
      MFP2 = MF+2
      DO 10 I=1,N
10    XN(I) = 1.
      DO 30 I=1,MFP1
      A(I,1) = 0.
      A(I,MFP2) = 0.
      DO 20 J=1,N
      A(I,1) = A(I,1)+XN(J)
```

```
      A(I,MFP2) = A(I,MFP2)+Y(J)*XN(J)
20    XN(J) = XN(J)*X(J)
30    CONTINUE
      DO 50 I=2,MFP1
      A(MFP1,I) = 0
      DO 40 J =1,N
      A(MFP1,I) = A(MFP1,I)+XN(J)
40    XN(J) = XN(J)*X(J)
50    CONTINUE
      DO 70 J=2,MFP1
      DO 60 I=1,MF
60    A(I,J) = A(I+1,J-1)
70    CONTINUE
      CALL LUDCMQ(A,MFP1,10)
      I = MF+1
      DO 90 J=1,I
90    C(J)=A(J,MFP2)
      CALL SOLNQ(A,C,I,10)
      RETURN
      END
C
      SUBROUTINE LUDCMQ(A,N,NDIM)
      DOUBLE PRECISION A(NDIM,NDIM)
      DO 30 I=1,N
      DO 30 J=2,N
      SUM = 0.0
      IF (J.GT.I) GO TO 15
      JM1 = J-1
      DO 10 K=1,JM1
10    SUM = SUM+A(I,K)*A(K,J)
      A(I,J) = A(I,J)-SUM
      GO TO 30
15    IM1 = I-1
      IF (IM1.EQ.0.) GO TO 25
      DO 20 K=1,IM1
20    SUM = SUM+A(I,K)*A(K,J)
25    IF(ABS(A(I,I)).LT.1.E-10) GO TO 99
      A(I,J) = (A(I,J)-SUM)/A(I,I)
30    CONTINUE
      GO TO 501
99    WRITE(6,100) I
100   FORMAT(1H0, 32H REDUCTION NOT COMPLETE BECAUSE ,
     &38H SMALL VALUE FOUND FOR DIVISOR IN ROW , I3)
501   CONTINUE
      RETURN
      END
```

```
C
      SUBROUTINE SOLNQ(A,B,N,NDIM)
      DOUBLE PRECISION A(NDIM,NDIM),B(NDIM)
      B(1) = B(1)/A(1,1)
      DO 20 I=2,N
      IM1 = I-1
      SUM = 0.0
      DO 10 K=1,IM1
10    SUM = SUM+A(I,K)*B(K)
20    B(I) = (B(I)-SUM)/A(I,I)
      DO 40 J=2,N
      NMJP2 = N-J+2
      NMJP1 = N-J+1
      SUM = 0.0
      DO 30 K=NMJP2,N
30    SUM = SUM+A(NMJP1,K)*B(K)
40    B(NMJP1) = B(NMJP1)-SUM
      RETURN
      END
```

Author: Atkins Mark D.
Name of thesis: Shock wave interaction with porous compressible foams.

PUBLISHER:
University of the Witwatersrand, Johannesburg
©2015

LEGALNOTICES:

Copyright Notice: All materials on the University of the Witwatersrand, Johannesburg Library website are protected by South African copyright law and may not be distributed, transmitted, displayed or otherwise published in any format, without the prior written permission of the copyright owner.

Disclaimer and Terms of Use: Provided that you maintain all copyright and other notices contained therein, you may download material (one machine readable copy and one print copy per page)for your personal and/or educational non-commercial use only.

The University of the Witwatersrand, Johannesburg, is not responsible for any errors or omissions and excludes any and all liability for any errors in or omissions from the information on the Library website.